

**DEVELOPMENT AND IMPLEMENTATION OF  
MAGNETO-RHEOLOGICAL FLUID DAMPER IN TWO-  
WHEELER VEHICLE WITH REAL-TIME CONTROL**

**Thesis**

*Submitted in partial fulfillment of the requirements for the degree of*

DOCTOR OF PHILOSOPHY

By

**PINJALA DEVI KIRAN**



DEPARTMENT OF MECHANICAL ENGINEERING  
NATIONAL INSTITUTE OF TECHNOLOGY KARNATAKA,  
SURATHKAL, MANGALORE – 575025

MAY 2023

**DEVELOPMENT AND IMPLEMENTATION OF  
MAGNETO-RHEOLOGICAL FLUID DAMPER IN TWO-  
WHEELER VEHICLE WITH REAL-TIME CONTROL**

**Thesis**

*Submitted in partial fulfillment of the requirements for the degree of*

DOCTOR OF PHILOSOPHY

By

**PINJALA DEVI KIRAN**

Under the Guidance of

**Dr. HEMANTHA KUMAR**

Associate Professor



DEPARTMENT OF MECHANICAL ENGINEERING  
NATIONAL INSTITUTE OF TECHNOLOGY KARNATAKA,  
SURATHKAL, MANGALORE – 575025

MAY 2023

## DECLARATION

I hereby *declare* that the Research Thesis entitled “**Development and Implementation of Magneto-Rheological Fluid Damper in Two-Wheeler Vehicle with Real-Time Control**” which is being submitted to the National Institute of Technology Karnataka, Surathkal in partial fulfillment of the requirements for the award of the Degree of Doctor of Philosophy in Department of Mechanical Engineering is a *bonafide report of the research work carried out by me*. The material contained in this Research *thesis* has not been submitted to any University or Institution for the award of any degree.

Register Number : 177161ME028

Name of the Research Scholar : PINJALA DEVI KIRAN

Signature of the Research Scholar



Department of Mechanical Engineering

Place: NITK, Surathkal

Date: 04-05-2023

## C E R T I F I C A T E

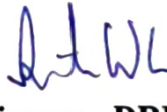
This is to *certify* that the Research Thesis entitled “**Development and Implementation of Magneto-Rheological Fluid Damper in Two-Wheeler Vehicle with Real-Time Control**” submitted by **Mr. PINJALA DEVI KIRAN. (Register Number: 177161ME028)** as the record of the research work carried out by him, is *accepted as the Research thesis submission* in partial fulfillment of the requirements for the award of degree of Doctor of Philosophy.

Research Guide

  
04/05/2023

**Dr. Hemantha Kumar**  
Associate Professor  
Department of Mechanical Engineering  
NITK Surathkal



  
2.5.2023

**Chairman - DRPC**  
Department of Mechanical Engineering  
NITK Surathkal

## ACKNOWLEDGEMENTS

With a deep sense of gratitude, I wish to express my sincere thanks to my supervisor **Dr. Hemantha Kumar**, Associate Professor, Department of Mechanical Engineering, National Institute of Technology Karnataka (N.I.T.K), Surathkal, for his continuous guidance and support throughout my research work. I received very useful, encouraging, excellent academic guidance and constant motivation from him, which has helped me in coming up with this thesis. His constant encouragement, help and review of the entire work during the course of the investigation were invaluable. I profoundly thank him.

I thank the Head of the Department, **Prof. Ravikiran Kadoli**, Professor, Department of Mechanical Engineering for his encouragement and support. I take this opportunity to thank former Heads of the Department, **Prof. Shrikantha S Rao**, **Prof. Narendranath** and **Prof. S.M. Kulkarni**, Professor, Department of Mechanical Engineering for their help, continuous and timely suggestions.

I wish to thank all the members of the Research Program Assessment Committee members, **Dr. Veershatti Gumtapure**, Associate Professor, Department of Mechanical Engineering and **Dr. R. Madhusudhan**, Head of the department & Associate Professor, Department of Mathematics and Computational Sciences, for their appreciation and valuable suggestions for this research work. I wish to express my sincere gratitude to all the faculty members of the Department of Mechanical Engineering, N.I.T.K Surathkal for their help, encouragement and support all through this research work.

I acknowledge and express gratitude for the funding support from **IMPRINT** project No. **IMPRINT/2016/7330**, titled with “Development of Cost Effective Magneto-Rheological (MR) Fluid Damper in Two wheelers and Four Wheelers Automobile to Improve Ride Comfort and Stability” under Ministry of Human Resource Development and Ministry of Road Transfer and Highways, Govt. of India.

I thank the technical support provided by Mr. Sahoo, Arya technocrats, Belgaum, for manufacturing of axial, radial and hybrid radial flux-based MR Dampers.

My heartfelt thanks to Mr. Abhinandan Hegale and Mr. N. P. Puneet for helping me in the design of one of my dampers and its experimentation. My sincere thanks to all my colleagues, Dr. Radhe Shyam, Dr. Rangaraj M Desai., Dr. Ravikumar., Dr. J. Vipin Allien, Mr. Suhas Aralikatti, Mr. Ashok K, Mr. M. J. Hussain, Dr. Subhash Acharya and Ms. Pendyala Shravya for their help and support to carry out this dissertation work. I am thankful to everybody who helped and encouraged me during this research work.

Finally, I would like to thank my wife Mrs. Pilla Durga Bhuvana and parents who have been a constant motivation and moral support to me throughout the completion of my research.

Pinjala Devi Kiran

## ABSTRACT

The present-day automotive systems are equipped with a combination of various electromechanical sensors, actuators and devices to improve the ride quality according to the preferences of the riders. Suspension systems are one of the most important areas in which tremendous amount of research was being pursued while different technologies have been developed and incorporated. Magneto-rheological dampers are one of the technologies which can be implemented in the vehicular suspension to obtain a varied damping with respect to the road profile. This study carries out various MR damper designs which can be fabricated and implemented in two-wheeler vehicles depending on the fixtures and complexities.

Two different piston designs namely axial flux based and radial flux-based designs are designed considered in the space and dimensional constrains of specific two-wheeler motor vehicles and E-bicycle (E-bike) i.e., Splendor plus (make: Hero motor corp.), Pulsar 200cc (make: Bajaj Auto) and Crest (make: Atlas cycles). The design parameters are considered by the Matlab optimization tool box considering the maximum dynamic range as the prime requirement. With the obtained dimensions, FEMM analysis is performed to obtain the magnetic flux density being produced in the fluid flow gap, estimating the flux produced for influencing the MR fluid in the damper. the designed MR dampers are fabricated and characterized for the force-velocity characteristics with respect to the changes in current under varied frequency sine excitation. These characteristics are considered for mathematical modelling.

The characterization results are utilized in mathematical modeling considering either parametric or non-parametric models for the designed damper modelling. Kwok model is considered in the parametric modeling whereas the polynomial model is considered in the nonparametric modeling. Due to the reduced complexities and ease of implementation polynomial model is considered for modeling most of the MR dampers in the studies performed. The mathematical model is used in the simulation of Quarter car and two-wheeler suspension with the designed MR damper.

Parallely with respect to the design parameters considered for, the designed MR damper is fit to the two-wheeler vehicle and tested for certain road conditions at specific velocities. The control logic is implemented with the help of FPGA based controller and data acquisition cards namely NI cRIO 9045, NI 9230, NI 9403 and NI 9205. Different control logics were implemented in this study and the nonlinear control model namely Sliding mode control was providing better performance in reducing the body vibrations of the vehicle. The obtained results show satisfactory performance results while implementing the MR damper in the rear suspension of the two-wheeler vehicle considering the sliding mode control strategy.

With the inspiration of axial and radial flux piston designs, a novel design namely hybrid radial flux piston design was designed and fabricated for a prototype MR damper. This damper utilized the orientation of the coil wound and the effective design to generate both the axial and radial fluxes with in the piston core. The characterization results of this damper also show observable change in the damping force with respect to the change in current supplied to the damper. Polynomial modeling of the damper designed is implemented in the quarter car and two-wheeler models in MATLAB / Simulink and the sprung mass acceleration is considered as priority. The obtained results confirm the effectiveness of the designed damper in vehicular implementation.

***Keywords:*** Axial flux, Radial flux, Hybrid radial flux, MR damper, Two-wheeler suspension, kwok model, Polynomial modelling, Real time implementation, Hybrid radial flux.



# CONTENTS

<b>ACKNOWLEDGEMENTS.....</b>	<b>i</b>
<b>ABSTRACT.....</b>	<b>iii</b>
<b>CONTENTS.....</b>	<b>v</b>
<b>LIST OF FIGURES.....</b>	<b>xi</b>
<b>LIST OF TABLES.....</b>	<b>xvii</b>
<b>1 INTRODUCTION.....</b>	<b>1</b>
1.1 SUSPENSION AND PARTS OF SUSPENSION SYSTEM.....	1
1.1.1 Spring.....	2
1.1.2 Damper.....	2
1.2 TYPES OF SUSPENSION SYSTEM.....	3
1.2.1 Passive suspension system.....	3
1.2.2 Active suspension system.....	4
1.2.3 Semi-active suspension system.....	5
1.3 MAGNETORHEOLOGICAL FLUID.....	6
1.3.1 MR dampers.....	8
1.4 MODELING OF MR DAMPERS.....	11
1.4.1 Parametric Modeling.....	11
1.4.2 Non-parametric Modelling.....	15
1.5 CONTROL STRATEGIES.....	16
1.5.1 PID Controller.....	16
1.5.2 Groundhook Controller.....	19
1.5.3 Skyhook controller.....	19
1.5.4 Fuzzy logic control.....	20
1.5.5 Sliding mode control.....	21
1.6 ORGANIZATION OF THE THESIS.....	22

<b>2</b>	<b>LITERATURE REVIEW.....</b>	<b>25</b>
2.1	INTRODUCTION.....	25
2.2	RHEOLOGICAL STUDY.....	25
2.3	MATHEMATICAL MODELLING OF MR FLUID DAMPERS..	27
2.4	OPTIMIZATION OF PISTON DESIGN AND CONFIGURATION.....	31
2.5	DESIGN BASED ON ELECTROMAGNETIC PISTON.....	35
2.6	DESIGN BASED ON FLOW VALVES.....	39
2.7	CURRENT CONTROLLER.....	39
2.8	CONTROL STRATEGY AND CONTROL ALGORITHM.....	40
2.9	APPLICATIONS OF MR DAMPER.....	42
2.10	RESEARCH GAP.....	43
2.11	OBJECTIVES.....	44
2.12	SCOPE.....	45
2.13	METHODOLOGY.....	45
2.14	SUMMARY.....	47
<b>3</b>	<b>DESIGN AND ANALYSIS OF AXIAL FLUX TWO-WHEELER MR DAMPER.....</b>	<b>49</b>
3.1	INTRODUCTION.....	49
3.2	DESIGN OF AXIAL FLUX TWO-WHEELER MR DAMPER...	49
3.3	AXIAL FLUX TWO-WHEELER MR DAMPER CHARACTERIZATION.....	53
3.4	MODELLING AND ANALYSIS OF AXIAL FLUX TWO- WHEELER MR DAMPER.....	57
	MODELLING OF AXIAL FLUX MR DAMPER USING KWOK MODEL.....	58
3.5	REAL TIME TESTING OF AXIAL FLUX MR DAMPER WITH CONSTANT CURRENT INPUT.....	73
3.6	SUMMARY.....	78

<b>4</b>	<b>DESIGN AND ANALYSIS OF RADIAL FLUX TWO-WHEELER MR DAMPER.....</b>	<b>79</b>
4.1	INTRODUCTION.....	79
4.2	SYNTHESIS AND CHARACTERIZATION OF MR FLUID.....	79
4.3	DESIGN OF RADIAL FLUX TWO-WHEELER MR DAMPER.	82
4.4	CHARACTERIZATION OF RADIAL FLUX TWO-WHEELER MR DAMPER.....	85
4.5	MODELLING OF RADIAL FLUX TWO-WHEELER MR DAMPER.....	89
4.6	SLIDING MODE CONTROL (SMC) FOR MATHEMATICAL ANALYSIS.....	93
4.7	RESPONSE OF MMT USING RADIAL FLUX TWO-WHEELER MR DAMPER.....	95
4.8	REAL-TIME CONTROL OF RADIAL FLUX MR DAMPER IN TWO-WHEELER VEHICLE.....	99
	4.8.1 Control laws implemented in real time control.....	102
4.9	RESULTS OF REAL-TIME CONTROL WITH SMC CONTROL ON TWO-WHEELER VEHICLE WITH RADIAL FLUX MR DAMPER.....	104
4.10	SUMMARY.....	109
<b>5</b>	<b>DESIGN AND ANALYSIS OF AXIAL FLUX AND RADIAL FLUX BASED MR DAMPERS FOR E-BICYCLE.....</b>	<b>111</b>
5.1	INTRODUCTION.....	111
5.2	SYNTHESIS AND CHARACTERISATION OF MR FLUID.....	111
5.3	DESIGN OF E-BICYCLE MR DAMPERS WITH AXIAL FLUX PISTON.....	113
5.4	CHARACTERIZATION OF AXIAL FLUX E-BICYCLE MR DAMPER.....	115
5.5	DESIGN OF E-BICYCLE RADIAL FLUX MR DAMPER.....	120

5.6	CHARACTERIZATION OF RADIAL FLUX MR DAMPER FOR E-BICYCLE.....	123
5.7	MODELLING OF AXIAL FLUX E-BICYCLE MR DAMPER...	127
5.8	RESPONSE OF MMQ USING AXIAL FLUX E-BICYCLE MR DAMPER.....	130
5.9	RESPONSE OF MMT USING AXIAL FLUX E-BICYCLE MR DAMPER.....	131
5.10	REAL TIME CONTROL IMPLEMENTATION OF AXIAL FLUX MR DAMPER IN E-BICYCLE.....	135
5.11	SUMMARY.....	140
<b>6</b>	<b>HYBRID RADIAL FLUX PISTON: NOVEL DESIGN OF ELECTRO-MAGNETIC PISTON FOR MAGNETO-RHEOLOGICAL DAMPERS.....</b>	<b>141</b>
6.1	INTRODUCTION.....	141
6.2	DESIGN OF HYBRID RADIAL FLUX PISTON (HRFP) BASED MR DAMPER.....	141
6.3	FINITE ELEMENT MAGNETOSTATIC ANALYSIS OF HRFP	144
6.4	CHARACTERIZATION OF MR DAMPER WITH HRFP.....	147
6.5	PULSED EXCITATION RESPONSE OF THE PROTOTYPE MR DAMPER.....	152
6.6	MODELLING OF HRFP BASED MR DAMPER.....	157
6.7	RESPONSE OF MMQ USING HRFP BASED MR DAMPER....	160
6.8	RESPONSE OF MMT USING HRFP BASED MR DAMPER....	162
6.9	SUMMARY.....	166
<b>7</b>	<b>SUMMARY AND CONCLUSIONS.....</b>	<b>167</b>
7.1	SUMMARY.....	167
	7.1.1 Axial flux design-based Two-wheeler motor vehicle MR damper.....	167
	7.1.2 Radial flux design-based Two-wheeler MR damper.....	168

7.1.3 E-bicycle Axial flux design-based MR damper.....	169
7.1.4 E-bicycle Radial flux design-based MR damper.....	170
7.1.5 Hybrid Radial Flux Piston based MR Damper.....	170
7.2 CONCLUSION.....	171
7.2.1 Comparison of Axial and Radial flux piston-based MR dampers.....	171
7.2.2 Real time control of two-wheeler and e-bicycle with MR damper.....	172
7.2.3 Hybrid Radial flux piston-based MR damper.....	172
7.3 SCOPE FOR THE FUTURE WORK.....	173
<b>REFERENCES.....</b>	<b>175</b>
<b>LIST OF PUBLICATIONS.....</b>	<b>191</b>
<b>APPENDIX .....</b>	<b>193</b>
<b>BIO DATA.....</b>	<b>210</b>



## LIST OF FIGURES

Figure 1.1	Typical bike suspension system.....	2
Figure 1.2	Types of vehicle suspension system.....	4
Figure 1.3	(a) Flow Mode (b) Shear Mode (c) Squeeze Mode.....	7
Figure 1.4	Schematic of a MR damper.....	9
Figure 1.5	Monotube damper.....	10
Figure 1.6	Twin tube damper.....	10
Figure 1.7	Bingham Model.....	12
Figure 1.8	Bouc-Wen Model.....	12
Figure 1.9	Modified Bouc-Wen Model.....	13
Figure 1.10	The Kwok model.....	15
Figure 1.11	Individual PID controllers (a) P controller (b) I controller (c) D controller.....	17
Figure 1.12	Block diagram of PID controlled MR Damper.....	18
Figure 1.13	Scheme of the skyhook controller.....	20
Figure 1.14	Fuzzy control schematic.....	21
Figure 2.1	Cross sectional view of axial design (Strecker et al. (2021)).....	28
Figure 2.2	Optimized design of axial flux MR damper (Krishna et al. (2017)).....	32
Figure 2.3	Radial flux design (side view) (Goldasz (2013)).....	34
Figure 2.4	Radial flux design (top view) (Goldasz (2013)).....	34
Figure 2.5	Design of twin tube damper (Desai et al. (2019)).....	35
Figure 2.6	Improved radial flux design with both annular gaps (Goldasz (2019)).....	36
Figure 2.7	8-pole radial flux design (Oliver et al (2002)).....	37
Figure 2.8	Dis-assembled view of axial flux MR damper (Nam and Park (2009)).....	38
Figure 2.9	Methodology involved in the performed research work.....	46
Figure 3.1	Nomenclature of MR damper piston.....	51
Figure 3.2	FEMM analysis of axial flux two-wheeler MR damper piston...	52

Figure 3.3	Developed axial flux two-wheeler MR damper.....	53
Figure 3.4	Damper testing machine with axial flux two-wheeler MR damper.....	54
Figure 3.5	(a) force-displacement and (b) force-velocity for 8mm amplitudes.....	55
Figure 3.6	(a) force-displacement and (b) force-velocity for 12mm amplitudes.....	56
Figure 3.7	(a) force-displacement and (b) force-velocity for 16mm amplitude.....	57
Figure 3.8	Experimental and Kwok model output for off state condition for (a) 8mm, and (b) 12mm.....	62
Figure 3.9	Quartercar Mathematical Suspension Model.....	64
Figure 3.10	Sprung mass acceleration response of MMQ with axial two-wheeler MR damper.....	65
Figure 3.11	Mathematical model of the Two-wheeler vehicle.....	66
Figure 3.12	Random Road profile (a) time domain (b) power spectral density.....	68
Figure 3.13	Block diagram representation of the PID control Strategy.....	70
Figure 3.14	Sprung mass RMS acceleration at different velocities.....	71
Figure 3.15	Pitch angle with different current inputs at different velocities..	71
Figure 3.16	Road holding of (a) front and (b) rear different current inputs...	72
Figure 3.17	Total suspension system for two-wheeler vehicle.....	74
Figure 3.18	MR Damper fitted to two-wheeler with control kit.....	75
Figure 3.19	Road with a speed bump for testing the semi active suspension.	76
Figure 3.20	PSD acceleration with variation in frequency.....	76
Figure 3.21	RMS sprung mass acceleration with current variation.....	77
Figure 4.1	Rheometer test setup for characterization of MR fluid.....	80
Figure 4.2	Shear rate vs shear stress at different currents.....	81
Figure 4.3	Shear rate vs viscosity at different currents of MR fluid.....	81
Figure 4.4	Currents vs Shear stress of MR fluid.....	82
Figure 4.5	Design of radial flux two-wheeler MR damper.....	83



Figure 4.6	FEMM results of radial flux two-wheeler MR damper piston...	84
Figure 4.7	Fabricated radial flux two-wheeler MR damper disassembled view.....	84
Figure 4.8	Characterization setup of radial flux two-wheeler MR damper..	85
Figure 4.9	(a) Force-displacement and (b) force-velocity curves at 1Hz....	86
Figure 4.10	(a) Force-displacement and (b) force-velocity curves at 1.5 Hz.	87
Figure 4.11	(a) Force-displacement and (b) force-velocity curves at 2Hz....	88
Figure 4.12	Force current curves at (a) 31.4mm/s (b) 47.1mm/s and (c) 62.8mm/s.....	92
Figure 4.13	Force velocity curves at different current inputs for radial flux MR damper.....	93
Figure 4.14	Block diagram representation of the SMC on two-wheeler suspension.....	97
Figure 4.15	(a) Sprung mass RMS acceleration and (b) pitch angle with SMC control.....	98
Figure 4.16	Road holding of (a) front and (b) rear different current inputs...	99
Figure 4.17	Road Profile for RT control of radial flux two-wheeler MR damper.....	100
Figure 4.18	Schematic for the RT control of radial flux two-wheeler MR damper.....	100
Figure 4.19	Two-wheeler RT experimentation test setup along with the controller.....	101
Figure 4.20	Realtime sprung mass acceleration response to the (a) Crest Road input and (b) trough.....	105
Figure 4.21	Real time sprung mass acceleration response to (a) crest and (b) trough road input in the frequency domain.....	107
Figure 4.22	Damper currents obtained at the impact of (a) crest and (b) trough.....	108
Figure 5.1	Shear rate vs shear stress at different currents of prepared MR fluid.....	112

Figure 5.2	Shear rate vs viscosity at different currents of prepared MR fluid.....	112
Figure 5.3	Currents vs shear stress of prepared MR fluid.....	113
Figure 5.4	FEMM result of axial flux piston designed for e-bicycle MR damper.....	114
Figure 5.5	Assembled and disassembled view of axial flux e- bicycle MR damper.....	115
Figure 5.6	Characterization setup housing the axial flux e-bicycle MR damper.....	116
Figure 5.7	(a) Force-displacement and (b) force-velocity curves at 1 Hz...	117
Figure 5.8	(a) Force-displacement and (b) force-velocity curves at 1.5 Hz.	118
Figure 5.9	(a) Force-displacement and (b) force-velocity curves at 2Hz....	119
Figure 5.10	FEMM analysis of radial flux e-bicycle MR damper.....	121
Figure 5.11	Assembled and disassembled view of the radial flux e-bicycle damper.....	122
Figure 5.12	Radial flux e-bicycle MR damper piston (a) side view (b) isometric view.....	123
Figure 5.13	(a) Force-displacement and (b) force-velocity curves at 1 Hz...	124
Figure 5.14	(a) Force-displacement and (b) force-velocity curves at 1.5 Hz.	125
Figure 5.15	(a) Force-displacement and (b) force-velocity curves at 2Hz....	126
Figure 5.16	Force current curves at (a) 31.4mm/s (b) 47.1mm/s and (c) 62.8mm/s.....	129
Figure 5.17	Force velocity curves at different current inputs for axial flux e-bicycle MR damper.....	130
Figure 5.18	Sprung mass acceleration of MMQ with axial two-wheeler MR damper.....	131
Figure 5.19	Block diagram representation of the SMC on e-bicycle suspension.....	133
Figure 5.20	(a) RMS Sprung mass acceleration and (b) pitch angle with varied velocities.....	134
Figure 5.21	Road holding of (a) front and (b) rear different current inputs...	135

Figure 5.22	Road Profile for RT control of axial flux e-bicycle MR damper	136
Figure 5.23	Schematic of the total setup for RT control.....	136
Figure 5.24	Real time test setup of MR damper fit e-bicycle along with the controller.....	137
Figure 5.25	Realtime sprung mass acceleration response to the road input...	138
Figure 5.26	Frequency plot of sprung mass acceleration response to the road input.....	139
Figure 5.27	Damper currents obtained at the impact of the undulations in road.....	140
Figure 6.1	Cross sectional view of HRFP.....	142
Figure 6.2	Magnetic flux lines in MR fluid and outer cylinder.....	144
Figure 6.3	Magnetic flux lines in piston poles of HRFP.....	145
Figure 6.4	Magnetic flux lines in piston core of HRFP.....	145
Figure 6.5	Developed MR damper with detailed view of Hybrid Radial Flux Piston.....	146
Figure 6.6	Damper testing machine with designed MR damper containing HRFP.....	147
Figure 6.7	(a) Force-displacement and (b) force-velocity curves at 0.8Hz..	148
Figure 6.8	(a) Force-displacement and (b) force-velocity curves at 1.2 Hz.	149
Figure 6.9	(a) Force-displacement and (b) force-velocity curves at 1.6Hz..	150
Figure 6.10	(a) Force-displacement and (b) force-velocity curves at 2Hz....	151
Figure 6.11	(a)Timer circuit schematic with (b) practical design for Pulsed excitation.....	154
Figure 6.12	(a) RL schematic of MRD and (b) the current trace for Pulsed excitation.....	155
Figure 6.13	Pulse excitation responses under (a) 1 Hz (b) 2 Hz (c) 3 Hz.....	156
Figure 6.14	Force Vs Current at (a) 20mm 0.8Hz (b) 20mm 1.2Hz.....	158
Figure 6.15	Force Vs Current at (a) 20mm 1.6Hz and (b) 20mm 2Hz.....	159
Figure 6.16	Force – velocity curves at different currents of HRFP based MR damper.....	160

Figure 6.17	Sprung mass acceleration of MMQ with HRFP based MR damper.....	161
Figure 6.18	Block diagram representation of the SMC on two-wheeler suspension.....	163
Figure 6.19	(a) Sprung mass RMS acceleration and (b) pitch angle with current inputs.....	164
Figure 6.20	Road holding of (a) front and (b) rear for different velocity inputs.....	165

## LIST OF TABLES

Table 3.1	Dimensions of damper piston.....	51
Table 3.2	Kwok model parameters for different conditions.....	60
Table 3.3	Parameters in terms of current for 12 mm amplitude.....	61
Table 3.4	Final representation of each Kwok model parameter.....	61
Table 3.5	Parameters of the MMQ with axial flux-based two-wheeler MR damper.....	65
Table 3.6	Parameters for MMT for Axial flux two-wheeler MR damper.....	69
Table 4.1	MR fluid composition for Radial flux two-wheeler MR damper...	80
Table 4.2	Optimal dimensions of Radial flux two-wheeler MR damper.....	82
Table 4.3	Maximum and minimum damping force at different current inputs.....	90
Table 4.4	Damping force equations with respect to velocity variations.....	91
Table 4.5	Force velocity equations at different currents.....	92
Table 4.6	Parameters for MMT with radial flux two-wheeler MR damper...	96
Table 4.7	Sprung mass acceleration in response to crest road profile.....	106
Table 4.8	Sprung mass acceleration in response to trough road profile.....	106
Table 5.1	Composition of MR fluid for e-bicycle damper.....	111
Table 5.2	Dimensions of axial e-bicycle damper.....	114
Table 5.3	Dimensions of Radial flux e-bicycle MR damper.....	120
Table 5.4	Maximum and minimum damping force obtained at different currents w.r.t. velocity.....	128
Table 5.5	Damping force equations with respect to velocity variations.....	128
Table 5.6	Force velocity equations at different currents.....	129
Table 5.7	Parameters of MMQ with axial flux e-bicycle MR damper.....	130
Table 5.8	Parameters for MMT employing axial flux e-bicycle MR damper	132
Table 5.9	Sprung mass acceleration in response to specific road profile.....	139
Table 6.1	Dimensions of HRFP.....	142
Table 6.2	Materials used for fabrication of HRFP MR damper.....	144
Table 6.3	The maximum and minimum forces with respect to current I.....	157

Table 6.4	Force - Current equations for HRFP based MR damper.....	158
Table 6.5	Force Velocity equations for HRFP based MR damper.....	159
Table 6.6	Parameters of the Quarter Car Model with HRFP based MR damper.....	161
Table 6.7	Parameters for two-wheeler mathematical model with HRFP MR damper.....	162

# **CHAPTER 1**

## **INTRODUCTION**

Automotive technology, a research area that is getting updated day by day with immense changes and improvements from the basic screw nut arrangements to the complex fuel and subsystem changes. One such field of automotive research, where, extensive growth has occurred is suspension systems. The work of suspension systems in the automotive field is to reduce or eliminate the vibrations caused in the vehicle due to the unevenness of the road at the passenger's end. It improves the road gripping as well as keeps the ride more comfortable for the passengers.

Improvement of vehicular suspension has been a main concern for automobile industry as well as the researchers as ride comfort and better road holding gained crucial importance. Semiactive suspension has become one of the rapidly growing technologies and gained importance of researchers as they provide a better ride comfort and stability in vehicular applications. Even though semi active suspension as a whole can be segregated based on the material design technology used etc., MR dampers are the best fit in semi active suspension for the vehicular applications, as its material properties and operating conditions lie well within the preview.

### **1.1 SUSPENSION AND PARTS OF SUSPENSION SYSTEM**

Vehicle suspension systems contain multiple parts and fixtures which can be embedded into inertial elements (masses), restoring elements (springs), and dissipative elements (dampers). The suspension system is passive in the sense that there is no external power added in order to control the system dynamics. The main feature of such systems is the cyclic interchange of kinetic and potential energy with some energy dissipation in damping devices. (Gołdasz and Sapiński (2015))

A system of springs and dampers that are used to connect the wheels to the chassis is known as the suspension system as shown in figure 1.1. It performs a dual job i.e., ride quality and road handling at the same time.

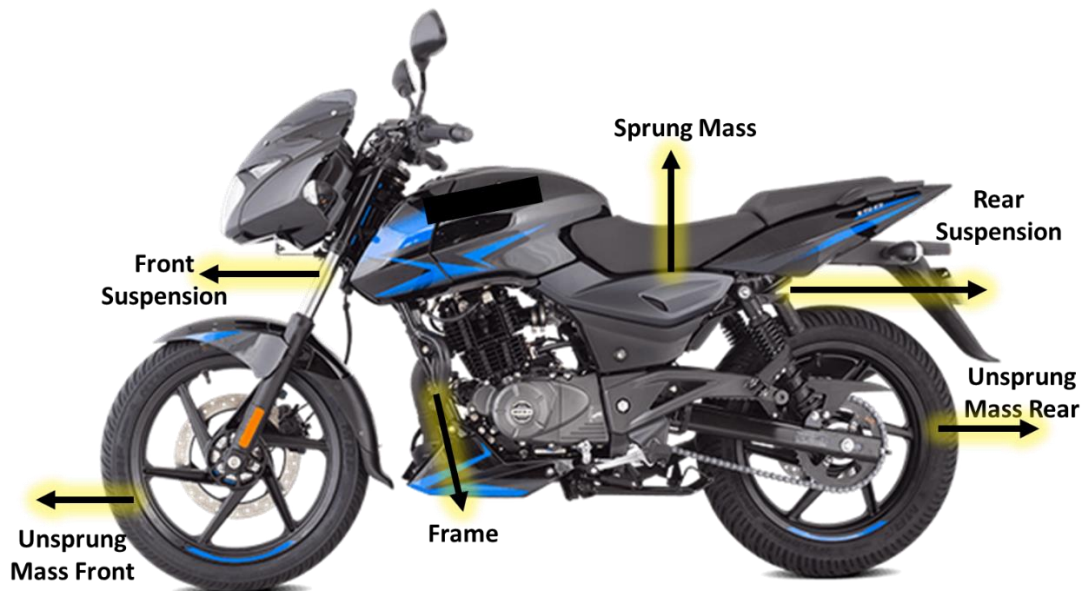


Figure 1.1 Typical bike suspension system (Gołdasz and Sapiński (2015))

### 1.1.1 Spring

The role of a spring is to compensate for irregularities in the road surface, maintain the suspension system at a predetermined height and support added weight without excessive sagging. Springs cushion the ride of a vehicle according to the principle of sprung-to-unsprung weight ratios. As a vehicle gains speed, the springs begin to absorb the impact of striking irregularities in the road surface as vehicle speed increases, a stiffer spring rate is required to keep the axles and wheels in contact with the road surface. This is why high-performance vehicles tend to use stiffer suspension systems than regular passenger vehicles.

### 1.1.2 Damper

As the wheel of a vehicle moves over a bump, energy is given to the spring due to which it deflects, when the bump is crossed, rebound or release of the stored energy takes place, and the spring is put into an oscillating motion before restores to its normal position. To provide a comfortable ride, the damper is used to absorb the energy stored



in the spring. This reduces the number of oscillations that occur between the initial bump and the return of spring to the rest position.

Hydraulic dampers are most commonly used today. The dissipation of the energy in these dampers occurs by the flow of oil through small orifices. Resistance of the hydraulic damper increases with the increase of the speed of spring deflection. The resistance to spring movement is applied at the rebound stroke where the energy received or stored by the spring is dissipated in the form of the frictional force created in the movement of the damper releasing the energy which is stored in the spring by converting into heat.

## **1.2 TYPES OF SUSPENSION SYSTEM**

As specified earlier the suspension system comprises of inertial elements, springs and the dampers. The suspension systems can therefore be classified based on the types of springs or the dampers used in the suspension. As the work in this study deals with the dampers, the suspension systems can be classified into three types based on the types of dampers used in the system. They are:

- Passive suspension system.
- Active suspension system.
- Semi-active suspension system.

### **1.2.1 Passive suspension system**

Passive suspensions are simple mechanical elements and they do not require any external energy for suppression of vibration. The suspension elements will provide the force necessary for the vibration suppression. A schematic representation of passive suspension system is shown in figure 1.2(a) which is an early design for automobile suspension systems focused on optimization of a passive suspension system, which has disadvantages unadaptable to the road condition and its parameters are generally fixed. It reacts automatically to the loads applied to them at the road surface. However, there is no absolutely active control over these reactions.

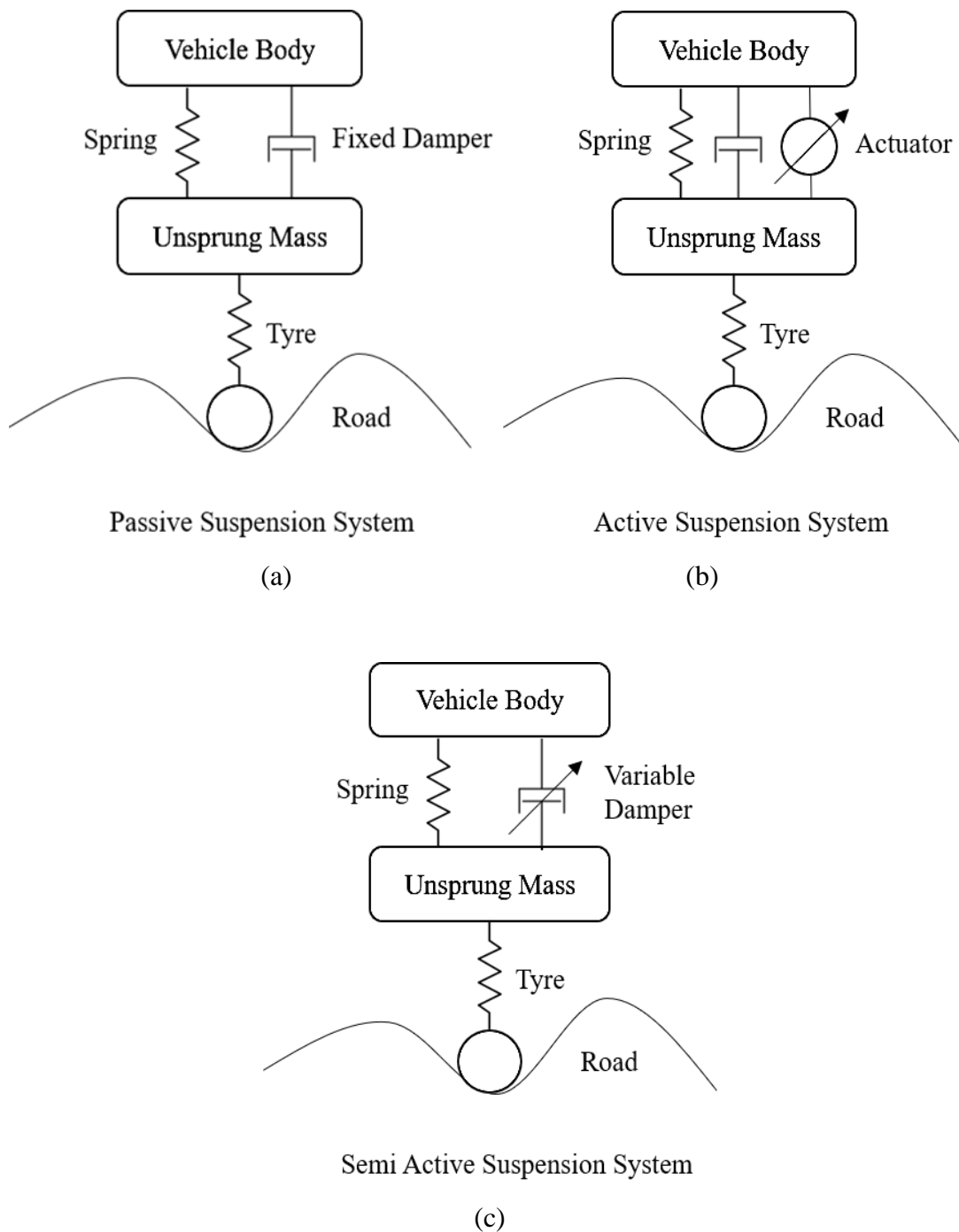


Figure 1.2 Types of vehicle suspension system (Gołdasz and Sapiński (2015))

### 1.2.2 Active suspension system

An active suspension system is shown in figure 1.2(b) in which the reactions to the applied loads are positively supplied by automatically controlled powered actuator. Typically, it consists of a spring, a shock absorber and a hydraulic actuator at each corner of the vehicle. Its role is to improve both driving comfort and road holding by

appropriately transmitting and filtering all forces between the body of the vehicle and the road.

### **1.2.3 Semi-active suspension system**

In a semi-active suspension, the active force generator is replaced with an adjustable damper as shown in figure 1.2(c) using this damper, the rate of energy dissipation can be changed depending on the instant condition of the suspension motion. In this suspension, the damping rate is determined by a controller with closed loop control, using sensory information as feedback.

Magnetorheological (MR) fluid and Electrorheological (ER) fluid are the most effective fluids for semi active suspension. These fluids can change instantaneously into a controllable semi solid with yield strength from a free flow fluid when exposed to a magnetic or electric field with power supply ranging from 0W to 50W. The basic difference between both the fluids is that MR fluid dampers use supply voltages ranging between 2V-25V while the ER fluid dampers use supply voltages from 2000V to 5000V (El-Kafafy et al. (2012)).

Since, the amount of voltage produced in the alternator and the battery in a vehicle generally ranges from 0V to 48V, MR dampers are the most preferable choice when compared with the ER dampers. Also, the yield strength of MR fluids is higher compared to ER fluids. Ferrous materials have high magnetic permeability and saturation. The average response time of MR fluid is around 4 ms with the dynamic range of 8 (Kubík et al. (2017)). MR dampers are thus used in a wide variety of applications not only in vehicular suspension but also in prosthetic applications eg: prosthetic knee (Saini et al. (2021)).

The MR damper based semi-active control system consists of a “system controller” and a “damper controller”. The system controller generates damping force depending upon the dynamic response from the vehicle. The damper controller adjusts the command voltage to the current driver to track the desired damping force. The damping force of the MR damper is monitored and then passed on to the damper

controller to generate command voltage according to the desired damping force generated by the system controller.

### **1.3 MAGNETORHEOLOGICAL FLUID**

MR Fluids consist of magnetic particles typically iron particles in a carrier fluid. In the presence of a magnetic field, the micron-sized particles link with each other and change the fluid to a semi-solid in fraction of seconds (milli seconds). When the magnetic field is removed, the fluid reverts back to its natural free-flowing state almost instantly.

The degree to which the fluid changes to a semi-solid is proportional to the strength of the magnetic field, giving the fluid infinite controllability and precision. Based on the method in which the fluid is made to flow, working behaviour of the MR fluid is classified into three basic modes as shown in the Figure 1.3. They are:

- Shear mode
- Flow mode
- Squeeze mode

The MR fluid flows due a pressure difference between two stationary planar or concentric surfaces in flow mode of operation as shown in figure 1.3 (a). The magnetic field is applied normal to the fluid flow direction which causes changes in the rheological properties of the fluid. MR dampers for vehicle suspensions are designed to operate in flow mode due to greater force which can be attained.

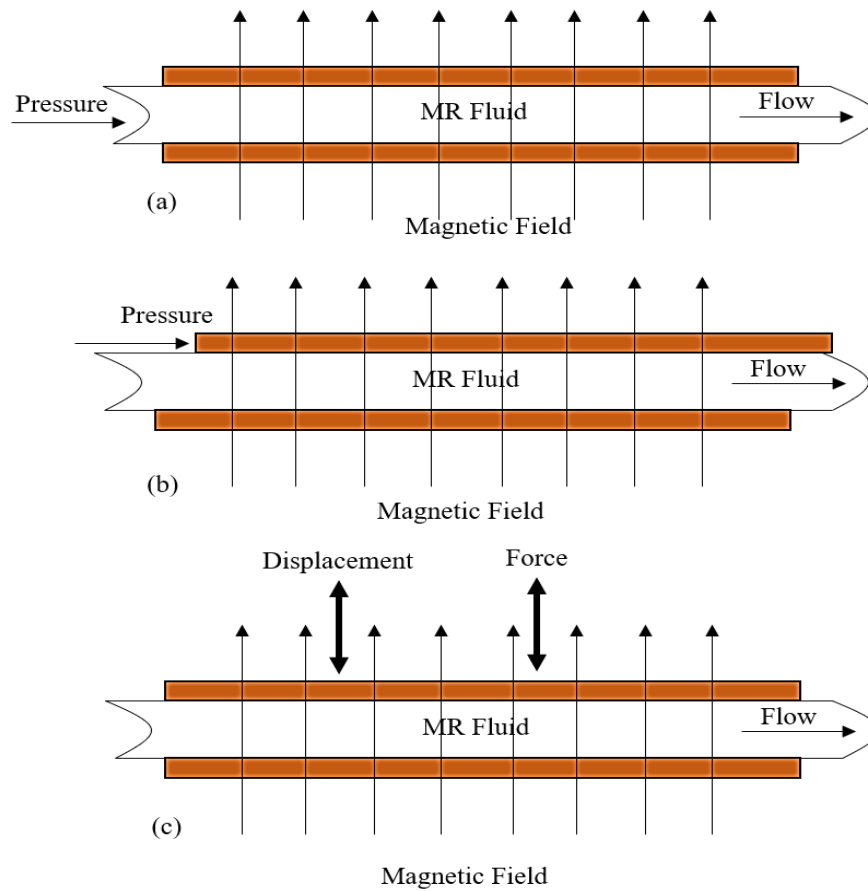


Figure 1.3 (a) Flow (b) Shear and (c) Squeeze mode (Gołdasz and Bogdan (2014))

Figure 1.3 (b) shows shear mode of operation of MR fluid in which fluid flows between two surfaces which move relative to each other and the magnetic field is perpendicular to the fluid flow direction. Rotary dampers, brakes, clutches and steering dampers are examples of devices which use this mode.

Figure 1.3 (c) shows MR fluid operating in Squeeze mode in which the MR fluid is contained between two planar parallel surfaces. Based on predetermined displacement or force input, the distance between the surfaces is varied. It is used in applications in which magnitude of vibration is small. Devices utilizing this mode include MR mounts and high force small stroke linear dampers (Gołdasz and Bogdan 2014).

### 1.3.1 MR dampers

A MR damper consists of a MR fluid that moves between different chambers via small orifices in the piston, converting the energy possessed by the spring into heat. Due to the presence of an electrical circuit in the piston assembly this energy dissipation can be varied as per the requirement. As electrical current is supplied to the damper, a coil inside the piston creates a magnetic field and instantaneously changes the properties of the MR Fluid in the piston. Consequently, the resistance of the damper can be continuously changed in real time by modulating electrical current to the damper. There are different types of MR dampers considering piston design, design elements and characteristics. Some of them are stated in the following sub sections.

MR fluid damper is a device which is filled with magnetorheological fluid whose dynamic characteristics can be varied by controlling the magnetic field applied to it. Construction of MR damper is similar to the conventional hydraulic damper with a housing for solenoid piston. Typical MR damper consists of a piston, accumulator, magnetic coils and MR fluid. Copper coils are wound on an iron core and fitted to the piston. The coils are excited by a DC source. Due to the road disturbances, the piston head moves inside the cylinder. The movement of the piston causes change in the volume which is compensated by compression and expansion of the compressed gas in the accumulator. The accumulator contains compressed gas (nitrogen), which has three main functions:

- (i) Compensates the change in volume due to movement of the piston;
- (ii) Accommodates the thermal expansion of MR fluid, and
- (iii) Avoids the cavitation in the fluid due to piston movements.

When magnetic field is applied to the coils, the particles in the MR fluid form dipoles and apparently increase the viscosity of the fluid. The input current of the magnetic coils determines the dynamic characteristics of the MR damper. Figure 1.4 shows the schematic of an MR damper.

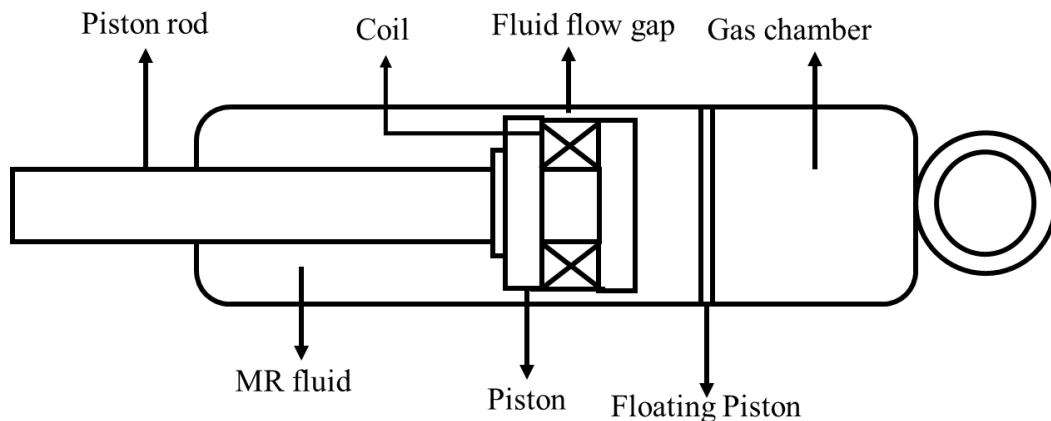


Figure 1.4 Schematic of a MR damper (Gołdasz and Sapiński (2015))

### 1.3.1.1 Monotube MR damper

Mono-tube dampers are by far the most common devices that utilize MR fluids. The mono-tube design has been a natural choice for MR applications due to its simplicity and few internal components. As already stated, the most common application of these dampers is a passenger vehicle suspension. From the standpoint of design, the automotive MR dampers are of a simple mono-tube design with no electromechanical valves and no small moving parts.

In principle, the design configuration of a typical gas-charged MR damper is similar to that of a passive valve-based damper. The cylinder tube houses the floating piston which separates the MR fluid from the high-pressure gas chamber. The main piston divides the MR fluid volume into the compression chamber (fluid volume between the floating piston and the main piston assembly) and the rebound chamber (fluid volume between the rod guide and the main piston). The piston assembly incorporates an annular gap to permit the fluid to flow between the chambers while in motion. The relative motion of the wheel and the body drives the fluid flow between the chambers through the annular gap in the piston. The gas high pressure in the chamber below the floating piston is necessary for cavitation-free operation. (Gołdasz and Sapiński 2015). Figure 1.5 shows a typical monotube MR damper.

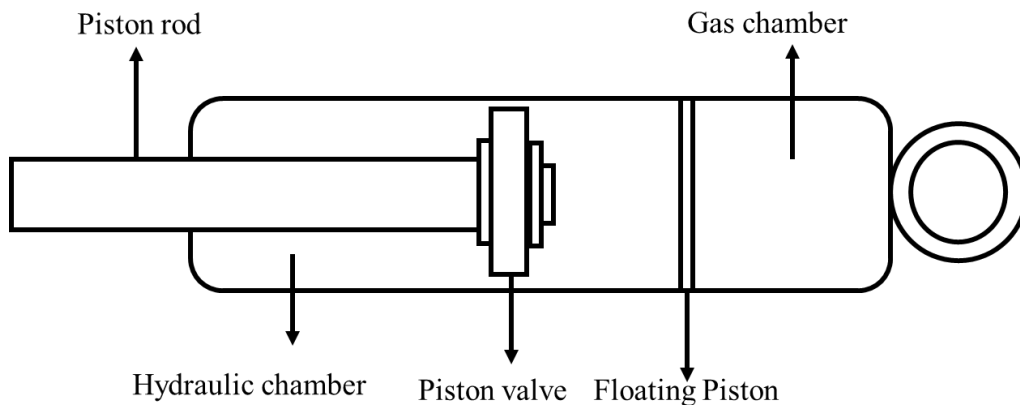


Figure 1.5 Monotube damper

### 1.3.1.2 Twin tube MR damper

Compared to mono-tube configurations, a standard twin-tube damper features concentric cylindrical tube. The inner cylinder houses a piston valve. The piston valve controls the flow between the adjacent fluid chambers and a base valve. In turn, the base valve regulates the flow between the fluid chamber below the piston in the inner cylinder (hydraulic chamber) and a reservoir. The reservoir (outer chamber) is partially filled with oil to accommodate volume changes due to piston rod displacement. The dampers work at a lower gas pressure, but only upright positions (or ones with low inclination angles) are possible in a vehicle suspension and they incorporate more valving components (Goldasz and Sapinski 2015). Figure 1.6 shows a typical twin tube MR damper.

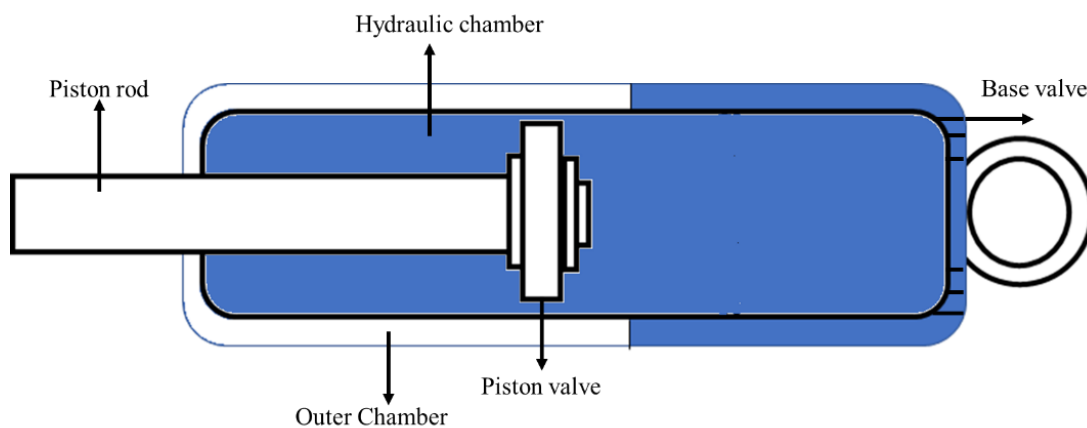


Figure 1.6 Twin tube damper



## 1.4 MODELING OF MR DAMPERS

Variable damper plays a key role in control of semi-active suspension system. Designing and analysis of the suspension system controller requires an accurate model of the damper. A practical damper exhibits non-linearity and hysteresis which must be taken into account in simulation studies in order to investigate the real time system performance. Modelling of the dampers can be broadly classified into two categories:

- a) Parametric modelling
- b) Non-parametric modelling

### 1.4.1 Parametric Modeling

In parametric modeling approach, the damper is represented as an interconnection of mechanical elements like springs and dash pots. Parameters of the model are obtained through experimental results and mathematical methods. Number of parametric models have been proposed in literature to describe the dynamic behaviour of MR damper. Some of the widely used models are:

- ❖ Bingham model
- ❖ Bouc-Wen model
- ❖ Modified Bouc-Wen model
- ❖ Kwok model

#### 1.4.1.1 Bingham Model

This is the most basic model which is used to predict the dynamic behaviour of MR dampers. It consists of a friction and dash pot element placed in parallel as shown in figure 1.7. This model does not map the force-velocity hysteresis relation (Kwok et al. (2006)). The mathematical equation for force generated by Bingham model is given by:

$$F = f_0 + f_c \operatorname{sgn}(\dot{x}) + C_o \dot{x} \quad (1.1)$$

Where,  $C_o$  is the damping coefficient,  $f_c$  is the frictional force and  $f_0$  is the offset force.

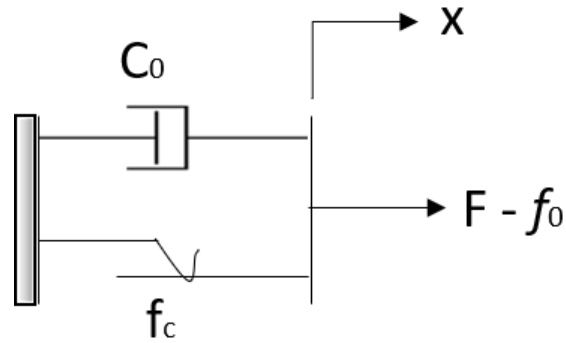


Figure 1.7 Bingham Model

#### 1.4.1.2 Bouc-Wen Model

Schematic representation of Bouc-Wen model is shown in figure 1.8. Bouc-Wen model can capture the hysteresis behaviour of the MR damper.

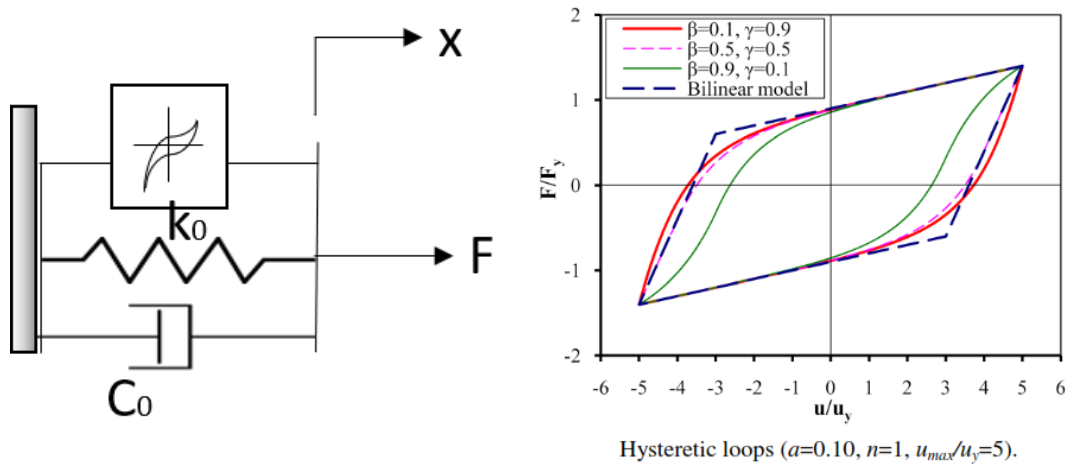


Figure 1.8 Bouc-Wen Model (Charalampakis (2010))

The damping force generated by Bouc-Wen model is given by:

$$F = C_0 \dot{x} + K_0 x + \alpha z \quad (1.2)$$

Where,  $z$  is given by:

$$\dot{z} = -\gamma z |\dot{x}| |z|^{n-1} - \beta \dot{x} |z|^n + \delta \dot{x} \quad (1.3)$$

Where  $K_o$  is the stiffness,  $C_o$  is the viscous coefficient,  $F_d$  is the damping force,  $\gamma$ ,  $\beta$ ,  $\delta$  and  $n$  are parameters of the Bouc-Wen model which define the shape of the hysteresis curve.

Bouc-Wen model is a versatile model which can characterize variety of hysteresis behaviours depending on the model parameters. However, it does not accurately model the characteristics in the regions where acceleration and velocity are having opposite signs and when the magnitudes of velocity are small.

### 1.4.1.3 Modified Bouc-Wen Model

Modified Bouc-Wen model was proposed by Spencer et al. (1997) which describes the dynamic characteristics of the MR damper more accurately. This model introduces an extra degree of freedom to the Bouc-Wen model and yields force-velocity maps of the MR damper which are very close to the experimental results. Figure 1.9 shows the modified Bouc-Wen model of an MR damper where a viscous damping element is connected in series to the Bouc-Wen model and a spring is connected in parallel to it.

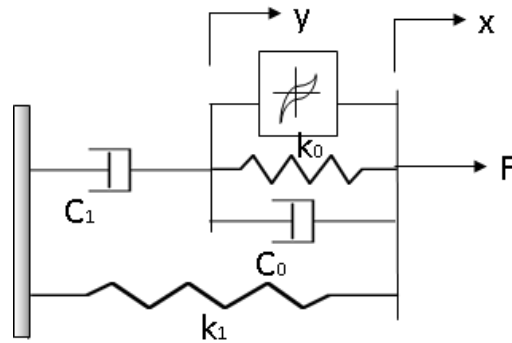


Figure 1.9 Modified Bouc-Wen Model (Spencer et al. (1997))

The damping force is given by:

$$F = C_1 \dot{y} + K_1(x - \dot{x}_o) \quad (1.4)$$

$$\dot{y} = \frac{1}{c_o + c_1} [\alpha z + C_o \dot{x} + K_o(x - y)] \quad (1.5)$$

$$\dot{z} = -\gamma z |\dot{x} - \dot{y}| |z|^{n-1} - \beta (\dot{x} - \dot{y}) |z|^n + \delta (\dot{x} - \dot{y}) \quad (1.6)$$

$$\alpha = \alpha(u) = \alpha_a + \alpha_b u \quad (1.7)$$

$$C_1 = C_1(u) = C_{1a} + C_{1b} u \quad (1.8)$$

$$C_o = C_o(u) = C_{oa} + C_{ob} u \quad (1.9)$$

$$\dot{u} = -\eta(u - v) \quad (1.10)$$

Where  $x$  is the displacement of the damper and  $F$  is the force generated it,  $K_1$  is the accumulator stiffness,  $C_1$  and  $C_o$  are the viscous damping coefficients observed at low and large velocities respectively.  $y$  is a fictitious variable known as internal displacement of the MR fluid damper and does not correspond to actual displacement.  $x_o$  corresponds to initial displacement of the accumulator gas.  $z$  is an evolutionary variable which describes the hysteresis effect of the MR damper.  $K_o$  controls the stiffness at large velocities.  $\alpha$  is the stiffness associated with displacement  $z$ .  $\gamma$ ,  $\delta$ ,  $n$  and  $\beta$  are parameters of Bouc-Wen model.  $u$  is introduced to account for the effect of voltage command  $v$  which is given to the current driver. Variable  $\eta$  is the gain filter.

#### 1.4.1.4 Kwok Model

The kwok model is similar to the bouc-wen model where the model is a hysteretic model based on hyperbolic tangent function proposed by Kwok et al. (2006) and is shown in figure 1.10. The root-mean-square error between the experimentally obtained force and the simulated force using this model is quite less as the degree of nonlinearity is less compared to the Bouc-Wen model. Linear functions which represent the stiffness and viscous, were combined with hyperbolic tangent function in Kwok model.

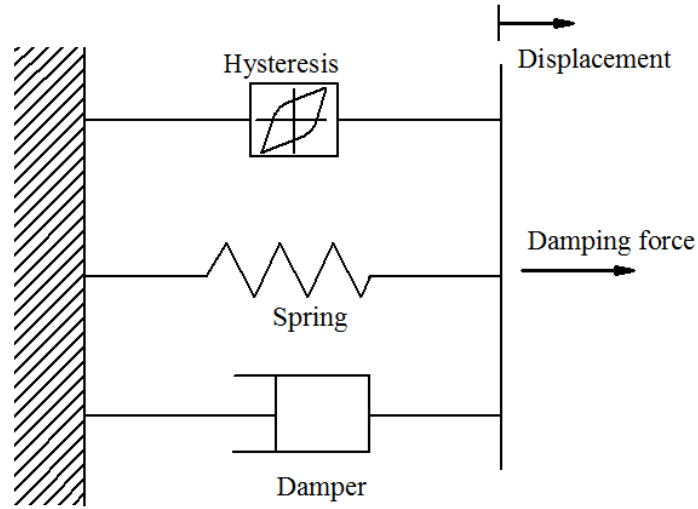


Figure 1.10 The Kwok model (Kwok et al. (2006))

The damping force through Kwok model is represented as,

$$F(t) = c_0\dot{x} + k_0x + \alpha z + f_0 \quad (1.11)$$

Where,  $z$  is the hysteretic variable given by,

$$z = \tanh[\beta\dot{x} + \delta \operatorname{sgn}(x)] \quad (1.12)$$

Where  $\delta$  determines the width of hysteresis and  $\beta$  decides the hysteretic slope. Parameters  $k_0$  and  $c_0$  represent conventional damper without hysteresis.  $\alpha$  is the deciding factor for height of the hysteresis and  $f_0$  is the offset shift of the hysteresis.

#### 1.4.2 Non-parametric Modelling

Non-parametric modelling describes the behaviour of the damper by analytic expressions that give the result close to experimental results. Non-parametric models need large amount of data to model the system. Non-parametric modeling methods are robust and can be applicable to linear, non-linear and system with hysteresis. Non-parametric models can be classified as follows:

- a) Polynomial based techniques
- b) Neural network-based methods

This work implements polynomial modelling for the designed MR dampers which actually works on the estimation of the damping force considering the maximum and minimum damping force obtained from the characterization curves.

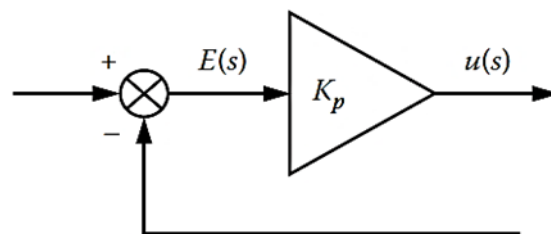
## 1.5 CONTROL STRATEGIES

MR dampers are very effective to control vibration, which use MR fluids to produce controllable damping force and provide both the reliability of passive systems and the facility of active control systems with a minimal power supply. Due to their mechanical simplicity, high dynamic range, low power requirements, large force capacity and robustness, offer an attractive means of vibration protection. In order to evaluate vibration control performance of a vehicle with MR suspension system, various control strategies are formulated and experimentally implemented.

### 1.5.1 PID Controller

An attractive controller to achieve desired damping force using MR damper system is a Proportional-Integral-Derivative (PID) controller. As it is well known, the PID controller is easy to implement in practice, and is very effective with robustness to system uncertainties. The control action of each P, I, and D is shown in figure 1.11. From the block diagram, the input is expressed by

$$\begin{aligned}
 u(s) &= k_p E(s), \quad \text{for } P \text{ action} \\
 u(s) &= \frac{k_i}{s} E(s), \quad \text{for } I \text{ action} \\
 u(s) &= k_d s E(s), \quad \text{for } D \text{ action}
 \end{aligned}
 \tag{1.13}$$



(a) P action

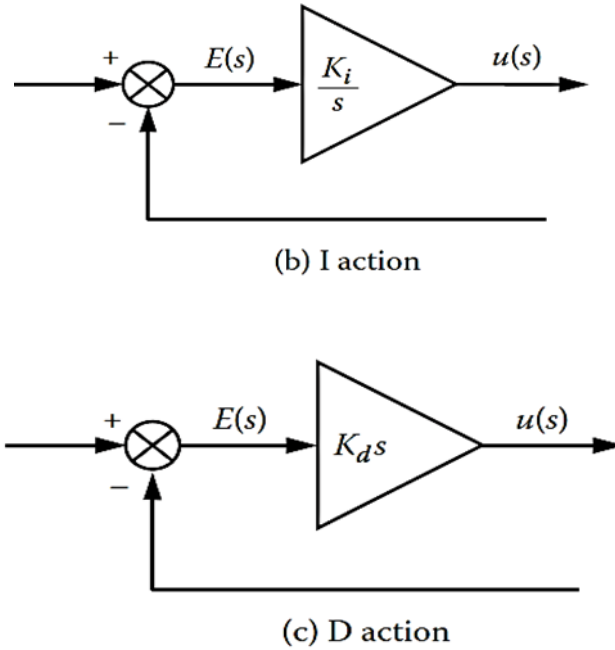


Figure 1.11 Individual P, I, D controllers (Kumar (2008))

In the above equations,  $s$  is the Laplace variable.  $k_p$ ,  $k_i$ , and  $k_d$  are control gains for P, I, and D components, respectively.  $E(s)$  is the feedback error signal between desired value and actual output value. (Kumar (2008)) Consequently, the form of PID controller is given by

$$u(s) = k_p E(s) + \frac{k_i}{s} E(s) + k_d s E(s) \quad (1.14)$$

The P controller is essentially an amplifier with an adjustable gain of  $k_p$ . If the  $k_p$  is increased, the response time of the control system becomes faster. But instability of the control system may occur using very high feedback gains of  $k_p$ . The value of the control  $u(t)$  is changed at a rate proportional to the actuating error signal  $e(t)$  by employing the I controller. For zero actuating error, the value of  $u(t)$  remains to be stationary. By employing the I controller action, the steady state error of control system can be effectively alleviated or eliminated. This is a very significant factor to be considered in the tracking control problem. In general, we can increase system stability by employing the D controller. However, the D control action may amplify noise signals and cause a saturation effect in the MR actuator. It is also noted that the D control action can never be implemented alone because the control action is effective

only during transient periods. An appropriate determination of control gains  $k_p$ ,  $k_i$ , and  $k_d$  to achieve superior control performance can be realized by several methods—Ziegler-Nichols, adaptive, and optimal. (Choi and Han, 2012)

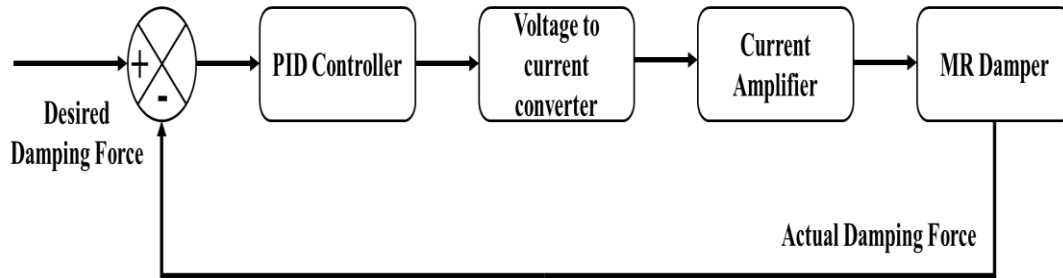


Figure 1.12 Block diagram of PID controlled MR Damper (Kumar (2008))

Figure 1.12 presents a block diagram to achieve the desired damping force of an MR damper using the PID controller. The desired damping force,  $F_d$ , to be tracked is stored in the microprocessor and compared with the actual damping force,  $F_a$ , generated from the MR damper. The actuating error signal is fed back to the PID controller, and hence control input is written by

$$u(t) = k_p E(t) + k_i \int_0^t e(t) + k_d \frac{de(t)}{dt}, \quad e(t) = F_d - F_a \quad (1.15)$$

PID controllers are used in a wide range of applications. These controllers are frequently designed in the frequency domain, and on the hypothesis of linearity. Therefore, they work well if this hypothesis is close to the actual behaviour of the system. If this is not the case, performance is likely to be poor. The actual response of a PID-controlled system depends on how close the linear model represents the actual behaviour of the real system. The major sources of uncertainty are due to parameter changes, unmodelled dynamics, time delays, changes in the operating point, sensor noise and unpredicted disturbance inputs. Although a PID controller is not supposed to perform well in conditions different from those for which it has been designed, its performance can be optimised using a robust design approach or by including an additional adaptive loop. In this way, it can be made to exhibit the desired performance over a larger range. A controller is said to be robust if it has low sensitivities, is stable and continues to meet its nominal specification over a typical range of parameter



variations. A robust control design is one that satisfactorily meets its control specification, even in the presence of parameter uncertainties and other modelling errors.

The design of a PID controller entails the choice of the proportional, integral and derivative gains. More generally the design of the controller transfer function entails defining its static gain, and its poles and zeroes. Classical linear control system theory offers a number of tools for controller design and stability analysis of the closed-loop response, such as the root locus, Bode and Nyquist diagrams etc., as well as several design criteria. The desirable features of a robust design in the frequency domain are the largest possible bandwidth and the largest possible loop gain, attained primarily in the controller and in the forward path transfer functions (in this way the disturbance rejection is increased). (Choi and Han, 2012)

### **1.5.2 Groundhook Controller**

Very few studies have been devoted to the possible improvement of road-holding, using a suspension actuator. Indeed, the usual main issue in suspension control is ride comfort for which such “actuators” have been considered. In recent years, studies on global chassis control have emphasized that the suspension system may also help in obtaining better road-holding and even handling. The Groundhook approach, which is in some sense the dual of the Skyhook one, is described below. It consists in increasing the damping, then reducing the deflection, to reduce the road-tire forces. As in the Skyhook case, the ideal Groundhook cannot be achieved and needs to be approximated.

This logic aims at reducing dynamic tyre force, thus improving handling and at the same time reducing road damage (particularly useful in the case of heavy vehicles). Like skyhook, the Groundhook damper is supposed to be hooked to a fixed point, in this case the ground.

### **1.5.3 Skyhook controller**

Skyhook controller is simple but very effective control algorithm. It is well known that the logic of the skyhook controller is easy to implement in the real field. The principle of this approach is to design an active suspension control so that the

chassis is “linked” to the sky in order to reduce the vertical oscillations of the chassis and the axle independently of each other. Thus, a fictitious damper is considered between the sprung mass and the sky frame, as shown in Figure 1.13. (Choi and Han, 2012).

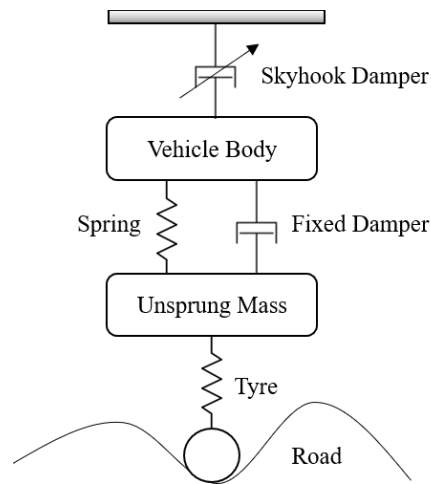


Figure 1.13 Scheme of the skyhook controller (El- Kafafy et al. (2012))

The desired damping force is set by

$$u = C_{sky} z_s \quad (1.16)$$

Where,  $C_{sky}$  is the control gain, which physically indicates the damping coefficient. (Gołdasz and Sapinski 2015)

#### 1.5.4 Fuzzy logic control

Bellman and Zadeh, (1970), observed that unlike computers, the human decision making includes a range of possibilities between YES and NO. Fuzzy Logic (FL) is a method of reasoning that resembles human reasoning. The approach of FL imitates the way of decision making in humans that involves all intermediate possibilities between digital values ‘Yes’ and ‘No’. The conventional logic block that a computer can understand takes precise input and produces a definite output as ‘True’ or ‘False’, which is equivalent to human’s ‘Yes’ or ‘No’.

The fuzzy logic works on the levels of possibilities of input to achieve the definite output. It can be implemented in systems with various sizes and capabilities

ranging from small micro-controllers to large, networked, workstation-based control systems. It can be implemented in hardware, software, or a combination of both.

It has four main parts as shown in Figure 1.14 –

- a) Fuzzification Module – It transforms the system inputs, which are crisp numbers, into fuzzy sets. It splits the input signal into different steps such as LP when  $x$  is Large Positive, MP when  $x$  is Medium Positive, S when  $x$  is Small, MN when  $x$  is Medium Negative, LN when  $x$  is Large Negative
- b) Knowledge Base – It stores IF-THEN rules provided by experts.
- c) Inference Engine – It simulates the human reasoning process by making fuzzy inference on the inputs and IF-THEN rules.
- d) Defuzzification Module – It transforms the fuzzy set obtained by the inference engine into a crisp value.

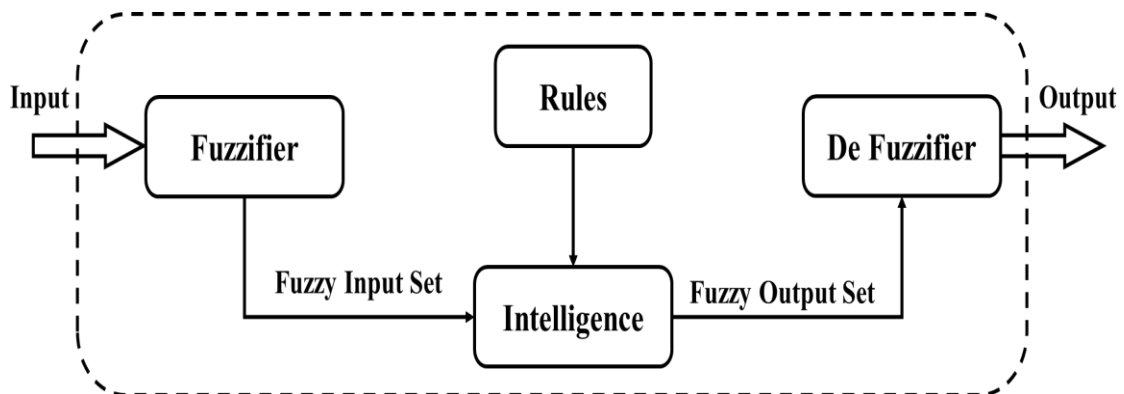


Figure 1.14 Fuzzy control schematic (Bellman and Zadeh, (1970))

### 1.5.5 Sliding mode control

Sliding mode control is variable structure control system (VSCS), which is characterized by a discontinuous feedback control structure that switches as the system crosses certain manifold in the state space to force the system state to reach, and subsequently to remain on a specified surface within the state space called sliding surface (Choi and Han, 2012). In order to guarantee control robustness of the control system featuring an MR device, a robust controller needs to be implemented to take account for system uncertainties. A sliding mode controller (SMC), also called a variable structure controller, is well known as one of the most attractive and robust

controls against system uncertainties and external disturbances. SMC control, in detail with respect to the specific application has been put forth in the upcoming chapters.

## **1.6 ORGANIZATION OF THE THESIS**

The entire thesis in short consists of the design modeling simulation control and real-time implementation of the MR damper in vehicular suspension. The thesis is thus categorised into chapters and briefing of each chapter is specified below.

**Chapter 1 Introduction:** Consists of the basics of suspension, types of suspension, smart materials and its applications (dampers) along with the organization of the thesis.

**Chapter 2 Literature Review:** This chapter presents a review of design, fabrication, modelling, simulation and real-time implementation of MR dampers in multiple applications along with Vehicular applications followed by research gap and the objectives for the entire study performed.

**Chapter 3 Design and Analysis of Axial flux two-wheeler MR Damper:** The chapter provides the design and fabrication of axial flux piston-based MR damper for two-wheeler light motor vehicle followed by its characterization. The chapter also deals with the modelling of the axial flux damper using kwok model and analysis of the damper when associated with the quarter car and two-wheeler mathematical model with PID control. Real time control of the two-wheeler vehicle (Splendor plus) employing the fabricated MR damper is analysed for the sprung mass acceleration reduction (body vibrations).

**Chapter 4 Design and Analysis of Radial flux two-wheeler MR Damper:** The chapter provides the design and fabrication of radial flux piston-based MR damper for two-wheeler light motor vehicle followed by its characterization. The chapter also deals with the modelling of the radial flux damper using polynomial model and analysis of the damper when associated with the two-wheeler mathematical model with sliding mode control. Real time control of the two-wheeler vehicle employing the fabricated radial flux damper is analysed for the sprung mass acceleration reduction (body vibrations).

**Chapter 5 Comparison and Analysis of Axial and Radial flux MR Damper for E-bicycle:** The chapter provides the design and fabrication of both axial and radial flux piston-based MR damper for e-bicycle followed by its characterization. based on the obtained results better design is selected and further proceeded for modelling and analysis of the quarter car and two-wheeler mathematical model employing the damper with sliding mode control. Real time control of the e-bicycle employing the fabricated axial flux damper is analysed for the sprung mass acceleration reduction.

**Chapter 6 Hybrid Radial Flux Piston based Magneto-Rheological Dampers:** This chapter provides the basic description and analysis of a new hybrid radial flux piston - based MR damper follower by its fabrication and characterization. The chapter also deals with the modelling of the hybrid radial flux damper using polynomial model and analysis of the damper when associated with the quarter car and two-wheeler mathematical model using sliding mode control.

**Chapter 7 Summary and Conclusion:** Consists of the conclusion part of the entire thesis which discusses the aspects of the designed MR damper(s) with the workflow of characterization modelling simulation and control and concluding with the real time implementation of MR damper(s) in vehicular suspension.



## **CHAPTER 2**

### **LITERATURE REVIEW**

#### **2.1 INTRODUCTION**

Many researchers have contributed to the growth of the field of semiactive suspension system in different categories like design, modelling, control, simulation etc. Most of the research performed on the magneto rheological applications are a combination of modelling a device, its characterization and its control. As this work concentrates on the improvement of MR dampers and its vehicular applications, most of the literature considered is on the MR dampers with varied designs, modelling and simulation of the damper systems in automotive applications. A few of the literature are stated below categorised based on the design variation and control implementation.

Rabinow (1948) can be considered as the father of magneto-rheological fluid and its applications as he was the first one to illustrate its application in a magnetic fluid clutch. He described MR fluid as a suspension of magnetizable particles in a liquid of low viscosity. When a magnetic field is applied to this fluid, the particles align with the magnetic flux lines forming chain like structures, resulting in increased resistance to flow and higher shear stress in yielding. Ahmadian (2017) studied the application of MR damper to increase automotive ride comfort and stability. With the help of previous studies, it was established that MR damper suspensions provide a definite advantage in performance when compared to passive suspensions. MR damper suspensions were shown to provide better compromise between the vehicle ride comfort and handling.

#### **2.2 RHEOLOGICAL STUDY**

While most of the research work available in the literature made use of commercially available MR fluid which are proprietary in nature, the present work uses an in-house prepared MR fluid whose composition is definitely known. It is an added advantage that it is also more economical. Moreover, instead of relying on material

specifications and technical data provided by the commercial MR fluid manufacturer, the MR fluid used in the present work was characterized experimentally in a rheometer. Bossis et al. (2002) carried out analysis on basic phenomenon of interparticle magnetic and hydrodynamic forces and an analytical prediction for yield stress, rheology with hysteresis and shear induced phase was also provided.

Gong et al. (2005) studied the dynamic properties, viscoelastic properties and microstructure of MR elastomers by changing the percentage amount of each component by weight in the fluid. In the first case, the weight of iron particles was kept constant and the weight of the silicon oil was changed and in the second case, vice versa. Jiang et al. (2011) developed a type of dimorphic MR fluid by adding Fe nanowires into conventional MR fluids. It was observed that in ON state, there was tremendous increase in shear yield stress and concluded that this might be the result of increased solid friction between the magnetic particles due to formation of complex networks. Kamble and Kolekar (2014) used silicon as carrier fluid with different amounts of iron carbonyl particles to synthesize a new MR fluid and studied its rheological properties. A plate and cone type rheometer was used to determine shear stress, shear strain rate, viscosity and shear modulus. Kumbhar and Patil (2014) tried to determine selection criteria for components of MR fluid and concluded that mineral oils were not fit to be used because of their sudden response to temperature change and also that the carbonyl iron particles were best suited for this use because of their nature to eliminate the shape anisotropy.

Kciuk and Turczyn (2009) studied the flow behaviour of MR fluid carrying iron Carbonyl particles under the influence of magnetic field and also tried to reduce the sedimentation of Carbonyl particles by adding fumed silica particles. Park et al. (2010) made use of single walled nanotubes in conventional MR fluid to solve the sedimentation problem and studied its effect on dynamic yield strength and magnetic field strength using the quoted universal equation. Hato et al. (2011) tried suspending submicron sized organoclay particles in the CI suspension to study its effect on rheological properties of the resulting fluid. It was found that presence of organoclay particles improved the dispersion stability of the MR fluid in solid like state. Upadhyay et al. (2013) used flakes of pure iron as the dispersed phase of the MR fluid with an intention to reduce the sedimentation rate. An increase in storage modulus and elastic



modulus was observed and it was predicted that this was due to field dependent solid friction between the particles. Aruna et al. (2019) performed a study to improve the sedimentation properties of carbonyl iron particles-based MR fluid. In particular, they studied the effect of adding different combinations of clay with additives to the MR fluid, during synthesis. It was demonstrated that the synthesized MR fluid was more cost effective and had better sedimentation properties when compared to commercially available MR fluid.

### **2.3 MATHEMATICAL MODELLING OF MR FLUID DAMPERS**

Zhang et al. (2021) reviewed the different mathematical models used to model MR damper divided into three main groups, pseudo static models, parametric models, and nonparametric models. Eshkabilov (2016) compared the force verses velocity and force verses displacement characteristic obtained by modelling the MR damper using different parametric models: Bingham model, Dahl model, LuGre model, Bouc-Wen models. Ambhore et al. (2013) presented the non-linear hysteric behaviour of magnetorheological damper in terms of force-velocity relationship using Bouc-Wen model and Modified Bouc-Wen model. To obtain the model that effectively predict the MR damper's damping force.

Meng and Zhou (2019) presented modelling and control of MR damper for semiactive vehicle suspension. The work presented the use of *hyperbolic tangent model* to characterise MR damper and then model was integrated with quarter car model with improved fuzzy control algorithm. The simulation results showed that the improved fuzzy controller enhanced the riding comfort when compared to passive suspension and greater adaptability under random road excitation. Results compare the fully active, ideal semi-active and conventional passive suspension. Simulation results, for the designed controller, show that with the controllable MR damper has a significant improvement for the vehicle road holding then its lateral stability as well as road damage in comparison with passive, fully active and ideal semi-active suspension systems Peng et al. (2014) has used Bingham model. Sapiński (2003) in his work has presented various non parametric models like polynomial model, fuzzy logic method and neural network model to model MR dampers. Chang and Zhou (2002) has used

neural network based non parametric model which takes 6 input neurons, twelve hidden neurons and one output neuron.

Du et al. (2006) represented the MR damper using evolving RBF networks based non parametric modelling, which takes four input neurons, fifty hidden neurons and an output neuron to represent the force-velocity and force-displacement characteristics of the MR damper. Simon et al. (2001) used the homogenization theory to study the effective magnetic behaviour of MR composite and employ a mathematical model for the same. Sunil and Jain (2009) used curve fitting method to determine coefficients of equations evaluated for fluid models of MR polishing fluids prepared by using different constituents of fluid models. Lv et al. (2021) presented a systematic review of the MR damper modelling techniques covering wide range of both parametric and non-parametric models.

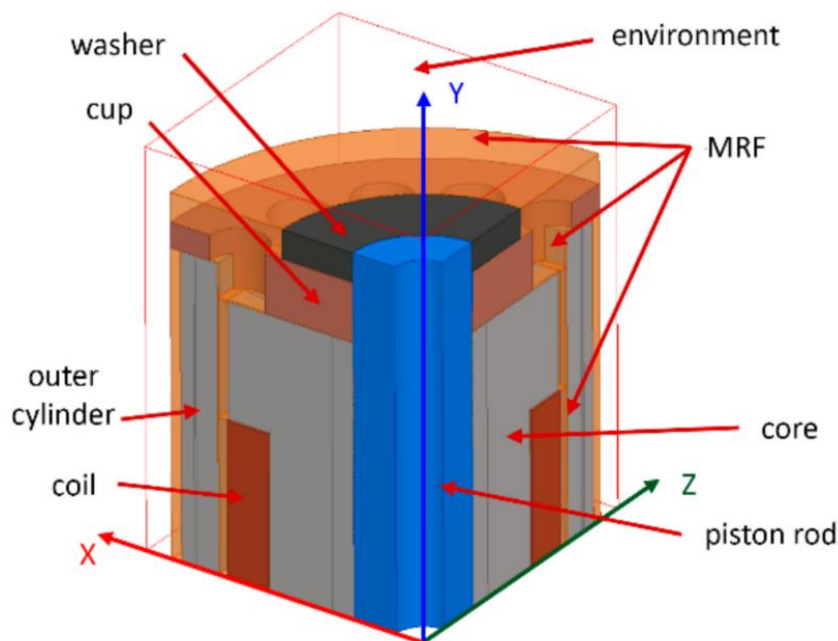


Figure 2.1 Cross sectional view of axial design (Strecker et al. (2021))

Strecker et al. (2021) have experimented and simulated different materials and suitable techniques in designing a fast activating MR damper. One of the main objectives of the study was to achieve the smallest time response using the material considered and the shape of the damper piston. The designed damper provided an innovative approach with the laminations on the inner periphery of the damper, creating a radial reduction in the eddy currents formed within the piston. The damper materials simulated for analysis were ferrite N87, vacoflux 50,

stainless steel 420A, cutting Steel, sintex SMC etc the obtained designs with ferrite N87 and sintex SMC were providing response less than 2.5 ms. Cortes et al. (2005) characterized MR damper based on fluid properties such as applied current and damper design parameters. Force, velocity and displacement were determined using load cell and Shimadzu system.

A numerical simulation of the suspension system was also conducted using ADAMS software. Hemanth et al. (2014) carried out magneto-static analysis of MR damper using ANSYS and found that in a single coil arrangement, magnetic saturation was observed for a supply of 0.7 A of current, which was also observed in the force vs velocity plot. A quarter car model was developed in MATLAB Simulink and was tested with both passive and semi-active dampers. It was concluded that the semi-active suspension system performed better than the passive one. A statistical model was developed by Shivaram and Gangadharan (2007) using design of experiments taking into consideration various factors that affect the performance of the MR damper such as magnetic field strength, volume fraction of the magnetic particle, shearing gap between piston and cylinder, amplitude and frequency of vibration. Guan et al. (2011) derived not only differential equations to represent the physical MR damper using the friction element, viscous element and spring element but also expression to determine the width of the hysteresis. Kim et al. (2017) used permanent magnet instead of electromagnet to activate the MR damper. The magnetic flux is controlled by the shape of the housing cylinder and the piston. Ferromagnetic housing cylinder of four different types are used to carry out analytical study with FEA. A prototype MR damper was fabricated using the triangular configuration and it was demonstrated that the force developed by the MR damper can be controlled by the position of the permanent magnet attached to the piston or by the shape of cylinder housing. Gurubasavaraju et al. (2018) used magnetostatic analysis to study the effect of choosing different materials for fabrication of MR damper on the strength of the magnetic field developed. It was found that low carbon steel and magnetic steel are ideal for piston head as they have high magnetic permeability resulting in maximum magnetic flux density. This in turn leads to higher damping force upon application of current.

Keshav et al. (2019) developed regression models to predict the density of magnetic flux in MR valve with current and geometric parameters of MR valve as

inputs. For this, they used ANSYS-APDL software and design of experiment (DoE) techniques. These models were further used for geometrical design optimization in MATLAB software.

Prabakar et al. (2013) modelled the MR damper using both Bingham model and modified Bouc-Wen models and obtained the parameters of the models using non-dominated sorting genetic algorithm. The work also obtained the controlled response of quarter car model with semi active suspension with MR damper modelled using above two models using random road profile as the input. Krishnan Unni and Tamilarasan (2018) used COMSOL multi-physics software for designing an MR damper for application in an all-terrain vehicle (ATV). The design was optimized using Taguchi method and DOE software. The aim was to improve the damping force with geometrical constraints so that the damper would fit in the ATV. Verros et al. (2005) presented a method for optimizing damping and stiffness value of quarter car suspension with random excitation as road input. They also studied the effect of road quality as well as other effects related to wheel hop. However, this was only a numerical study and experimental work with a physical damper was not involved.

Rao and Narayanan (2008) implemented a look ahead preview control for the response of a four degree of freedom half car model with semi-active suspension. The vehicle moves with constant velocity on random road surface. The vehicle response is optimized for better road holding, control force and suspension stroke. Prabakar et al. (2009) studied the stationary response of a half car vehicle model moving over rough road with uniform velocity. The control of the suspension using MR dampers is considered. Monte-Carlo simulation was used to verify the control and response of vehicle model obtained using equivalent linearization method.

Sultoni et al. (2014) investigated the performance of a regenerative electromagnetic shock absorber with the help of a quarter car dynamic model. The effect of vehicle acceleration and excitation due to road irregularity were studied using numerical simulations on quarter car model. The power generated by the damper and the RMS value of suspension velocity when the vehicle moves over different classes of road were analysed. Jamali et al. (2017) developed a MATLAB Simulink model to study the dynamic behaviour of a passive suspension system used in an electric vehicle. A two degree of freedom quarter car model was used for the study. Transmissibility

ratio was plotted against frequency of excitation for different values of damping. A match between results of simulation and theoretical calculation showed that the Simulink model was accurate.

Omar et al. (2017) designed and implemented experimental test rigs for quarter car suspensions. Performance of an electro-hydraulic active suspension was compared with passive suspension using both experiments and numerically. A single degree of freedom quarter car model was used. Hemanth et al. (2018) performed dynamic analysis of MR damper-based suspension using half car model. A Bouc-Wen mathematical model was used to predict the force developed by the prototype MR damper. Using the half-car model, the ride comfort and road holding of passive and semi-active suspension with MR damper are compared to show that the performance of the MR damper suspension is better.

Nguyen et al. (2009) presented a design and characterization of MR shock absorber for vehicular suspension system. The work presented finite element analysis of damper piston to obtain the optimal damper design parameters. Bingham model was used to model the damper and a skyhook control was employed to provide the required current input to damper. The results show that the vehicular model provided better suspension when employed with the control logic. Hegale et al. (2020) presented the ride comfort analysis with change in inclination angle of shock absorber of two-wheeler vehicle by considering a commercial viscous damper of two-wheeler vehicle.

Ericksen and Gordaninejad (2000) presented a theoretical model for damping force of a magneto-rheological fluid (MRF) shock absorber of an off-road motorcycle. The theoretical model was based on Bingham plastic model. FEM analysis was used to study the magnetic field distribution with input current. The theoretical model was evaluated by comparing it with experimental results. Theoretical and experimental force-displacement curves demonstrated excellent match.

## **2.4 OPTIMIZATION OF PISTON DESIGN AND CONFIGURATION**

Krishna et al. (2017) optimized the electromagnetic circuit of an MR damper to maximize the magnetic flux density. This was done as the force developed by the MR damper is highly influenced by the strength of the magnetic field developed at the fluid

flow gap. Genetic algorithm and design of experiments approach was used for the optimization and the results showed that a fluid flow gap of 1.12 mm was optimum.

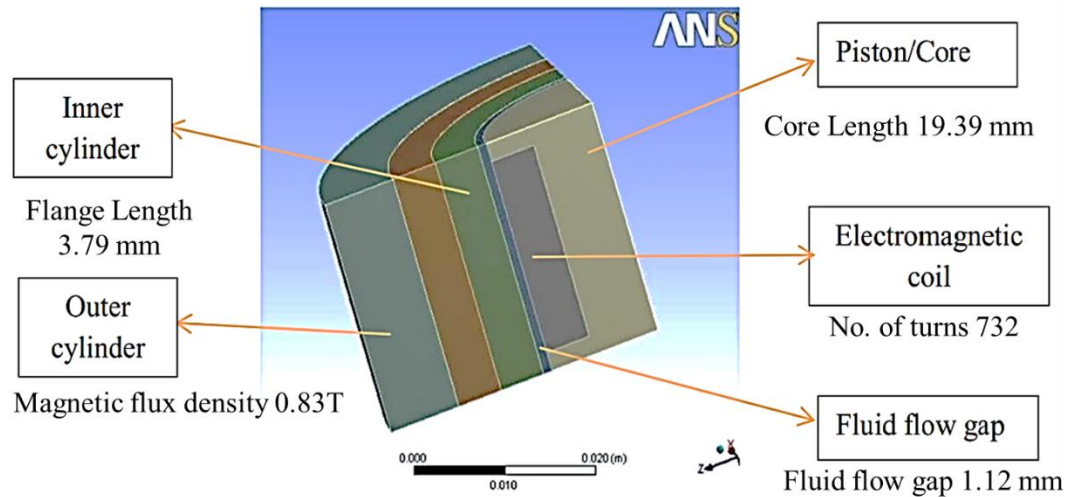


Figure 2.2 Optimized design of axial flux MR damper (Krishna et al. (2017))

Rahman et al. (2017) reviewed recent advances in MR damper technology and presented various applications of MR dampers and optimization methods for designing MR dampers. Different configurations for fabricating MR dampers were explored and an overview of different MR damper models were presented. Namuduri et al (2001) have designed and fabricated an MR damper which has concentric flow gaps formed between the mounted flux rings in the core of the piston. The patent states the multiple annular flow gap makes the design an optimized piston for the linearity in the obtained damping force.

Cheng et al. (2018) presented a novel MR damper, which had a meandering magnetic path in the piston so as to improve the performance of the damper. By using materials of different magnetic properties, the magnetic flux was guided to obtain a much higher controllable force when compared to traditional MR damper. Manjeet and Sujatha (2018) performed optimization of MR valve using Herschel-Bulkley (HB) model of MR fluid. Multi objective minimization was done with an aim to improve the dynamic range and reduce the inductive time constant of the MR damper. Care was taken to see that the magnetic flux density does not reach the saturation limit of the materials used in the MR valve. Genetic algorithm was used for the optimization and

Pareto fronts were found in MATLAB environment. However, experimental validation of the optimization results was not discussed in the article.

Georgiou et al. (2007) performed multi-objective optimization of semi-active and passive suspension systems with the help of two degrees of freedom quarter car models. Optimum values of spring stiffness and damping coefficient were selected for suspension subjected to road excitation. Suitable methodologies were used to capture the dynamics of the vehicle when it moves with constant speed over roads with geometric irregularity. The aim was to improve the vehicle ride comfort, road holding and suspension travel.

Chi et al. (2008) performed comparative study of three optimization algorithms for optimizing vehicle suspension design using a quarter vehicle model. With the help of numerical simulation, it was shown that the suspension design can be improved significantly by optimizing the design variables. Investigations were also done on how vehicle velocity and road irregularity affect the design variables to get better ride quality. Liu et al. (2019) proposed and applied general theory of skyhook control strategy to semi active suspension system of vehicle. The work employed adaptive fish swarm algorithm to optimise the control parameters. The results indicate that the proposed control strategy has superior performance over the traditional skyhook control and passive suspension system. Simulation study of MR damper for bump road profile.

Considering the Amperes law and Gauss laws an axial flux MR damper with a magnetic circuit has been designed for the implementation of the MR damper piston by Guo et al (2018). The designed circuital model considers the magnetic saturation, hysteresis and eddy currents formed with in the damper. As per the results of the FEM analysis, the model was able to predict the magnetic saturations, eddy currents and the hysteresis effect in the designed piston. A model was designed to combine bingham model of fluid with the designed magnetic circuit. The produced magnetic field lags the damping force in case of low frequency varying magnetic field and increases with increase in the frequency of the magnetic field.

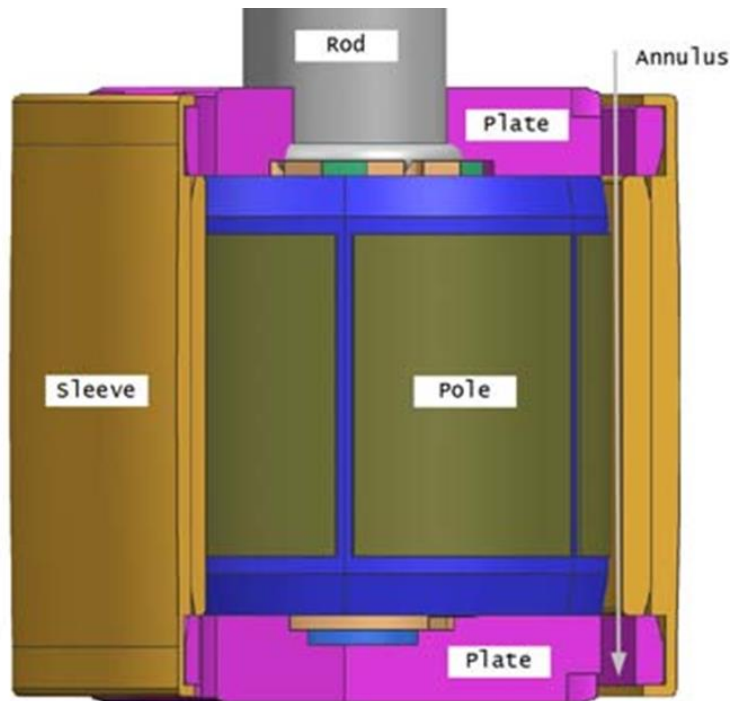


Figure 2.3 Radial flux design (side view) (Goldasz (2013))

Goldasz (2013) designed a radial flux-based design with 6 poles excited with alternate poles so as to generate a flux with high magnetic permeable area ratio and analysed the piston behaviour in terms of the magnetic field generated considering 36 turns per pole with 24 AWG winding with the current ratings touching up to 5A.

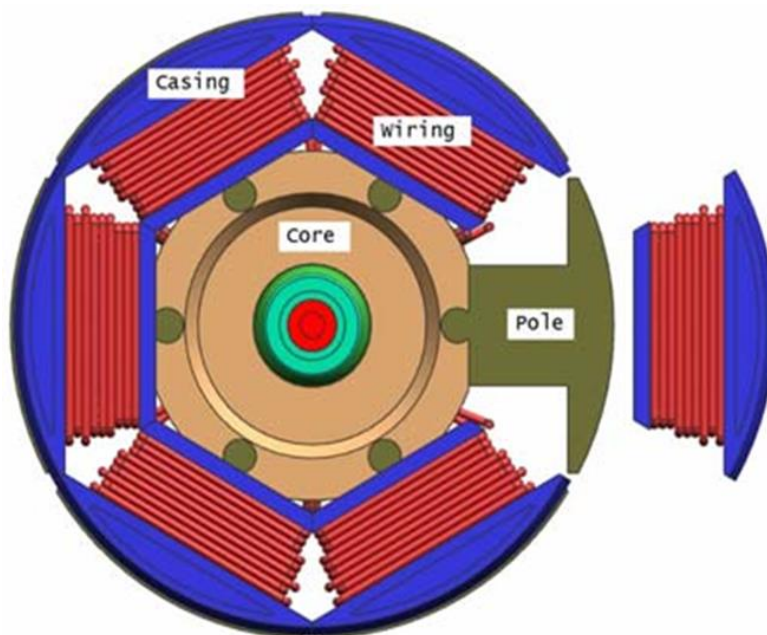


Figure 2.4 Radial flux design (top view) (Goldasz (2013))



The core was assumed to be made of laminations with 1mm thickness so as to reduce the effect of eddy currents on the generated magnetic flux density.

Seid et al. (2019) used the conventional mono tube damper structure to analyse the performance indices which includes damping ratio, power consumption, damping range, force etc. Desai et al. (2019) have designed a conventional twin tube damper to replace the passive damper that provides constant damping force with all displacements in the passenger van to control the damping force with displacement.

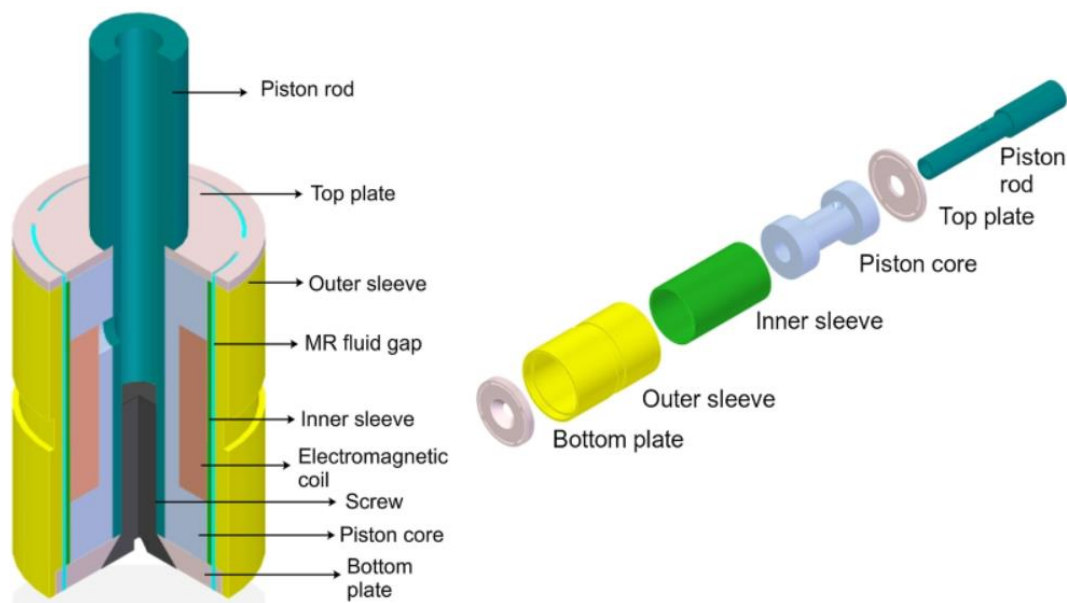


Figure 2.5 Design of twin tube damper (Desai et al. (2019))

## 2.5 DESIGN BASED ON ELECTROMAGNETIC PISTON

Goldasz (2019) has designed a piston with similar poles and two annular gaps in the piston with the holding sleeve in between. The study shows the dual gap MR piston shows the presence of the valve reduces the magnetic flux flow in the fluid flow gap which creates an accountable change in the damping force in fabricated piston with the consideration. The laminations in the design reduce the eddy current effect providing improved flux flow.

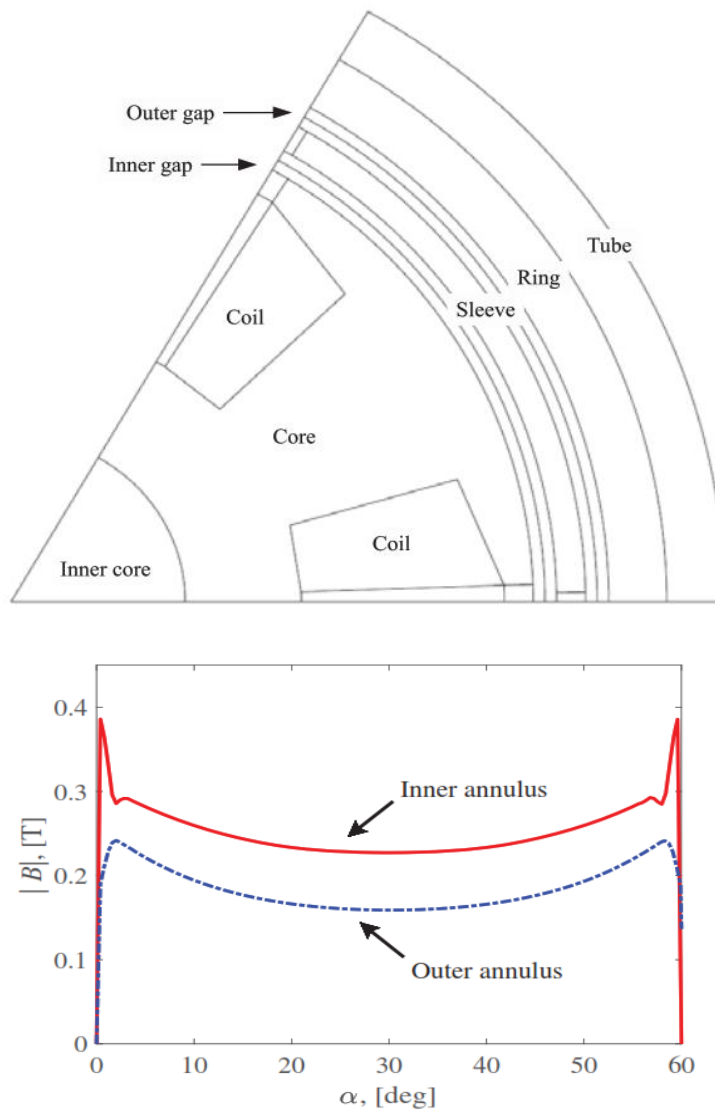


Figure 2.6 Improved radial flux design with both annular gaps (Goldasz (2019))

Oliver et al (2002) patented a design of 8 pole radial flux design consisting of the alternate adjacent poles with the coil drawn between the poles from the centre of the piston through the bottom end of the piston to the pole coils. However, the patent design states only about the damper design and does not state any other detail regarding its fem analysis or the characteristics of the designed MR damper.

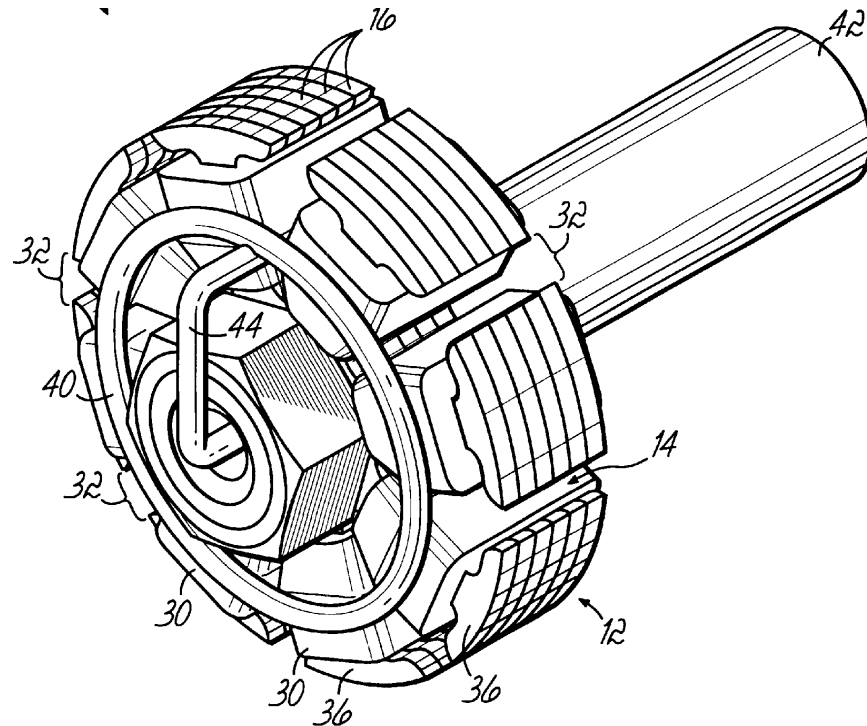


Figure 2.7 8-pole radial flux design (Oliver et al (2002))

Nehl et al (2012) designed a simple MR damper with an axial flux design where the coil wound space was the novelty in the design. The coil spacing was coaxially aligned with the central longitudinal axis, thus, making certain part of the coil buried under the piston pole. The patent also discusses about the differential multipole axial design with similar coil packing assembly.

Goldasz et al (2005) has patented a high-performance piston design in which the core consists of two piston cylinders. The design specifies the magnetic coupling of the first and the second cylinder with the piston centre longitudinally disposed. The piston center was made of high-performance magnetic materials such as Silicon Steel (SiFe), Cobalt Steel (CoFe), Vanadium steel etc. Jaehwan and Kyoung-Mi (2004) analysed the effect of magnetic field on MR fluid in high frequency range to explore the applications of smart structures. They also investigated the effect of magnetic field applied orthogonally and parallel to the direction of wave propagation.

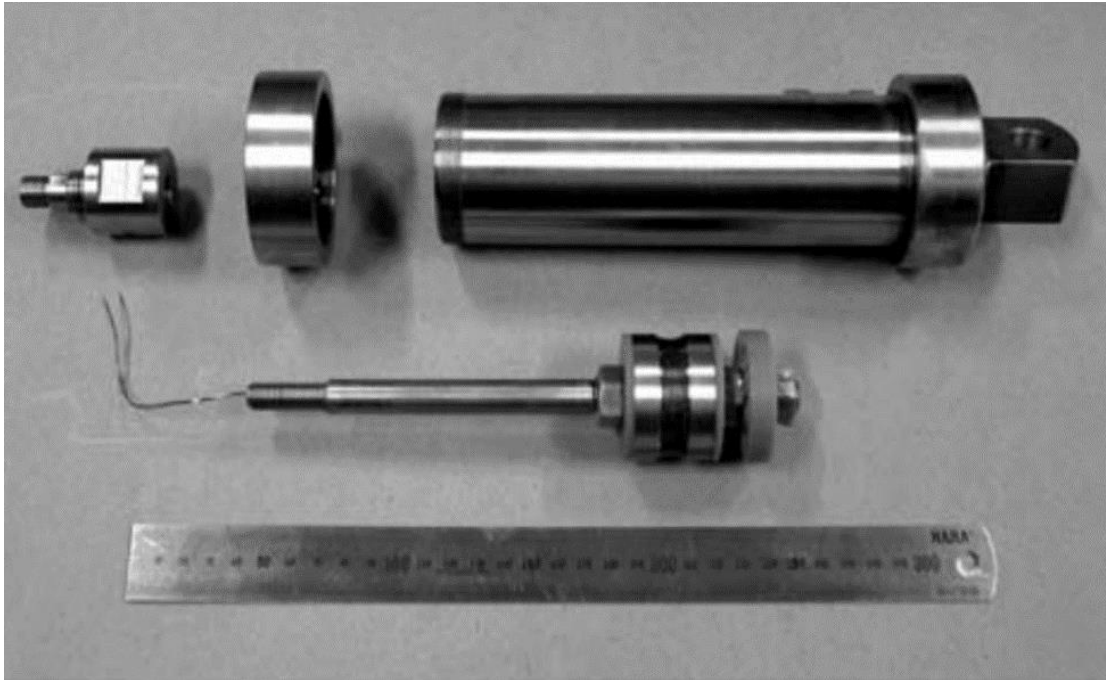


Figure 2.8 Dis-assembled view of axial flux MR damper (Nam and Park (2009))

Nam and Park (2009) proposed a design methodology for a better performing electromagnetic circuit of the MR damper. The aim was to improve the static and dynamic characteristics of the MR damper by reducing the magnetic flux path and increasing the reluctance of the magnetic circuit.

Shiao et al. (2013) proposed a new piston design consisting of multi-pole magnetic core and special polarization causing almost all the magnetic flux to penetrate orthogonally in MR fluid gap, thus increasing the MRF chaining area significantly and it was found that the MR damper with this piston design performed very well compared to the conventional design. Goldsaz (2013) also proposed a new design similar to the one discussed previously. This particular design has radially projecting arms made out of a stacked silicon steel lamination. The advantage of this design was to disturb the formation of eddy currents during the transient response of the device. Another design was given by Imaduddin et al. (2013) with multiple radial and annular gap in order to increase the pressure drop of the MR valve without increasing the size and it was found that the size of outer annular gap zone contributes to viscous pressure drop and radial gap size contributes to pressure drop due to magnetic field

## **2.6 DESIGN BASED ON FLOW VALVES**

Lopez et al (2013) have patented an axial flux-based design consisting of a radial inner surface flow passage. The design shows multiple passages and the flux flows from the centre of the piston through the fluid flow gap into the piston cylinder and through the fluid flow gap returns back to the piston centre. Wang et al. (2009) proposed an MR damper that increases the effective damping length where the flux was perpendicular to fluid flow. This was done by using both annular and radial flow paths. This increase in effective damping length improved the damping force to large extent.

Boese et al. (2010) has designed an MR damper with fail safe behaviour. The design used two permanent magnets apart from conventional magnetic circuit. This improved the minimum damping force in the absence of electric input. The design also improved the dynamic range of damping force. This design used both annular flow and radial flow to improve the active length and thus the damping force.

Hu et al. (2016) designed an MR damper with inner, middle and outer channels that were serially connected through fluid flow. The design improved the active length by about 3 times the conventional damper thus improved the damping force for same current. Zhang et al. (2006) studied the importance of energy dissipated and controllable force as performance parameters in MR damper. It was concluded that both were closely related to magnetic flux density that can be reached in MR fluid flow gap.

## **2.7 CURRENT CONTROLLER**

Yerrawar and Arakerimath (2017) presented a methodology to implement semi active suspension using MR damper. A current controller was developed to vary the current between 0.1 A and 1 A. Ride comfort was optimized with the help of design of experiments (DOE) and Taguchi method. Relationships between the suspension parameters and their effect on ride comfort is studied with the help of a quarter car test rig. Ata and Salem (2017) performed a theoretical study to find a suitable semi-active control strategy for tracked vehicle MR damper suspension. A suspension model of the tracked vehicle with MR damper, having seven degrees of freedom, was developed to compare performance of three different controllers. Different vehicle speeds over bump

and sinusoidal road profiles are simulated and the results are compared with a typical passive suspension in time and frequency domains. The results showed a marked improvement in performance of MR damper based semi-active suspension. Morales et al. (2018) studied semi-active suspension which employed pneumatic spring of variable stiffness and MR dampers with variable damping to increase vehicle ride comfort and handling when compared to passive suspension. Vehicle velocity and road information gathered using GPS system were used to control the semi-active suspension resulting in 30% improvement in ride comfort and maintaining same roll angle as a comparable passive suspension.

## **2.8 CONTROL STRATEGY AND CONTROL ALGORITHM**

Salem and Aly (2009) compared fuzzy control and PID control for active suspension using a two degree of freedom quarter car suspension model in MATLAB simulations. The application of fuzzy logic technique for a continuously variable damping suspension system was illustrated and the vehicle response for a range of input road conditions were studied. Havelka and Musil (2012) studied optimal preview control strategy with MR damper-based quarter car model using sensor data of approaching road disturbances. MR damper was represented by a non-linear hysteretic model and the effect of tyre lift was studied.

Park et al. (2016) used a quarter car model to compare the performance of two different designs of MR damper. A skyhook controller was used for semi-active suspension and simulations were carried out for two different road profiles, bump and random road excitations. One of the MR dampers had a bypass hole provided in the piston to reduce the slope of pre-yield damping force. The damping force characteristics are studied using both numerical simulations and experiments. The results showed that the MR damper with bypass holes provide better ride comfort.

Hu et al. (2017) used a hyperbolic tangent model to represent the nonlinear damping of MR damper. Using this model, a quarter car model with MR damper was established and a new hybrid fuzzy PID controller was developed to improve the performance of the semi-active suspension. Results of the numerical simulation showed that sprung mass acceleration, tyre displacement and damper deflection can be reduced

effectively under sinusoidal excitation from road. Jamadar et al. (2020) presented the dynamic analysis of quarter car model with semi active suspension. Analysis was done using commercially available magnetorheological damper. The presented work employed skyhook control and PID control.

Chen (2009) presented a two degree of freedom dynamic model of vehicular suspension system in MATLAB/SIMULINK and implemented a skyhook surface sliding mode control to it. The results show that the ride comfort of vehicle was improved with the implementation of control logic into the suspension model. Hudha et al. (2005) presented an investigation of performance effectiveness of modified skyhook, modified ground hook and modified hybrid skyhook-ground hook control strategies by applying these strategies to MR damper. Damper was modelled using non parametric model and integrated with the quarter car model. Ahmadian et al. (2008) presented a study to evaluate the performance of magnetorheological front fork suspension system for motorcycle. MR damper with skyhook control is used in front suspension system to provide better handling and rider comfort compared to conventional motorcycle suspension. The damper was tested and the test rig showed that the MR damper was more adaptable to road disturbance. The damper was implemented in the motorcycle and on road testing was done to evaluate its performance for different velocities and suspension settings.

El-kafafy et al. (2012) studied the performance of MR fluid damper for improving automotive ride comfort with use of Bouc Wen model and implementing it in quarter car model. The sliding mode control was used to control damping force of MR damper. The model was tested on two excitations, the first is a road hump with severe peak amplitude and the second is a statistical random road.

Rajendiran et al. (2017) studied the performance of the quarter car with single and dual actuators considering the driver model for the seat suspension. Fuzzy sliding mode control was implemented for active suspension and also compared with a unique fractional order sliding mode controller.

Chen et al. (2011) simulated a Macpherson strut based semi active suspension considering the nonlinearity of the entire system. Sliding mode control was

implemented in the control of the modelled semi active damper and is compared with the passive and constant current states. The SMC control was providing an effective reduction in the body vibrations with respect to the other controls.

Wen et al. (2011) implemented a fuzzy based dynamic sliding mode control for quarter car active suspension system. Takagi-Sugano fuzzy model was used in this process and the results show effective vibration reduction in comparison with similar passive suspension.

## **2.9 APPLICATIONS OF MR DAMPER**

Pavel et al. (2003) studied the flow of MR fluids in packed beds of magnetic and non-magnetic spheres and cylindrical porous media. Jun et al. (2005) evaluated magnetic field response of MR fluid made out of 30% weight of monodisperse magnetic composite (MMC) particle. Spaggiari et al. (2019) reviewed three different types of smart materials, which included MR fluids also. Commercial application of MR fluid in semi-active devices such as dampers, brakes or clutches were examined. The physics behind the working of these smart materials was explained with the help of equations, which would help a designer in an industrial context. Oliver (2003) have designed and fabricated bypass valve included MR damper piston at the damper was designed to be fit between the body of the vehicle and the wheel. The damper was adjustable and the control valve opens at the compression stage of the damper and vice versa there were two passageways in the design and it can be observed that both the flow passages can be controlled independently or combinedly as per the requirement of the application.

Kruckemeyer (2001) designed an improved MR damper which can transition from allowed and peak force at near zero velocity to extreme damping at peak acceptable velocities. The designed damper please actually and axial works damper with a group in the fluid flow path towards the outer cylinder creating a possibility of reduced of state force the patent claims that with the increase in the velocity the damping force obtained can be varied from a critical zero to a maximum permissible limit. Shiao et al. (2015) designed and implemented magnetorheological suspension system as well as a brake for bicycle applications. The damper designed was a



multilayered piston damper and to provide an adaptive damping a linkage mechanism was applied to MR brake in order to obtain better control.

Jastrzebski and Sapinski (2017) evaluated an automotive MR damper under varying mechanical and electrical excitations and studied its force response and energy dissipated. The results of the experiment would help the engineers in designing an energy harvesting device for the MR damper. The effect of amplitude of piston displacement and piston velocity are analysed. Chen et al. (2018) proposed and implemented self-powered magnetorheological damper for motorcycle suspension. The proposed design uses the energy that is obtained from vibration of damper due to road disturbances. It converts vibration energy to electrical energy and which in turn is used to power the MR damper through direct feedback mechanism. The work also presented the results of on road testing of self-powered MR damper with Sachs Madass 125 model motorcycle. Results compared the RMS acceleration of sprung mass with conventional MR damper and self-powered MR damper, it is observed that both peak acceleration and RMS acceleration was reduced in case of self-powered MR damper.

Breese and Gordaninejad (2000) presented the development and evaluation of field-controllable, semi-active magnetorheological fluid (MRF) shock absorbers for a mountain bicycle. The dampers were theoretically modelled and then the two MRF dampers were designed and tested for use in front and rear suspension system of mountain bicycle. The designed dampers emulated the OEM dampers at passive state and the damping force has drastically changed with the application of current to it. Li and Du (2003) presented the design, fabrication and testing of a magnetorheological (MR) steering damper for motorcycles. Three designs were proposed to be employed in steering dampers; the final design was selected using concept scoring matrix. MR damper was fabricated and tested at different values of current inputs.

## **2.10 RESEARCH GAP**

As per the literature review performed on the design and control of semi active and active suspension systems, there are different types of design and control algorithms which serve the purpose. The design of electromagnetic piston depends on

the placement of the piston and the core design. The literature review suggests the design of piston with the coil wound perpendicular to the piston rod which is the axial flux design. The axial flux piston designs with further modifications were presented and designed by the researchers with research on the radial flux design quite seldom.

Sliding mode control, on the other hand, is one of the robust and effective way in dealing the system uncertainties in the case of road nonlinearities as well as the external disturbances. Many researchers have proposed different improvements in this field of control to reduce or eliminate the chattering effect present in the conventional sliding mode controller like observer based sliding mode control, fuzzy sliding mode control, adaptive fuzzy sliding mode control etc. Most of the proposed methods have been introduced and implemented only in the simulation of the system and the actual hardware issues and implementation are not described or discussed. Most of these algorithms rely on the change in the displacement between the unsprung mass and the sprung mass i.e., the displacement in the suspension system which is a difficult task to attain as these sensors are quite difficult to build and even expensive to use in practical applications. Sliding mode control with a proper error consideration and calculating from the accelerometer data can create a better alternative and effective real time control approach to these problems.

## **2.11 OBJECTIVES**

1. To design and develop axial and radial flux MR damper(s) for two-wheeler vehicular applications
2. To design and develop prototype MR damper(s) on e-bicycle with axial and radial flux piston designs.
3. To mathematically model the fabricated MR damper(s) and analyse it in two-wheeler systems using suitable control scheme.
4. To design and develop a novel MR damper with hybrid radial flux piston and its characterization.
5. Real time implementation and testing of developed MR damper with current controller in two-wheeler vehicle(s) using various control strategies.

## **2.12 SCOPE**

The specified objectives require unique research on the specific vehicular constrains for the damper. Also, quite a high-level hardware support is needed to analyse the vibrations in the vehicular body considering the vehicle with the MR damper in off-state and on state conditions. The on-state condition can signify two things i.e., with or without (constant current) any control implementation. Thus, the scope of the research is restricted to the specified works below.

- To conduct finite element analysis studies for symmetric and unsymmetric piston designs in order to understand the magnetic behaviour of the specified piston designs.
- The suspension parameters other than the damper are considered to be linear in the analysis of quarter car and two-wheeler model.
- Simplified mathematical modelling of MR damper is considered such that the complexity of the model does not hamper the execution of the real-time controller.
- Utilisation of damper testing machine for understanding the pulse excitation behaviour of the specified MR damper using a custom-made pulsating circuit.
- To perform real-time vehicular testing by using suspension with MR dampers for various controlled current conditions considering the hardware facilities available in the institution.

## **2.13 METHODOLOGY**

The work projected in this thesis comprises of the design optimization and manufacturing of multiple dampers with control for specific vehicles with different piston designs. The methodology followed in reaching the specified objectives is as shown in figure 2.9. The process involves in designing the prototype dampers considering the space complicity of the vehicle and the dimensional constrains involved in fitting the damper to the vehicle.

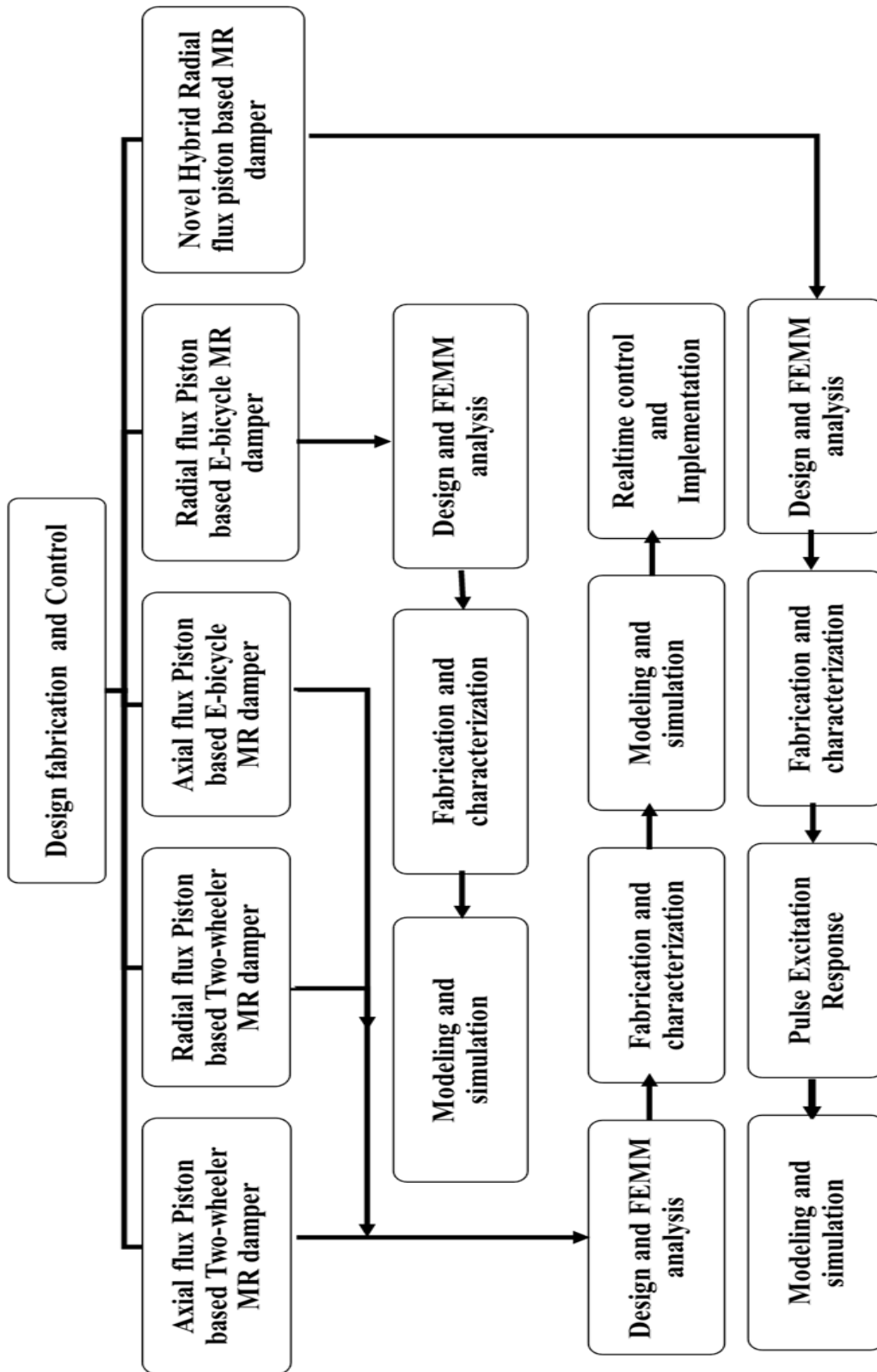


Figure 2.9 Methodology involved in the performed research work

The damper is fabricated and tested for its characteristics and its response in the form of damping force with respect to the change in current. The mathematical modelling of the prototype damper is then obtained using the parametric or non-parametric modeling analysis which is further substituted in the simulation of quarter car and two-wheeler in MATLAB / Simulink and also the modelling is used in the real-time implementation of sliding mode control with the prototype MR damper in two-wheeler vehicles i.e., Splendor plus (make: Hero Motocorp.), Pulsar (make: Bajaj Auto.) and E-bicycle, which is a custom modification of Crest bicycle (make: Atlas cycles ltd.).

## **2.14 SUMMARY**

The chapter briefly describes about the research work of various researchers in the fields of rheology of MR fluids, design, modelling and analysis of MR dampers. The chapter also puts focus on design of current controller and other applications of MR dampers. With the groundwork of the prior specified literature survey, research gaps are found and objectives of the performed research were set. The methodology (work flow) to attain the objectives was manifested and followed.



## **CHAPTER 3**

### **DESIGN AND ANALYSIS OF AXIAL FLUX TWO-WHEELER MR DAMPER**

#### **3.1 INTRODUCTION**

The axial flux flow design piston is basically a solenoid design with two poles at the top and the bottom respectively creating an 'I' section and the flux flow path in the parallel to the piston rod. This flux flow is possible when the coil is wound in the plane perpendicular to the piston rod. The design, fabrication and analysis of the damper with this design is discussed in the sub sections. The fabrication process of this damper piston is quite simple and the solenoid coil winding to the piston is also a simpler process compared to that of the radial flux design.

This chapter gives a complete picture of the axial flux two-wheeler MR damper designed considering the constraints of the two-wheeler vehicle splendor plus. The damper parameters are optimised and analysed for the magnetic flux density generated in the fluid flow gap of the damper. At the time of fabrication, the damper is retrofitted to a commercially available accumulator followed by its characterization.

The characterization results are used in mathematical modelling of the prototype MR damper using the Kwok model. The modelled MR damper is used to analyse the response of quarter car and two-wheeler suspension models using PID controller. The damper is then fitted to actual two-wheeler vehicle and the sprung mass acceleration (body vibrations) are analysed considering a constant current input to the damper from a current controller.

#### **3.2 DESIGN OF AXIAL FLUX TWO-WHEELER MR DAMPER**

An objective of this study is to implement a monotube shear mode MR damper into two-wheeler vehicle. One of the crucial points in designing MR damper is dynamic

range  $D_r$ , which is defined as the ratio of controllable force C.F. to the uncontrollable force U.F.

$$D_r = \frac{C.F.}{U.F.} = \frac{F_\tau}{F_\mu + F_f} \quad (3.1)$$

Where,  $F_\tau$  is the force due to field induced shear,  $F_\mu$  is the force due to viscosity and  $F_f$  is the frictional force. The design procedure in this work is based on maximum damping expected and dynamic range. The field induced shear force and the plastic viscous force can be expressed according to Bingham model (Acharya et al. (2019)) as,

$$F_\mu = \left(1 + \frac{wgV}{2Q}\right) \frac{12\mu QLA_p}{wg^3} \quad (3.2)$$

$$F_\tau = \left(2.07 + \frac{12Q\mu}{12Q\mu + 0.4wg^2\tau_y}\right) \frac{\tau_y p A_p}{g} \text{sgn}(V) \quad (3.3)$$

Where, volumetric flow rate is denoted by  $Q$ , the piston effective cross section is denoted by  $A_p, A_p = \pi(d_p^2 - d^2)/4$ , The diameter of piston rod, relative velocity between cylinder and piston and the pole length, are denoted by  $d, V, p$  respectively.

Considering the entire length of axial pole as  $L$  it can be calculated by  $L = (m + p)$ , where,  $w$  is the average circumference of annular flow path,  $w = \pi(d_p + g)$ ,  $d_p$  is the diameter of piston head,  $\mu$  is the apparent viscosity of MR fluid without magnetic field (off-state),  $\tau_y$  is the yield shear strength of fluid and  $g$  is gap of annular flow path. Frictional force is neglected for the analysis purpose. Figure 3.1 shows the nomenclature of the MR damper piston and its dimensions considered for the equations 3.2 and 3.3. The dynamic range  $D_r$  and the expected force should be kept high for a good MR damper design. Hence, the piston dimensions should be optimized for the required objectives. Piston dimension optimization was subjected to reaching higher damping force of 1kN with dynamic range of at least 2 at operating velocity 0.2 m/s.

Thus, the optimization problem is defined as



$$D_r - \frac{F_\tau}{F_\mu + F_f} = 0 \quad (3.3)(a)$$

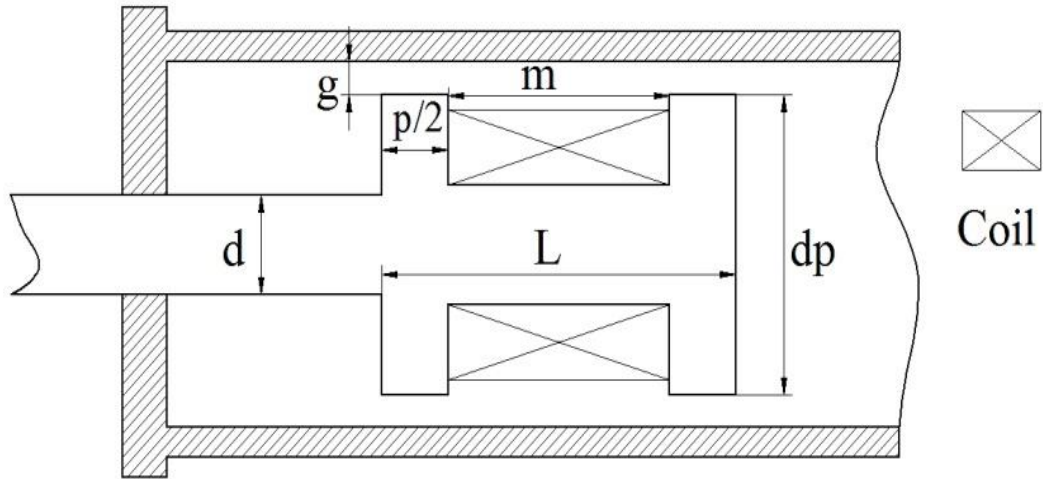


Figure 3.1 Nomenclature of MR damper piston

The variables  $\{d_p, d, p, L, g\}$  were considered as design parameters and dynamic range as objective function. The maximum damping force was taken as constraint. The outer cylinder dimensions were considered as constraints, since it must fit in the vehicle. Fluid properties such as off-state viscosity ( $\mu$ ), induced shear stress ( $\tau_y$ ) of commercially available MR fluid (from Lord corporation) were used in the design. Optimization function ‘fmincon’ from MATLAB optimization tool box was used for the optimization problem. The optimized design parameters of the MR damper are listed in the table 3.1.

Table 3.1 Dimensions of damper piston

Design parameters	Dimensions in mm
Piston head diameter ( $d_p$ )	27.82
Piston rod diameter ( $d$ )	12
Pole length ( $p$ )	8
Total length of axial pole ( $L$ )	44.91
Height of annular flow gap ( $g$ )	0.8

The magnetic analysis of the piston is a prerequisite for the manufacturing as the simulation specifies the approximate flux density obtained with respect to the input current to the coil. This analysis is performed using Finite Element Method Magnetics (FEMM) tool which is an open-source software used for electromagnetic analysis.

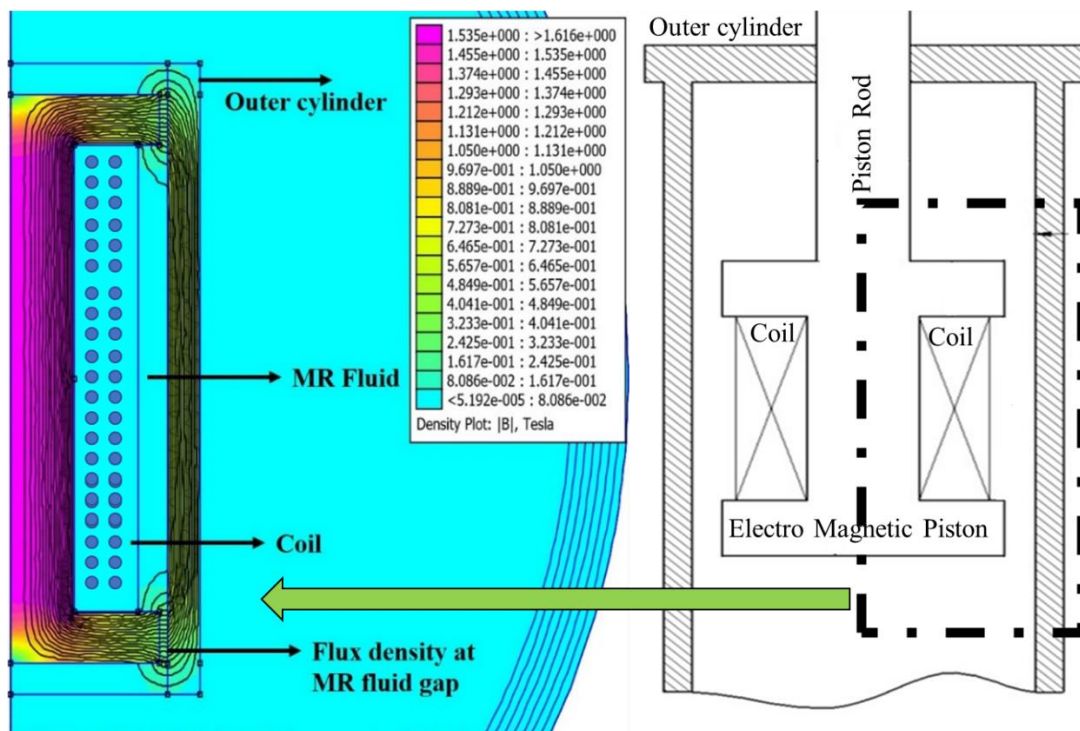


Figure 3.2 FEMM analysis of axial flux two-wheeler MR damper piston

The analysis is performed with respect to the piston dimensions as in table 3.1 and for 1.5A and 200 turns of the coil and by using commercially available MR fluid (from Lord corporation) as the operating fluid. The analysis shows a magnetic flux density of 0.307T in the fluid flow gap adjacent to the poles. The simulation result of the FEMM tool is shown in figure 3.2.

AISI 1018 steel was utilized in the fabrication of MR damper, which is known for good magnetic permeability. The piston was wound with AWG 26 copper wire for about 190 turns for producing electromagnetic effect. The fabricated MR damper for two-wheeler application is shown in figure 3.3. A commercial MR fluid from Lord Corporation (MRF 132 DG) was used in the damper for characterization and on road testing.

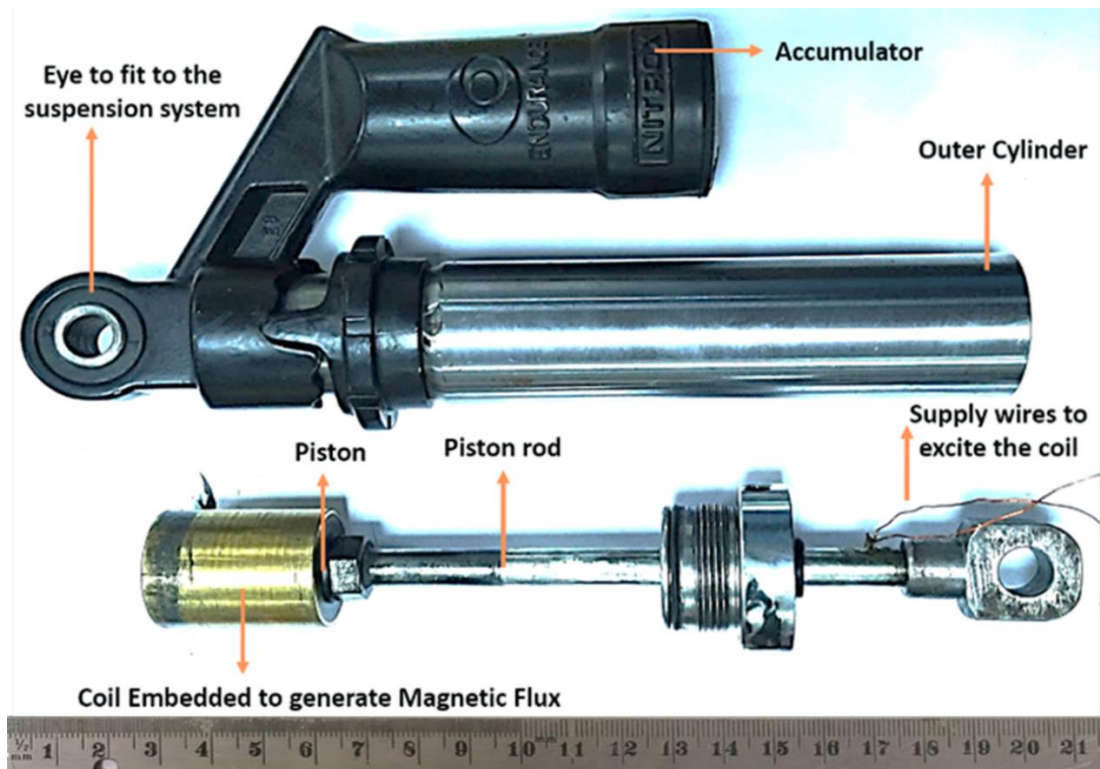


Figure 3.3 Developed axial flux two-wheeler MR damper

### 3.3 AXIAL FLUX TWO-WHEELER MR DAMPER CHARACTERIZATION

The designed MR damper was tested in the damper testing machine (DTM) to explore the dynamic characteristic of the damper in terms of force versus displacement curves. The DTM (Make: HEICO Ltd.) comprises of hydraulic actuator and is capable to generate a force of  $\pm 20$  kN at peak velocity of 1.2 m/s. The DTM is aided with linear position transducer for measuring displacement and load cell for force measurement. Required input signal is sent through and the experimental data is fetched from MOOG control unit which acts as data acquisition unit too. The set-up of DTM is shown in figure 3.4.

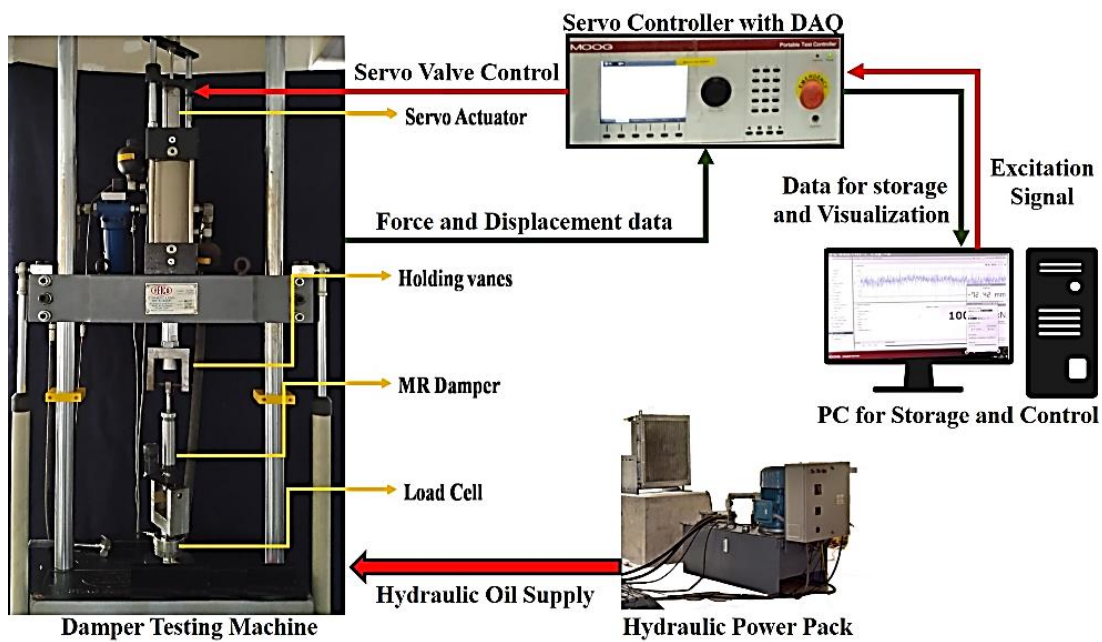
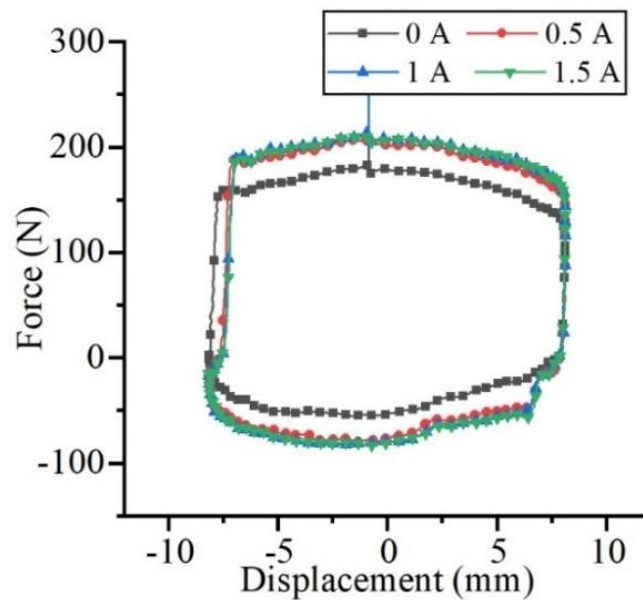
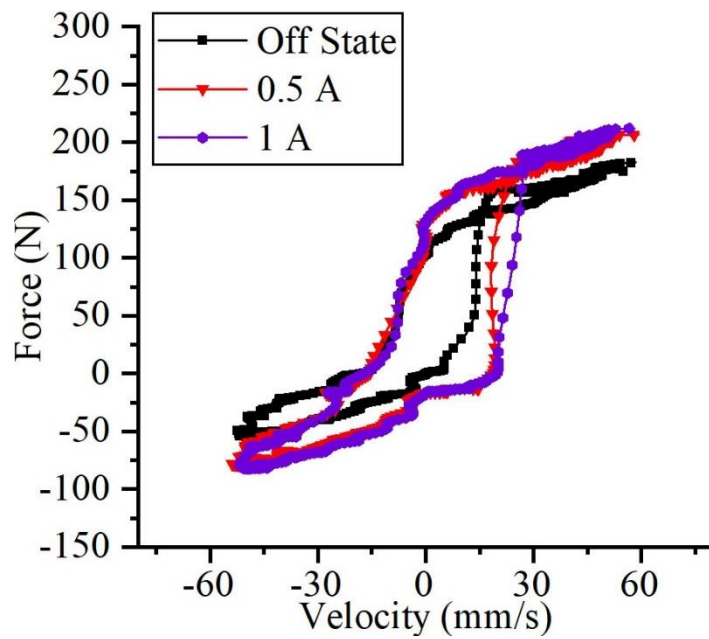


Figure 3.4 Damper testing machine with axial flux two-wheeler MR damper

Damper characterization experiments are generally carried out for required amplitude and frequency conditions. In this work, all experiments were carried out at 1 Hz operating frequency and by choosing 8mm, 12mm and 16mm amplitude conditions.



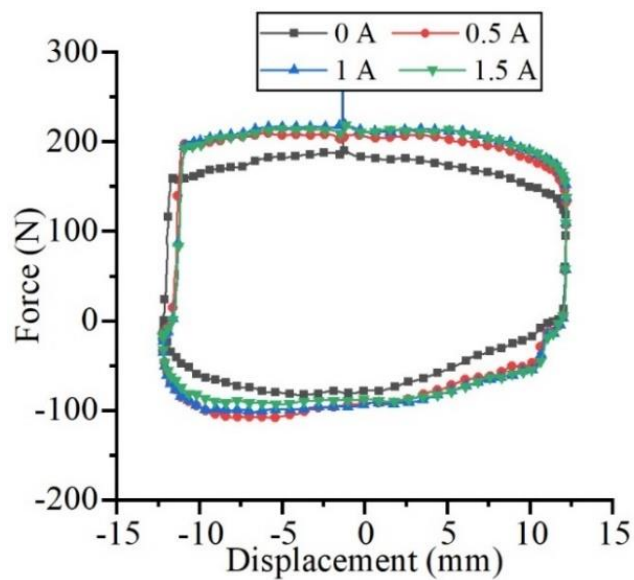
(a)



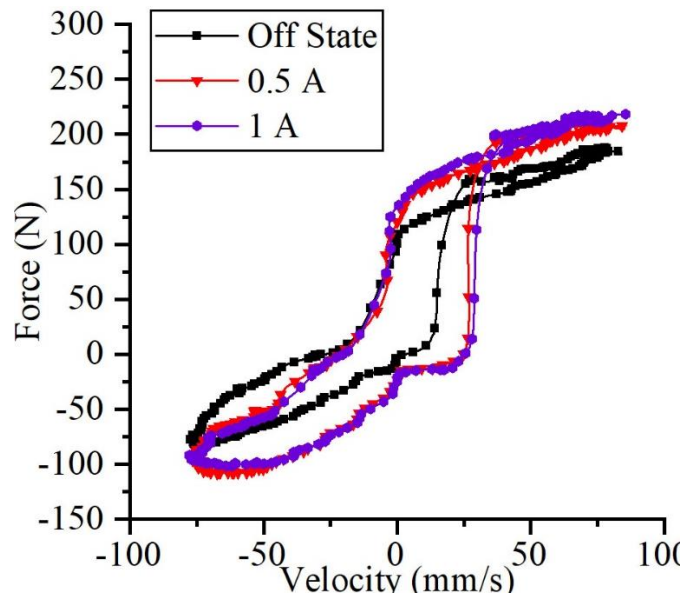
(b)

Figure 3.5 (a) force-displacement and (b) force-velocity for 8mm amplitudes

The electromagnetic piston of the damper was actuated by supplying 0.5A and 1A of DC current supply.



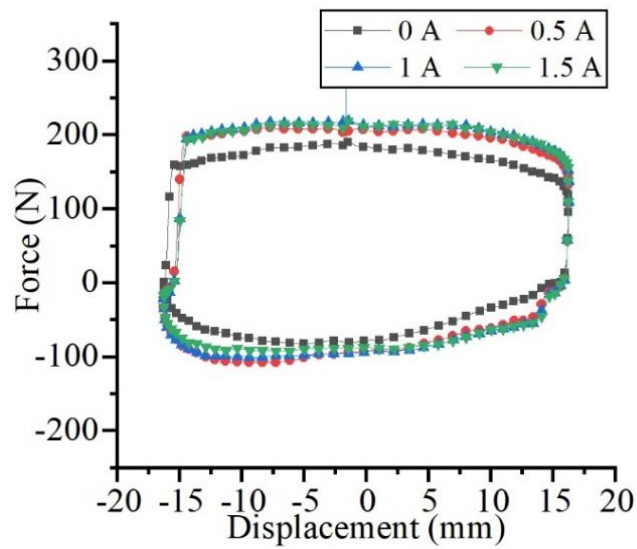
(a)



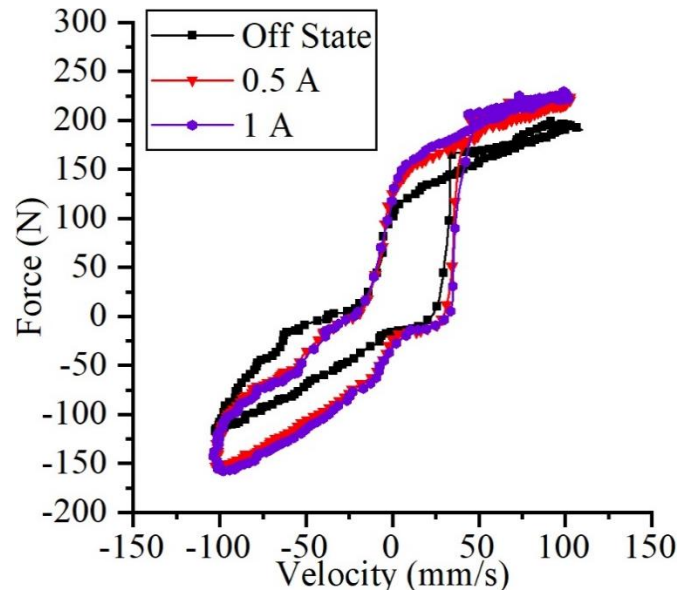
(b)

Figure 3.6 (a) force-displacement and (b) force-velocity for 12mm amplitudes

Experiments were carried out in off-state conditions too i.e., without supplying current to MR damper. Damper characterization results are shown in figure 3.5, 3.6 and 3.7.



(a)



(b)

Figure 3.7 (a) force-displacement and (b) force-velocity for 16mm amplitude

Results of characterization clearly distinguish the effect of MR damper in on-state and off-state. For instance, a total damping force of 195 N was produced in off-state condition whereas 231 N force was seen with 1 A current supply at 16 mm amplitude condition. The figures Fig. 3.5(a), 3.6(a), and 3.7(a) state the change in the force at the set displacement with respect to the current changes. The variation in the force with respect to the current from 0A to 0.5A is clearly visible whereas the change in force from 0.5A to 1.5A is barely visible as the piston core is not able to deliver the required flux. The brass fitting in the electromagnetic piston creates an earliest saturation of the damping force with respect to current.

### 3.4 MODELLING AND ANALYSIS OF AXIAL FLUX TWO-WHEELER MR DAMPER

The modelling of MR damper can be performed considering either parametric modeling or non-parametric modeling depending on the application. Parametric modelling and non-parametric modeling can be implemented for analysing the damper in suspension system models like quartercar and two-wheeler model. Multiple researchers went with the parametric modeling as they tried to fit the characteristic curves into parametric models like bingham plastic, modified bingham, bouc-wen and

modified bouc-wen models. The Bingham model consists of five parameters whereas the Bouc-Wen Model consists of seven parameters. Therefore, bingham model is a favourable model among researchers in the field.

With the increase in the number of parameters in the modelling, the accuracy of the force prediction increases, making modified bouc-wen modelling one of the most models. Kwok model is one model which works on the hysteretic model based on hyperbolic tangent function consisting of 6 parameters. Modified bouc-wen model has 14 parameters in the process of predicting the damping force which makes this model one of the most complex models and kwok model also provides a considerable prediction of damping force with just 6 parameters.

Non parametric modeling on the other hand does not depend on any of the parameters or specific formulated equations rather works by predicting the damping force considering the data from the characteristic curves like relative displacement, velocity, prior damping force etc. Some of the non-parametric models are polynomial model, algebraic model, black box models etc.

The model used in this study is kwok model and the parameters of this model are optimized by genetic algorithm. The root-mean-square error between the experimentally obtained force and the simulated force using this model is quite less as the degree of nonlinearity is less compared to the Bouc-Wen model. Due to the simplicity of the model and lesser number of parameters, the parameter identification efficiency outperforms the Bouc-Wen model

#### **3.4.1 Modelling of axial flux MR Damper using Kwok model**

Mathematical modelling of any dynamic system is an important stage which is used to predict the system performance for desired conditions. Mathematically, hyperbolic tangent function can represent hysteretic behaviour in a simplistic and efficient manner. A hysteretic model based on hyperbolic tangent function was proposed in the study by Kwok et al. (2006) and is shown in figure 1.10. With reference to the Kwok et al. (2006), Kwok model has the ability to represent the hysteretic relationship between the damping force and the velocity with reduced number of



parameters while still maintaining the physical interpretations of viscous damping and spring stiffness intact when compared to the bouc-wen model. Furthermore, Kwok et al. (2006) states computational efficiency and predictability of the kwok model is better than the Bouc-wen model. This was the prime reason for choosing the kwok model for modelling of axial flux MR damper. Linear functions which represent the stiffness and viscous, were combined with hyperbolic tangent function in Kwok model. The damping force through Kwok model is represented as,

$$F(t) = c_0\dot{x} + k_0x + \alpha z + f_0 \quad (3.4)$$

Where,  $z$  is the hysteretic variable given by,

$$z = \tanh[\beta\dot{x} + \delta \operatorname{sgn}(x)] \quad (3.5)$$

Where  $\delta$  determines the width of hysteresis and  $\beta$  decides the hysteretic slope. Parameters  $k_0$  and  $c_0$  represent conventional damper without hysteresis.  $\alpha$  is the deciding factor for height of the hysteresis and  $f_0$  is the offset shift of the hysteresis.

MR damper behaviour can be mathematically represented with proper identification of Kwok model parameters i.e.,  $c_0$ ,  $k_0$ ,  $f_0$ ,  $\alpha$ ,  $\beta$ ,  $\delta$ . The damping force, displacement and velocity data obtained using damper characterization in damper testing machine, were used in parametric identification. Parametric identification process was treated as an optimization problem where model parameters were considered as variables. The variables were identified against the objective function of minimizing the error between experimental and theoretical damping force. The genetic algorithm toolbox in MATLAB was used for optimal parameter identification.

MR damper was characterized for three different amplitudes (8mm, 12mm and 16mm) with three different current supplies to damper (0A, 0.5A and 1A) at 1 Hz frequency. Parameters were identified for each characterization data obtained from DTM. Table 3.2 represents Kwok model parameters obtained for various conditions.

Table 3.2 Kwok model parameters for different conditions

Amplitude (mm)	Current supply (A)	c <sub>0</sub>	k <sub>0</sub>	f <sub>0</sub>	β	α	δ
8	0	1106.65	1523.23	59.99	159.23	57.42	1.15
12	0	1116.03	1534.55	57.07	169.04	44.60	1.71
16	0	1171.93	1446.18	47.47	173.27	35.46	3.47
8	0.5	1530.34	1330.43	57.66	193.98	63.16	3.66
12	0.5	1200.27	1410.03	49.04	148.02	62.36	3.35
16	0.5	1350.91	1101.87	45.53	195.91	50.94	6.72
8	1	1879.93	1473.43	55.69	362.27	53.94	7.82
12	1	1443.03	1048.26	55.08	257.85	59.10	7.16
16	1	1157.67	1351.29	46.05	164.36	64.88	5.39

Kwok model parameters for each condition are listed in table 3.3. The purpose of mathematical model lies in its application in control system. But parameters listed above hold good corresponding to their dynamic condition. Therefore, modelling is essential in such a way that it is effective in all dynamic conditions.

To make this happen, each Kwok model parameter was represented in terms of current in against each displacement by curve fitting method in the form of,

$$\text{Parameter} = AI^2 + BI + C \quad (3.6)$$

Where,  $A$ ,  $B$  and  $C$  are coefficients of above-mentioned equation and  $I$  is the current supply.

A sample of equation fitting for 12 mm amplitude is shown in table 3.4. Similar technique was adopted for 8 mm and 16 mm displacement too. Now each parameter has been represented in terms of current. But still all these parameters are restricted to corresponding displacement conditions. Hence a method was adopted by which coefficient from each equation (from table 3.4) for each parameter was represented in terms of displacement.

Table 3.3 Parameters in terms of current for 12 mm amplitude

Parameter	Expression in terms of current (I)
$c_0$	$317I^2 + 9.986I + 1116$
$k_0$	$-474.4I^2 - 11.79I + 1534$
$f_0$	$28.16I^2 - 30.16I + 57.07$
$\beta$	$261.7I^2 - 172.9I + 169.0$
$\alpha$	$-42.04I^2 + 56.54I + 44.60$
$\delta$	$4.361I^2 + 1.083I + 1.719$

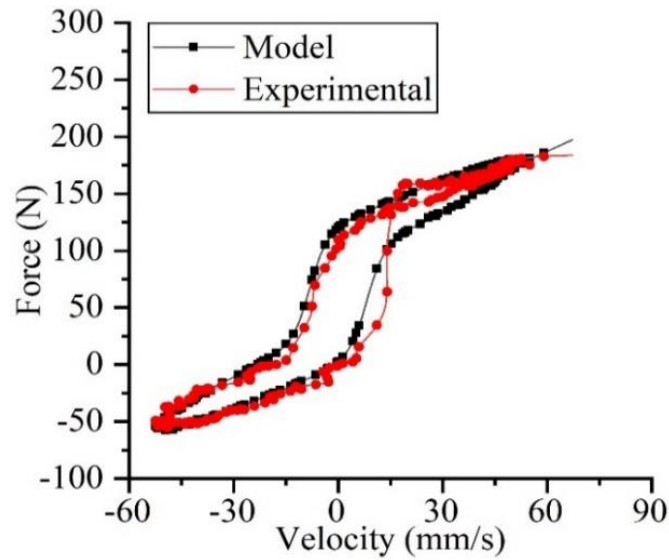
Again, curve fitting method was implemented to arrive at equations for each coefficient against all parameters. Finally, each Kwok model parameter was represented in terms of current ( $I$ ) and the displacement ( $x$ ).

Table 3.4 Final representation of each Kwok model parameter

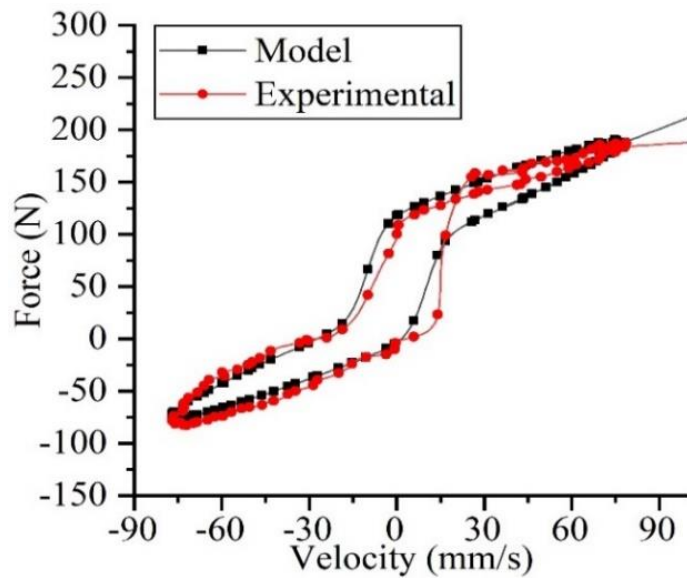
Parameter	Representation in terms of current( $I$ ) and displacement( $x$ )
$c_0$	$(-5 \times 10^7 x^2 + 10^6 x - 5658)I^2 + (5 \times 10^7 x^2 - 10^6 x + 7638)I + (8125x + 1033)$
$k_0$	$(9 \times 10^7 x^2 - 2 \times 10^6 x + 11385)I^2 + (-6 \times 10^7 x^2 + 10^6 x - 8079)I + (-3 \times 10^6 x^2 + 64625x + 1204)$
$f_0$	$(-2 \times 10^6 x^2 + 38544x - 206.2)I^2 + (2 \times 10^6 x^2 - 36894x + 192.2)I + (-20875x^2 + 3445x + 45.79)$
$\beta$	$(-10^7 x^2 + 22661x - 816.5)I^2 + (10^7 x^2 - 26545x + 1297)I + (1750x + 146.1)$
$\alpha$	$(2 \times 10^6 x^2 - 34952x + 147.5)I^2 + (-2 \times 10^6 x^2 + 41366x - 196.1)I + (-2745x + 78.76)$
$\delta$	$(-45540x^2 + 9374x - 42.55)I^2 + (38378x^2 - 8249x + 44.80)I + 290.5x - 1.371$

Comparison between experimental and values extracted from Kwok model is presented in figure 3.8. It is clear from the figure that the output from Kwok model is

comparable with the experimental values with minimum difference. The hysteretic behaviour from Kwok model is in good agreement with actual nature of the dynamic data.



(a)



(b)

Figure 3.8 Experimental and Kwok model output for off state condition for (a) 8mm, and (b) 12mm

The final representation of Kwok model consists of parameters in terms of current and displacement only. This makes the model suitable for application of control system for variety of road input conditions.

Control is the most important aspect in the effective working of the MR damper. Multiple control strategies are available considering different formulations and parameters for the estimation of the damping force required for obtaining the current required to drive the MR damper with respect to the road input.

Any MR Damper employed in a suspension system requires a controller which instantaneously detects the suspension deflection and relatively provides the required current for the deflection to be nullified. A robust controller which can obtain the desired damping force with MR damper suspension system is a PID controller. Being a well-known control, it is a simple yet effective to implement practically, with a key feature of robustness to system uncertainties. The PID control consists of the three individual controllers, 'P' 'I' and 'D' where P control is an adjustable gain amplifier with ' $k_p$ ' as the gain.

The response time of the control system decreases with increase in  $k_p$  and vice versa. P control alone brings the system output to an error between the expected value and the actual value. This error is determined as steady state error and it can only be reduced by the implementation of integral control. If there is a steady state error the integral gain tries to eliminate it by applying the control effect based on the historic cumulative error. Once the steady state error is reduced to zero, the integral gain ceases to increase resulting in the suppression of proportional control. This can be reduced by the implementation of derivative control. As the steady state error gets eliminated the derivative control seeks to reduce influence of the rate of change of error. The higher the change, the more effective the control (damping) of the integral influence.

In this study PID control is used in the quarter car suspension model and two-wheeler suspension model employing the kwok model of the MR damper. The system is analysed for the sprung mass acceleration reduction in both the suspension models.

### 3.4.1.1 Mathematical Model of Quarter-car (MMQ)

The basic quarter car suspension system includes spring and a damper connected between the sprung and the unsprung masses. Here the figure 3.9 describes a two degree of freedom mechanical suspension system which represents the quarter car model with both passive and MR damper.

The vehicular body mass is represented by  $M_s$ , typically the sprung mass and the wheel mass including all the fixtures and the other components associated with it is considered as the unsprung mass and is represented by  $M_{us}$ .

The vertical displacements are represented with  $Z_s$  and  $Z_{us}$  respectively for both the sprung and unsprung masses. The road undulation or profile or simply the vertical disturbance is indicated with  $Z_r$ , the spring stiffness and tire stiffness are labelled as  $K_s$  and  $K_{us}$ . The damping force provided by the tyre is neglected as it is quite small compared to the entire damping of the system. The force produced by the MR Damper is indicated as  $F_d$ .

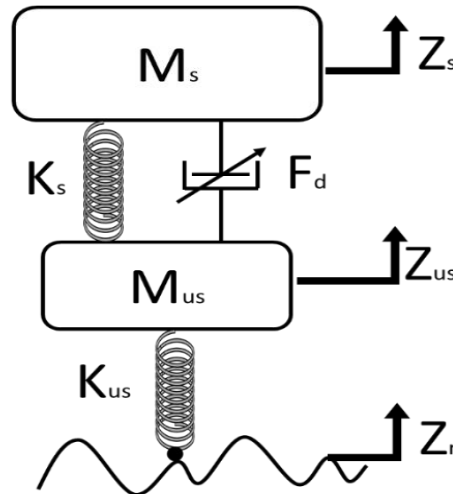


Figure 3.9 Quartercar Mathematical Suspension Model

Thus, by applying Newton's second law, equations of motion for sprung and unsprung masses are as follows (El-Kafafy et al. (2012)):

$$M_s \ddot{Z}_s + k_s (Z_s - Z_{us}) + F_d = 0 \quad (3.7)$$

$$M_{us} \ddot{Z}_{us} - k_s (Z_s - Z_{us}) + k_{us} (Z_r - Z_{us}) - F_d = 0 \quad (3.8)$$

The quarter car model considering the parameters specified in table 3.5 in association with the kwok model have been implemented with the PID control strategy. The analysis of quarter car suspension model with off state PID control and 1A constant current semi-active suspension system has been carried out under a continuous sine wave with an amplitude of 0.01m, 3Hz frequency excitation are considered for the road input profile.

Table 3.5 Parameters of the MMQ with axial flux-based two-wheeler MR damper

Quarter car Parameters	Value of the parameter
Sprung Mass $M_s$	150 Kg
Unsprung Mass $M_{us}$	15.82 Kg
Sprung stiffness $K_s$	24000 N/m
Unsprung stiffness $K_{us}$	180000 N/m

The vertical acceleration responses of suspension are illustrated in figure 3.10. It is observed that the peak sprung mass acceleration has been reduced to 4.07% in case of PID controlled suspension system when compared with the off state.

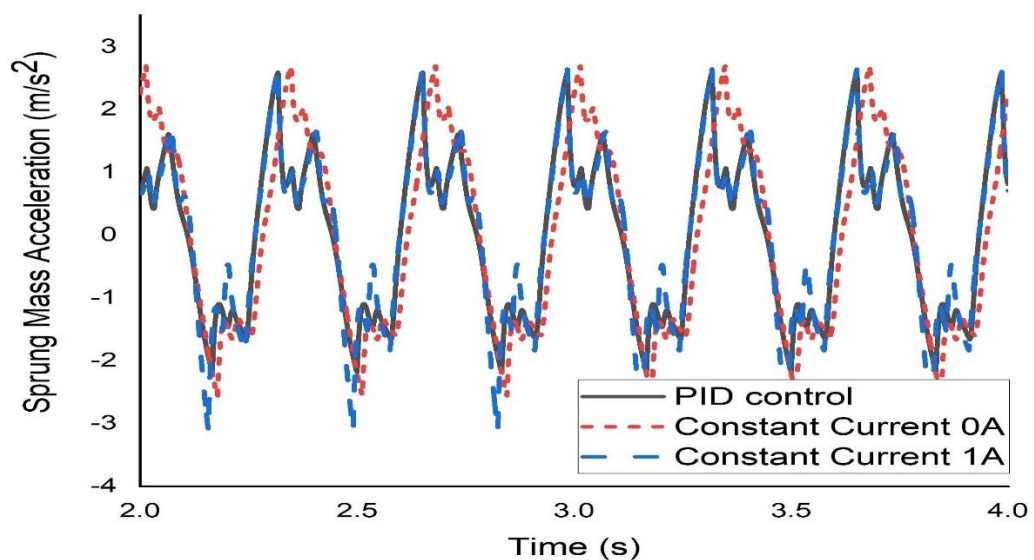


Figure 3.10 Sprung mass acceleration response of MMQ with axial two-wheeler MR damper

The RMS acceleration response of the quarter car system specifies  $1.506\text{m/s}^2$  and  $1.275\text{ m/s}^2$  with MR damper off-state and the implementation of PID control having P, I, D values to be 20.1, 0, 10.6 respectively. Road holding can be measured as the relative displacement between road and unsprung mass. The road holding characteristics of the suspension system provides  $0.009496\text{m}$  with off-state and  $0.008036\text{m}$  stability to the vehicle with PID control by making significant contact with the ground. Quantitatively, lesser the magnitude of road holding better is the vehicle stability. Thus, the control provides an improvement of 10.56% on RMS acceleration and 15.37% of RMS road holding with respect to the off-state response of the MR damper.

### 3.4.1.2 Mathematical Model of Two-wheeler (MMT) with axial flux MR damper

The two-wheeler automobile suspension system can be represented by a mathematical model with two unsprung masses and a single sprung mass balanced on the unsprung using the suspension system parameters. Thus, the two-wheeler model with four degrees of freedom system as shown in figure 3.11 is analysed by considering vertical displacement ( $x_s$ ) and pitch movement or pitch angle ( $\theta$ ) of vehicle body, vertical displacement of front ( $x_{uf}$ ) and rear unsprung ( $x_{ur}$ ) masses. (Kumar (2008))

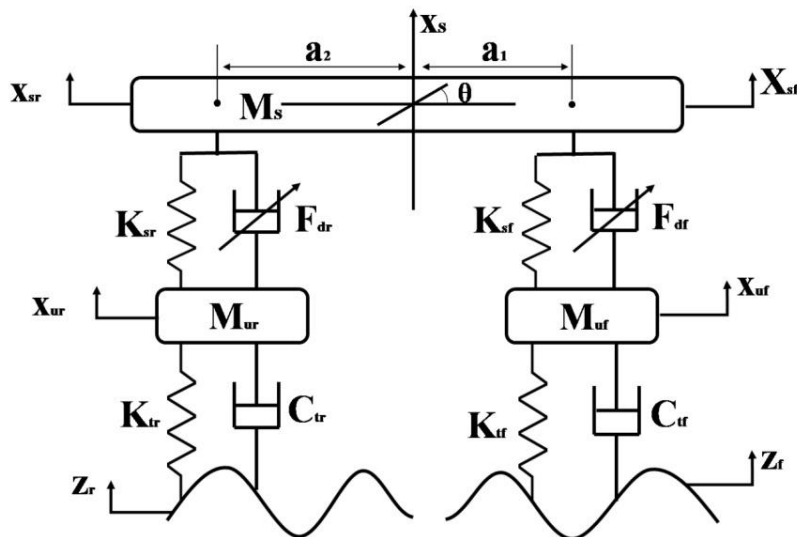


Figure 3.11 Mathematical model of the Two-wheeler vehicle



The displacement at each corner of the sprung mass is expressed in terms of bounce, pitch.

$$x_{sf} = x_s + a_1\theta \quad (3.9)$$

$$x_{sr} = x_s - a_2\theta \quad (3.10)$$

The equation of motion of a two-wheeler model can be described as follows

Sprung mass bounce

$$M_s\ddot{x}_s + K_{sf}(x_{sf} - x_{uf}) + K_{sr}(x_{sr} - x_{ur}) + F_{df} + F_{dr} = 0 \quad (3.11)$$

Sprung mass pitch

$$I_y\ddot{\theta} + a_1K_{sf}(x_{sf} - x_{uf}) - a_2K_{sr}(x_{sr} - x_{ur}) + a_1F_{df} - a_2F_{dr} = 0 \quad (3.12)$$

Unsprung mass bounce

$$M_{uf}\ddot{x}_{uf} + C_{tf}(\dot{x}_{uf} - \dot{z}_f) + K_{tf}(x_{uf} - z_f) - K_{sf}(x_{sf} - x_{uf}) - F_{df} = 0 \quad (3.13)$$

$$M_{ur}\ddot{x}_{ur} + C_{tr}(\dot{x}_{ur} - \dot{z}_r) + K_{tr}(x_{ur} - z_r) - K_{sr}(x_{sr} - x_{ur}) - F_{dr} = 0 \quad (3.14)$$

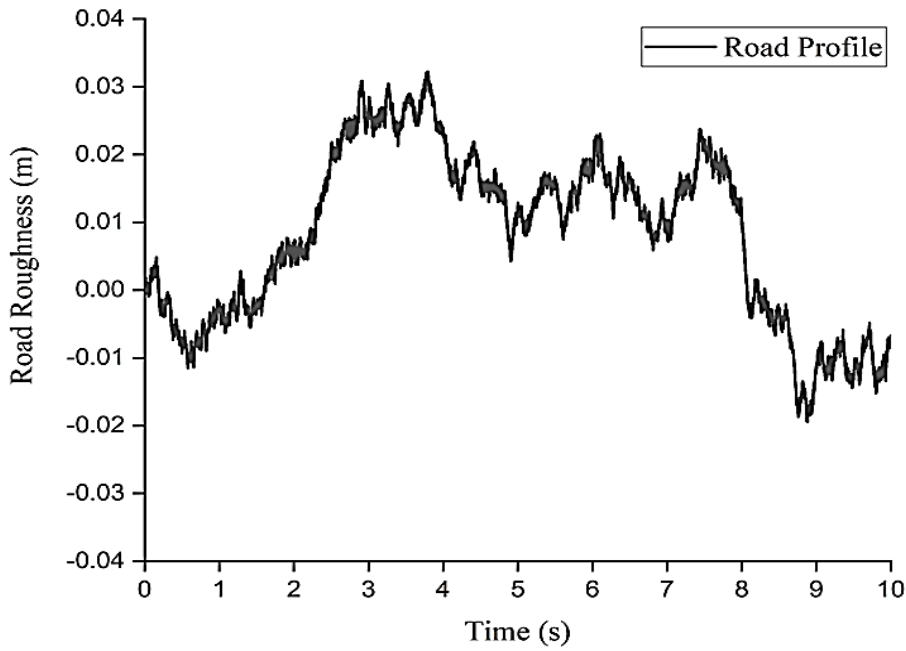
Where,  $\ddot{x}_s$  is sprung mass acceleration,  $\ddot{x}_{uf}$  is front unsprung acceleration,  $\dot{x}_{uf}$  is front unsprung velocity,  $\ddot{x}_{ur}$  is rear unsprung acceleration,  $\dot{x}_{ur}$  =Rear unsprung velocity,  $F_{dr}$  =Semi active damping force (rear),  $F_{df}$  is semi active damping force (front),  $z_f$  is road displacement (front),  $z_r$  is road displacement (rear).

The entire work in the simulations were considered with a random road profile implemented with the following equation.

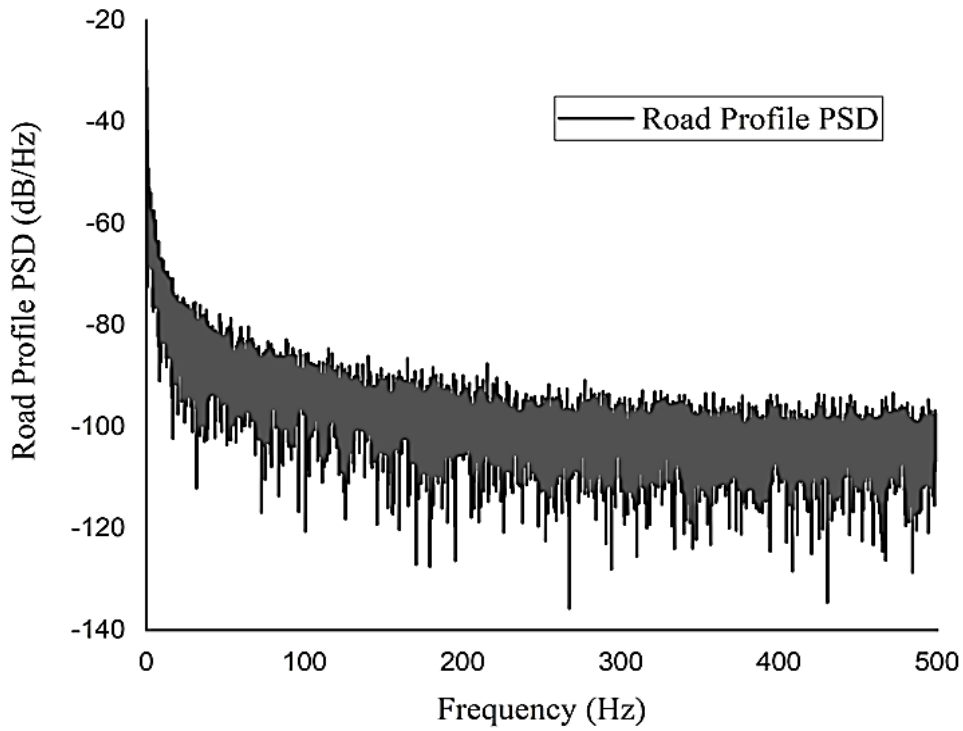
$$\dot{S}_r(t) = -2\pi m_0 S_r(t) + \sqrt{G_i(\lambda_0)v} w(t) \quad (3.15)$$

Where,  $\dot{S}_r(t)$  is the road irregularity,  $G_i(\lambda_0)$  is the roughness coefficient at  $\lambda_0 = 0.1\text{rad/min}$ ,  $v$  is velocity,  $w(t)$  is the white noise and  $m_0$  is the special frequency. All test runs were carried out on ‘poor’ road condition with roughness coefficient of  $256 \times$

$10^{-6} \text{ m}^2/\text{cycle}/\text{m}$ . The figure 3.12 shows the random road profile in time domain with its corresponding power spectral density plot.



(a)



(b)

Figure 3.12 Random Road profile (a) time domain (b) power spectral density

The parameters of the two-wheeler vehicle were considered with reference to Karanam (2016) to develop the two-wheeler model. The parameters are listed in table 3.6. The two-wheeler mathematical model was subjected to random road excitation as specified in the equation 3.15.

In this study a PID controller is designed to control the two-wheeler suspension model. The suspension deflection is measured and sent to the PID controller to produce the required control signal. This control signal is fed to the current amplifier to produce the required current for the MR damper.

Table 3.6 Parameters for MMT for Axial flux two-wheeler MR damper

<b>Parameters</b>	<b>Value</b>
Wheelbase ( $a_1 + a_2$ )	1.26 m
Sprung mass ( $M_s$ )	155.6 kg
Front unsprung mass ( $M_{uf}$ )	12.28 kg
Front tire damping ( $C_{tf}$ )	700 Ns/m
Distance of front unsprung from center of gravity ( $a_1$ )	0.6237 m
Front tire stiffness ( $K_{tf}$ )	180000 N/m
Front spring stiffness ( $K_{sf}$ )	24000 N/m
Distance of rear unsprung from centre of gravity ( $a_2$ )	0.6363 m
Rear unsprung mass ( $M_{ur}$ )	15.82 kg
Rear tire damping ( $C_{tr}$ )	700 Ns/m
Rear tire stiffness ( $K_{tr}$ )	180000 N/m
Rear spring stiffness ( $K_{sr}$ )	24000 N/m
Inertia ( $I_y$ )	1105 kgm <sup>2</sup>

In order to ensure that the current fed to the damper is under the physical limitation of the damper, a current limiter is provided to limit the current between 0 to 1.5 A. The bounded current (limited current) including the suspension deflection are fed to the MR damper.

The detailed design of the control strategy is illustrated in the figure 3.13. The PID control parameters were selected and optimized based on the ‘PID tuner’ app available in the MATLAB. This app linearizes the entire Simulink file and considers the output PID parameters accordingly. The obtained PID values are  $P = 20.1$ ,  $I = 1.53$ ,  $D = 1$ .

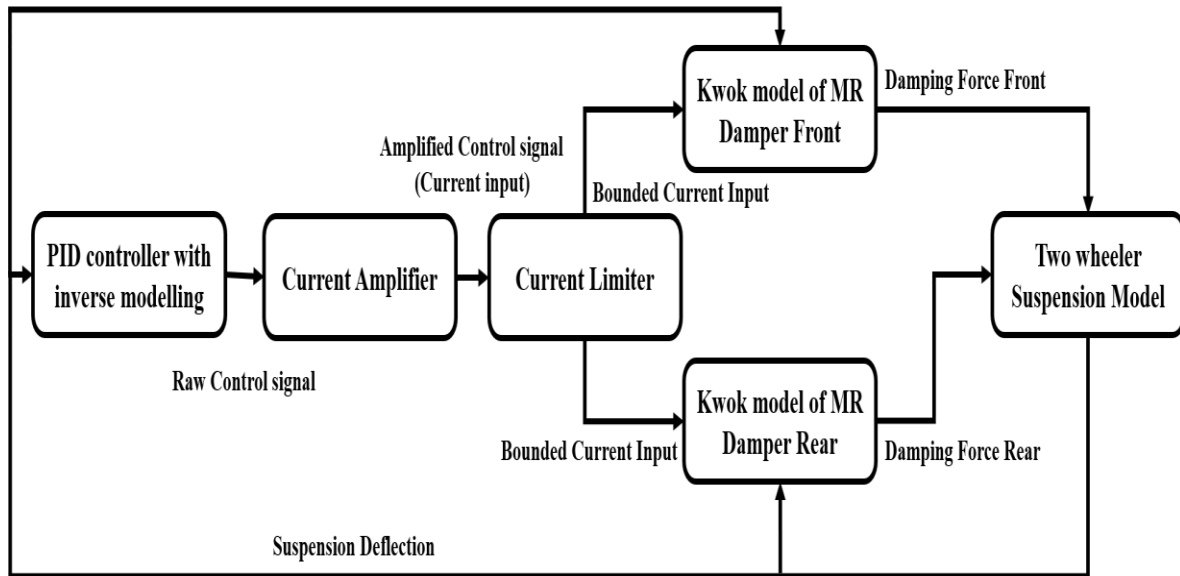


Figure 3.13 Block diagram representation of the PID control Strategy

The analysis of two-wheeler semi active suspension model with off state PID control and 1A constant current semi-active suspension system has been carried out under random irregularities for different vehicle velocities.

The vertical acceleration responses of semi-active two-wheeler suspension at various speeds are illustrated in figure 3.14. It is observed that sprung mass acceleration has been reduced to 19.3% in case of PID controlled suspension system when compared with the off state at 5 m/s vehicular velocity.

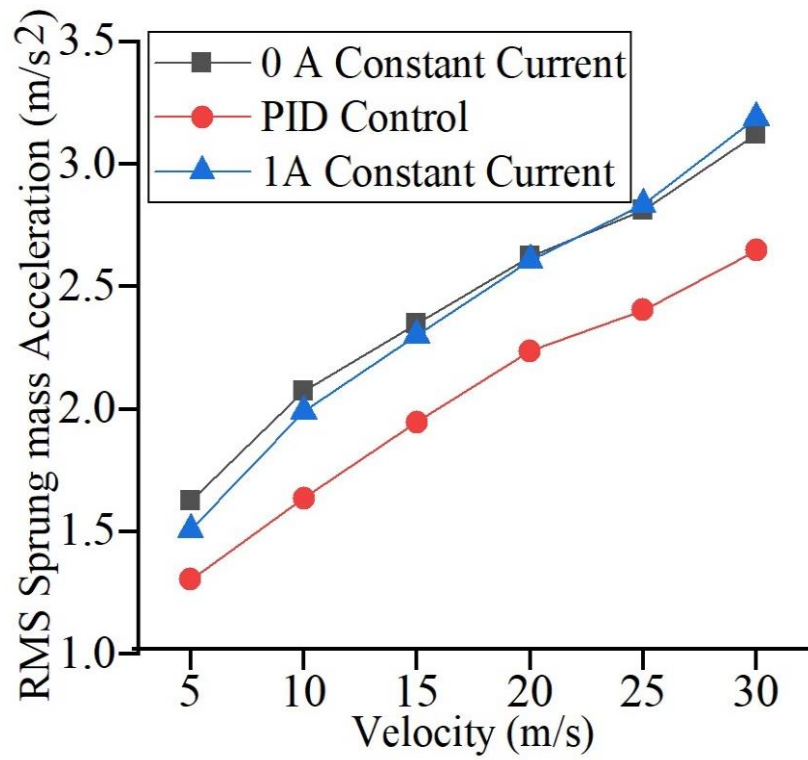


Figure 3.14 Sprung mass RMS acceleration at different velocities

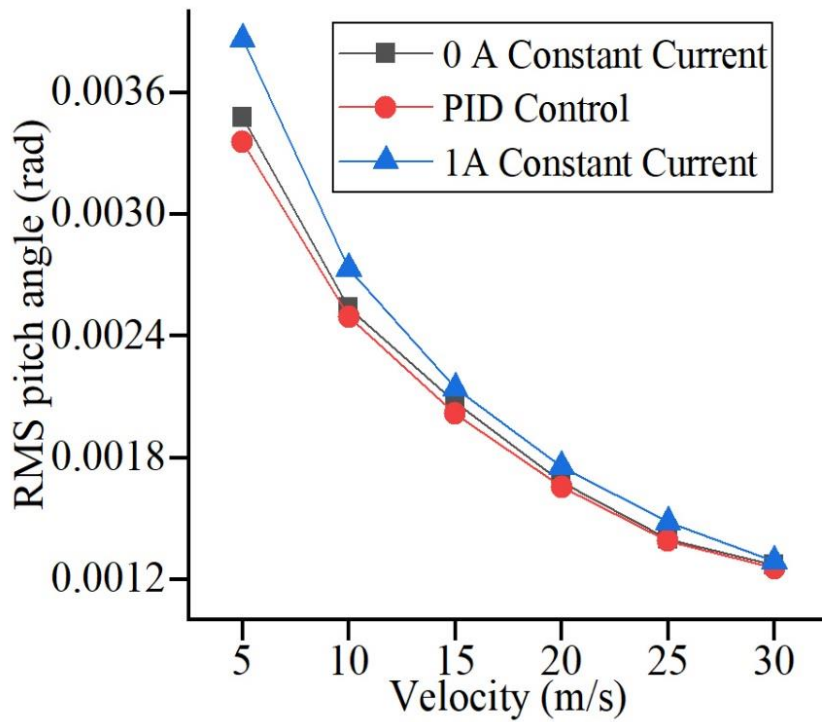
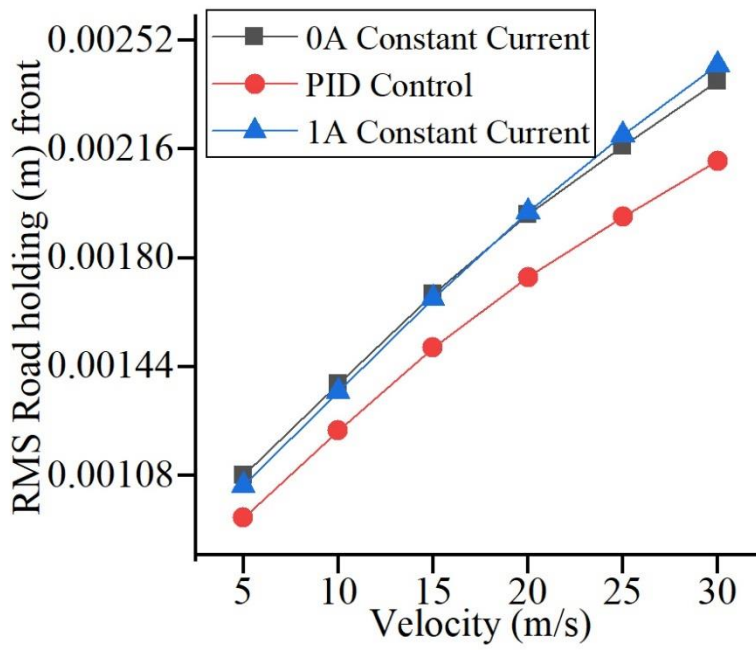
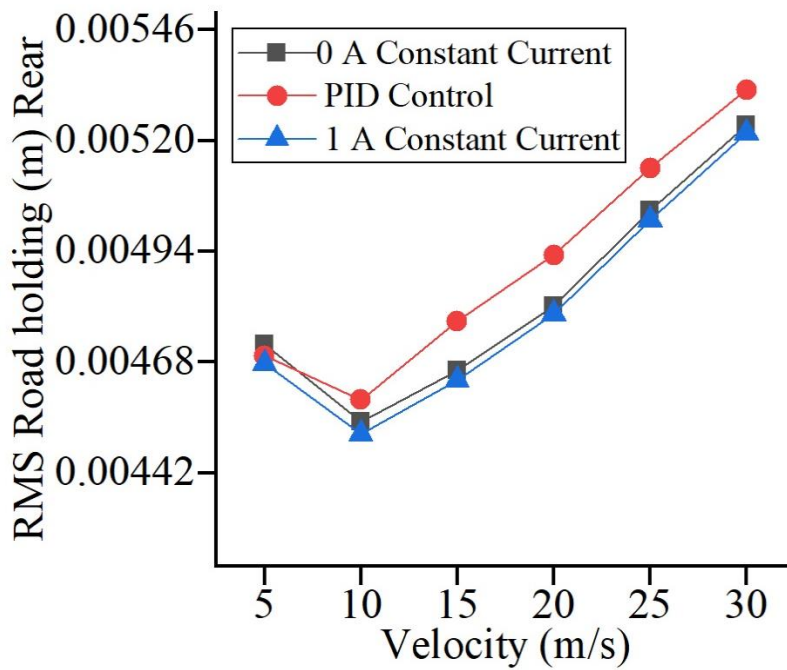


Figure 3.15 Pitch angle with different current inputs at different velocities

Figures 3.16(a) and 3.16(b) demonstrate the road holding nature of the two-wheeler suspension at front and rear wheel, respectively, with different vehicle velocity.



(a)



(b)

Figure 3.16 Road holding of (a) front and (b) rear different current inputs

It is observed that two-wheeler model with developed Kwok modelled MR based suspension system provides about 12% improved road holding (at front wheel) with PID controlled current input than with off-state condition. But it was also observed that the performance of the system was not up to the mark at rear position in terms of road holding. Hence, still there is a scope for improving the damper performance at rear position.

The analysis of pitch angle motion of the sprung mass showed very little improvement using MR damper with PID controller when compared to off-state condition (figure 3.15). The developed MR damper in two-wheeler semiactive suspension model showed a good improvement in performance with PID controller in terms of RMS acceleration of sprung mass and road holding at front unsprung position of the vehicle.

### **3.5 REAL TIME TESTING OF AXIAL FLUX MR DAMPER WITH CONSTANT CURRENT INPUT**

The designed Axial flux MR damper is implemented in a light weight two-wheeler vehicle (Splendor, Make: Hero corporation). The on-road experimentation is carried out on the random road where MR dampers are placed on the either side of the two-wheeler vehicle. The excitation coil wires of the damper are connected to the current controller via a current sensor to measure the amount of current entering the coil of the MR damper.

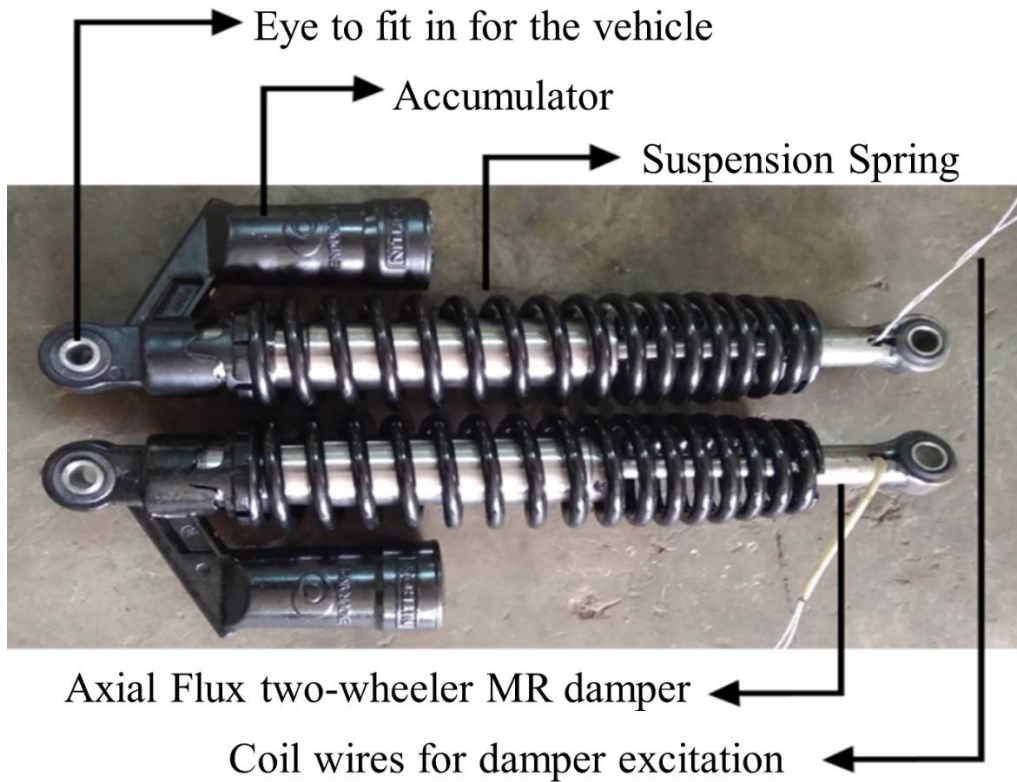


Figure 3.17 Total suspension system for two-wheeler vehicle

The current controller is in turn powered by a LiPo battery of 11.1V and 5000mAH consisting of three individual 3.7V cells. The current controller can adjust the current as per the requirement using a variac. Either side of the damper are fed with equal current as both the dampers are connected in series. The final suspension system to be connected to the two-wheeler vehicle is shown in the figure 3.17. The vibration (acceleration) on either side of the suspension system (sprung and unsprung mass) is measured using accelerometers by connecting it to the NI hardware using the BNC cables.



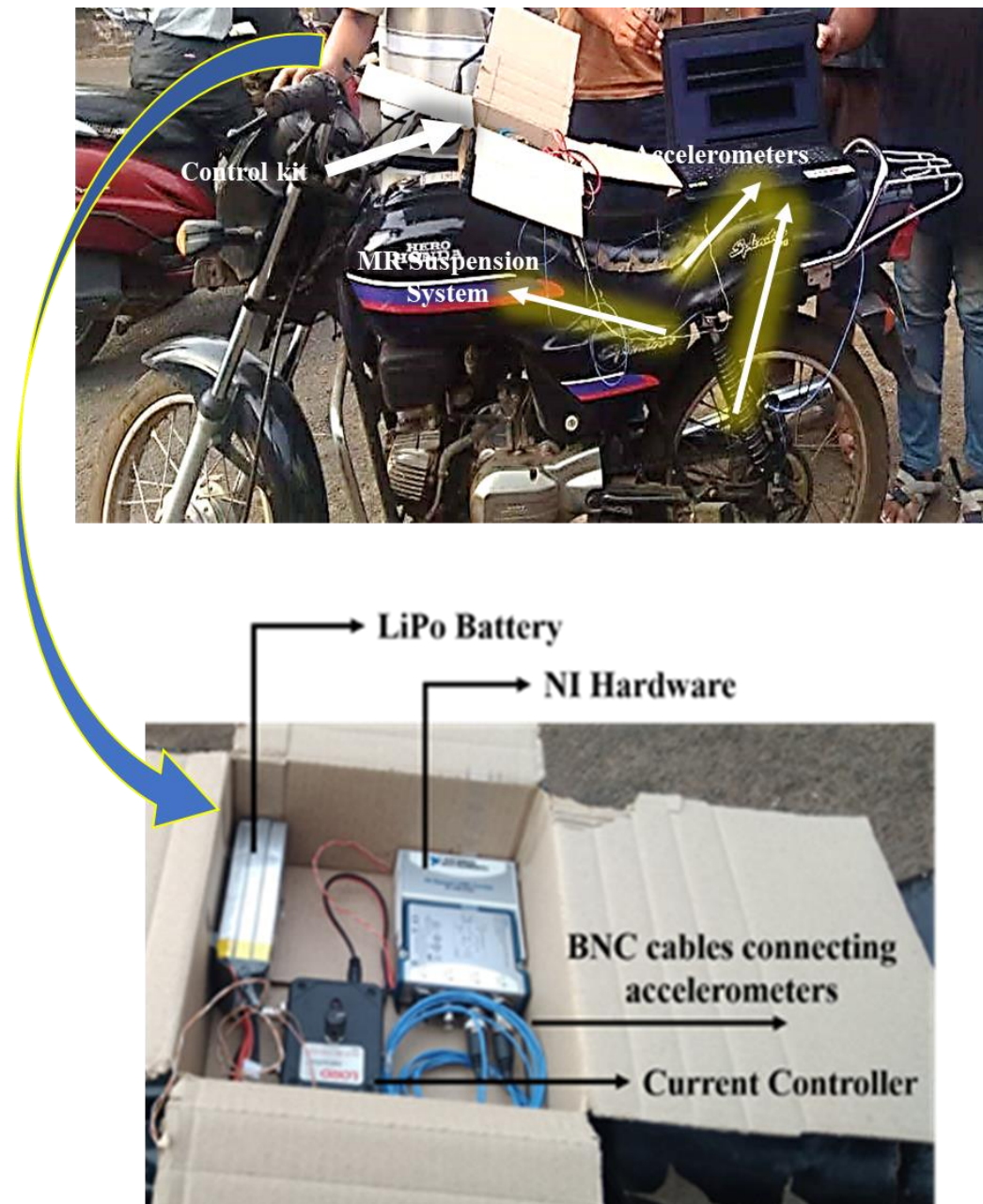


Figure 3.18 MR Damper fitted to two-wheeler with control kit

The damper fixation to the two-wheeler vehicle and the control kit placed before the rider is displayed in the figure 3.18. The NI hardware used here is the USB C DAQ with NI 9234 for accessing data.



Figure 3.19 Road with a speed bump for testing the semi active suspension

All vehicle testing were performed over a road with hump shown in the figure 3.19. The vehicle velocity was maintained at 30 kmph throughout the testing. But there is no surety that vehicle has followed same line path at same time intervals, during every testing. Hence, time domain data do not provide the clear idea on the performance of the damper. Hence, representation in frequency domain provides a better picture on the performance variation. The sprung mass acceleration with current variation is represented in frequency domain as shown in figure 3.20.

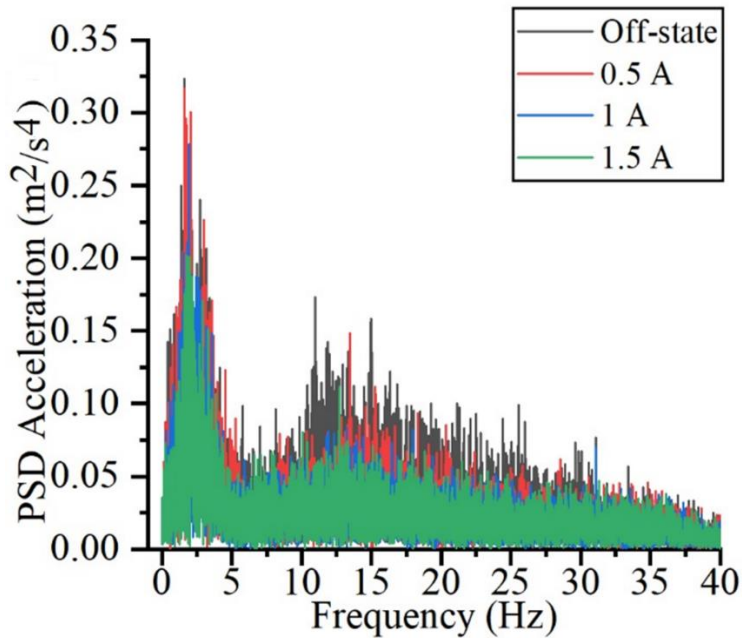


Figure 3.20 PSD acceleration with variation in frequency

The peak amplitudes were observed near 2 Hz frequency and the amplitude reduction was observed with increase in current showing improved damping performance with MR damper.

It is a general practice to measure the comfort of passenger with RMS acceleration of the sprung mass. Figure 3.21 shows the sprung mass acceleration variation against the current supply. 40% reduction in the sprung mass RMS acceleration was observed for 1.5A current supply when compared against off-state condition.

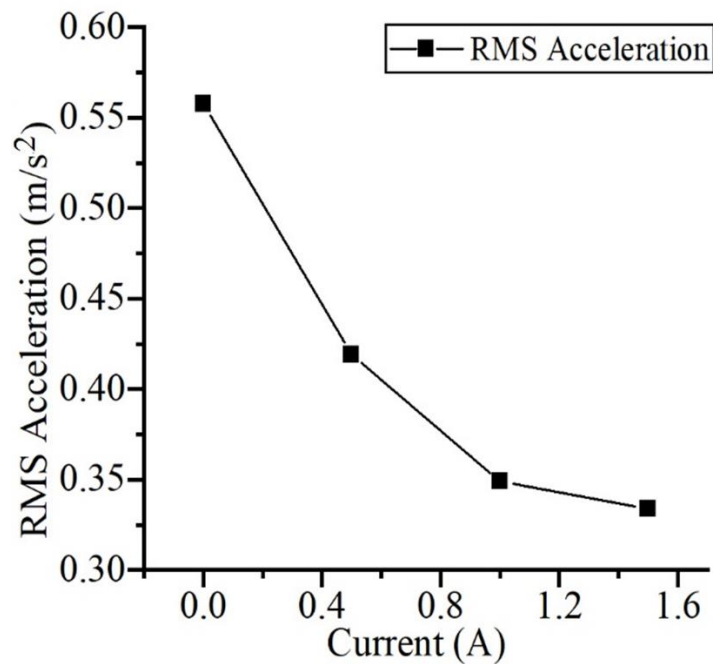


Figure 3.21 RMS sprung mass acceleration with current variation

This shows a significant reduction in sprung mass RMS acceleration with MR effect. The results showed a significant performance improvement showing the capability of MR damper to provide better passenger comfort.

Even though significant change in the MR damper implementation is observed in the vehicular implementation at constant current inputs there is a need for the implementation of control algorithms in the vehicles for more effective and proper reduction of the body vibrations. This work is carried out in the upcoming dampers for the reduction of sprung mass acceleration (body vibrations).

### **3.6 SUMMARY**

The designed damper was providing a magnetic flux density of 0.3 T within the fluid flow gap and was able to provide a considerable change in the damping force with respect to change in the current supply to the damper. The analysis of the damper in quarter car and two-wheeler mathematical models has shown improvement in the sprung mass acceleration reduction. Also, the constant current on road testing of the vehicle (splendor plus) was able to provide 40% reduction in the RMS sprung mass acceleration when compared to the off-state condition.

## **CHAPTER 4**

# **DESIGN AND ANALYSIS OF RADIAL FLUX TWO-WHEELER MR DAMPER**

### **4.1 INTRODUCTION**

The design of the Radial flux MR damper is quite different from that of the axial in terms of both the design and coil wound to it in order to make it a solenoid. The fabrication process is quite complex and requires wire EDM or a laser cut machining in order to obtain a precise and smooth fabricated design. The flux generated from the piston poles is also perpendicular to the piston rod throughout the pole length. An I house MR fluid was designed to fill the damper as the commercial fluid was costly. The detailed description of the designed and fabricated damper along with the MR fluid used is specified in the following sub sections of this chapter.

### **4.2 SYNTHESIS AND CHARACTERIZATION OF MR FLUID**

When the MR fluid is brought in the vicinity of magnetic field, its viscosity changes, making it a smart fluid. MR fluid is made by suspending magnetic particles in non-magnetic carrier fluid. An additive material is added to prevent the sedimentation of magnetic particles in the carrier fluid. In general, carbonyl iron particles are used as magnetic particles. In the absence of magnetic field, the MR fluid acts as a conventional fluid. With the application of magnetic field, the magnetic particles form chain like structures and resist the flow of fluid which indicates the change in viscosity.

The change in viscosity depends on the strength of magnetic field applied and number of magnetic particles present in the fluid. The prior axial flux piston-based MR damper used the Lord MR fluid which is a commercial MR fluid whereas the fluid used in this damper is an inhouse made fluid consisting of micron sized carbonyl iron particles suspended in fork oil with a viscosity of 40 cSt that acts as carrier fluid. Grease is added as additive to prevent the carbonyl iron particles sedimentation in the fork oil

medium. The composition of MR fluid used to carry out the further work is mentioned in the Table 4.1.

Table 4.1 MR fluid composition for Radial flux two-wheeler MR damper

<b>Ingredients</b>	<b>Weight percentage</b>
Carbonyl Iron particles	65.97%
Fork oil	27.73%
Grease	6.29%

To obtain the rheological properties of the MR fluid, rheometer is used. Figure 4.1 shows the parallel plate type rheometer used for rheological testing of MR fluid.

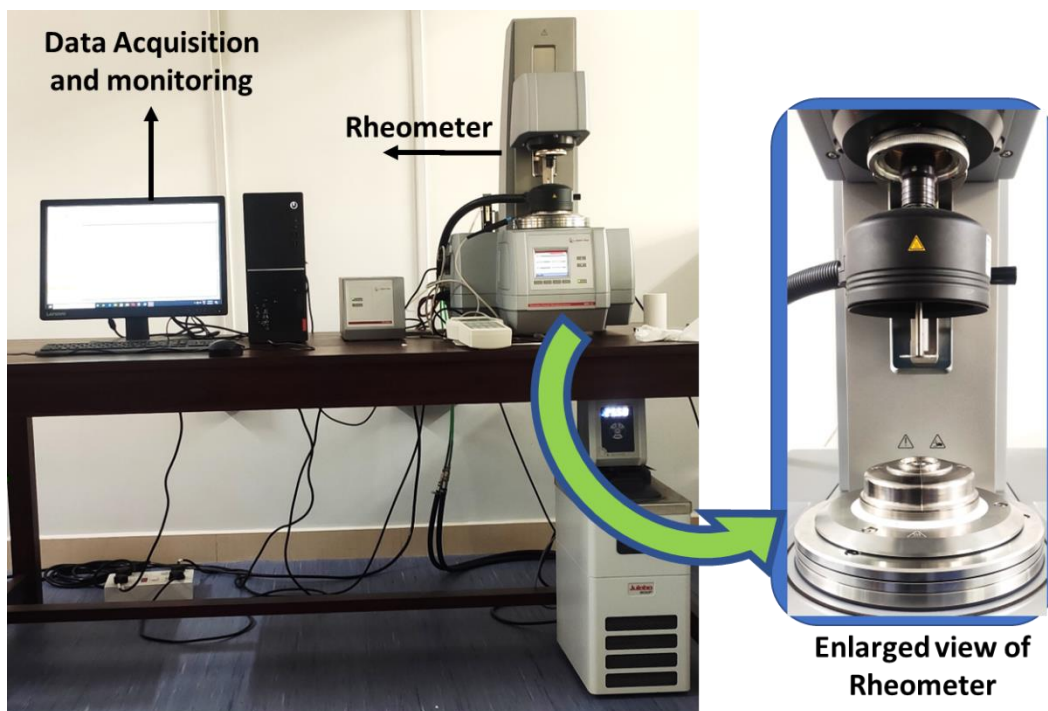


Figure 4.1 Rheometer test setup for characterization of MR fluid

A MR device cell was employed to apply different magnetic field strength to the test fluid sample and the figures 4.2 to 4.4 represents the various rheometric results obtained. Figure 4.2 represents the shear rate vs shear stress plots obtained at currents of 0A, 1A, 2A, and 3A.

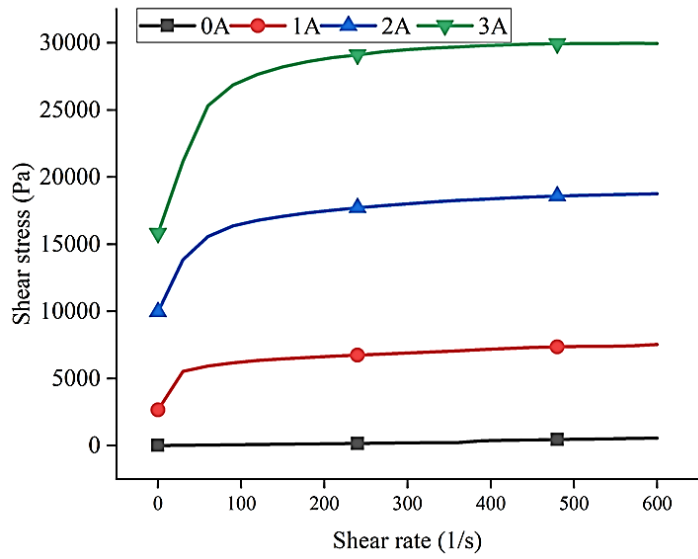


Figure 4.2 Shear rate vs shear stress at different currents

In the absence of magnetic field i.e., at 0A the shear stress varies linearly with shear rate. With the application of external current, the shear rate shear stress relation becomes nonlinear. The maximum shear stress obtained at 0A, 1A, 2A and 3A are 560.15Pa, 7529.6Pa, 18,768 Pa and 29,964 Pa respectively.

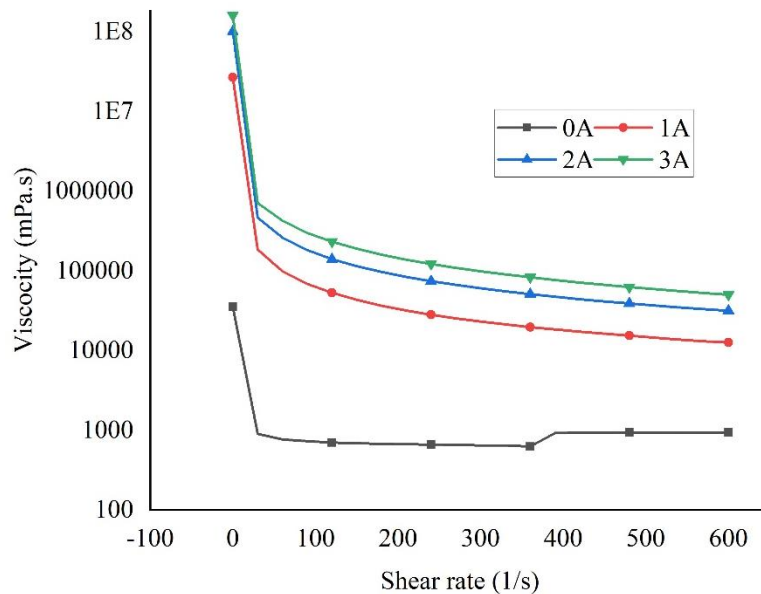


Figure 4.3 Shear rate vs viscosity at different currents of MR fluid

Figure 4.3 represents the shear rate vs viscosity plots obtained at currents of 0A, 1A, 2A, and 3A. The maximum viscosity obtained at 0A, 1A, 2A and 3A are 25,190 mPa-s,  $2.66 \times 10^7$  mPa-s,  $1 \times 10^8$  mPa-s and  $1.59 \times 10^8$  mPa-s respectively.

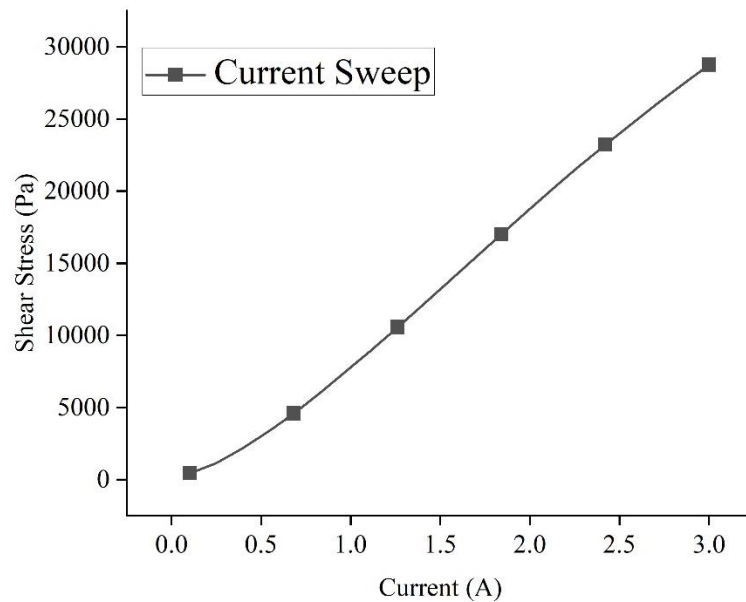


Figure 4.4 Currents vs Shear stress of MR fluid

Figure 4.4 represents the current vs shear stress plot at constant Shear rate. A maximum shear stress of 28,752 Pa is obtained at current of 3A.

### 4.3 DESIGN OF RADIAL FLUX TWO-WHEELER MR DAMPER

As specified in the previous chapters, the design procedures are followed towards radial flux-based two-wheeler MR damper by using equations 3.1 to 3.4. The optimized dimensions of damper piston are given in the table 4.2.

Table 4.2 Optimal dimensions of Radial flux two-wheeler MR damper

Parameter	Dimension (mm)
Piston rod diameter (d)	14.02
Piston head diameter (D)	31.13
No. of poles	4
Fluid flow gap (g)	1
Pole length (L)	22.3



The design details and structure of the piston are picturized in figure 4.5 which is said to be a radial flux MR damper. A radial flux MR damper differs from the conventional piston design with respect to the placement of the wound coil when compared to the axial flux design.

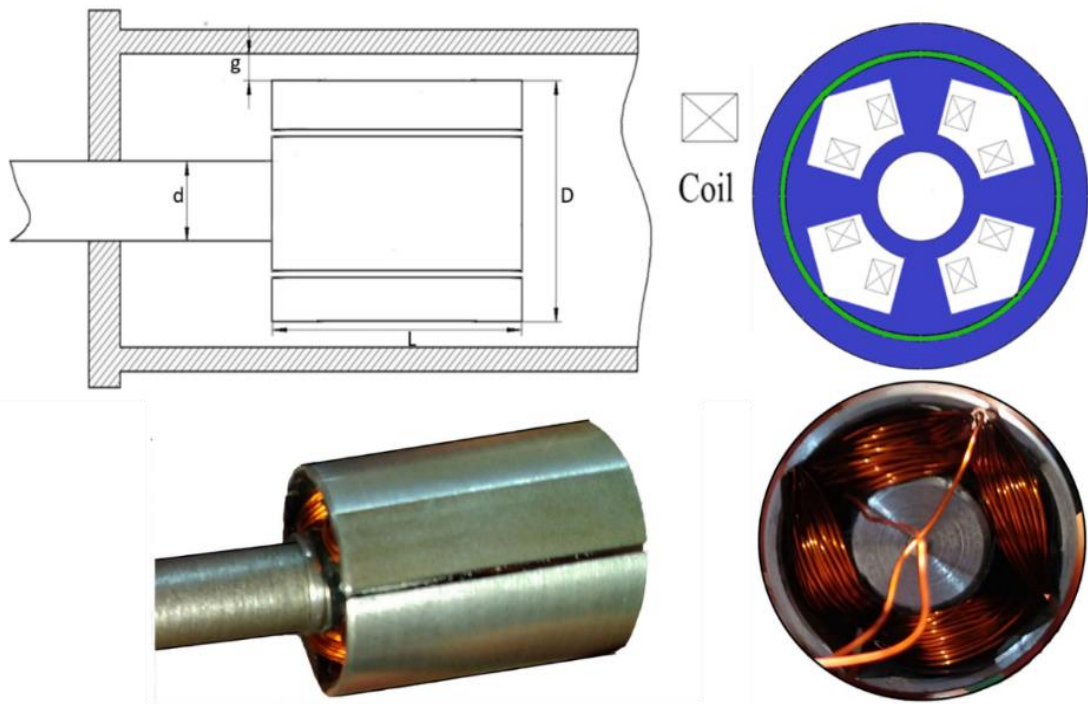


Figure 4.5 Design of Radial flux two-wheeler MR damper

In this design the coil is wound to generate a magnetic field which flows radially outwards rather than the axial design which generates the field flowing parallel to the piston rod. In order to obtain the effectiveness of the design, i.e., MR damper piston that gives significant magnetic field in the fluid flow gap, the magnetic analysis of the damper piston was performed using Finite element method magnetics (FEMM) tool. The FEMM analysis was performed for a radial flux MR damper piston with 4 poles with each pole having wound 55 turns of copper coil.

The results of FEMM analysis in figure 4.6 shows the presence of magnetic field of 0.36T in the MR fluid flow gap. The magnetic flux in the fluid flow gap increased by 20% as compared to conventional design with similar space constrains for rear suspension system of the two-wheeler vehicle.

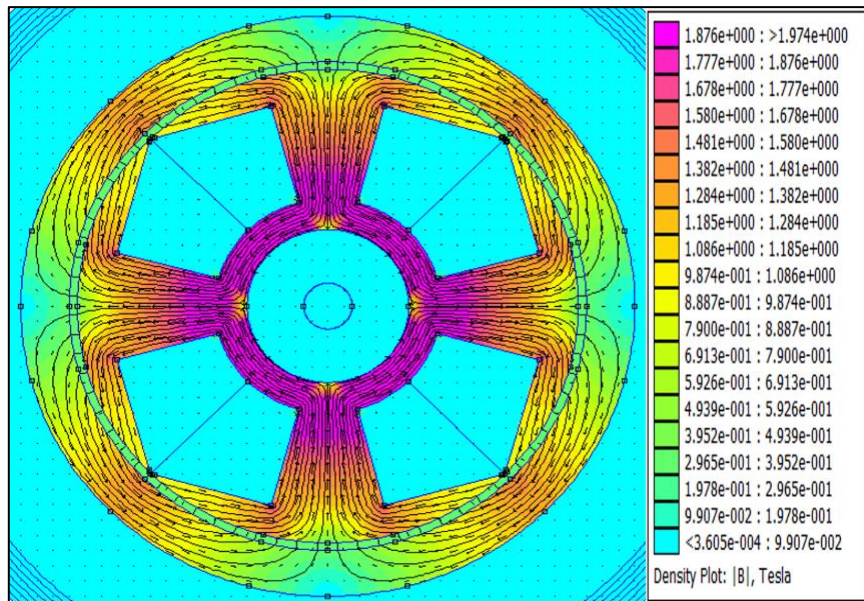


Figure 4.6 FEMM results of radial flux two-wheeler MR damper piston

The designed prototype damper was fabricated using AISI 1018 steel, a good magnetic permeability material. AWS copper of gauge 28 was wound on the electromagnetic piston to produce magnetic field. The fabricated radial flux MR damper is shown with a disassembled view in the figure 4.7.

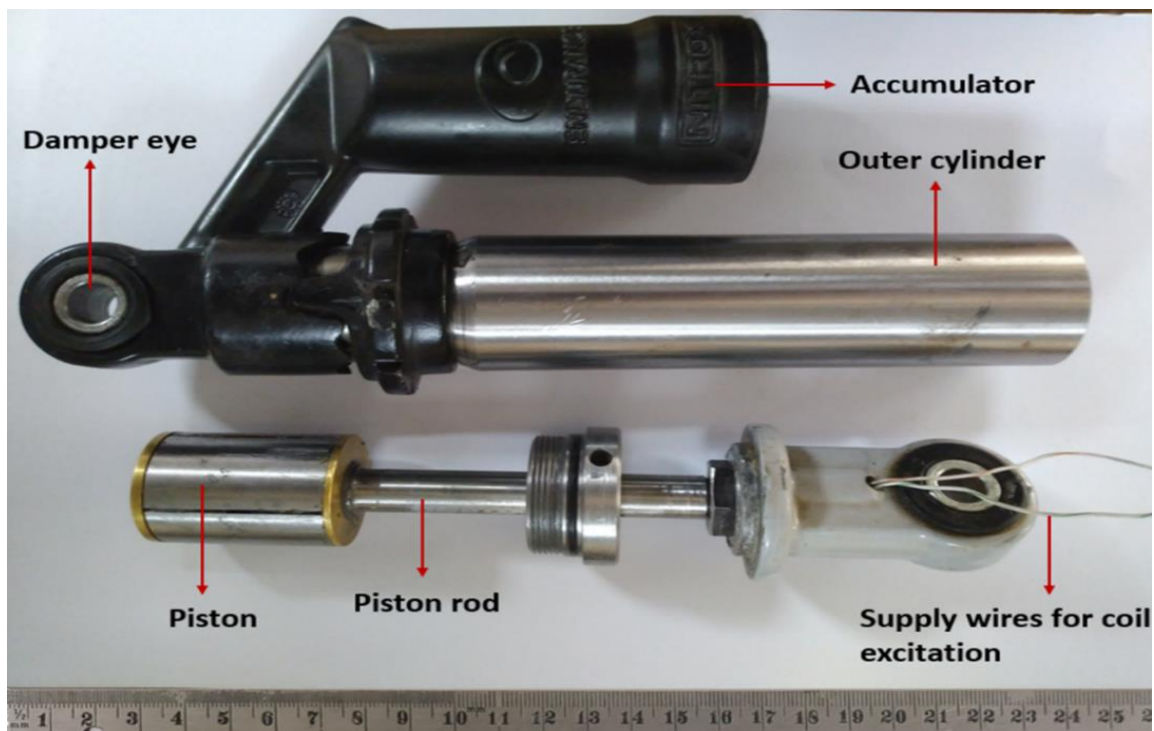


Figure 4.7 Fabricated radial flux two-wheeler MR damper disassembled view

#### 4.4 CHARACTERIZATION OF RADIAL FLUX TWO-WHEELER MR DAMPER

Damper characterization involves obtaining the force-velocity and force-displacement curves for required amplitude and frequency of sinusoidal input. Figure 4.8 shows the experimental setup used to test the damper.

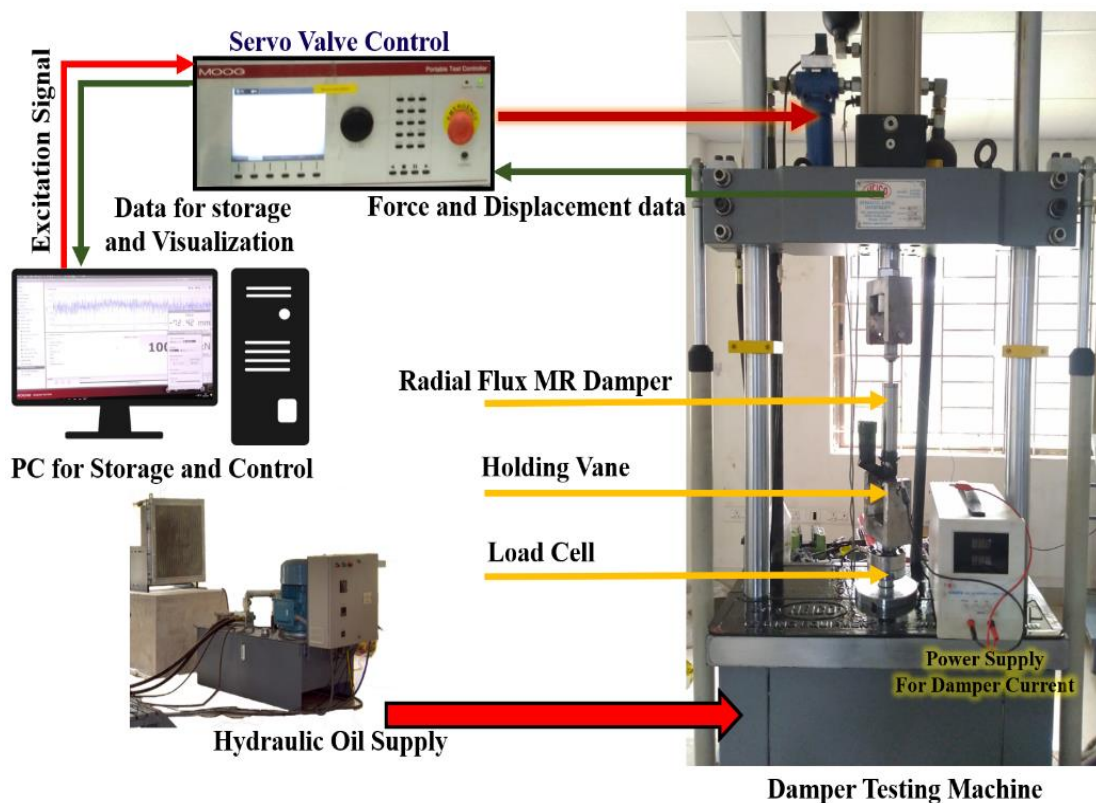
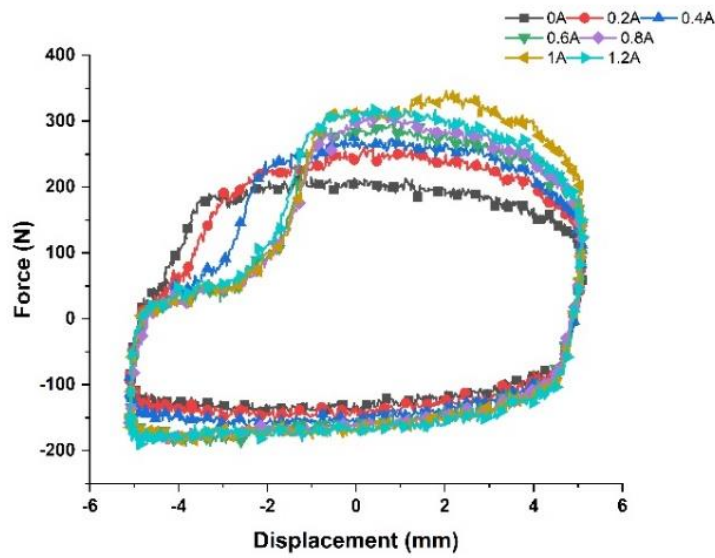


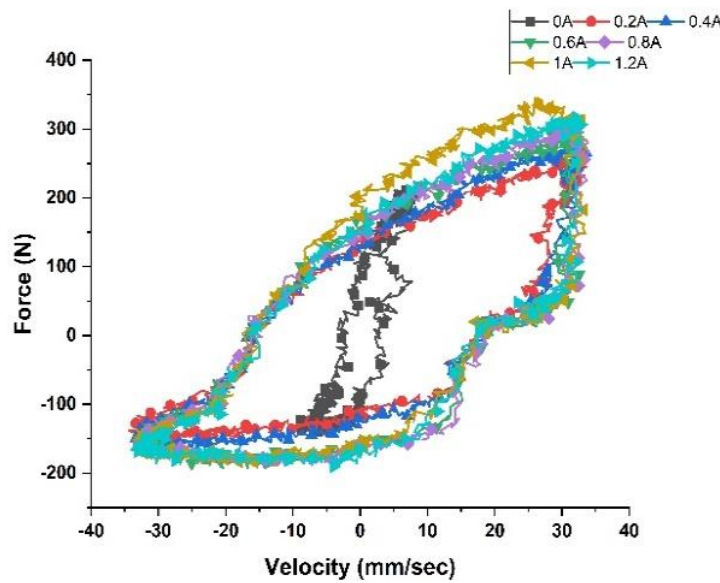
Figure 4.8 Characterization setup of radial flux two-wheeler MR damper

This work involves the characterization of damper for sinusoidal profile of frequencies 1Hz, 1.5Hz and 2Hz with an amplitude of 5mm.

The custom-made MR fluid with the characteristics specified earlier was used in the characterization of the damper and the piston of the damper was excited with current inputs ranging from 0A to 1.2A with a step increment of 0.2A.



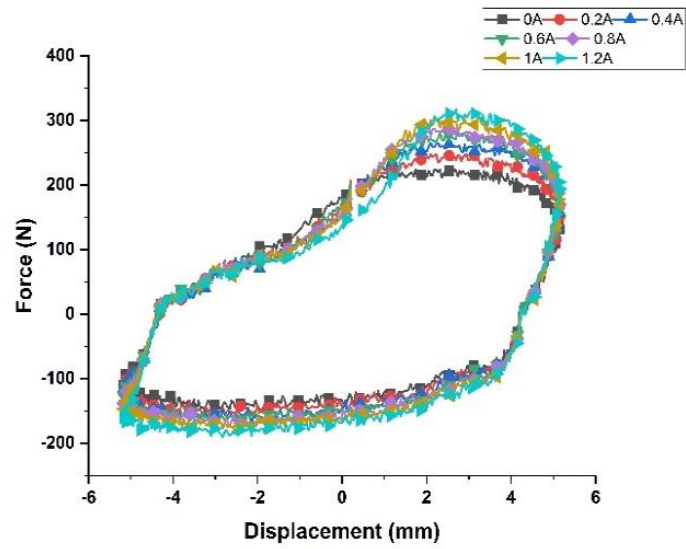
(a)



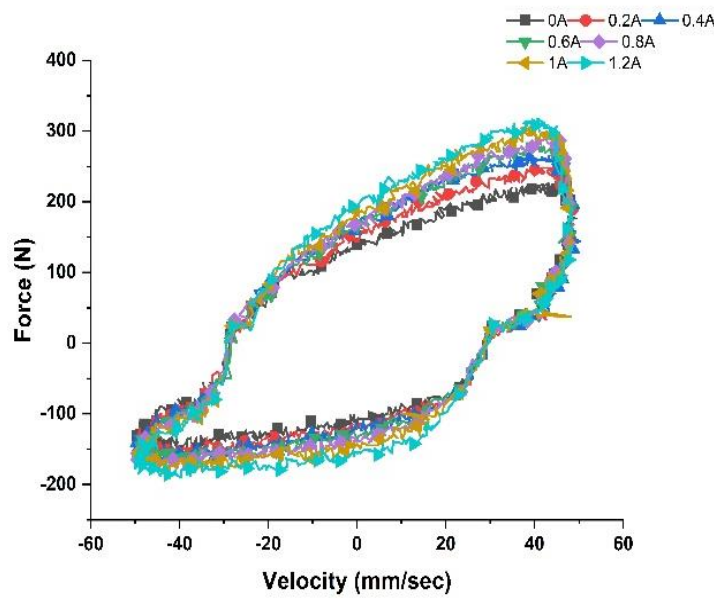
(b)

Figure 4.9 (a) Force-displacement and (b) force-velocity curves at 1Hz

From the figure 4.9 the maximum force obtained at compression and rebound with 1Hz frequency at 0A is 144.8N and 215.2N respectively. Whereas, the maximum force obtained at compression and rebound 1.2A is 190.4N and 321.5N respectively.



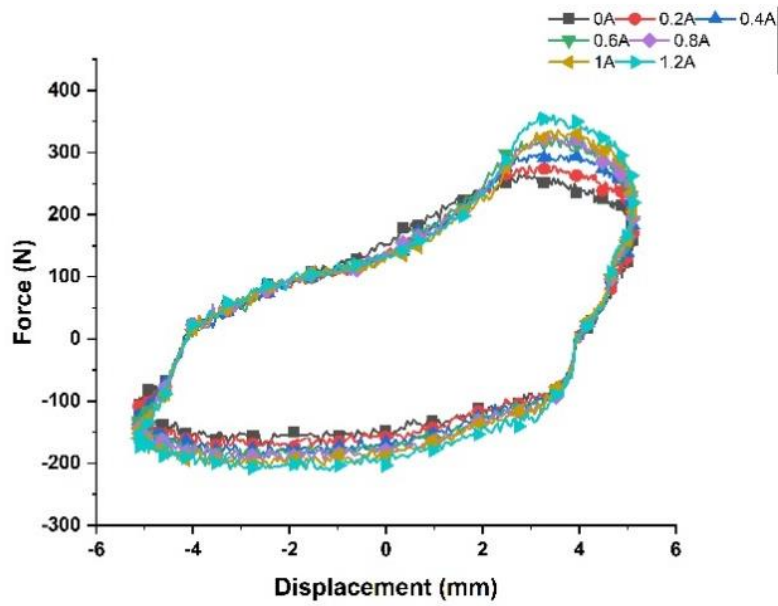
(a)



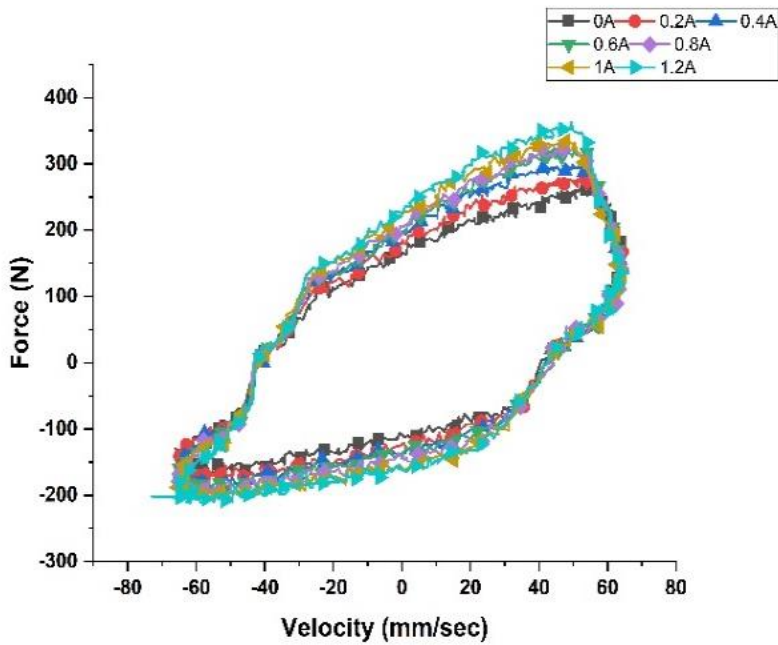
(b)

Figure 4.10 (a) Force-displacement and (b) force-velocity curves at 1.5 Hz

From the figure 4.10 the maximum force obtained at compression and rebound with 1.5 Hz frequency at 0A is 149.2N and 226.1N respectively. Whereas, the maximum force obtained at compression and rebound 1.2A is 190.4N and 317.1N respectively.



(a)



(b)

Figure 4.11 (a) Force-displacement and (b) force-velocity curves at 2Hz

From the figure 4.11 the maximum force obtained at compression and rebound with 2Hz frequency at 0A is 212.8N and 215.2N respectively. Whereas, the maximum force obtained at compression and rebound 1.2A is 212.1N and 362.7N respectively.

Results show that there is a significant improvement in maximum damping force signifying the presence of the MR effect in the damper.

#### **4.5 MODELLING OF RADIAL FLUX TWO-WHEELER MR DAMPER**

Although the kwok model and the PID control are providing a good modeling of the damper and control there are a few drawbacks with the existing modelling and control they are:

- The optimization of the parameters to be performed in the modeling of kwok model need Matlab optimisation tool box with genetic algorithm which was supported by Matlab has come to an end from 2019a version.
- The characteristic curves i.e., the Force velocity curves of the MR damper need to be accurately traced with the help of hyperbolic tangent function. Any distortion in the well-known hysteresis shape may lead to significant error between theoretical and experimental characteristic curves.
- The number of iterations and the execution time are high and requires complex calculation which are hard to be implemented in real time control (NI FPGA).
- PID control also requires inbuilt tuning option provided by the Matlab Simulink and LabView to obtain the parametric gain values of P, I, D.

The most effective and simplified solution for this issue is replacing the kwok modeling and PID control with the non-parametric polynomial model and Sliding mode control respectively. The reason for substituting with polynomial modeling is the ease of determining the dampers response considering only the maximum and minimum forces from the force velocity curves at a given current conditions. The model thus predicts polynomial equations based on the obtained forces and currents with the variable of the equations to be the velocities at that instant. On the other hand, the sliding mode control is a tracker-based control strategy, however the error signal obtainment and the process of making the system to slide over the sliding surface is quite similar to the PD control with the self-estimation of the parameters with respect to the system it is applied on. Thus, further studies are carried out considering the polynomial model with sliding mode control as the damper model and the control for the said dampers respectively.

The radial flux two-wheeler MR damper discussed in this section is modelled considering the drawbacks encountered in the implementation of the kwok model and the PID control implementation in the Axial design stated earlier. Polynomial modelling along with the sliding mode control is implemented for the radial flux piston design and the other designs stated in further chapters.

To obtain the model of MR damper, polynomial fitting was used which is a non-parametric modeling technique. Considering the three different velocities i.e., 31.4mm/s, 47.1mm/s and 62.8mm/s, the damping force  $F$ , velocity  $v$  and the damper current input  $I$  relation is modelled using polynomial fitting method by considering the maximum force (table 4.3) at rebound stroke and the minimum force at compression stroke.

Table 4.3 Maximum and minimum damping force at different current inputs

Current (A)	31.4mm/s		47.1mm/s		62.8mm/s	
	Max Force (N)	Min Force (N)	Max Force (N)	Min Force (N)	Max Force (N)	Min Force (N)
0A	215.219	-144.853	226.064	-149.191	262.939	-168.713
0.2A	260.770	-153.53	247.755	-157.868	278.123	-175.221
0.4A	278.123	-168.713	265.108	-173.052	297.649	-190.404
0.6A	259.476	-192.574	282.465	-170.883	328.012	-192.573
0.8A	314.998	-190.404	293.307	-177.39	328.012	-196.912
1A	345.365	-188.235	304.152	-181.728	336.689	-207.757
1.2A	321.505	-190.404	317.167	-190.404	362.718	-212.096

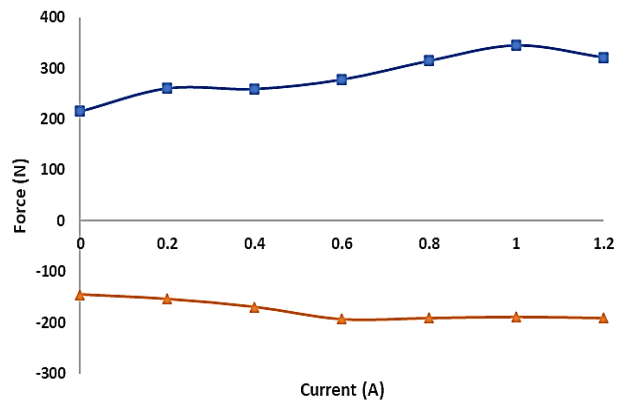
Corresponding Force Current equations for 31.4mm/s, 47.1mm/s and 62.8mm/s are given in the table 4.4 and the corresponding force current curves are represented in figure 4.12.



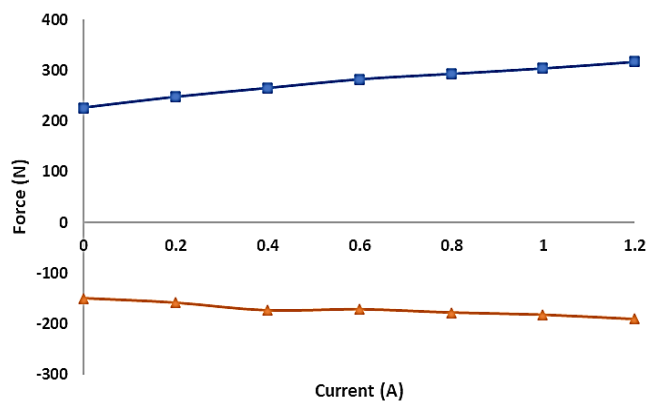
Table 4.4 Damping force equations with respect to velocity variations

Velocity	Equation
31.4mm/s	$F = -1143I^4 + 2690.5I^3 - 1976.1I^2 + 561.71I + 213.99$ for $F > 0$ $F = -302.98I^4 + 764.8I^3 - 555.21I^2 + 50.829I - 145.23$ for $F < 0$
47.1mm/s	$F = 395.42I^4 - 911.33I^3 + 616.83I^2 - 28.351I + 263.4$ for $F > 0$ $F = -10.263I^4 + 9.5647I^3 + 17.272I^2 - 53.993I - 168.02$ for $F < 0$
62.8mm/s	$F = 22.595I^3 - 67.143I^2 + 123.82I + 225.81$ for $F > 0$ $F = -45.191I^3 + 92.321I^2 - 80.7I - 148.31$ for $F < 0$

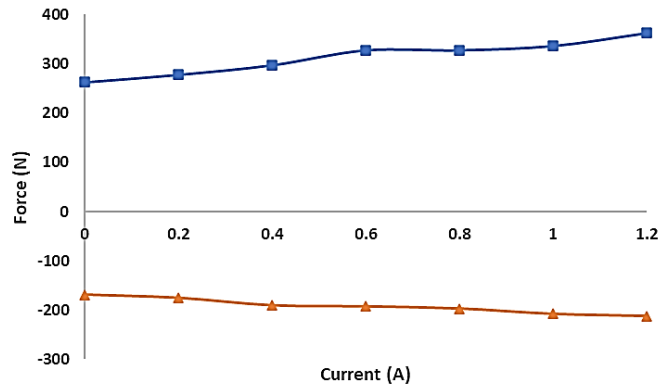
The entire process of curve fitting and estimating the polynomial curve can be performed either manually or by means of prediction algorithms. The graphs from the figure 4.22 and 4.13 clearly state the rise in the damping force with respect to the current and the damper velocity.



(a)



(b)



(c)

Figure 4.12 Force current curves at (a) 31.4mm/s (b) 47.1mm/s and (c) 62.8mm/s

The force-velocity equations for a range of currents were obtained by using polynomial fitting method considering the damping forces at seven different currents with maximum and minimum values.

Table 4.5 Force velocity equations at different currents

Current	Equation
0A	$F = 807483v^4 - 621417v^3 + 52.634v^2 + 5787.7v + 34.346$
0.2A	$F = 4E+06v^4 - 805414v^3 - 18752v^2 + 6654.2v + 68.556$
0.4A	$F = 1E+06v^4 - 806563v^3 - 3675v^2 + 6947.9v + 47.731$
0.6A	$F = -1E+06v^4 - 881022v^3 + 14513v^2 + 7457.6v + 29.664$
0.8A	$F = 3E+06v^4 - 1E+06v^3 - 12101v^2 + 8046v + 71.625$
1A	$F = -1E+06v^3 - 4339.4v^2 + 8444.4v + 78.421$
1.2A	$F = 3E+06v^4 - 959442v^3 - 11157v^2 + 8200.2v + 73.7$

The polynomial equations for the currents form 0A to 1.2A are represented in table 4.5 and the Force-velocity plot is represented in the figure 4.13.

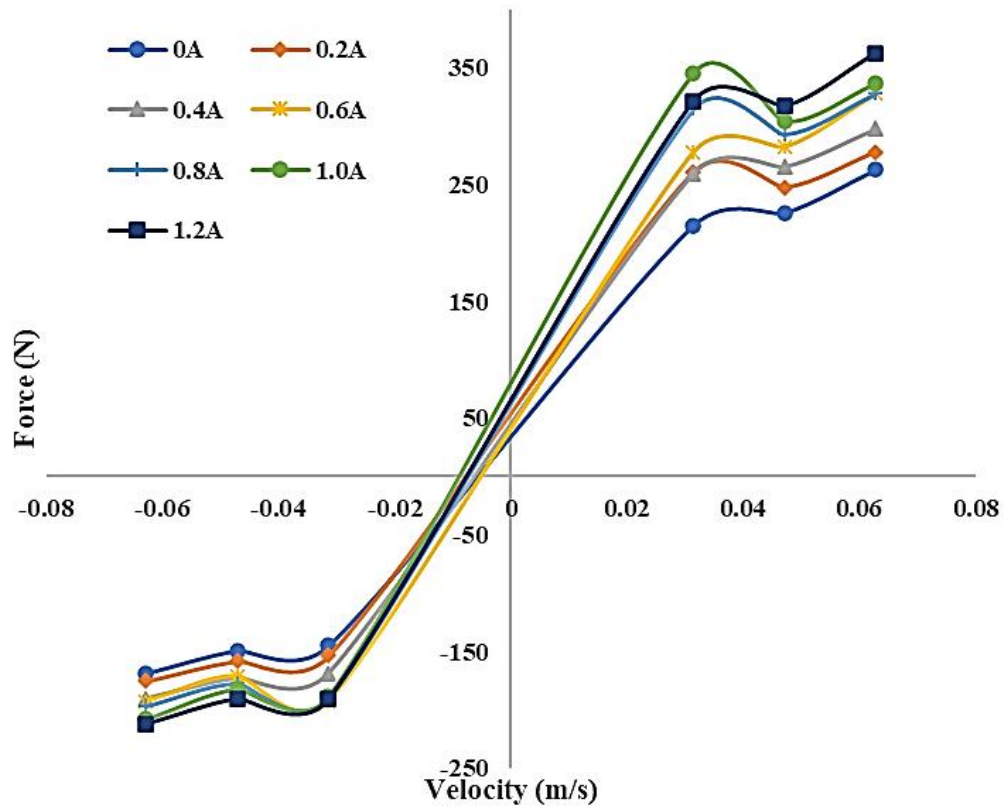


Figure 4.13 Force velocity curves at different current inputs for radial flux MR damper

The polynomial modelling of the prototype MR damper is further implemented in the analysis of the quarter car and two-wheeler suspension along with the real time control. In this aspect sliding mode control strategy is implemented in the analysis of quarter car and two-wheeler suspension.

#### 4.6 SLIDING MODE CONTROL (SMC) FOR MATHEMATICAL ANALYSIS

SMC strategy is a nonlinear tracker-based control algorithm which alters the dynamics where the system is made to move on a specific path more precisely to slide along its normal behavior depending on the control signal fed to the system. Sliding mode control well known as one of the most attractive and robust controls against system uncertainties and external disturbances. In order to attain a control law, the error equation to be formulated and it can be done in multiple ways considering the condition that

$$S \dot{S} < -\sigma |S| \quad (4.1)$$

Where,  $S$  is the sliding surface and  $\sigma$  is a positive real number. As quarter car suspension system is considered to be the plant system, being a second order system, the error equation can be considered based on the deflection of the masses or its rate of change of deflection or both depending on the which state can provide a better control law on the whole. Thus, the sliding surface  $S$  can be defined as

$$S = \dot{y}_2 + \lambda y_1 \quad (4.2)$$

$$\dot{S} = \ddot{y}_2 + \lambda \dot{y}_1 \quad (4.3)$$

Where  $y_1$  and  $y_2$  are the state variables of the system where they need to be stabilized in order to obtain the desired response of the system. In order to make the system stay on the sliding surface,  $\dot{S} = 0$ . The error input to Sliding mode control for a quarter car is the suspension deflection and the equation of sliding surface is given by:

$$S = \dot{e} + \lambda e \quad (4.4)$$

$$\dot{S} = \ddot{e} + \lambda \dot{e} \quad (4.5)$$

Where  $e$  is the suspension deflection i.e.,  $Z_s - Z_{us}$  and  $\dot{e}$  is the instantaneous velocity of the suspension deflection. The derivative of the sliding surface tends to zero as the systems slides through sliding surface

$$\dot{S} = 0 \quad (4.6)$$

Which on substitution of the values in equation 4.7 we have

$$\ddot{e} + \lambda \dot{e} = 0 \quad (4.7)$$

$$(Z_s - Z_{us}) + \lambda(Z_s - Z_{us}) = 0 \quad (4.8)$$

On substitution of the obtained sprung mass acceleration in the quarter car model in equations 4.15 and after simplification we have

$$F_d = \lambda M_s \dot{Z}_s - K_s(Z_s - Z_{us}) \quad (4.9)$$

The obtained force from the equation 4.11 is with the consideration that the system is sliding on the said sliding surface. Even though the system is not sliding

through the considered sliding surface it can be brought by formulating the control force based on the position of the system on either side of the surface and can be lured towards the sliding surface by means of a gain constant  $K_d$

$$F'_{mr} = F_d - K_d \text{sign}(S) \quad (4.10)$$

Substituting the quarter car equations, we have

$$F'_{mr} = (\dot{Z}_s)(\lambda M'_s) - K_s(Z_s - Z_{us}) - K_d \text{sign}(S) \quad (4.11)$$

Where  $M'_s$  is the sprung mass,  $K_s$  is the spring constant, where  $F'_{mr}$  is the control force to make the vehicular suspension tend towards the sliding surface. In order to estimate the current, an inverse modeling needs to be done which can be performed by applying a constant  $G$  which is proportional gain to obtain the currents and the limits are applied to the control current so that excess current does not enter the MR damper and damage the coil. The final control logic can be defined as

$$\begin{aligned} \text{If } G(F'_{mr}) > i_{max}, i &= i_{max} \\ \text{Else If } G(F'_{mr}) < i_{min}, i &= i_{min} \\ \text{Else } i &= G(F'_{mr}) \end{aligned} \quad (4.12)$$

Here  $i_{max}$  and  $i_{min}$  are 1.2A and 0A respectively for all the MR dampers designed in this study except for the axial flux bike damper and Hybrid radial flux piston damper, these dampers can have current limit of  $i_{max}=2A$ . If the control is implemented in two-wheeler suspension model, then two different controllers are implemented in the front and the rear suspension separately. The idea of implementation of these sliding mode control equations in this thesis is considered from the research papers of El-Kafafy et al. (2012) and Rajendiran et al. (2017).

#### **4.7 RESPONSE OF MMT USING RADIAL FLUX TWO-WHEELER MR DAMPER**

The parameters of the two-wheeler vehicle were considered with reference to Karanam (2016) to develop the two-wheeler model.

Table 4.6 Parameters for MMT with radial flux two-wheeler MR damper

Parameters	Value
Wheelbase ( $a_1 + a_2$ )	1.26 m
Sprung mass ( $M_s$ )	155.6 kg
Front unsprung mass ( $M_{uf}$ )	12.28 kg
Front tire damping ( $C_{tf}$ )	700 Ns/m
Distance of front unsprung from center of gravity ( $a_1$ )	0.6237 m
Front tire stiffness ( $K_{tf}$ )	180000 N/m
Front spring stiffness ( $K_{sf}$ )	24000 N/m
Distance of rear unsprung from centre of gravity ( $a_2$ )	0.6363 m
Rear unsprung mass ( $M_{ur}$ )	15.82 kg
Rear tire damping ( $C_{tr}$ )	700 Ns/m
Rear tire stiffness ( $K_{tr}$ )	180000 N/m
Rear spring stiffness ( $K_{sr}$ )	24000 N/m
Inertia ( $I_y$ )	1105 kgm <sup>2</sup>

The parameters are listed in table 4.6. The two-wheeler mathematical model was subjected to random road excitation as specified in the equation 3.15.

The suspension deflection is measured and sent to the SMC controller to produce the required control signal. This control signal is fed to the current amplifier to produce the required current for the MR damper. In order to ensure that the current fed to the damper is under the physical limitation of the damper, a current limiter is provided to limit the current between 0 to 1.2 A.

The bounded current (limited current) including the suspension deflection are fed to the MR damper. The detailed design of the control strategy is illustrated in the figure 4.14. The sliding mode control parameters i.e.,  $\lambda$  and G which are sliding mode constant and the current gain are selected based on the obtained expected force and the damping force. The obtained values for the MR damper fit MMT  $\lambda=1$  and  $G=0.3$ .

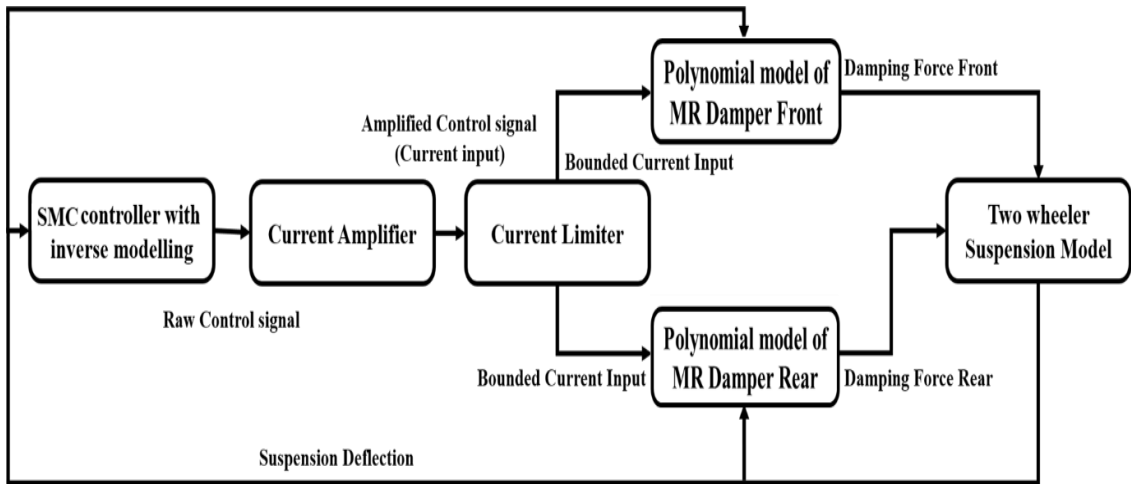
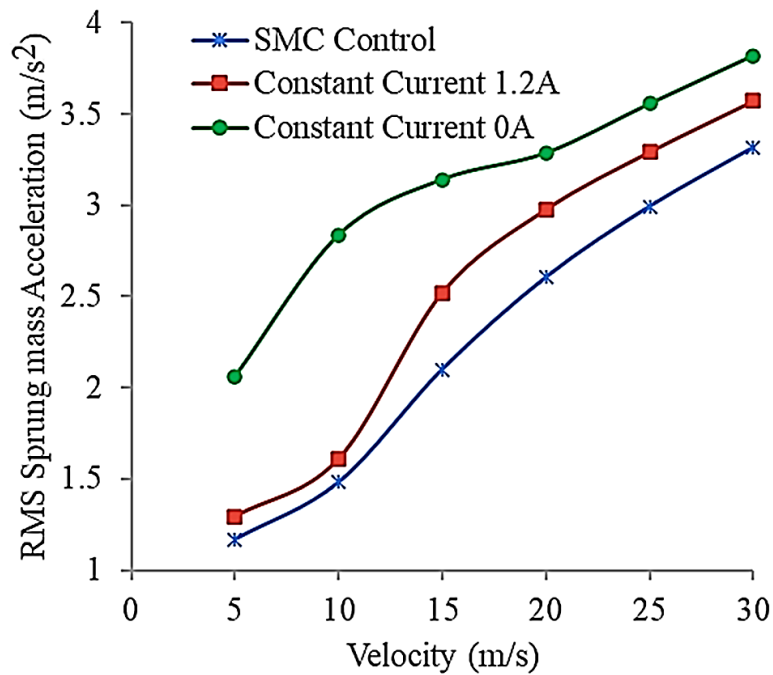
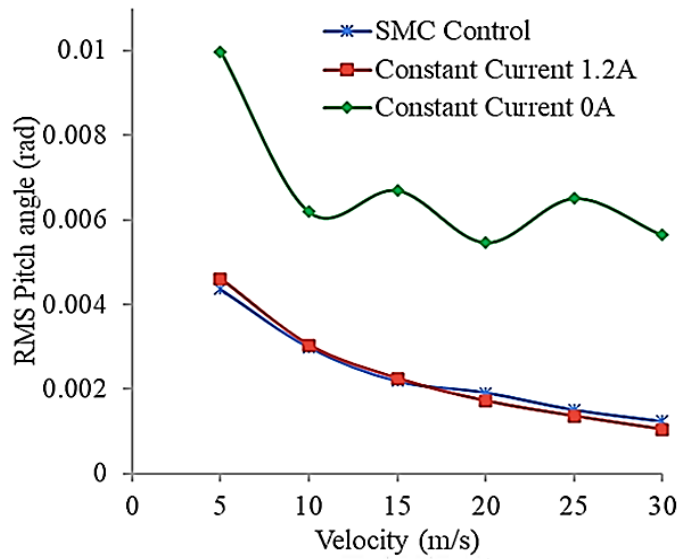


Figure 4.14 Block diagram representation of the SMC on two-wheeler suspension

The analysis of two-wheeler semi active suspension model with off state, sliding mode control and 1.2 A constant current semi-active suspension system has been carried out under random irregularities for different vehicle velocities. The vertical acceleration responses of semi-active two-wheeler suspension at various speeds are illustrated in figure 4.15(a). It is observed that sprung mass acceleration has been reduced to 43.4% in case of sliding mode-controlled suspension system when compared with the off-state response at 5 m/s vehicular velocity.



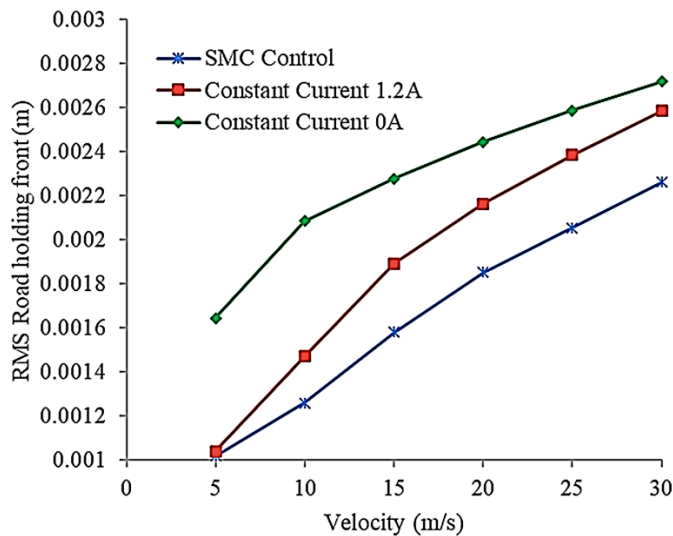
(a)



(b)

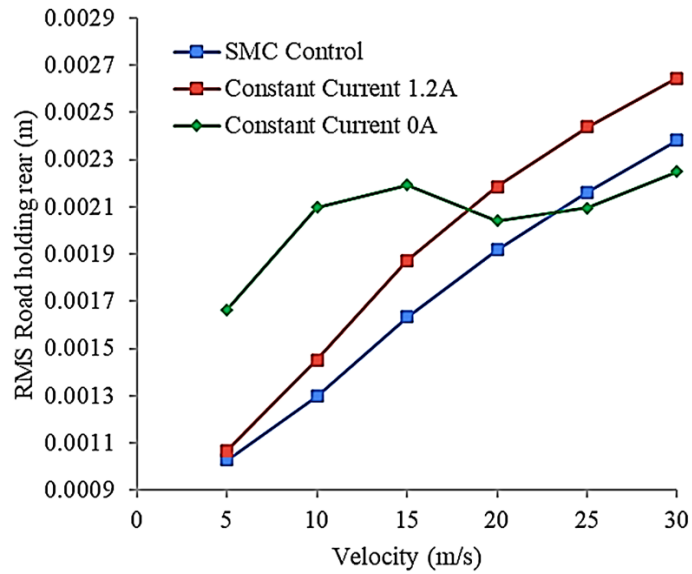
Figure 4.15 (a) Sprung mass RMS acceleration and (b) pitch angle with SMC control

Figures 4.16 (a) and (b) demonstrate the road holding nature of the two-wheeler suspension at front and rear wheel, respectively, with different vehicle velocity. It is observed that two-wheeler model with developed polynomial modelled MR based suspension system provides about 38% improved road holding (at front wheel) with sliding mode controlled current input. It was also observed that the performance of the system was not up to the mark at rear position in terms of road holding. Hence, still there is a scope for improving the damper performance at rear position.



(a)





(b)

Figure 4.16 Road holding of (a) front and (b) rear different current inputs

The analysis of pitch angle motion of the sprung mass showed very little improvement using MR damper with SMC controller when compared to off-state condition (figure 4.15(b)). The developed MR damper in two-wheeler semiactive suspension model showed a good improvement in performance with SMC controller in terms of RMS acceleration of sprung mass and road holding at front unsprung position of the vehicle.

#### 4.8 REAL-TIME CONTROL OF RADIAL FLUX MR DAMPER IN TWO-WHEELER VEHICLE

The MR damper was designed to be fitted and controlled on the rear end of the vehicle in order to provide better suspension deflection in order to provide minimal variation in the sprung mass velocity. The fabricated prototype MR damper is fit to a two-wheeler light motor vehicle (Pulsar 200, Make: Bajaj corporation) and real-time (RT) experimentation is carried out considering a road of profile as shown in figure 4.17.

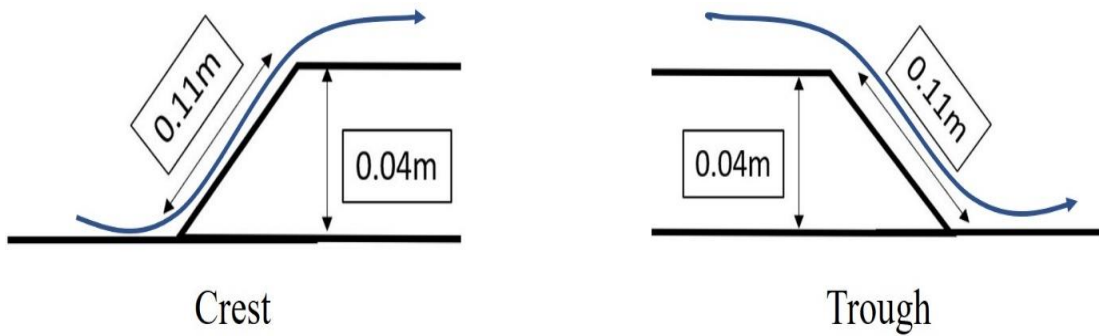


Figure 4.17 Road Profile for RT control of radial flux two-wheeler MR damper

The MR dampers are fit to the rear end of the vehicle on either side with the ends of the piston coil connected to a current controller by means of a current sensor (ACS712) in order to acquire the real time power consumed by the damper. The entire control is pictorially illustrated in figure 4.18.

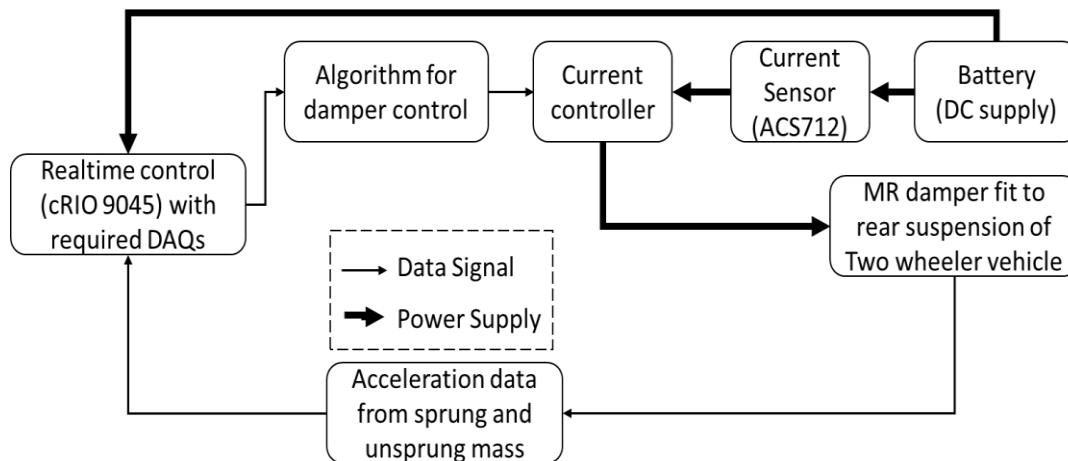


Figure 4.18 Schematic for the RT control of radial flux two-wheeler MR damper

The setup is energized using a Li-polymer battery of 11.1V 3S with a capacity of 5000mAH. An equal amount of current is fed to both sides of the damper and each of the dampers is connected to an individual current controller. The pictorial representation of the total setup is specified in figure 4.19. The resultant vibrations created by the road profile are measured using uniaxial accelerometers with a sensitivity of 100mV/g connected to both sprung as well as unsprung masses of vehicle considering the rear suspension system. These accelerometers work on 4mA constant current source fed through the NI hardware and data acquisition board

namely NI 9230 which is connected to the accelerometers by means of BNC cables. The data acquisition card 9230 takes the acceleration variation as input and sends the data to the actual control board with chassis for housing the data acquisition as well as control. NI-cRIO-9045 with an 8-slot chassis is used for data acquisition as well as control. Considering NI 9230 card for acceleration data acquisition, the NI 9205 is used for reading instantaneous current fed to the MR dampers.



Figure 4.19 Two-wheeler RT experimentation test setup along with the controller

The digital input output card namely 9403 is used for generating the PWM control pulse which triggers the current controller thereby providing a controlled current to be fed to the damper.

#### 4.8.1 Control laws implemented in real time control

Skyhook, Ground hook and SMC control strategies are implemented in the real time implementation of the prototype MR damper on vehicular systems. SMC control was implemented considering two different error signals. The error signal sprung mass deflection and both suspension deflection and sprung mass velocity are considered in SMC1 and SMC2. A brief explanation on the control laws used is specified in the following sub sections.

##### 4.8.1.1 Skyhook and Groundhook control

Skyhook and ground hook control algorithms are basic algorithms which are based on the sprung mass velocity and unsprung mass velocity irrespective of the system parameters. Skyhook and Groundhook controls can be implemented by ON-OFF control considering the error signal to be the relative velocity of the vehicular body (sprung mass) and the wheel of the vehicle (unsprung mass) associated with the sprung mass for skyhook control and unsprung mass for ground hook control. When the error signal is greater than zero the damper is set to on state with maximum current and nil current otherwise. The equation for the current is as follows:

$$\left\{ \begin{array}{l} \dot{Z}_s (\dot{Z}_s - \dot{Z}_{us}) > 0, i = i_{\max} \\ \dot{Z}_s (\dot{Z}_s - \dot{Z}_{us}) \leq 0, i = i_{\min} \end{array} \right\} \text{skyhook} \quad (4.13)$$

$$\left\{ \begin{array}{l} -\dot{Z}_{us} (\dot{x}_{sp} - \dot{Z}_{us}) < 0, i = i_{\max} \\ -\dot{Z}_{us} (\dot{Z}_{sp} - \dot{Z}_{us}) \geq 0, i = i_{\min} \end{array} \right\} \text{groundhook} \quad (4.14)$$

##### 4.8.1.2 Sliding mode control with different control laws

In order to attain a control law, the error equation to be formulated and it can be done in multiple ways considering the condition that

$$S \dot{S} < -\sigma |S| \quad (4.15)$$

Where, S is the sliding surface and  $\sigma$  is a positive real number. As quarter car suspension system is considered to be the plant system, being a second order system, the error equation can be considered based on the deflection of the masses or its rate of change of deflection or both depending on the which state can provide a better control law on the whole. Thus, the sliding surface S can be defined as

$$S = \dot{y}_2 + \sigma y_1 \quad (4.16)$$

$$\dot{S} = \ddot{y}_2 + \sigma \dot{y}_1 \quad (4.17)$$

Where  $y_1$  and  $y_2$  are the state variables of the system where they need to be stabilized in order to obtain the desired response of the system. In order to make the system stay on the sliding surface,  $\dot{S} = 0$ . In this work two different control strategies SMC1 and SMC2 considering different sliding surfaces i.e., suspension deflection and suspension deflection along with velocity are considered as the error signals. They are mathematically stated below.

$$S_1 = (\dot{x}_{sp} - \dot{x}_{ref}) + \sigma(x_{sp} - x_{ref}) = \dot{x}_{sp} + \sigma x_{sp} \quad (4.18)$$

$$\dot{S}_1 = \ddot{x}_{sp} + \sigma(\dot{x}_{sp}) \quad (4.19)$$

where  $x_{ref} = 0$  (initial reference value = 0)

$$S_2 = \dot{x}_{sp} + \sigma(x_{sp} - x_{usp}) \quad (4.20)$$

$$\dot{S}_2 = \ddot{x}_{sp} + \sigma(\dot{x}_{sp} - \dot{x}_{usp}) \quad (4.21)$$

replacing the  $\ddot{x}_{sp}$  from the quarter car equations we have

$$F'_{mr1} = (\dot{x}_{sp})(\sigma M'_{sp}) - K_{sp}(x_{sp} - x_{usp}) \quad (4.22)$$

$$F'_{mr2} = (\dot{x}_{sp} - \dot{x}_{usp})(\sigma M'_{sp}) - K_{sp}(x_{sp} - x_{usp}) \quad (4.23)$$

Where  $M'_{sp}$  is the sprung mass,  $K_{sp}$  is the spring constant,  $F'_{mr1}$  is the control force obtained of the quarter car model when the system is stable or when the system

is sliding on the sliding surface. When the system is outside the sliding surface the equilibrium is attained by

$$F_{c1} = F'_{mr1} - K_o M'_{sp} \text{sign}(S_1) \quad (4.24)$$

$$F_{c2} = F'_{mr2} - K_o M'_{sp} \text{sign}(S_2) \quad (4.25)$$

Where  $F_{c1}$ ,  $F_{c2}$  are the control forces to make the vehicular suspension tend towards the sliding surface. In order to estimate the current, an inverse modeling needs to be done which can be performed by applying a constant  $G$  which is proportional gain to obtain the currents and the limits are applied to the control current so that excess current does not enter the MR damper and damage the coil. The final control logic can be defined as

$$\text{If } G (F_c - F_a) \text{sign}(F_a) > i_{max}, i = i_{max}$$

$$\text{Else If } G (F_c - F_a) \text{sign}(F_a) < i_{min}, i = i_{min} \quad (4.26)$$

$$\text{Else } i = G (F_c - F_a) \text{sign}(F_a)$$

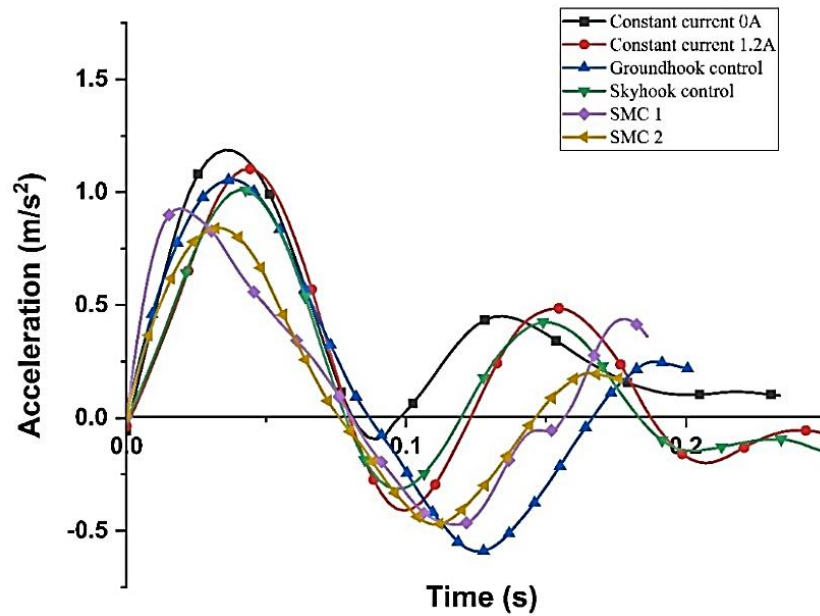
Here  $i_{max}$  and  $i_{min}$  are 1.2A and 0A respectively for each MR damper and the  $F_a$  is the actual force estimated considering the polynomial modeling of the MR damper presented in the previous sub sections for their respective dampers.

#### **4.9 RESULTS OF REAL-TIME CONTROL WITH SMC CONTROL ON TWO-WHEELER VEHICLE WITH RADIAL FLUX MR DAMPER**

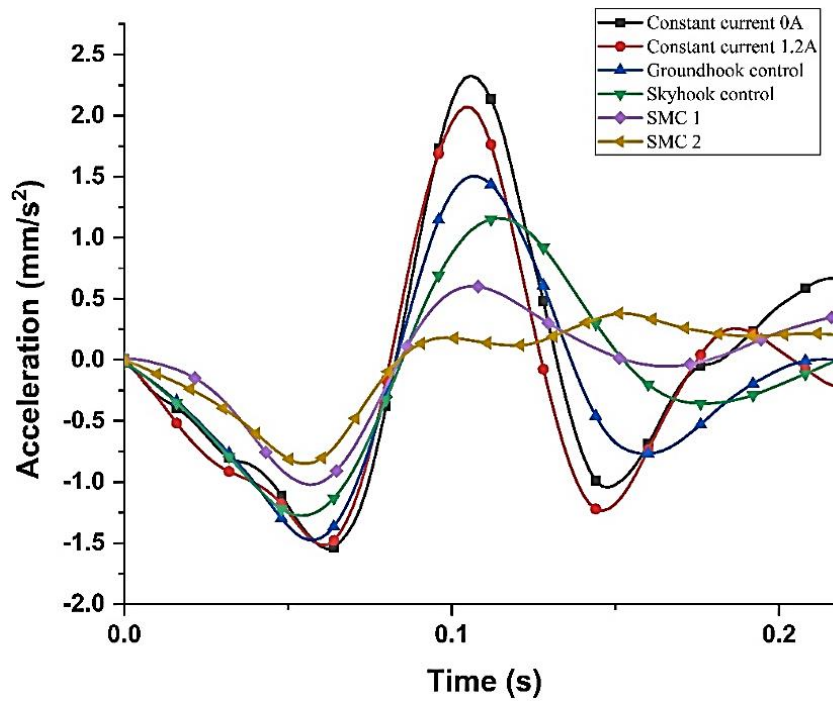
The control equipment with cRIO 9045 with data acquisition cards, current sensor, battery, including the current controller are fit in a carton box placed in front of the rider and verified for no electric leakages. The entire vehicle testing was conducted maintaining a vehicular velocity of 20kmph.

Although vehicular velocity is maintained, the path in which the vehicle exactly follows is uncertain which makes the time domain data unreliable for analyzing the performance of the damper. Therefore, filtering the data shows a better understanding of the damper performance.

A third order Butterworth lowpass filter was used in filtering the noise and engine vibrations as the cutoff frequency was set to 20Hz.



(a)



(b)

Figure 4.20 Realtime sprung mass acceleration response to the (a) Crest Road input and (b) trough

The time domain representations of sprung mass acceleration for road irregularities are picturized in figure 4.20.

Table 4.7 Sprung mass acceleration in response to crest road profile

<b>Control Logic</b>	<b>Peak Value (m/s<sup>2</sup>)</b>	<b>% Reduction</b>
Constant Current 0A	1.1872	
Constant Current 1.2A	1.1036	7.04
Groundhook Control	1.0555	11.09
Skyhook Control	1.0092	14.99
Sliding Mode Control 1 (SMC1)	0.9277	21.8
Sliding Mode Control 2 (SMC2)	0.8409	29.17

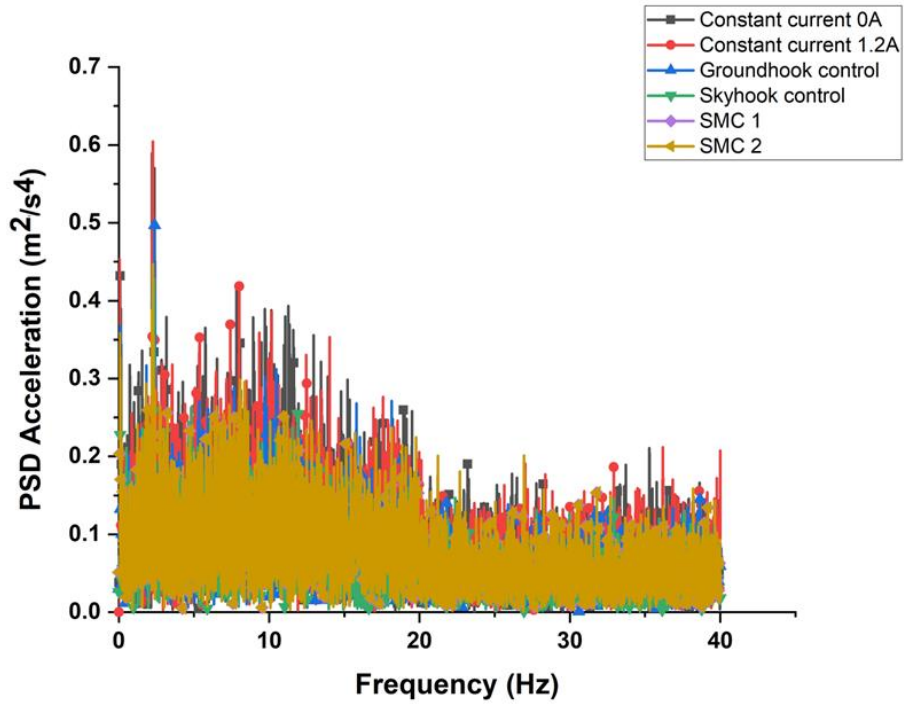
The peak acceleration recording of the sprung mass is observed using the time domain graphs and are tabulated in table 4.7 and 4.8. It is observed that with the change in control logic, the amplitude reduction is observed for SMC2 more than SMC1 and other control strategies.

Table 4.8 Sprung mass acceleration in response to trough road profile

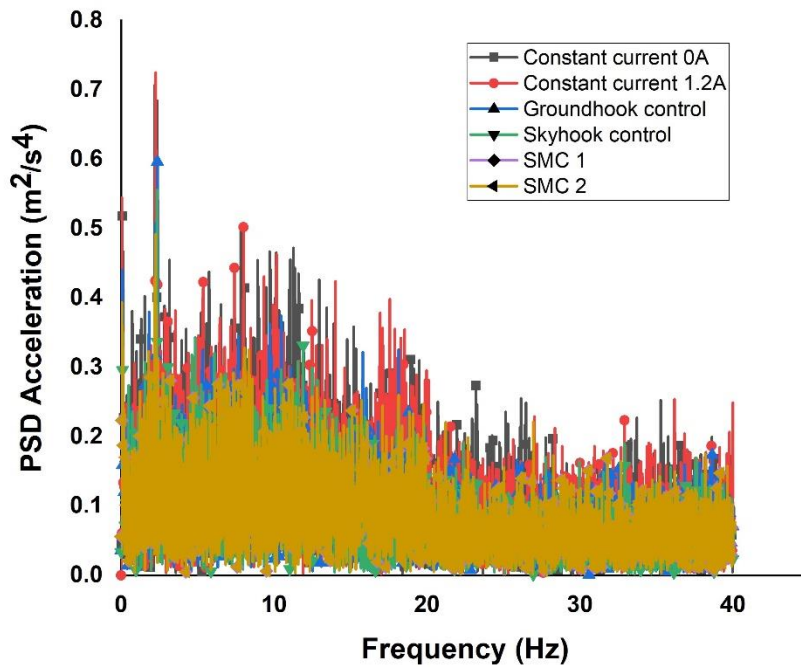
<b>Control Logic</b>	<b>Minimum Value</b>	<b>% Reduction</b>
Constant Current 0A	-1.54864	
Constant Current 1.2A	-1.51535	2.15
Groundhook Control	-1.47576	4.77
Skyhook Control	-1.27594	17.6
Sliding Mode Control 1 (SMC1)	-1.16088	25.03
Sliding Mode Control 2 (SMC2)	-1.0949	29.30

The results of the frequency domain graph (figure 4.21) also specifies that the vehicular acceleration is reduced by the application of sliding mode control when compared with the off-state of MR damper. It can also be observed that the natural frequency of the vehicle is about 2.4Hz.





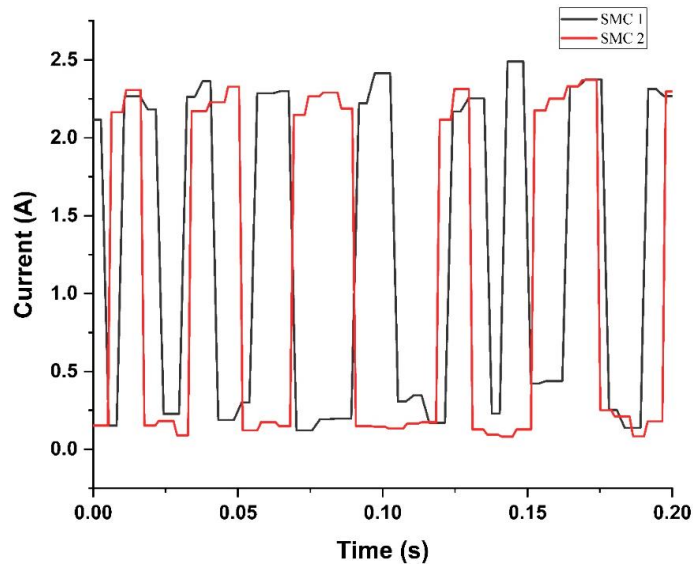
(a)



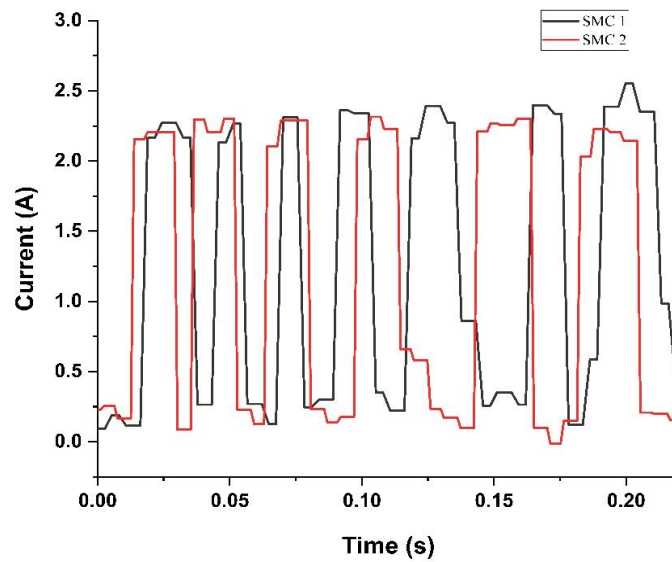
(b)

Figure 4.21 Real time sprung mass acceleration response to (a) crest and (b) trough road input in the frequency domain

The damper currents in figures 4.22 (a) and (b) are the currents generated from the battery and are tabulated by means of a current sensor connected at the output of the battery. This means that the graph shows total drawn current from the battery by both the dampers installed. From the graph it is clearly observed that the maximum current drawn is 2.5A and minimum current drawn is 0A.



(a)



(b)

Figure 4.22 Damper currents obtained at the impact of (a) crest and (b) trough

#### **4.10 SUMMARY**

The designed damper was providing a magnetic flux density of 0.36 T within the fluid flow gap which is 20% higher than the axial design and was able to provide a considerable change in the damping force with respect to change in the current supply to the damper. The analysis of the damper in quarter car and two-wheeler mathematical models has shown improvement in the sprung mass acceleration reduction. Also, real-time control of the dampers fit to the vehicle (pulsar 200) was able to provide 29.17% and 29.3% reduction in the peak sprung mass acceleration for crest and trough road profiles when compared to the off-state condition.



## CHAPTER 5

### DESIGN AND ANALYSIS OF AXIAL FLUX AND RADIAL FLUX BASED MR DAMPERS FOR E-BICYCLE

#### 5.1 INTRODUCTION

As specified in the previous sub sections, similar designs of MR damper were considered with a smaller packing fraction so as to fit the final fabricated product in an e-bicycle which is a modification of a basic bicycle named crest of atlas bicycles make. The detailed description of the designed and fabricated dampers along with the MR fluid used is specified in the following sub sections of this chapter.

#### 5.2 SYNTHESIS AND CHARACTERISATION OF MR FLUID

MR fluid in this study is a combination of three components. Fork oil was taken in a container and grease was added into it. This mixture was allowed to stir for up to an hour. Then carbonyl iron particles were added into it and allowed to stir for 12-14 hours until properly mixed. The prepared MR fluid is then used for tests. MR fluid was prepared by mixing base fluid, magnetic particles and additives. This work uses micron sized carbonyl iron particles as magnetic particles and fork oil with a viscosity of 40 c.s.t as carrier fluid. Grease is used as an additive to prevent sedimentation in the carrier fluid. Table 5.1 shows the composition of MR fluid used in this work.

Table 5.1 Composition of MR fluid for e-bicycle damper

<b>Ingredients</b>	<b>Weight Percentage</b>
Carbonyl iron particles	50
Fork oil	45
Grease	5

To obtain the rheological properties of the MR fluid, rheometer is used. The Rheology of MR fluid prepared is obtained using a rheometric test and the figure 5.1 to 5.3 represents the various rheometric results obtained.

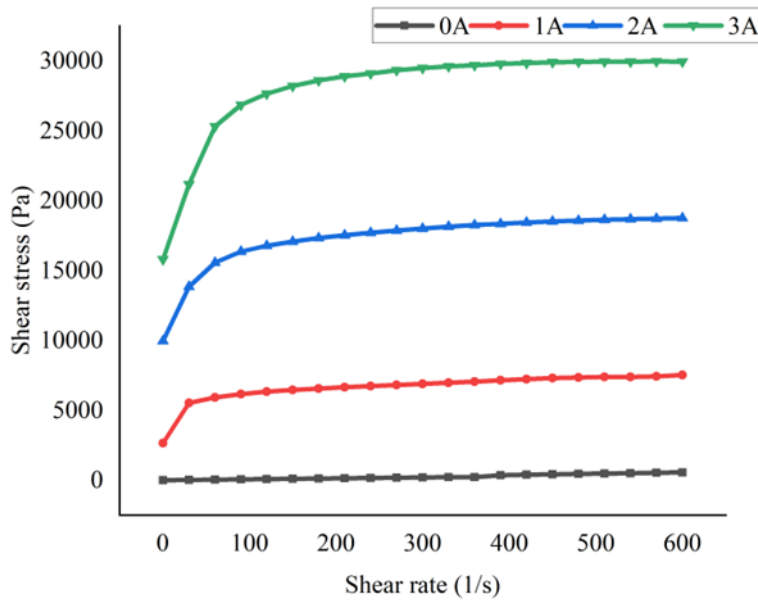


Figure 5.1 Shear rate vs shear stress at different currents of prepared MR fluid

Figure 5.1 represents the shear rate verses shear stress plots obtained at currents of 0A, 1A, 2A, and 3A. In the absence of magnetic field i.e., at 0A the Shear stress varies linearly with Shear rate.

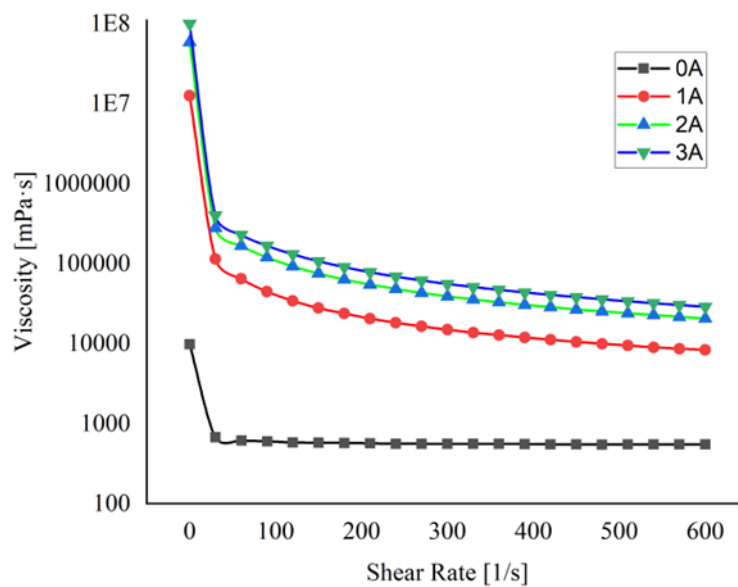


Figure 5.2 Shear rate vs viscosity at different currents of prepared MR fluid

With the application of external current, the relation between shear rate and shear stress becomes nonlinear. The maximum shear stress obtained at 0A, 1A, 2A and 3A are 328.55Pa, 5016.9Pa, 12313Pa and 17274Pa respectively.

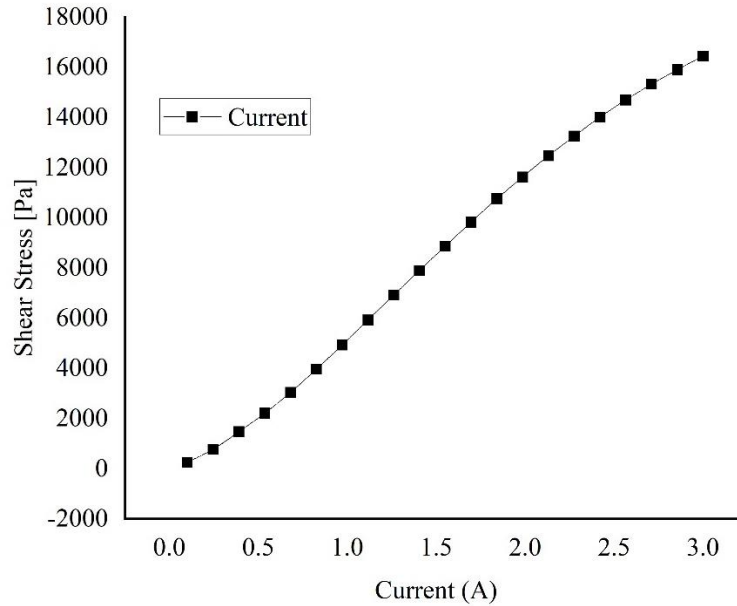


Figure 5.3 Currents vs shear stress of prepared MR fluid

Figure 5.2 represents the shear rate verses viscosity plots obtained at currents of 0A, 1A, 2A, and 3A. The maximum viscosity obtained at 0A, 1A, 2A and 3A are 9811.5 mPa.s,  $1.26 \times 10^7$  mPa.s,  $5.86 \times 10^7$  mPa.s and  $9.88 \times 10^7$  mPa.s respectively. Figure 5.3 illustrates the change in shear stress with respect to current. This signifies the effect of magnetic field on the fluid as the shear stress of the fluid acts almost linearly increasing with increase in the applied current in the rheometer.

### 5.3 DESIGN OF E-BICYCLE MR DAMPERS WITH AXIAL FLUX PISTON

As specified in the previous chapters, the design procedures are followed towards axial flux-based e-bicycle MR damper by using equations 3.1 to 3.4. The optimized dimensions of damper piston are given in the table 5.2.

Table 5.2 Dimensions of axial e-bicycle MR damper

Design Parameters	Dimensions in mm
Piston head diameter	22
Piston rod diameter	10
Cylinder outer diameter	28
Cylinder inner diameter	24
Fluid flow gap	1
Piston size (length)	15

Finite Element Method Magnetics (FEMM) tool was used to perform the magnetic analysis of MR damper piston. The analysis was performed for axial flux piston-based MR damper bearing a 100 turns of coil winding.

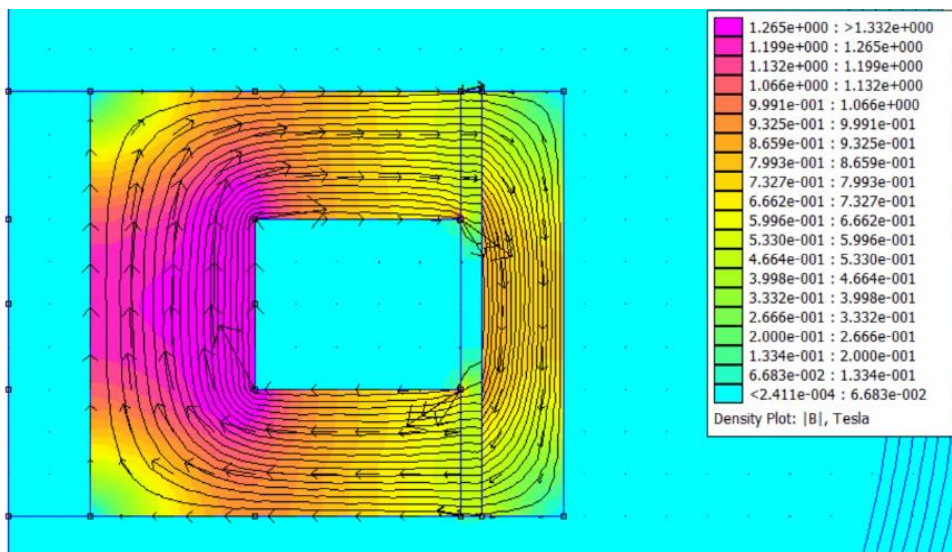


Figure 5.4 FEMM result of axial flux piston designed for e-bicycle MR damper

The pole design is similar to the solenoid design and adjacent poles are wound in opposite directions so as to create opposite magnetic flux. Figure 5.4 shows the FEMM analysis results of MR damper piston. The FEMM analysis results shows that there is a magnetic flux density of 0.48T in MR fluid flow gap.

The damper analysis in FEMM constitutes of the cross-sectional view of the MR damper as the produced magnetic field forms a closed path from one pole to another



as the poles are wound with coil winding in plane which provides the generated flux in parallel with the piston rod.

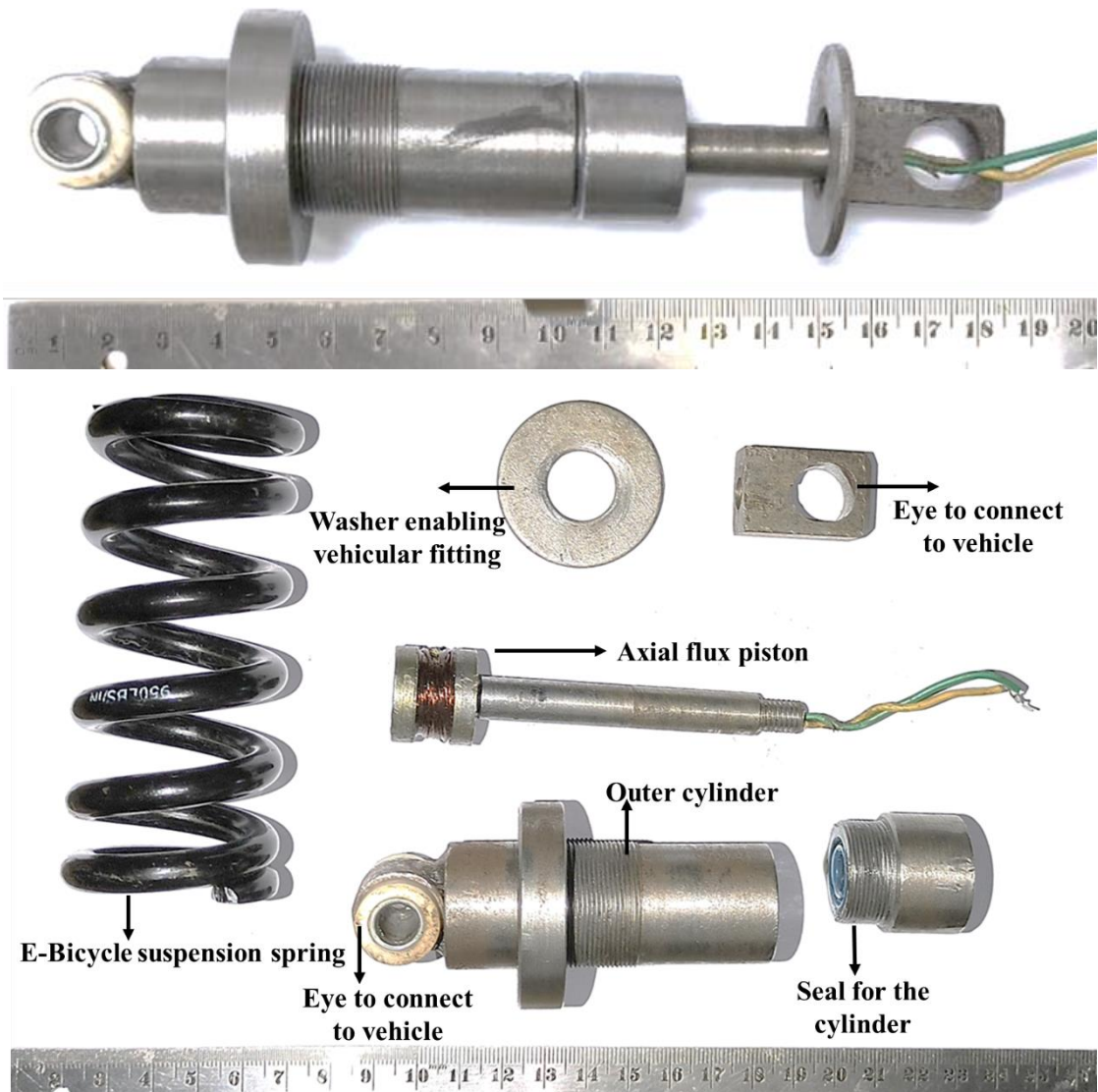


Figure 5.5 Assembled and disassembled view of axial flux e- bicycle MR damper

The material used in fabrication of this MR damper is mild steel. Figure 5.5 shows the images of fabricated damper in its assembled and disassembled view.

#### 5.4 CHARACTERIZATION OF AXIAL FLUX E-BICYCLE MR DAMPER

Using the damper testing machine (figure 5.6), the force-displacement characteristics of a specially built MR damper are measured. To understand the

damper's dynamic behaviors, a sinusoidal profile with a range of amplitudes and frequencies is typically used for characterization of the MR damper.

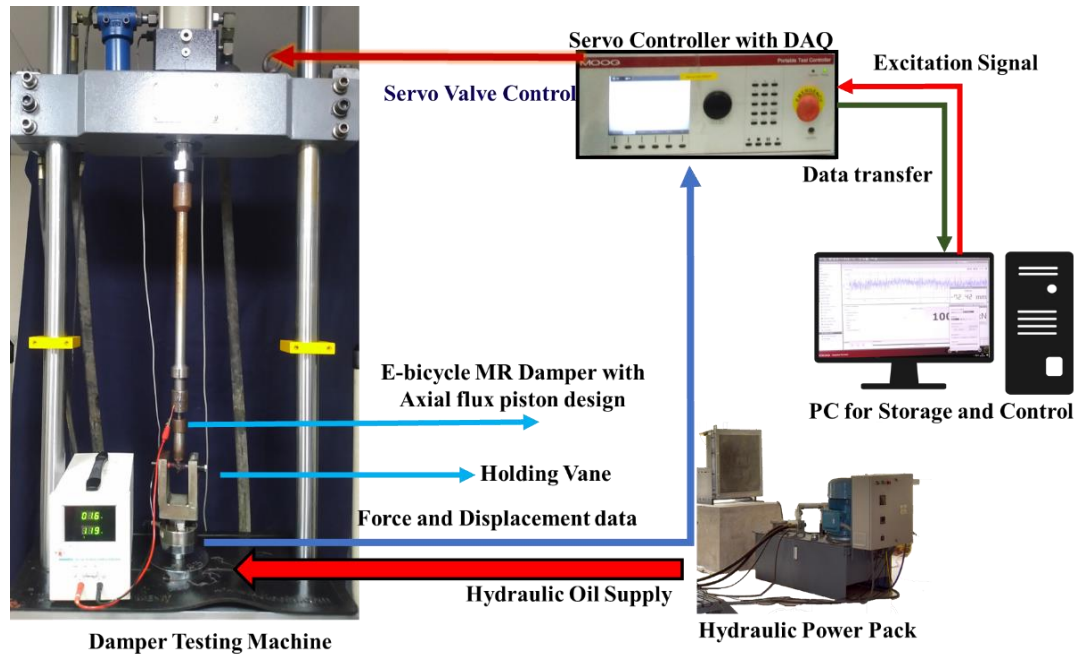
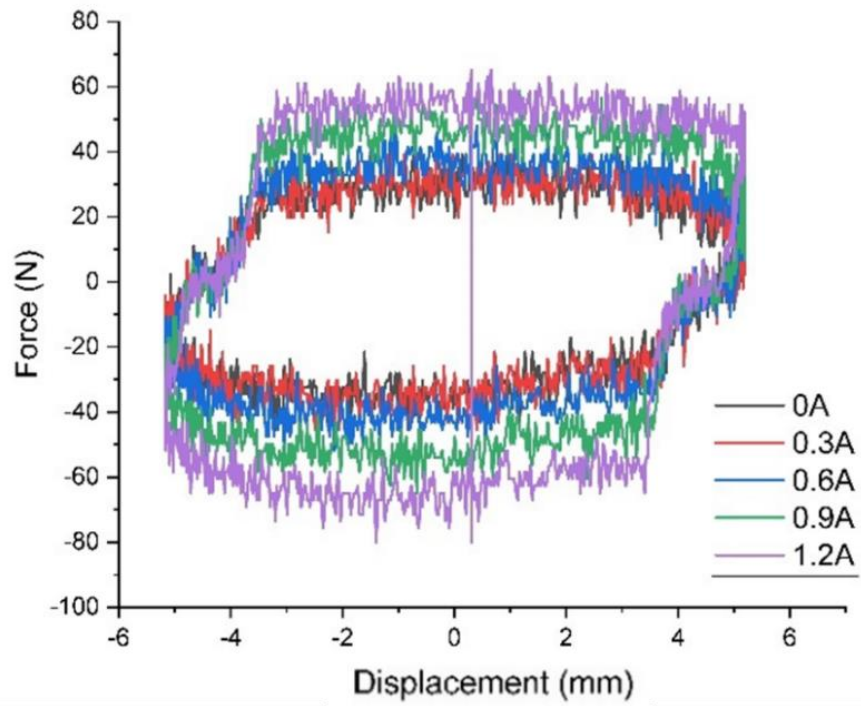
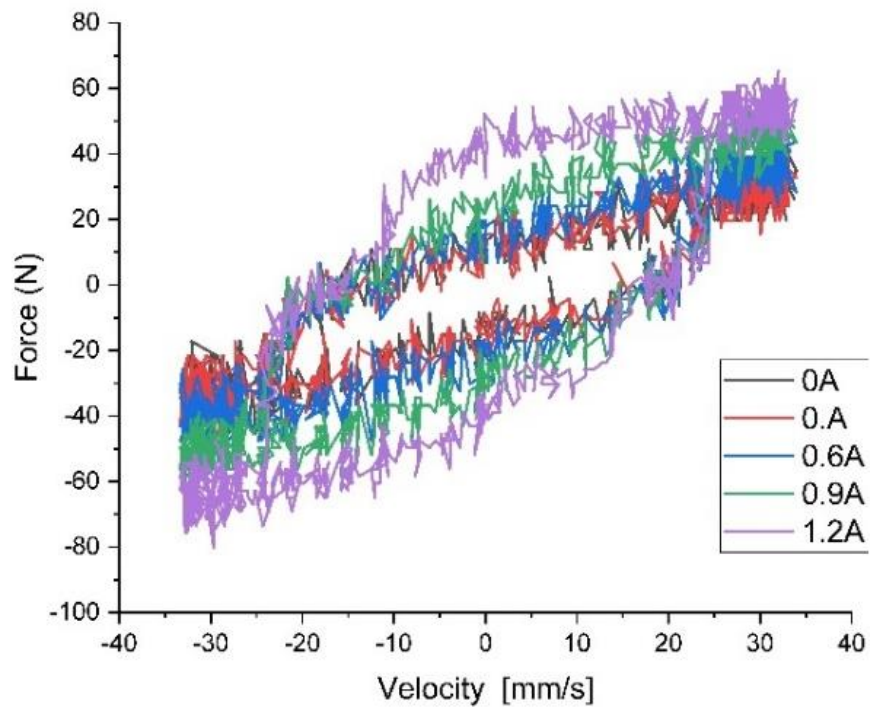


Figure 5.6 Characterization setup housing the axial flux e-bicycle MR damper

To understand the damper's dynamic behaviors, a sinusoidal profile with a range of amplitudes and frequencies is typically used as a characterization. In this study, the damper is characterized for a sinusoidal profile with amplitude of 5mm for frequencies 1Hz, 1.5Hz and 2Hz for input currents from 0A to 1.2A in steps of 0.3A. From the figure 5.7, the maximum force obtained at compression and rebound with 1Hz frequency at 0A is 41.3N and 45.3N respectively. Whereas, the maximum force obtained at compression and rebound 1.2A is 65.2N and 80.1N respectively

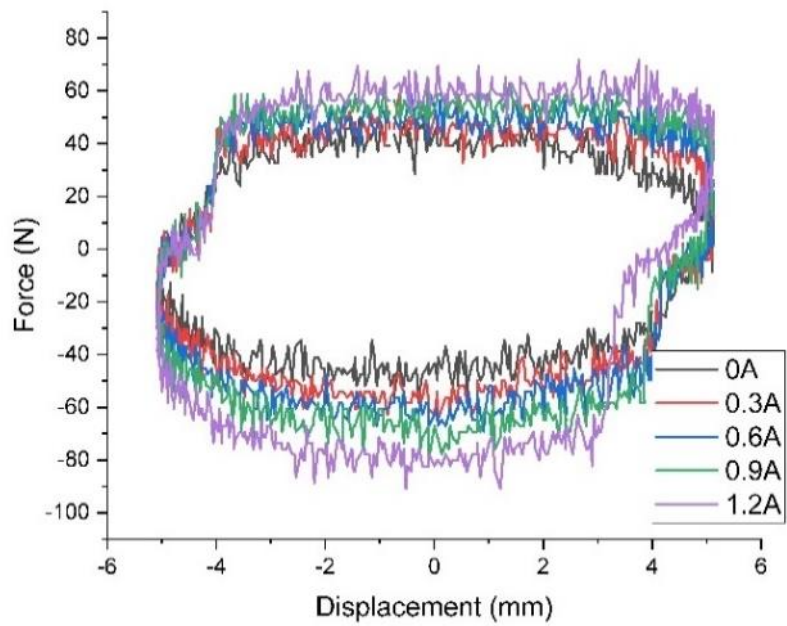


(a)

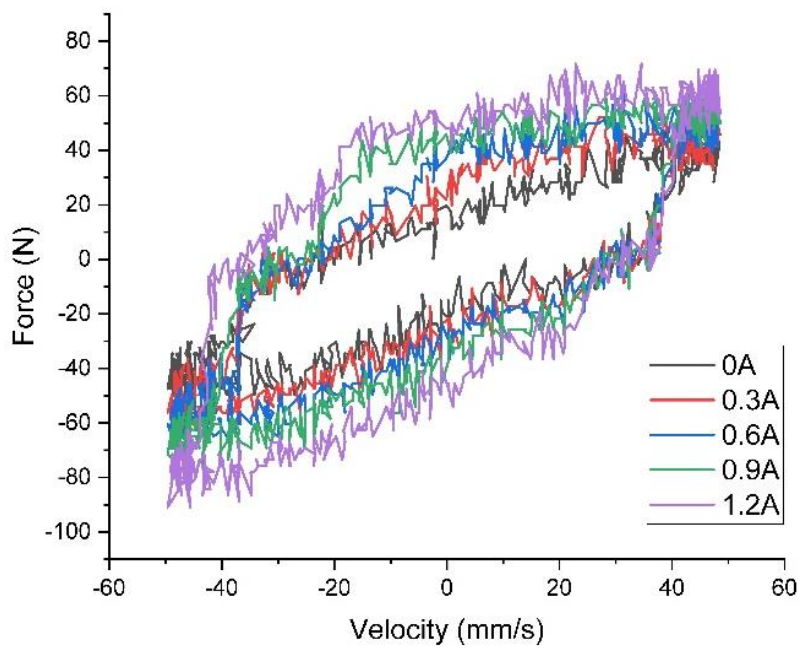


(b)

Figure 5.7 (a) Force-displacement and (b) force-velocity curves at 1 Hz



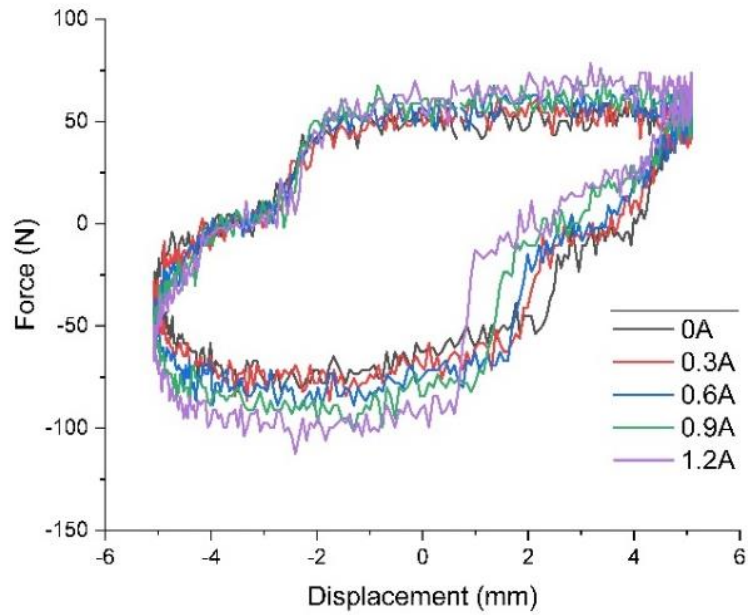
(a)



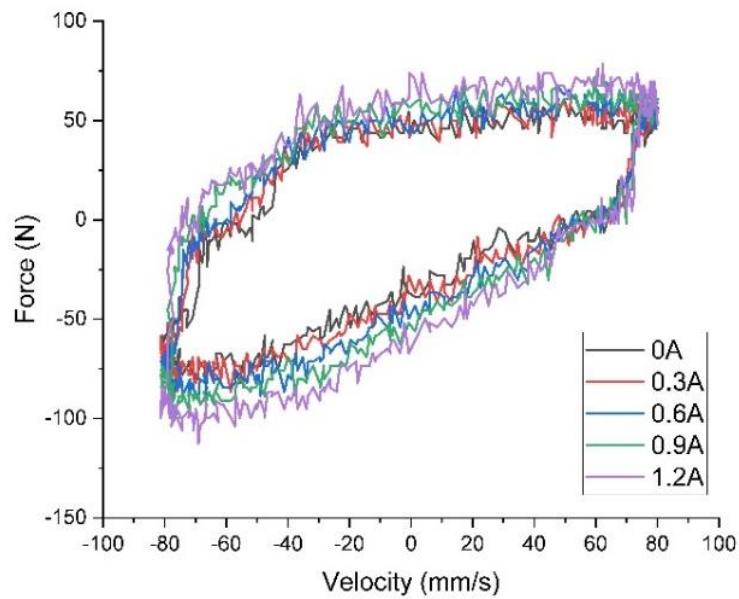
(b)

Figure 5.8 (a) Force-displacement and (b) force-velocity curves at 1.5 Hz

From the figure 5.8, the maximum force obtained at compression and rebound with 1.5 Hz frequency at 0A is 52.2N and 58.4N respectively. Whereas, the maximum force obtained at compression and rebound 1.2A is 71.7N and 90.9N respectively.



(a)



(b)

Figure 5.9 (a) Force-displacement and (b) force-velocity curves at 2Hz

From the figure 5.9, the maximum force obtained at compression and rebound with 2Hz frequency at 0A is 60.9N and 69.2N respectively. Whereas, the maximum force obtained at compression and rebound 1.2A is 78.2N and 99.6N respectively. This improvement in force signifies the presence of MR effect in the damper and is suitable for implementation in the vehicle it is designed for.

## 5.5 DESIGN OF E-BICYCLE RADIAL FLUX MR DAMPER

The design of the radial flux MR damper for bicycle application is similar to that of the radial flux two-wheeler design in terms of both the design and coil wound to it. The only difference is that the entire dimensions are reduced and the outer cylinder of the damper is shaped to fit to the e-bicycle. The fabrication process is more complex due to reduced size and wire EDM makes the damper fabrication process costlier than the vehicle itself. A simpler process of drilling and cutting for the coil space and pole design was used in fabricating the damper. The in-house MR fluid specified in section 5.1 was used to fill the damper as the commercial fluid. The detailed description of the designed and fabricated damper along with the MR fluid used is specified in the following sections of this chapter.

As followed in the previous designs the dynamic range and expected force must be kept high, in order to do that the piston dimensions of MR damper were optimized. The optimized dimensions of damper piston are given in the table 5.3.

Table 5.3 Dimensions of Radial flux e-bicycle MR damper

<b>Design Parameters</b>	<b>Dimensions in mm</b>
Piston head diameter	22
Piston rod diameter	10
Cylinder outer diameter	28
Cylinder inner diameter	24
Fluid flow gap	1
No. of poles	4

Finite Element Method Magnetics (FEMM) tool was used to perform the magnetic analysis of MR damper piston. The analysis has been performed for radial flux piston-based MR damper with 4 poles bearing a 25 turns of coil winding for each pole.

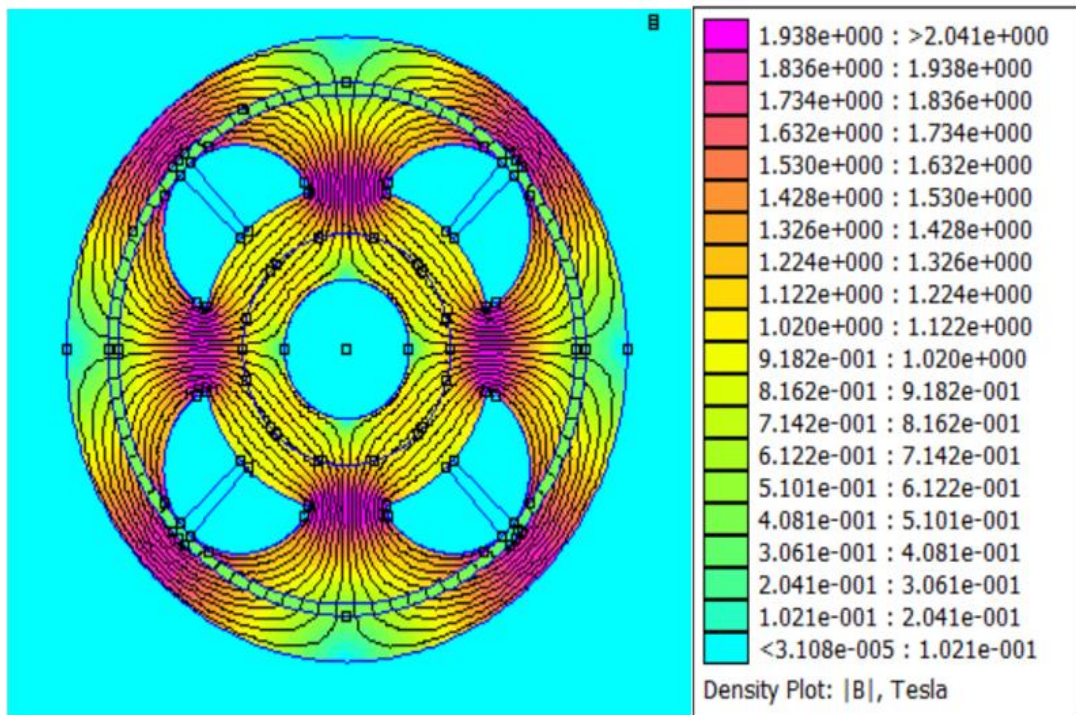


Figure 5.10 FEMM analysis of radial flux e-bicycle MR damper

The pole design is similar to the electrical motor poles with concentrated winding and adjacent poles are wound in opposite directions so as to create opposite magnetic flux. Figure 5.10 shows the FEMM analysis results of MR damper piston. The FEMM analysis results shows that there is a magnetic flux density of 0.51T in MR fluid flow gap.



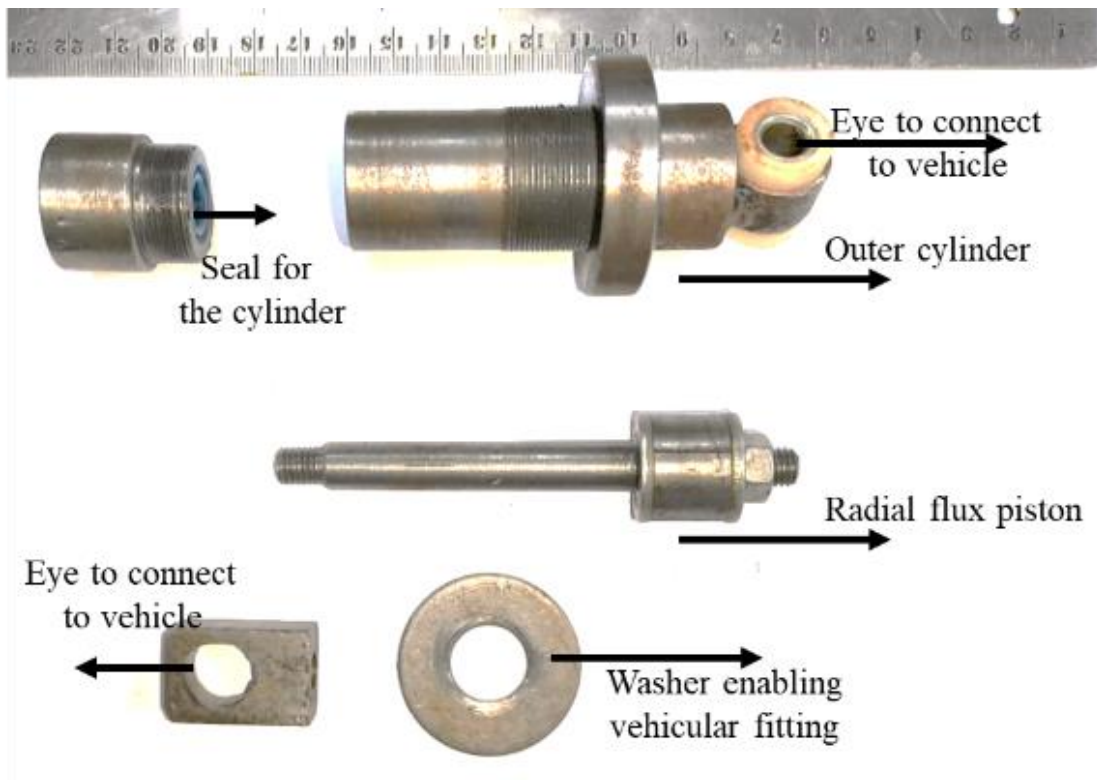


Figure 5.11 Assembled and disassembled view of the radial flux e-bicycle damper

The damper analysis in FEMM was performed using the cross-sectional layering of the MR damper perpendicular to the piston rod. As the produced magnetic field forms a closed path from one pole to another, the poles are wound with coil winding in plane parallel to the piston rod which is quite different when compared to the axial flux piston design.

The material used in fabrication of this MR damper is mild steel. Figure 5.11 shows the images of fabricated damper assembled and disassembled view and figure 5.12 shows the radial flux MR damper piston.



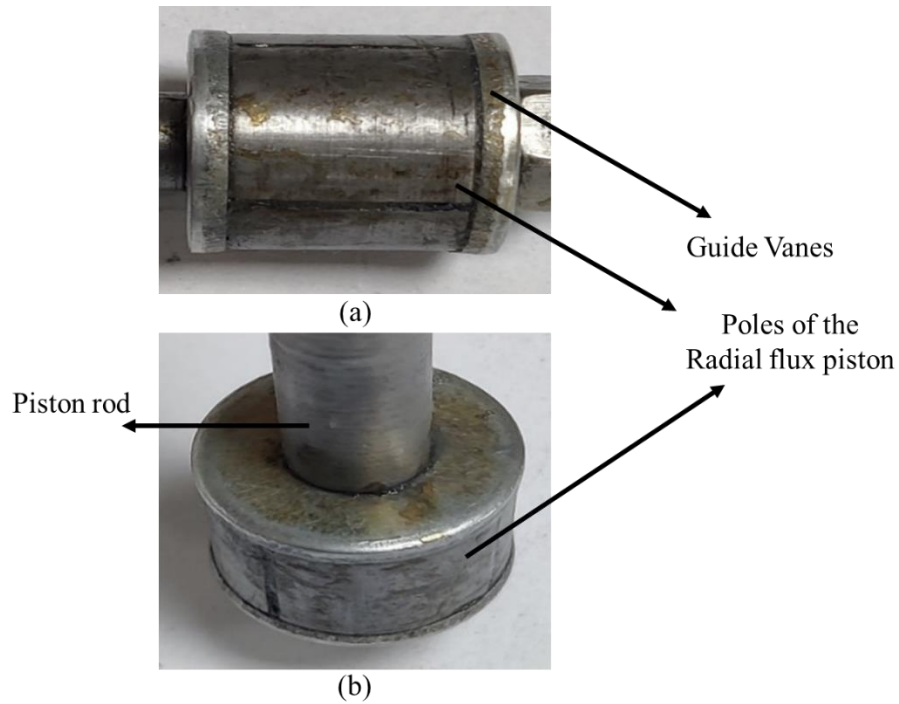
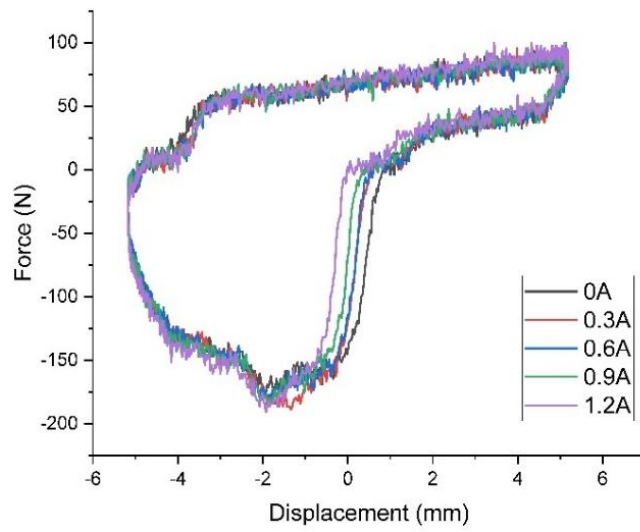


Figure 5.12 Radial flux e-bicycle MR damper piston (a) side view (b) isometric view

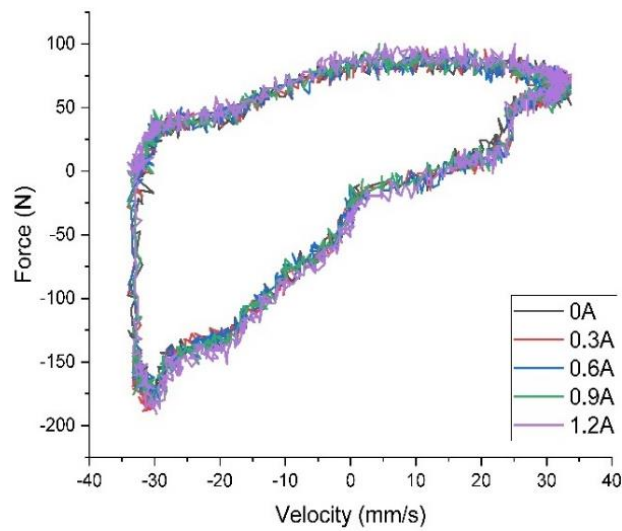
## 5.6 CHARACTERIZATION OF RADIAL FLUX MR DAMPER FOR E-BICYCLE

The force-displacement characteristics of custom-made MR damper are obtained by testing the damper using the damper testing machine. The damper is usually characterised for sinusoidal profile with different amplitudes and frequencies in order to understand their dynamic behaviour. Under these characterisations we obtain force-displacement curves scaling the damper's ability to the specified input range.

In this work, the damper is characterised for sinusoidal profile of amplitude 5mm and frequency 1Hz. The damper is characterised for off state and current inputs of 0.4A, 0.8A and 1.2A. The force-displacement curves are shown as in the figures 5.13 to 5.15.



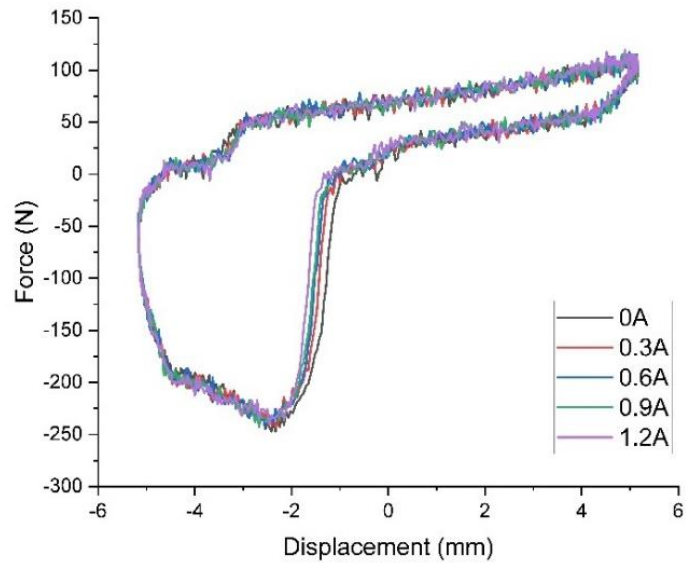
(a)



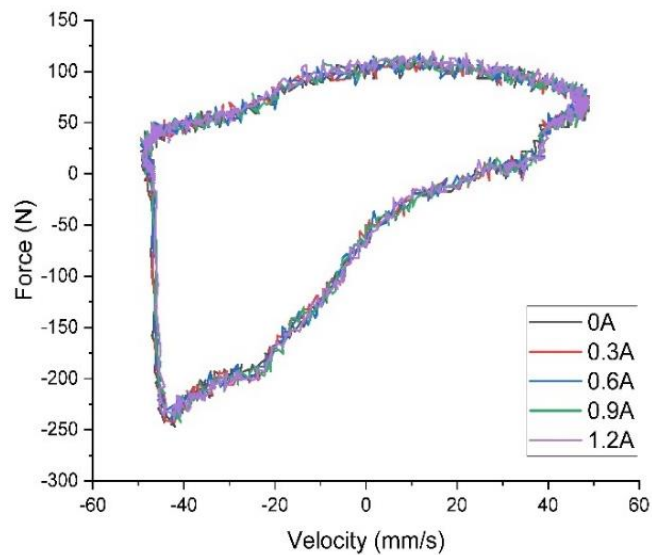
(b)

Figure 5.13 (a) Force-displacement and (b) force-velocity curves at 1 Hz

From the figure 5.13 the maximum force obtained at compression and rebound with 1Hz frequency at 0A is 105.3N and 186.3N respectively. Whereas, the maximum force obtained at compression and rebound 1.2A is 105.5N and 186.5N respectively



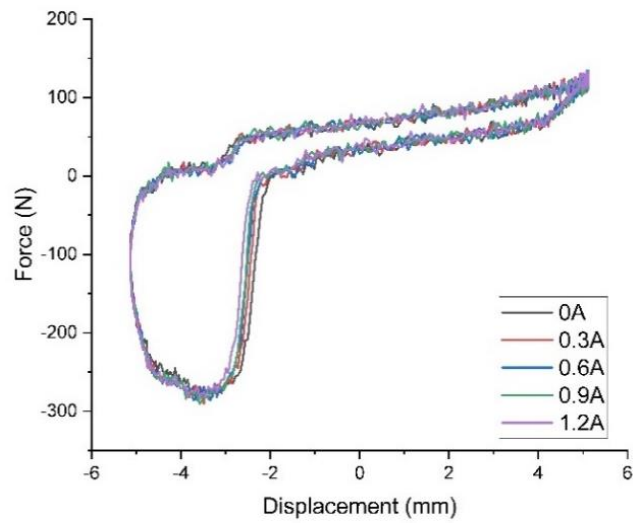
(a)



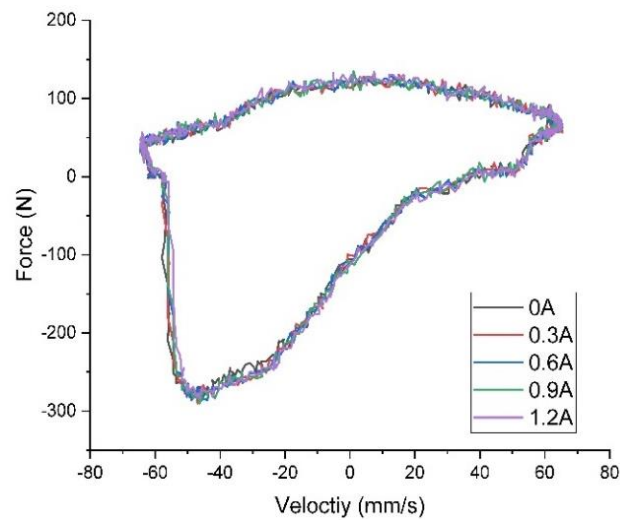
(b)

Figure 5.14 (a) Force-displacement and (b) force-velocity curves at 1.5 Hz

From the figure 5.14 the maximum force obtained at compression and rebound with 1.5 Hz frequency at 0A is 124.5N and 259.4N respectively. Whereas, the maximum force obtained at compression and rebound 1.2A is 124.7N and 259.9N respectively.



(a)



(b)

Figure 5.15 (a) Force-displacement and (b) force-velocity curves at 2Hz

From the figure 5.15 the maximum force obtained at compression and rebound with 2Hz frequency at 0A is 142.5N and 294.1N respectively. Whereas, the maximum force obtained at compression and rebound 1.2A is 78.2N and 99.6N respectively.

The characteristics signify a very low MR effect present in the damper with change in current from 0A to 1.2A by showing the minimum and maximum damping force value without and with MR effect as 64 N and 65 N respectively for 1hz frequency response. Even though there is a change in the variation of force it is quite negligible

as the shape of the curve is not even close to the ideal force-velocity and force-displacement curves.

Thus, this particular design for e-bicycle applications is not considered for the practical implementation. The obtained MR effect is also not sufficient to implement in a vehicle for variable damping as the change in the damping force with respect to the change in the current is negligible. The reasons for this might be due to

- The irregular shaping of the poles and the bottlenecks created in the flux flow path of the piston. The finishing of the damper was not proper as the cost and complexity of the design are quite high considering the vehicle it needs to be deployed in.
- The flux passage might have a severe issue with the internal passage drilled for coil through the piston. The size of the hole reduces the maximum material in the piston between the poles creating a bottleneck for the magnetic flux to pass through.

## **5.7 MODELLING OF AXIAL FLUX E-BICYCLE MR DAMPER**

As the radial flux piston-based e-bicycle damper was not able to fulfil the basic necessities, axial flux e-bicycle MR damper is used in further analysis.

To obtain the model of MR damper, polynomial fitting was used which is a non-parametric modeling technique. Considering the three different velocities i.e., 31.4mm/s, 47.1mm/s and 62.8mm/s, the damping force  $F$ , velocity  $v$  and the damper current input  $I$  relation is modelled using polynomial fitting method by considering the maximum force (table 5.4) at rebound stroke and the minimum force at compression stroke.

Table 5.4 Maximum and minimum damping force at different currents w.r.t. velocity

	31.4mm/s		47.1mm/s		62.8mm/s	
<b>Current (A)</b>	<b>Max Force (N)</b>	<b>Min Force (N)</b>	<b>Max Force (N)</b>	<b>Min Force (N)</b>	<b>Max Force (N)</b>	<b>Min Force (N)</b>
0A	41.38658	-45.3778	52.23212	-58.3925	60.90856	-69.238
0.3A	45.7248	-45.3778	58.7395	-64.8998	60.9086	-77.9145
0.6A	52.2321	-51.8852	60.9086	-69.238	63.0777	-82.2527
0.9A	58.7395	-64.8998	63.0777	-80.0836	67.4159	-88.76
1.2A	65.2468	-80.0836	71.7541	-90.9292	78.2614	-99.6056

Corresponding force-current equations for 31.4mm/s, 47.1mm/s and 62.8mm/s are given in the table 5.5 and the corresponding force current curves are represented in figure 5.16. The entire process of curve fitting and estimating the polynomial curve can be performed either manually or by means of fitting algorithms.

Table 5.5 Damping force equations with respect to velocity variations

<b>Velocity</b>	<b>Equation</b>
31.4mm/s	$F = -6.6949I^3 + 15.494I^2 + 10.931I + 41.356$ for $F > 0$ $F = 13.39I^3 - 53.367I^2 + 15.838I - 45.44$ for $F < 0$
47.1mm/s	$F = 33.474I^3 - 56.81I^2 + 36.238I + 52.201$ for $F > 0$ $F = -6.6948I^3 - 0.0002I^2 - 17.473I - 58.609$ for $F < 0$
62.8mm/s	$F = 13.39I^3 - 5.1648I^2 + 1.3773I + 60.847$ for $F > 0$ $F = -26.78I^3 + 43.039I^2 - 38.39I - 69.3$ for $F < 0$

The graphs from the figure 5.16 and 5.17 clearly state the rise in the damping force with respect to the current and the damper velocity.

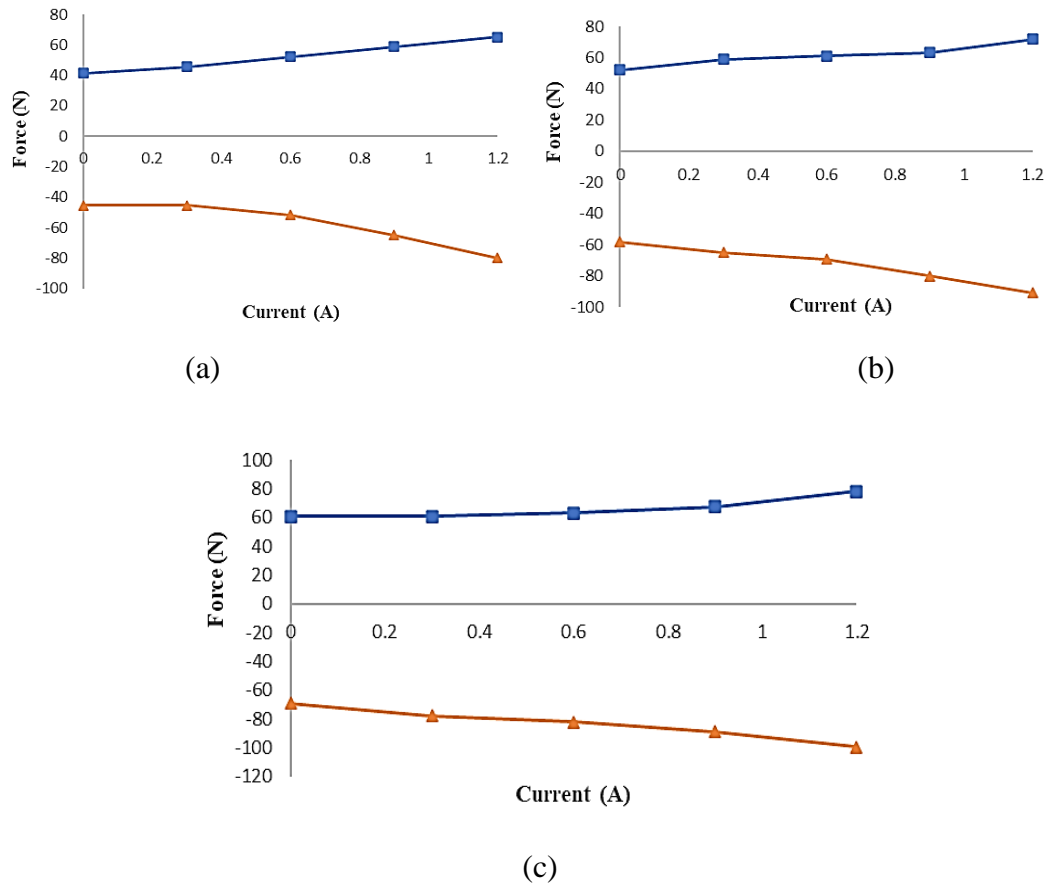


Figure 5.16 Force current curves at (a) 31.4mm/s (b) 47.1mm/s and (c) 62.8mm/s

The force-velocity equations for a range of currents were obtained by using polynomial fitting method considering the damping forces at seven different currents with maximum and minimum values.

Table 5.6 Force velocity equations at different currents

Current	Equation
0A	$F = 3E+07v^5 + 85015v^4 - 263572v^3 - 1152.4v^2 + 1612.5v - 0.942$
0.3A	$F = -3E+06v^5 - 170010v^4 - 103427v^3 - 2095.2v^2 + 1555.3v + 2.4046$
0.6A	$F = 3E+07v^5 + 127488v^4 - 326132v^3 - 3928.5v^2 + 1948.5v + 3.9229$
0.9A	$F = 7E+07v^5 + 1E+06v^4 - 585531v^3 - 7804.8v^2 + 2479v + 3.5821$
1.2A	$F = 1E+08v^5 + 382530v^4 - 797390v^3 - 2985.8v^2 + 3003v - 4.8464$

The polynomial equations for the currents from 0A to 1.2A are represented in table 5.6 and the Force-velocity plot is represented in the figure 5.17.

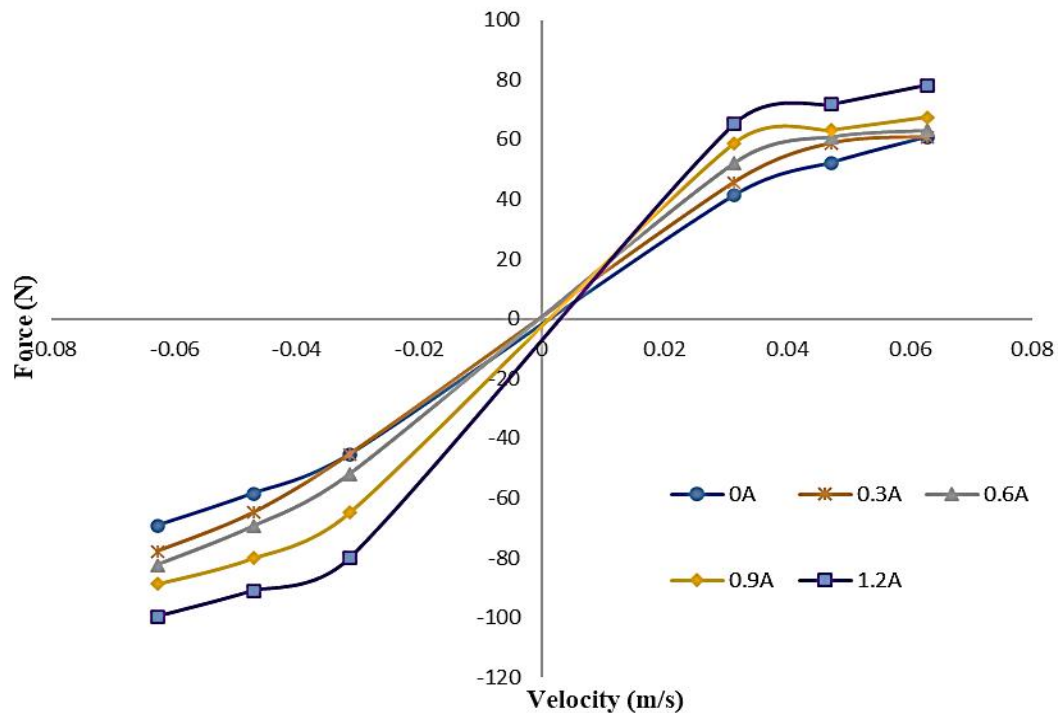


Figure 5.17 Force velocity curves at different current inputs for axial flux e-bicycle MR damper

## 5.8 RESPONSE OF MMQ USING AXIAL FLUX E-BICYCLE MR DAMPER

The quarter car model considering the parameters specified in table 5.7 in association with the polynomial model have been implemented with the sliding mode control strategy. The analysis of quarter car suspension model with off-state, sliding mode control and 1.2 A constant current semi-active suspension system has been carried out under a continuous sine wave with an amplitude of 0.01m, 3hz frequency excitation are considered for the road input profile.

Table 5.7 Parameters of MMQ with axial flux e-bicycle MR damper

Quarter car Parameters	Value of the parameter
Sprung mass $M_s$	35 Kg
Unsprung mass $M_{us}$	4 Kg
Sprung stiffness $K_s$	2950 N/m
Unsprung stiffness $K_{us}$	35055 N/m



The sprung mass acceleration responses of suspension are illustrated in figure 5.18. It is observed that the peak sprung mass acceleration has been reduced to 8.21% in case of sliding mode-controlled suspension system when compared with the off state.

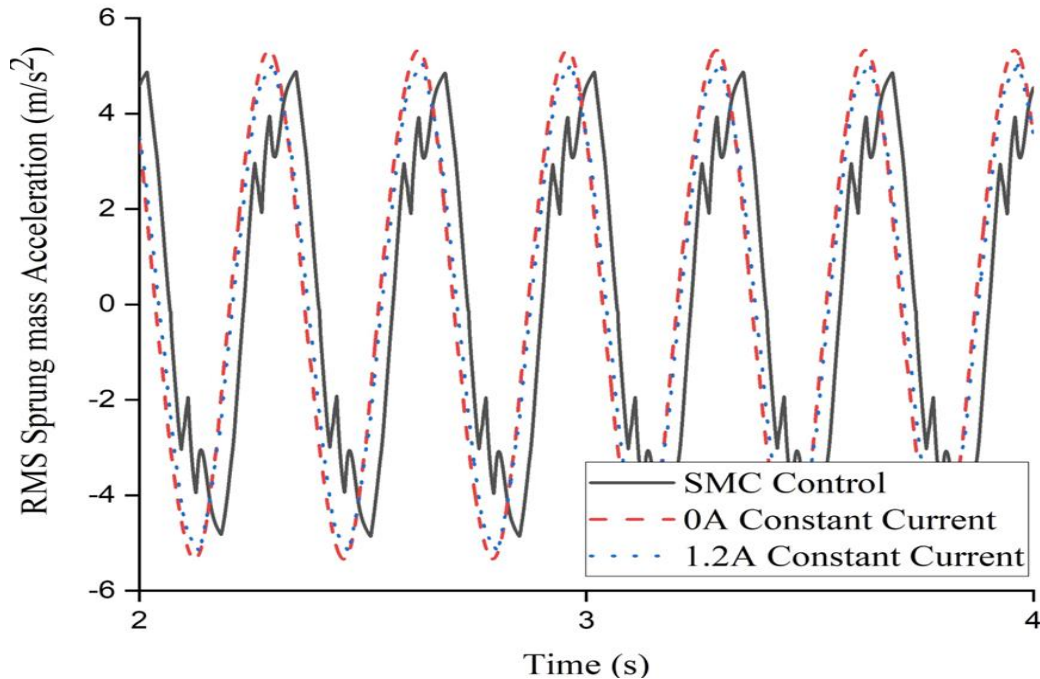


Figure 5.18 Sprung mass acceleration of MMQ with axial two-wheeler MR damper

The RMS acceleration response of the quarter car system specifies  $3.775\text{m/s}^2$  and  $3.211\text{ m/s}^2$  with MR damper off-state and the implementation of sliding mode control respectively. The road holding characteristics of the suspension system provides  $0.00886\text{m}$  with off-state and stability  $0.006054\text{m}$  to the vehicle with sliding mode control by making significant contact with the ground. Road holding is measured as the relative displacement between road and unsprung mass which in turn provides the amount of road gripping. Quantitatively, lesser the magnitude of road holding better is the vehicle stability. Thus, the control provides an improvement of 14.94% on RMS acceleration and 31.67% of RMS road holding with respect to the off-state response of the MR damper.

## 5.9 RESSPONSE OF MMT USING AXIAL FLUX E-BICYCLE MR DAMPER

The parameters of the two-wheeler vehicle were considered with weight measurement of each of the parts of e-bicycle to develop the two-wheeler model. The

parameters are listed in table 5.8. The two-wheeler mathematical model was subjected to random road excitation as specified in the equations 3.15.

Table 5.8 Parameters for MMT employing axial flux e-bicycle MR damper

Parameters	Value
Wheelbase ( $a_1 + a_2$ )	1.00 m
Sprung mass ( $M_s$ )	60 kg
Front unsprung mass ( $M_{uf}$ )	3 kg
Front tire damping ( $C_{tf}$ )	105 Ns/m
Distance of front unsprung from center of gravity ( $a_1$ )	0.64 m
Front tire stiffness ( $K_{tf}$ )	35055 N/m
Front spring stiffness ( $K_{sf}$ )	2950 N/m
Distance of rear unsprung from centre of gravity ( $a_2$ )	0.36 m
Rear unsprung mass ( $M_{ur}$ )	4 kg
Rear tire damping ( $C_{tr}$ )	105 Ns/m
Rear tire stiffness ( $K_{tr}$ )	35055 N/m
Rear spring stiffness ( $K_{sr}$ )	2950 N/m
Inertia ( $I_y$ )	18.51 kgm <sup>2</sup>

In this study sliding mode control is designed to control the two-wheeler suspension model. The suspension deflection is measured and sent to the SMC controller to produce the required control signal. This control signal is fed to the current amplifier to produce the required current for the MR damper. In order to ensure that the current fed to the damper is under the physical limitation of the damper, a current limiter is provided to limit the current between 0 to 1.2 A.

The bounded current (limited current) including the suspension deflection are fed to the MR damper. The detailed design of the control strategy is illustrated in the figure 5.19. The sliding mode control parameters i.e.,  $\lambda$  and G which are sliding mode constant and the current gain are selected based on the obtained expected force and the damping force. The obtained values for the MR damper fit MMT  $\lambda=1$  and  $G=0.8$ .

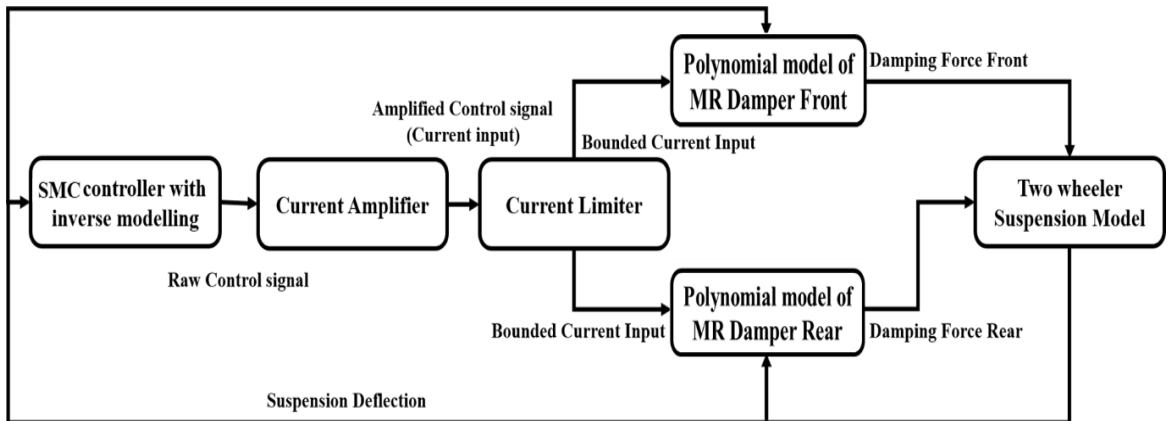
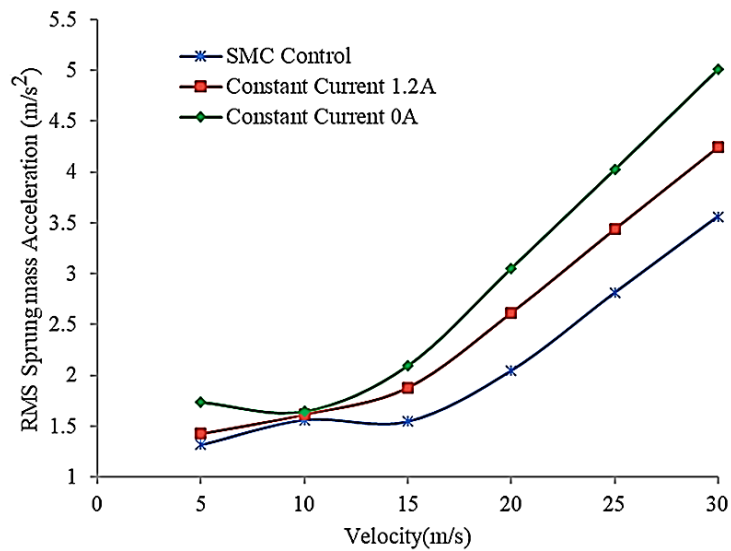
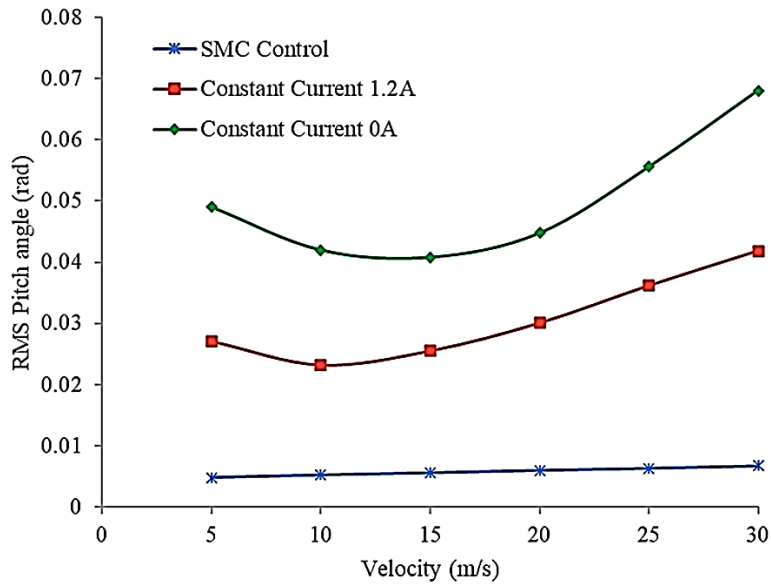


Figure 5.19 Block diagram representation of the SMC on E-bicycle suspension

The analysis of two-wheeler semi active suspension model with off state, sliding mode control and 1.2 A constant current semi-active suspension system has been carried out under random irregularities for different vehicle velocities. The vertical acceleration responses of semi-active two-wheeler suspension at various speeds are illustrated in figure 5.20(a). It is observed that sprung mass acceleration has been reduced to 24.26% in case of sliding mode-controlled suspension system when compared with the off state at 5 m/s vehicular velocity.



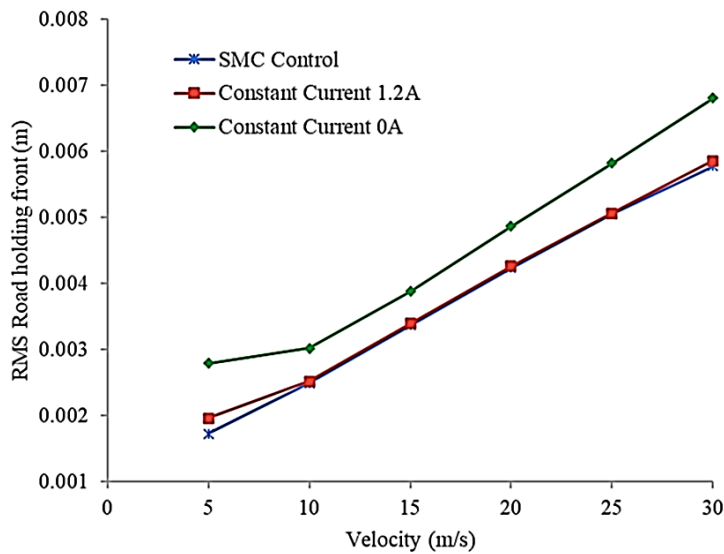
(a)



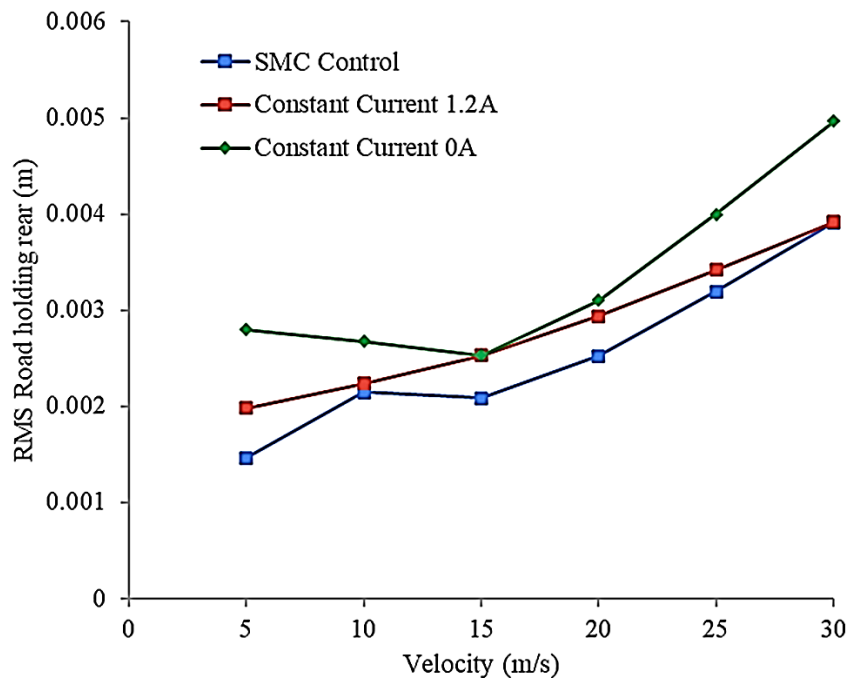
(b)

Figure 5.20 (a) RMS Sprung mass acceleration and (b) pitch angle with varied velocities

Figures 5.21 (a) and (b) demonstrate the road holding nature of the two-wheeler suspension at front and rear wheel respectively with the increment of vehicular velocities by 5m/s. It is observed that two-wheeler model with developed polynomial modelled MR damper-based suspension system provides about 38.02% improved road holding (at front wheel) with sliding mode controlled current input than with off-state condition at 5m/s velocity.



(a)



(b)

Figure 5.21 Road holding of (a) front and (b) rear different current inputs

It was also observed that the performance of the system was not up to the mark at rear position in terms of road holding. Hence, still there is a scope for improving the damper performance at rear position. The analysis of pitch angle motion of the sprung mass showed very good improvement using MR damper with SMC controller when compared to off-state condition (figure 5.20(b)). The developed MR damper in two-wheeler semiactive suspension model showed a good improvement in performance with SMC controller in terms of RMS acceleration of sprung mass and road holding at front unsprung position of the vehicle.

### 5.10 REAL TIME CONTROL IMPLEMENTATION OF AXIAL FLUX MR DAMPER IN E-BICYCLE

The MR damper was designed to be fitted and controlled on the rear end of the E- bicycle in order to provide better suspension deflection in order to provide minimal variation in the sprung mass velocity. The fabricated axial flux MR damper is fit to a custom-made E-bicycle which is converted from a normal mountain bicycle

(Crest, make: Atlas cycles ltd.) and real-time experimentation is carried out considering a road with a bump profile created using an iron base (manually created obstruction) as shown in figure 5.22.

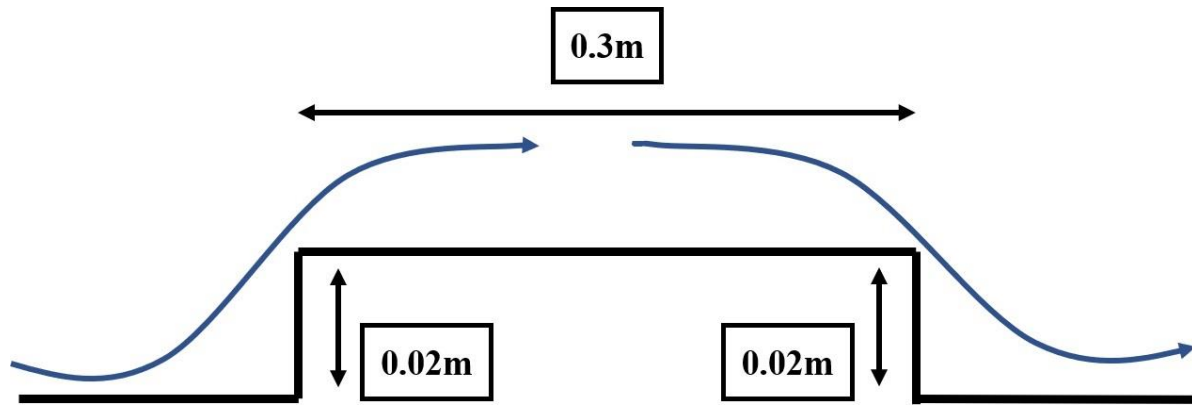


Figure 5.22 Road Profile for RT control of axial flux e-bicycle MR damper

The MR dampers are fit to the rear end of the vehicle on either side with the ends of the piston coil connected to a current controller by means of a current sensor (ACS712) in order to acquire the real time power consumed by the damper.

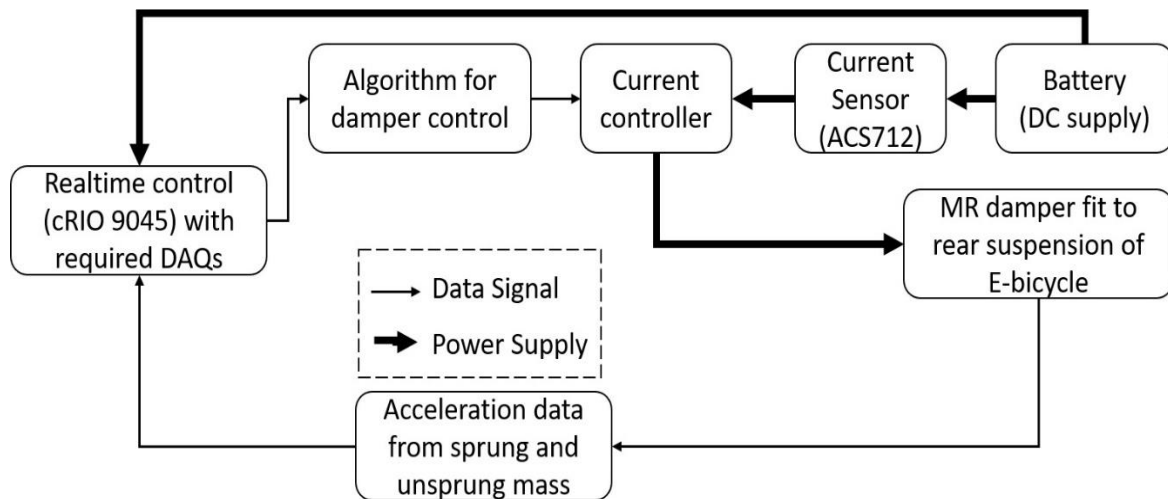


Figure 5.23 Schematic of the total setup for RT control

The setup is energized using a Li-polymer battery of 11.1V 3S with a capacity of 5000mAH. current is fed to the damper by means of an individual current controller. The schematic diagram of the total setup is specified in figure 5.23.



- |                |                            |
|----------------|----------------------------|
| 1 NI CRIO 9045 | 4 NI 9205                  |
| 2 NI 9230      | 5 ACS712                   |
| 3 NI 9403      | 6 Damper control Indicator |

Figure 5.24 Real time test setup of MR damper fit e-bicycle along with the controller

The resultant vibrations created by the road profile are measured using uniaxial accelerometers with a sensitivity of 100mV/g connected to both sprung as well as unsprung masses of vehicle considering the rear suspension system. These accelerometers work on 4mA constant current source fed through the NI hardware and data acquisition board namely NI 9230 which is connected to the accelerometers by means of BNC cables.

The data acquisition card 9230 takes the acceleration variation as input and sends the data to the actual control board with chassis for housing the data acquisition as well as control. NI-cRIO-9045 with an 8-slot chassis is used for data acquisition as well as control. Considering NI 9230 card for acceleration data acquisition, the NI 9205 is used for reading instantaneous current fed to the MR dampers. The digital input output card namely 9403 is used for generating the PWM control pulse which

triggers the current controller thereby providing a controlled current to be fed to the damper.

The control equipment with cRIO 9045, current sensor, battery, including the current controller are fit in a carton box placed in front of the rider and verified for no electric leakages. The real time experimentation test setup is picturized in figure 5.24. The entire vehicle testing was conducted maintaining a vehicular velocity of 20kmph. Although vehicular velocity is maintained, the path in which the vehicle exactly follows is uncertain which makes the time domain data unreliable for analyzing the performance of the damper. Therefore, filtering the data shows a better understanding of the damper performance. A third order Butterworth lowpass filter was used in filtering the noise and engine vibrations as the cutoff frequency was set to 20Hz. The time domain representations of sprung mass acceleration for road irregularities are picturized in figure 5.25.

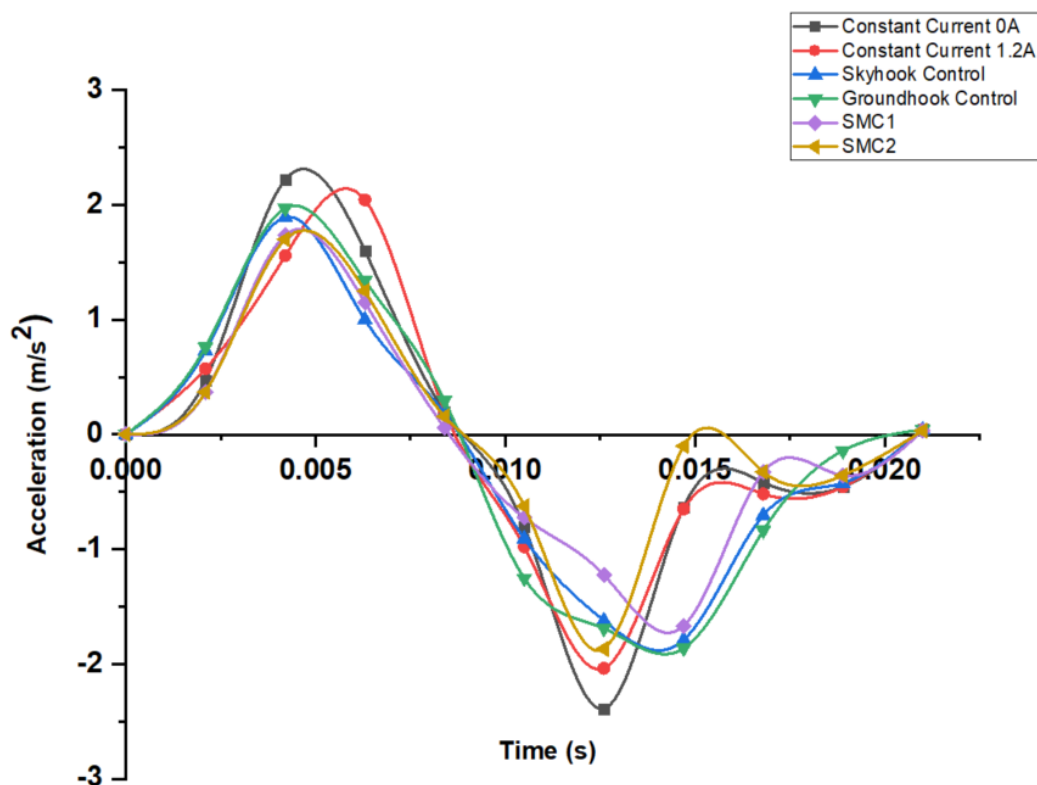


Figure 5.25 Realtime sprung mass acceleration response to the road input



The peak acceleration recording of the sprung mass is observed using the time domain graphs and are tabulated in table 5.9. It is observed that with the change in control logic, the amplitude reduction is observed for SMC2 more than SMC1 and other control strategies.

Table 5.9 Sprung mass acceleration in response to specific road profile

Control Logic	Maximum Value	% Reduction
Constant Current 0A	1.1872	
Constant Current 1.2A	1.1036	7.04
Groundhook Control	1.0555	11.09
Skyhook Control	1.0092	14.99
Sliding Mode Control 1	0.9277	21.8
Sliding Mode Control 2	0.8409	24.07

The results of the frequency domain graph (figure 5.26) also specifies that the vehicular acceleration is reduced by the application of sliding mode control when compared with the off-state of MR damper.

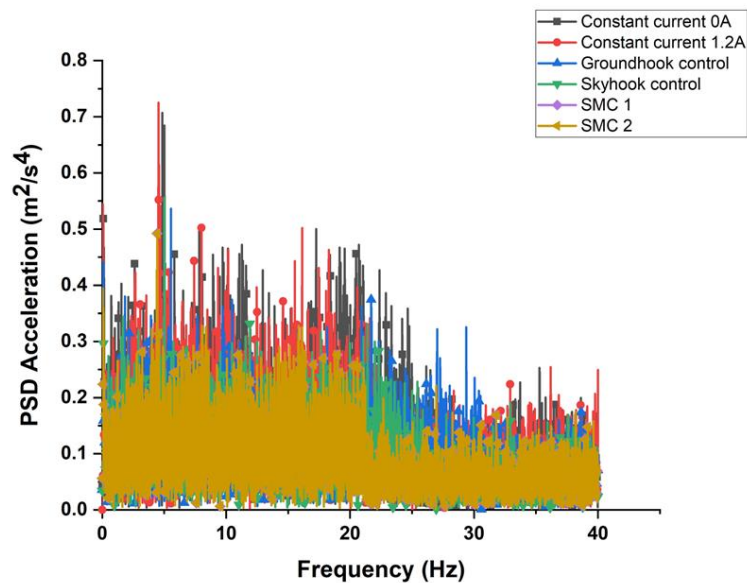


Figure 5.26 Frequency plot of sprung mass acceleration response to the road input

The damper currents in figures 5.27 are the currents generated from the battery and are tabulated by means of a current sensor connected at the output of the battery. This means that the graph shows total drawn current from the battery which of both the dampers combined. From the graph it is clearly observed that the maximum current drawn is 0.8A and minimum current drawn is 0A (the negative currents are due to minute sensitivity and calibration issues as the ACS712 is calibrated considering 2.4A as its maximum current).

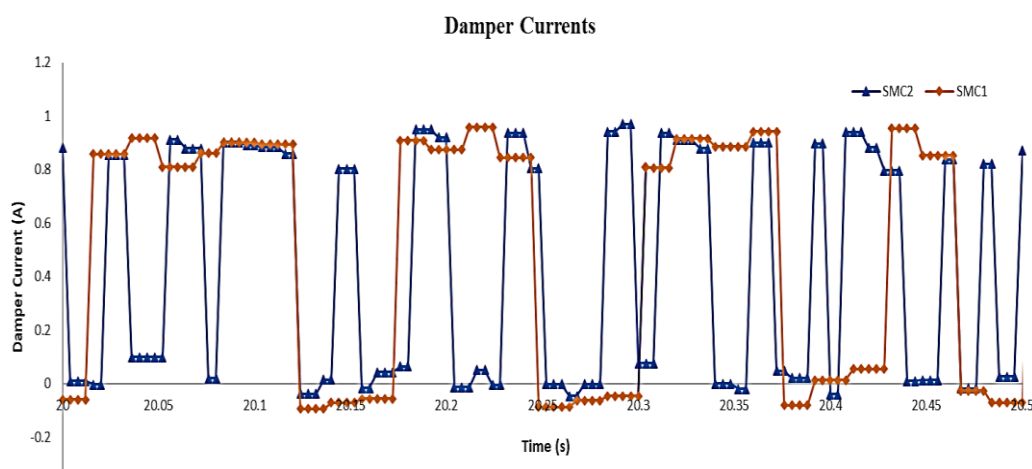


Figure 5.27 Damper currents obtained at the impact of the undulations in road

## 5.11 SUMMARY

The designed dampers were providing a magnetic flux density of 0.48 T and 0.51T with axial and radial flux-based designs respectively within the fluid flow gap. The fabricated axial flux damper was providing better damping force with respect to the change in current, whereas, the radial flux damper was not able to provide change in the damping force with respect to the changes in the current input. The probable reasons for this issue might be due to the bottlenecks created in the flux flow path and irregularities in the design. The axial flux-based e-bicycle MR damper was further used for the analysis in quarter car and two-wheeler mathematical models, which in turn shows good improvement in the sprung mass acceleration reduction. Also, real-time control of the dampers fit to the vehicle (Crest) was able to provide 24.07% reduction in the peak sprung mass acceleration for the provided road profile when compared to the off-state condition.

## **CHAPTER 6**

# **HYBRID RADIAL FLUX PISTON: NOVEL DESIGN OF ELECTRO-MAGNETIC PISTON FOR MAGNETO- RHEOLOGICAL DAMPERS**

### **6.1 INTRODUCTION**

The literature review defines only two types of piston designs namely axial and radial flux designs with either single layer core or multi-layered stacking (for differential fluxes). Multi layered designs even though could produce differential field can produce only either axial or radial fluxes but not both in the piston core. This drawback of the conventional designs can be eliminated by the Hybrid radial flux Piston (HRFP). In this study novel design namely “Hybrid radial flux Piston” has been proposed which can create both axial as well as radial fluxes in the fluid flow gap of the designed MR damper. This design has been analysed using FEM analysis in ANSYS software. Based on the piston analysis, MR damper has been fabricated, characterized and tested for dynamic testing and for pulsed excitation response. The characterized damper results are then used in formulating a polynomial model fit to the Quarter car modeling in Simulink with sliding mode control in comparison with the constant current and no current fed to the MR damper.

### **6.2 DESIGN OF HYBRID RADIAL FLUX PISTON (HRFP) BASED MR DAMPER**

As specified in the previous chapters, the design procedures are followed towards HRFP based MR damper by using equations 3.1 to 3.4.

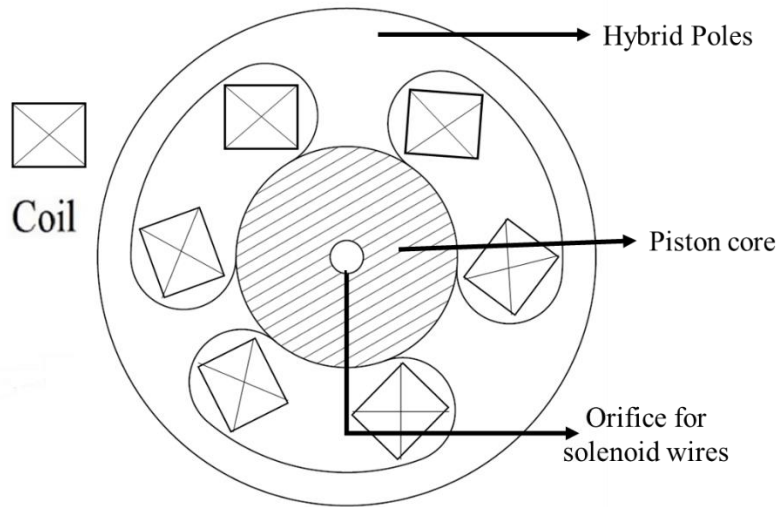


Figure 6.1 Cross sectional view of HRFP

The cross-sectional view of HRFP and the design parameters used in the development of the MR damper are specified in figure 6.1 and table 6.1 respectively.

Table 6.1 Dimensions of HRFP

Design parameter	Dimension in mm
Pole length ( $p/2$ )	10 mm
Coil gap (m)	10 mm
Piston diameter ( $d_p$ )	45mm
Piston poles	3per layer
No. of layers	2
Piston pole covering	6 mm hollow cylinder

The axial flux design consists of the electromagnetic piston with coil wound at its centre generating the magnetic flux parallel to the direction of motion. On the contrary, the radial flux design has coil wound perpendicular to the direction of motion. Each design has its own merits and demerits making them unique in their aspects. Considering axial flux magnetic field piston design the major advantage of the damping system is it provides uniform magnetic field in the MR fluid gap.

One of the major disadvantages in this design is it generates a distributed magnetic field in the poles of the piston. When it comes to the radial flux damper piston, the design provides concentrated magnetic flux in the annular fluid flow gap which is a major advantage of this design yet lacks effectiveness due to the build-up of the remanent magnetic flux in the piston poles making the MR Fluid viscosity higher for a longer period of time disrupting the dynamic range capability. One solution for this problem is to use a very low viscous MR fluid in the annular fluid flow gap. This reduces the problem to some extent but it does not work effectively if a higher viscous MR fluid is inevitable with a smaller annular gap.

The design of Hybrid Radial Flux Piston is slightly different to the traditional axial and radial flux designs in terms of the placement of the coil and the flux flow path. The entire piston area is divided into two or more layers with respect to the vertical axis of the piston core. Each layer consists of multiple poles to house coil on each pole. The number of poles and their sizes on each layer can be optimally designed based on the pole length and the areal consumption of the coil combined. A gap between the adjacent layers is needed so as to provide spacing for the wound coil on the pole and also to provide separation from one layer to another. The gap between piston and the outer cylinder can be between 0.5mm to 1mm in diameter in order to provide sufficient spacing for the MR fluid flow and to alter the viscosity of the fluid by the change in magnetic field respectively. This design how ever has some compulsions which are specified below:

1. The poles present in a particular layer must be wound with the copper coil in a certain way that all the poles generate magnetic flux in similar direction (either radially inwards or outwards) if the outer layer is interconnected else alternative generation of magnetic flux can be produced, provided, the consecutive layers with respect to the vertical axis are of opposing poles.
2. The poles are offset by a certain angle in comparison with the adjacent layers to provide an average uniform flux in the entire fluid gap between the piston and outer cylinder.

- An effective gap between the layers is required to be maintained to accommodate the turns of both the adjacent layer coils.

### 6.3 FINITE ELEMENT MAGNETOSTATIC ANALYSIS OF HRFP

In order to understand the magnetic flow line behaviour due to the designed HRFP, the finite element analysis is performed. The analysis is focused on the magnetic flux nature over the MR fluid region. The materials chosen for the MR damper re listed in table 6.2.

Table 6.2 Materials used for fabrication of HRFP MR damper

Part	Material
Outer Cylinder	Mild steel
Piston	SAE 1018
Piston rod	Mild steel
Flow separators	Aluminum
Coil	Copper (AWG 26)

The magnetic flux lines in the MR fluid surrounding the current piston design are shown in figure 6.2 below.

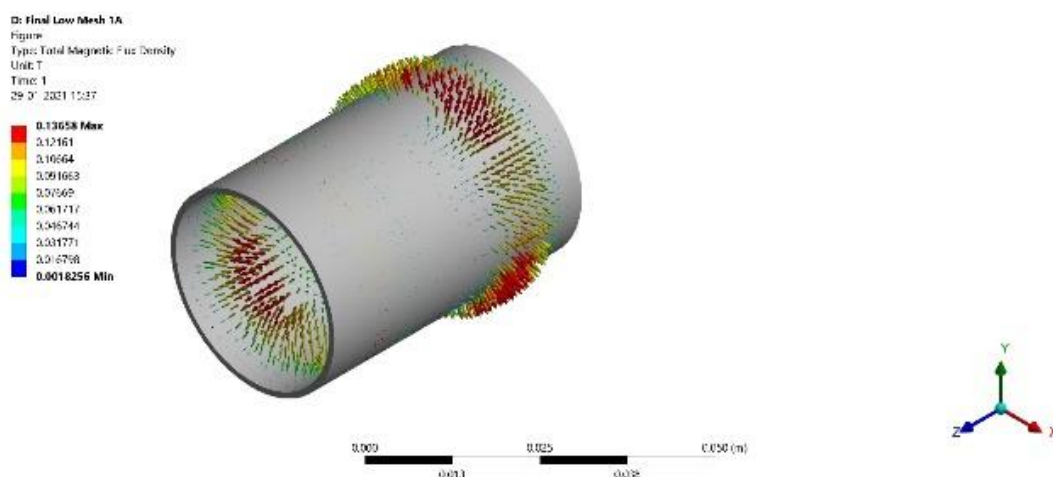


Figure 6.2 Magnetic flux lines in MR fluid and outer cylinder

As observed in Figure 6.3, the lines of magnetic flux are radiating outwards near the bottom pole and are radially projecting inwards at the top pole.

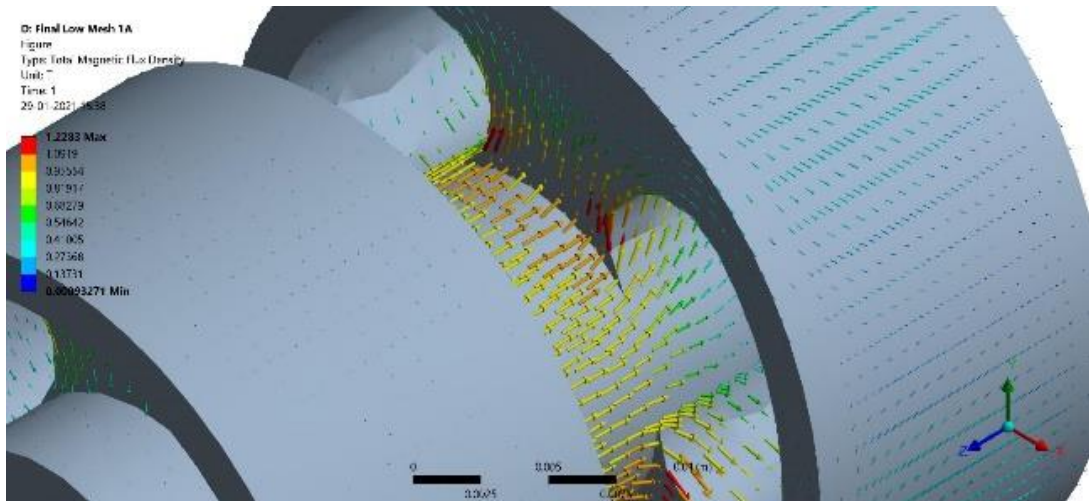


Figure 6.3 Magnetic flux lines in piston poles of HRFP

As shown in figure 6.3, the center portion connecting the top and bottom poles has magnetic flux in the axial direction. Also, from figure 6.3 and 6.4, the flux lines are projected radially in the active pole regions. Therefore, the design produces both axial and radial flux lines through the piston core.

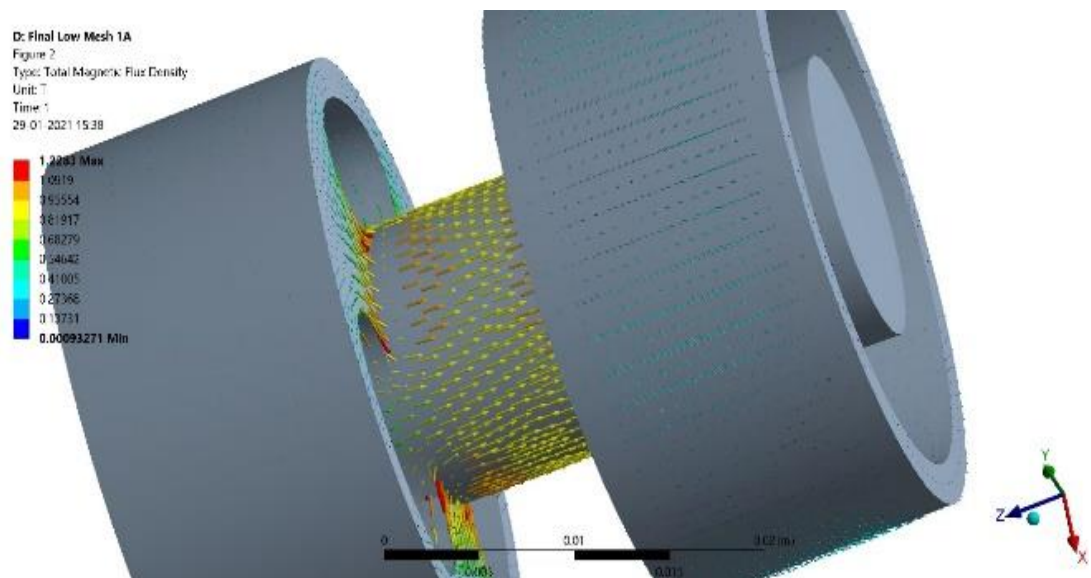


Figure 6.4 Magnetic flux lines in piston core of HRFP

An MR damper with the present piston configuration has been fabricated based on a sample set of dimensions. An outer cylinder with a thickness of 4mm and a fluid flow gap of 0.5 mm between the cylinder and the piston was chosen for initial testing.

The piston is insulated with insulation enamel or insulation tapes so as to prevent short circuit of the coil winding with the piston core. Each pole is wound with 50 coil turns in order to produce the required Magnetic flux in the core. The damper cylinder is filled with an in-house MR fluid to obtain enhanced damping force.



Figure 6.5 Developed MR damper with detailed view of Hybrid Radial Flux Piston



In-house MR fluid has been prepared with a particle proportion of 65.97% by weight of carbonyl iron powder, 27.73% by weight of fork oil along with grease with 6.29% by weight as specified in chapter 4. In order to avoid uneven magnetic field, the MR damper is filled such that no air bubbles are left out. The designed MRD including the cross-sectional view is presented in figure 6.5.

#### 6.4 CHARACTERIZATION OF MR DAMPER WITH HRF

The performance evaluation of the damper can be accessed by exploring its dynamic characteristics using the dynamic testing machine. The dynamic testing machine housing the prototype damper is pictured in figure 6.6.

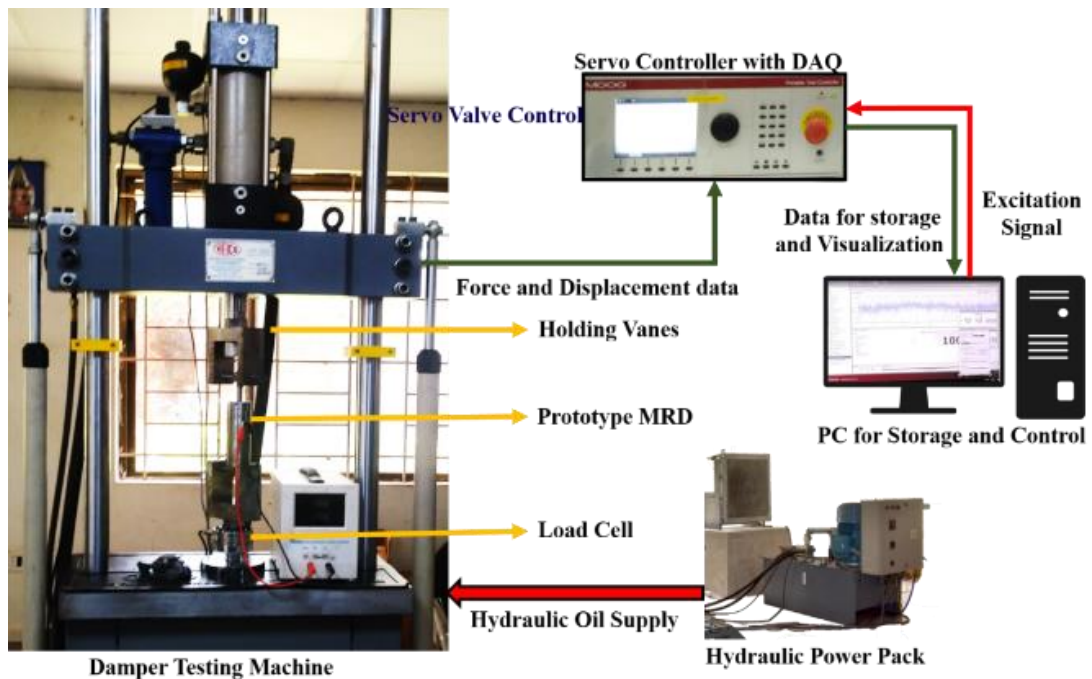
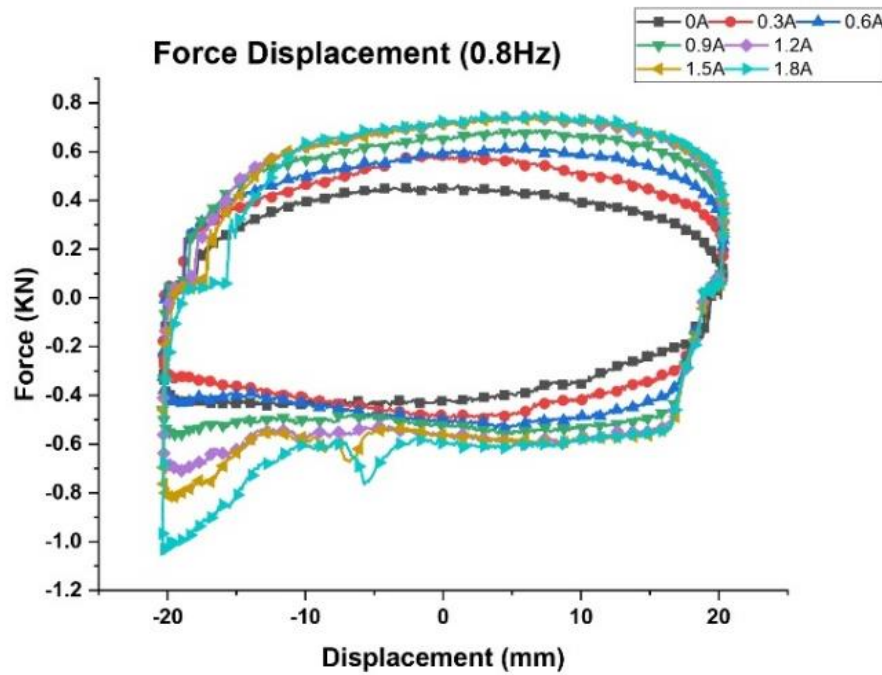


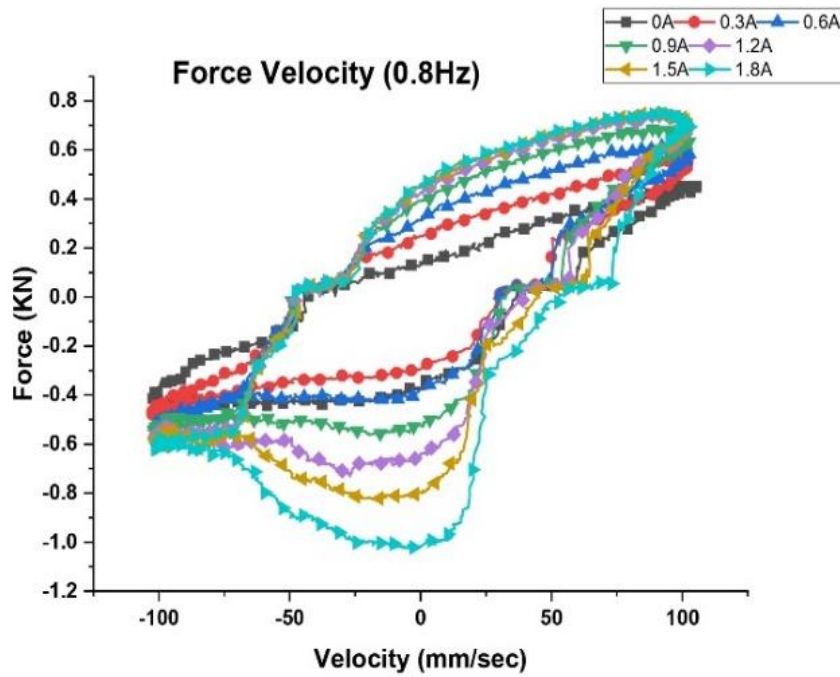
Figure 6.6 Damper testing machine with designed MR damper containing HRF

Experiments for damper characterisation are generally performed for the required frequency and amplitude conditions. The experimentation for this damper is carried out for 0.8Hz, 1.2Hz and 1.6Hz, 2Hz frequencies with a displacement of 20mm. The above specified inhouse MR fluid is used in analysis and 0.3 - 2A current was provided to the piston coil in steps using a Regulated DC power supply. Experiments were also carried out in off-state i.e., at no current input to the MR damper.

The custom-made MR fluid was used with the characteristics specified earlier and the piston of the damper was excited with current inputs ranging from 0A to 1.8A with a step increment of 0.3A.



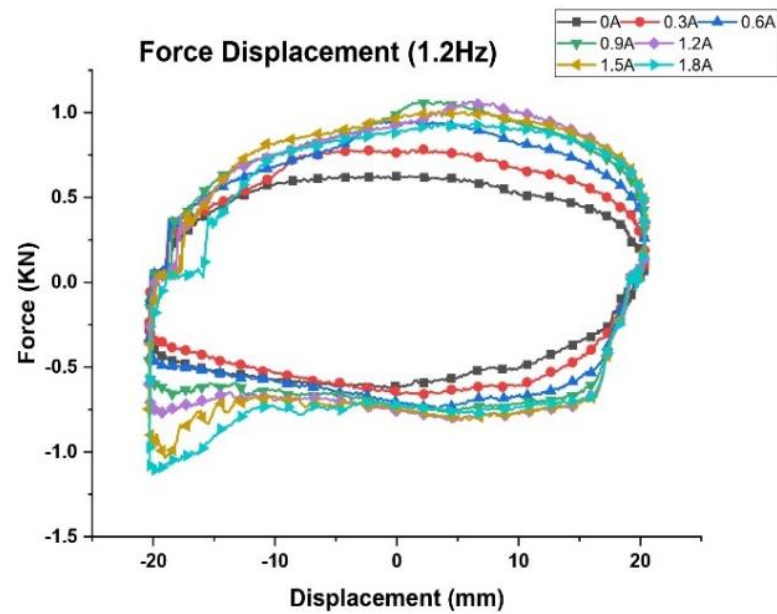
(a)



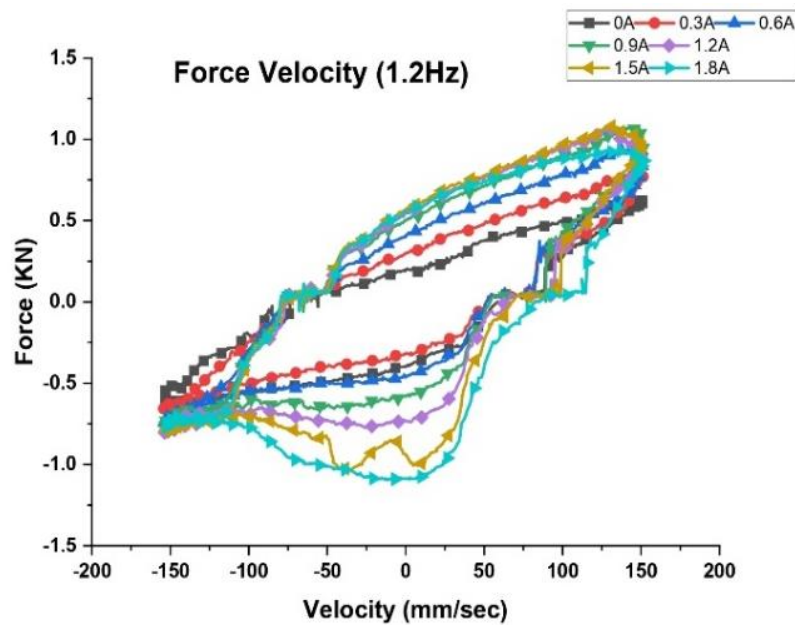
(b)

Figure 6.7 (a) Force-displacement and (b) force-velocity curves at 0.8Hz

From the figure 6.7, the maximum force obtained at compression and rebound with 0.8Hz frequency at 0A is 458.16N and 444.19N respectively. Whereas, the maximum force obtained at compression and rebound 1.8A is 755.33N and 1025.51N respectively.



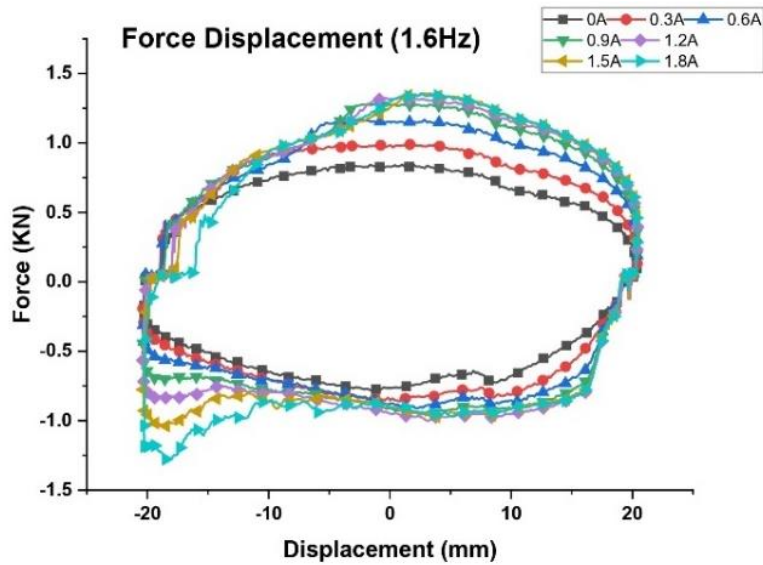
(a)



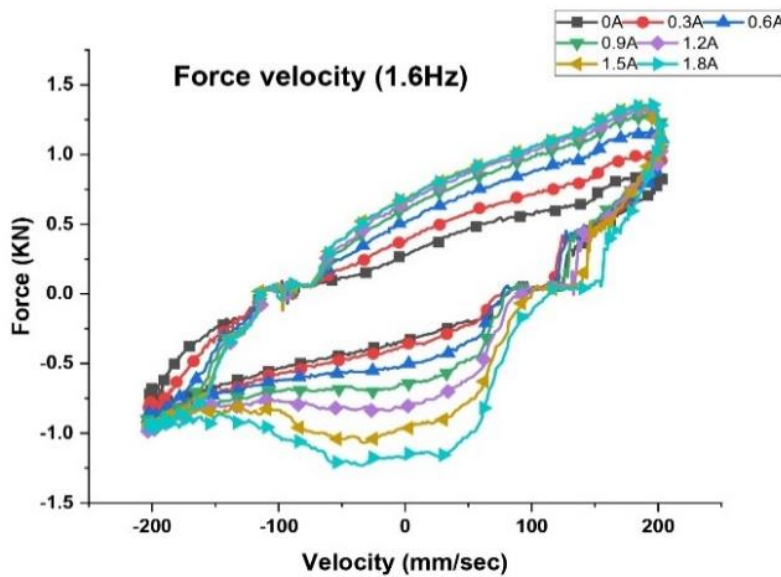
(b)

Figure 6.8 (a) Force-displacement and (b) force-velocity curves at 1.2 Hz

From the figure 6.8, the maximum force obtained at compression and rebound with 1.2 Hz frequency at 0A is 627.35N and 619.89N respectively. Whereas, the maximum force obtained at compression and rebound 1.8A is 933.19N and 1092.75N respectively.



(a)

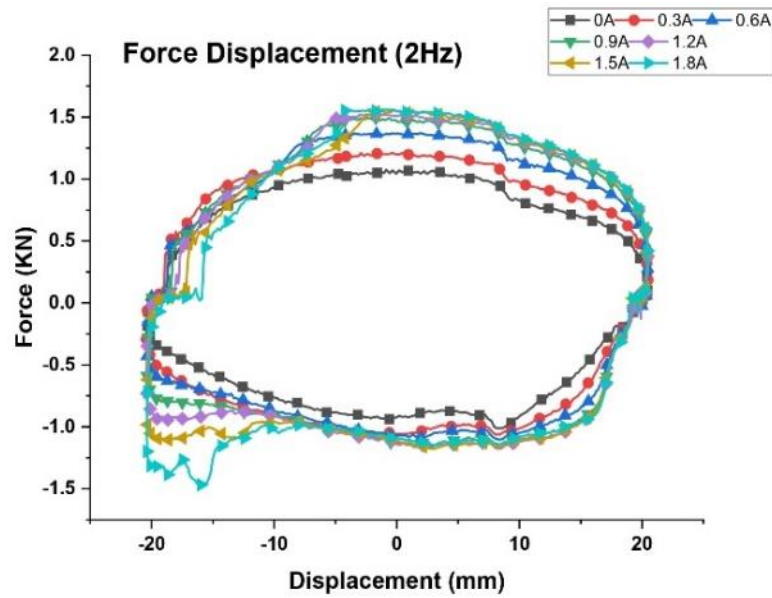


(b)

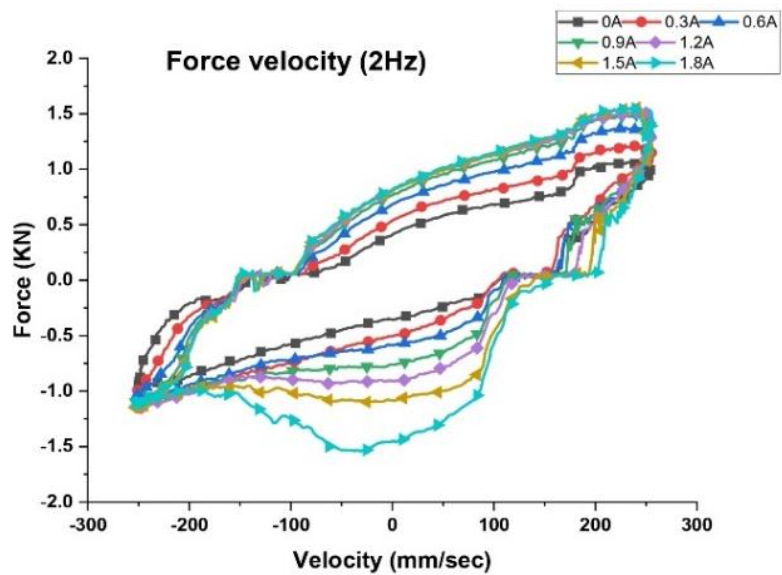
Figure 6.9 (a) Force-displacement and (b) force-velocity curves at 1.6Hz

From the figure 6.9, the maximum force obtained at compression and rebound with 1.6Hz frequency at 0A is 1067.68N and 786.91N respectively. Whereas,

the maximum force obtained at compression and rebound 1.8A is 1371.35N and 1231.58N respectively.



(a)



(b)

Figure 6.10 (a) Force-displacement and (b) force-velocity curves at 2Hz

From the figure 6.10 the maximum force obtained at compression and rebound with 2Hz frequency at 0A is 1067.68N and 1025.51N respectively. Whereas, the maximum force obtained at compression and rebound 1.8A is 1551.39N and 1541.76N

respectively. Results show that there is a significant improvement in maximum damping force signifying the presence of the MR effect in the damper. The obtained results clearly indicate the MR effect in the damper with and without the supply current. For instance, 1kN and 1.6kN damping force was obtained at off state and 1.8A current respectively at 2Hz producing an effective change magnetic flux for producing the required damping force. The force displacement curves also specify a uniform distribution of the force until saturation which indicates a uniform distribution of magnetic flux and effective magnetization of the piston core.

## 6.5 PULSED EXCITATION RESPONSE OF THE PROTOTYPE MR DAMPER

In order to obtain an instantaneous response of the MR damper in terms of the resultant force, supplying a pulsed excitation to the damper is an inevitable choice as it can provide with the force overshoot at a certain instance. This experimentation not only accesses the instantaneous increase in force but also tests the strength of the MRD for sudden changes in voltage ( $dv/dt$ ) and current ( $di/dt$ ). In order to obtain the pulsed voltages (which in turn generates the pulsed currents) a circuit was designed to generate pulses with frequencies between 0 to 10Hz. This circuit is basically an astable multivibrator with 555 timers as the base IC. rheostats are connected between 8,7 and 7,6 pins of the timer IC. A diode is connected antiparallel to the resistor connected between 7 and 6 pins of the IC. A capacitor is connected between the 6 and ground pins. All the rheostats are of  $10K\Omega$  and timing capacitor of  $100\mu f$ . The equation for pulse on time and duty cycle are as follows.

$$T_{ON} = 0.693(R_X C) \quad (6.1)$$

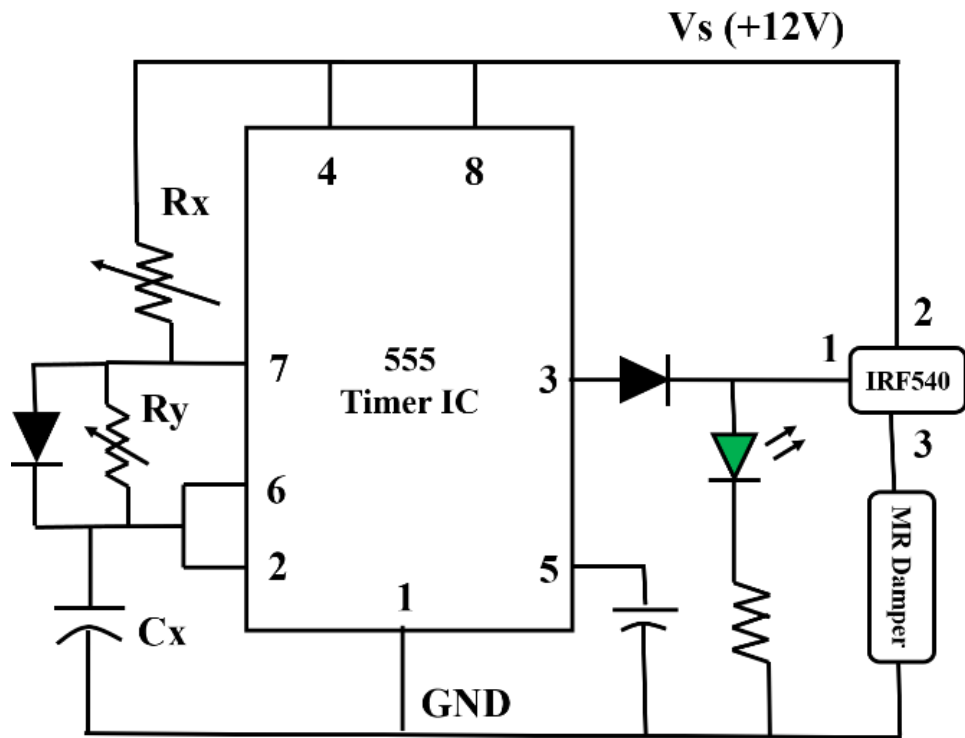
$$T_{OFF} = 0.693(R_Y C) \quad (6.2)$$

$$T_{total} = 0.693(R_X + R_Y)C \quad (6.3)$$

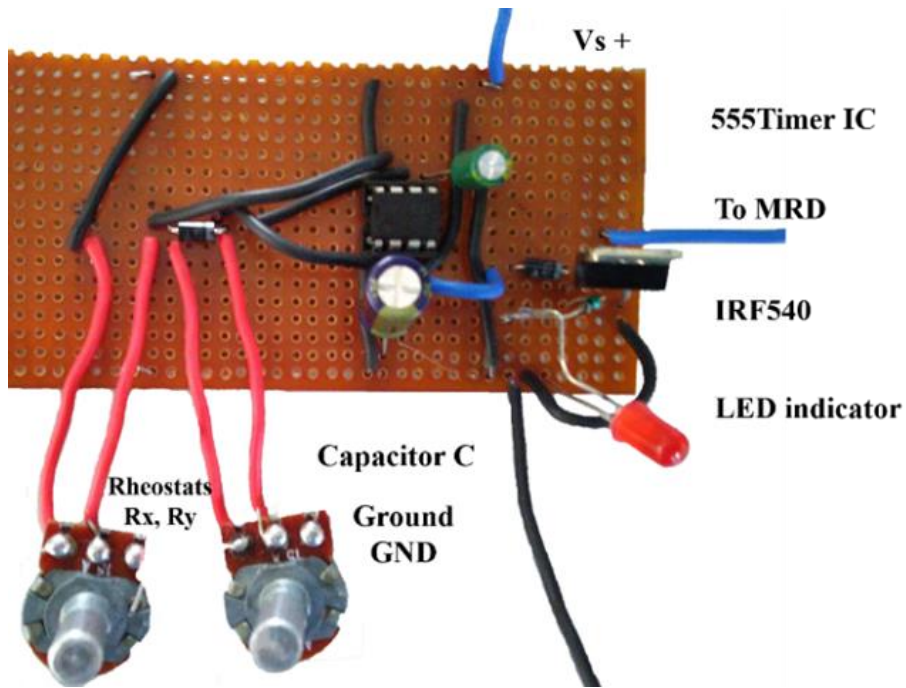
$$f = 1/[0.693(R_X + R_Y)C] \quad (6.4)$$

$$D = R_X / (R_X + R_Y) \quad (6.5)$$

Where  $R_x$  and  $R_y$  are the rheostat values and  $C$  is the timing capacitor value and  $D$  represents the duty cycle respectively. The circuit diagram for pulse generation can be observed in Figure 6.11. As it can be observed the output pin of the 555 timer IC is connected to the base of a IRF540 mosfet through a PN junction diode. A led is connected from the base of the mosfet through a  $1k\Omega$  resistor to ascertain the operation of pulse generation circuit. The damping force data while experimentation is obtained from the load cell of the DTM and the pulse characteristics are obtained by a voltage sensor DAQ NI 9215. this study was carried out for different frequency inputs using the DTM under 1Hz, 2Hz and 3Hz frequency conditions with  $\leq 10\%$  duty cycle and its respective force outputs are presented in the figure 6.13.



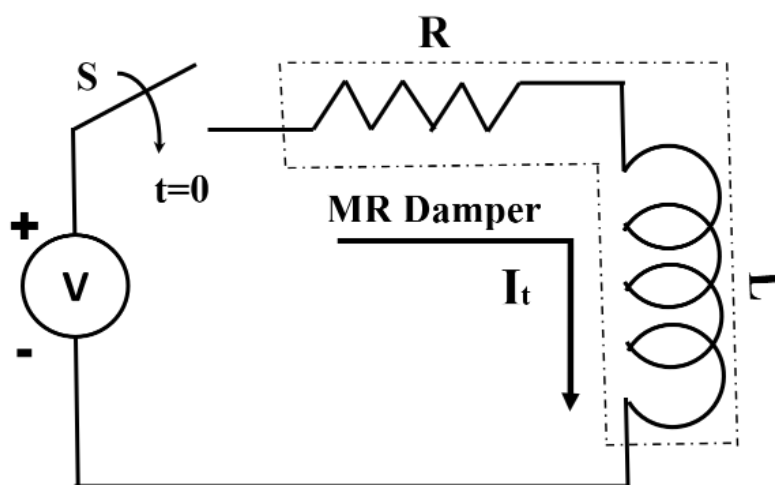
(a)



(b)

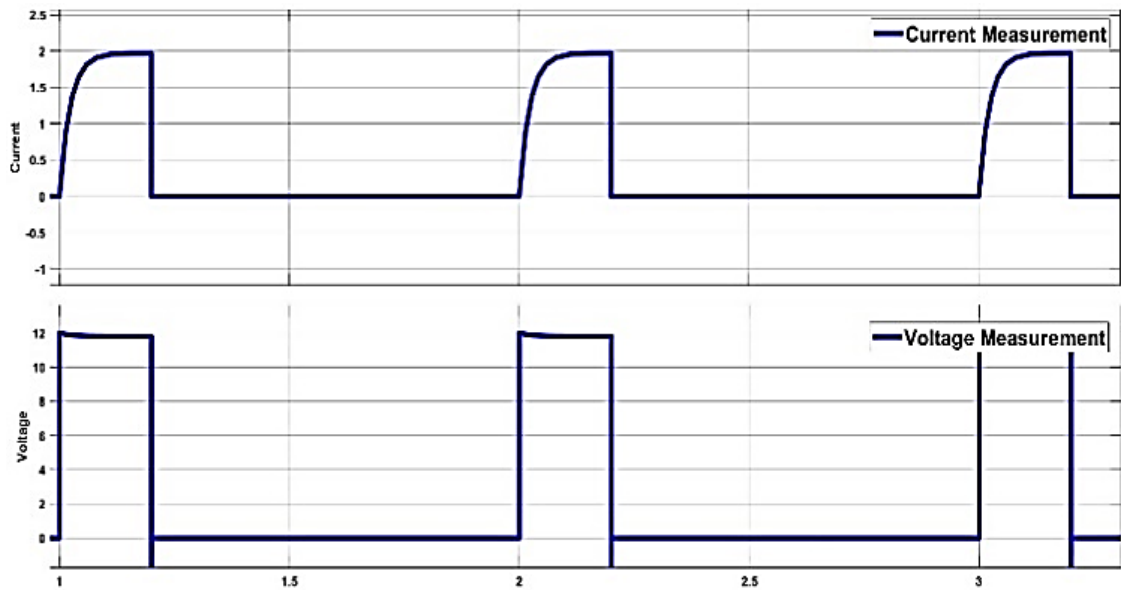
Figure 6.11 (a) Timer circuit schematic with (b) practical design for Pulsed excitation

The force overshoot can be clearly observed in all the experimented frequencies as shown in the figure 6.12. the pattern of the over shoot can be analysed by the RL circuit under transient response conditions. As we observe in the figure 6.12 (b), the rise in the current overshoot steadily increases to a certain point in a linear format as a parabolic path.



(a)



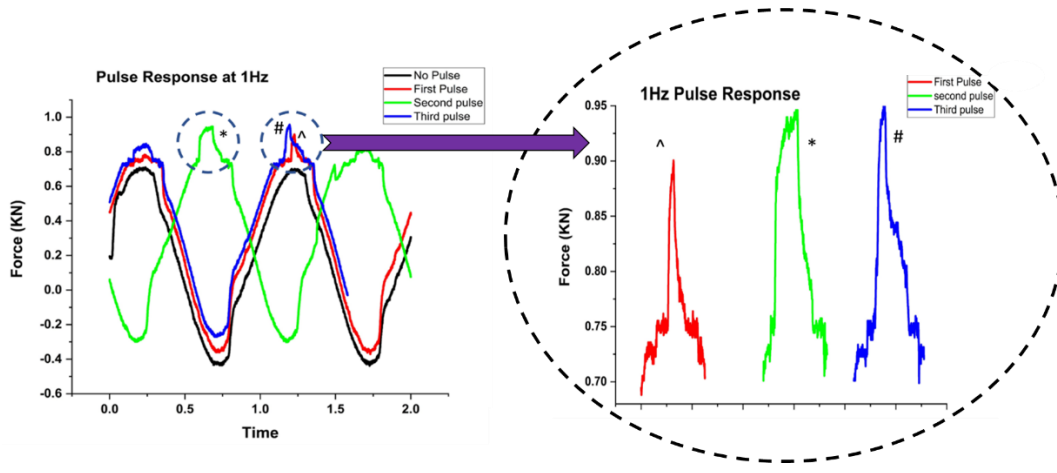


(b)

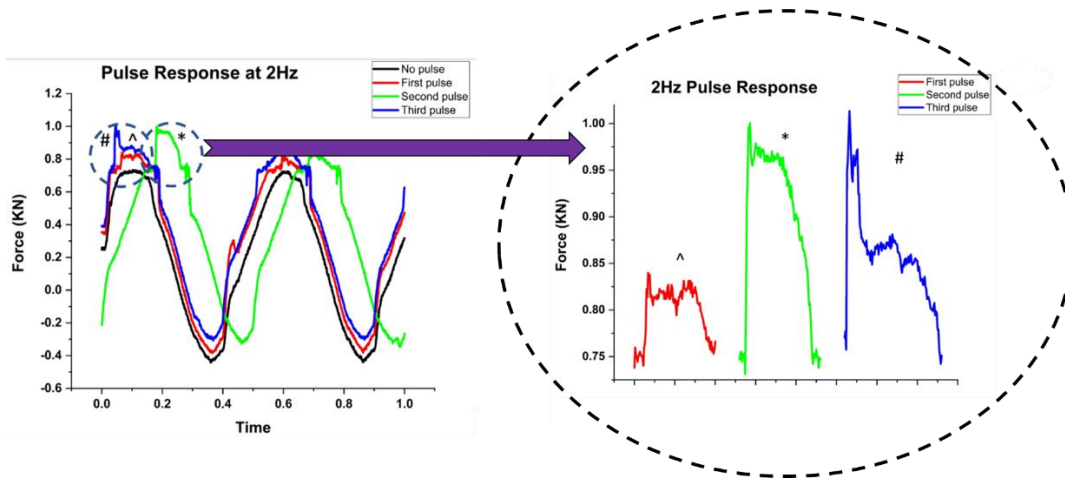
Figure 6.12 (a) RL schematic of MRD and (b) the current trace for Pulsed excitation

This is due to the inductive effect of the coil. As each pole is wound with 50 turns the total piston comprises of 300 turns and this accounts for a certain inductance value which results in such effect. Furthermore, the steepness of the parabolic curve is proportional to the length of the coil used and inversely proportional to the cross section of the coil size. Although this effect is certain for every electromagnetic circuit this phenomenon has a negligible effect on continuous control of the MR damper if the coil length to cross section ratio is less, which means that the overall impedance of the coil must be as low as possible. The internal resistance and inductance of the damper used in this study is around  $3\Omega$  and 144.25 mH respectively.

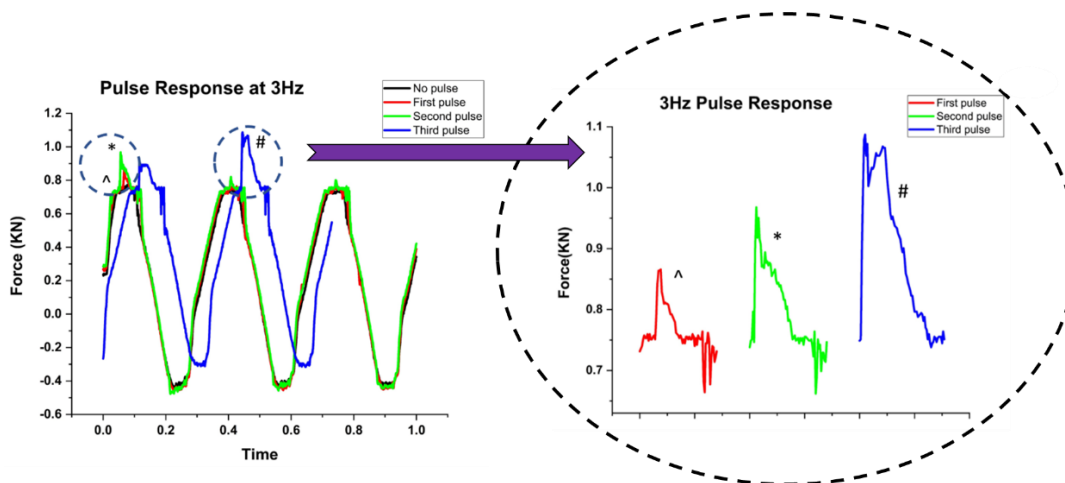
$$I_t = \frac{V}{R} [1 - e^{-Rt/L}] \quad (6.6)$$



(a)



(b)



(c)

Figure 6.13 Pulse excitation responses under (a) 1 Hz (b) 2 Hz (c) 3 Hz

The obtained damping force graphs for different pulse inputs can be observed from the figure 6.13. These indicate the parabolic increment of the damping force with respect to the coil rate of change of charge (current) which is internally dependent on the applied voltage pulses and the coil resistive and inductive properties. In other words, the obtained force responses are quite similar to the transient response of the rise and fall of the current in RL circuit with a certain delay in time.

## 6.6 MODELLING OF HRFP BASED MR DAMPER

Polynomial fitting based non parametric modelling is used to model the MR damper. The Force  $F$  and Current  $I$  relation is obtained by taking maximum and minimum forces for rebounding stroke and compression stroke for four dynamic conditions are shown in table 6.3.

Table 6.3 The maximum and minimum forces with respect to current  $I$

	20mm 0.8Hz		20mm 1.2Hz		20mm 1.6Hz		20mm 2Hz	
Current (A)	Max Force (N)	Min Force (N)	Max Force (N)	Min Force (N)	Max Force (N)	Min Force (N)	Max Force (N)	Min Force (N)
0	458.16	-444.19	627.35	-619.89	850.77	-786.9	1067.68	-1025.5
0.3	579.63	-489.74	781.36	-678.45	991.76	-856.3	1217.35	-1086.2
0.6	627.35	-537.46	957.05	-747.87	1176.14	-919.2	1375.69	-1114.4
0.9	692.42	-561.32	1076.36	-769.56	1278.08	-958.2	1494.99	-1162.1
1.2	742.31	-730.51	1067.68	-821.62	1330.14	-1008.1	1527.53	-1188.2
1.5	755.33	-823.78	1082.86	-1040.7	1356.17	-1068.8	1555.73	-1181.6
1.8	755.33	-1025.5	933.1	-1092.7	1371.3	-1231.5	1551.3	-1541.7

The force  $F$  and Current  $I$  equations for different dynamic conditions are as in table 6.4.

Table 6.4 Force - Current equations for HRFP based MR damper

Operating Condition	Force Current relation
20 mm 0.8 Hz	$F = -107.3I^2 + 354.8I + 464.87$ for $F > 0$ $F = -171.87I^2 - 0.7702I - 457.15$ for $F < 0$
20 mm 1.2 Hz	$F = 53.764I^4 - 302.9I^3 + 169.3I^2 + 537.49I + 624.06$ for $F > 0$ $F = 1041.5I^5 - 4355I^4 + 6110.4I^3 - 3313.8I^2 + 369.55I - 620.38$ for $F < 0$
20 mm 1.6 Hz	$F = -201.13I^2 - 653.06I + 841.06$ for $F > 0$ $F = -147.29I^3 + 334.57I^2 - 371.52I - 782.16$ for $F < 0$
20 mm 2 Hz	$F = -210.88I^2 - 650.98I + 1059.5$ for $F > 0$ $F = -862.89I^5 + 3367.7I^4 - 4585.4I^3 + 2578.5I^2 - 653.75I - 1025.2$ for $F < 0$

The entire process of curve fitting and estimating the polynomial curve can be performed either manually or by means of curve fitting and tracing algorithms. The graphs from the figure 6.14 and 6.15 clearly state the rise in the damping force with respect to the current and the damper velocity.

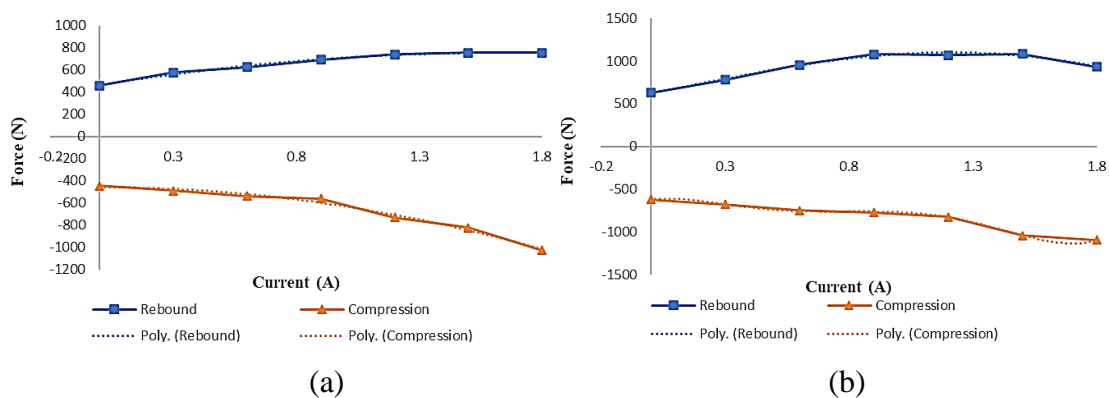


Figure 6.14 Force Vs Current at (a) 20mm 0.8Hz (b) 20mm 1.2Hz

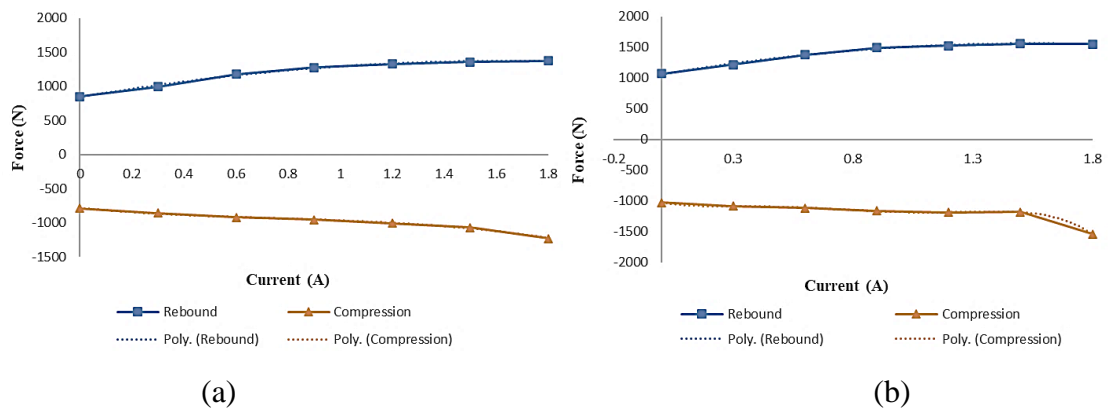


Figure 6.15 Force Vs Current at (a) 20mm 1.6Hz and (b) 20mm 2Hz

Force F, Velocity V relation at different values of currents i.e., 0A, 0.3A, 0.6A, 0.9A, 1.2A and 1.5A was obtained using polynomial fitting and are represented in table 6.5.

Table 6.5 Force Velocity equations for HRF based MR damper

Current (A)	Force Velocity equation
0	$F = 337287v^5 - 14304v^4 - 29604v^3 + 1440.6v^2 + 4695.4v - 10.875$
0.3	$F = 441412v^5 - 12483v^4 - 45296v^3 + 1346.1v^2 + 5688.8v + 30.993$
0.6	$F = 146733v^5 - 57529v^4 - 28132v^3 + 5736.3v^2 + 6142.3v - 3.698$
0.9	$F = 179964v^5 - 99707v^4 - 37245v^3 + 8623.9v^2 + 6902.2v + 10.243$
1.2	$F = 605230v^5 - 106842v^4 - 77189v^3 + 10693v^2 + 7877.6v - 83.036$
1.5	$F = 648387v^5 - 55762v^4 - 93960v^3 + 8492.3v^2 + 8792.5v - 123.14$
1.8	$F = 1E+06v^5 - 143897v^4 - 131777v^3 + 13644v^2 + 9570.3v - 275.8$

The equations provide a profile of the force velocity curves which can be implemented in modelling of the damper. The obtained results of the polynomial fitting, represented in table 6.5 are obtained from the force-velocity curves in presence of the damper currents from the figure 6.16.

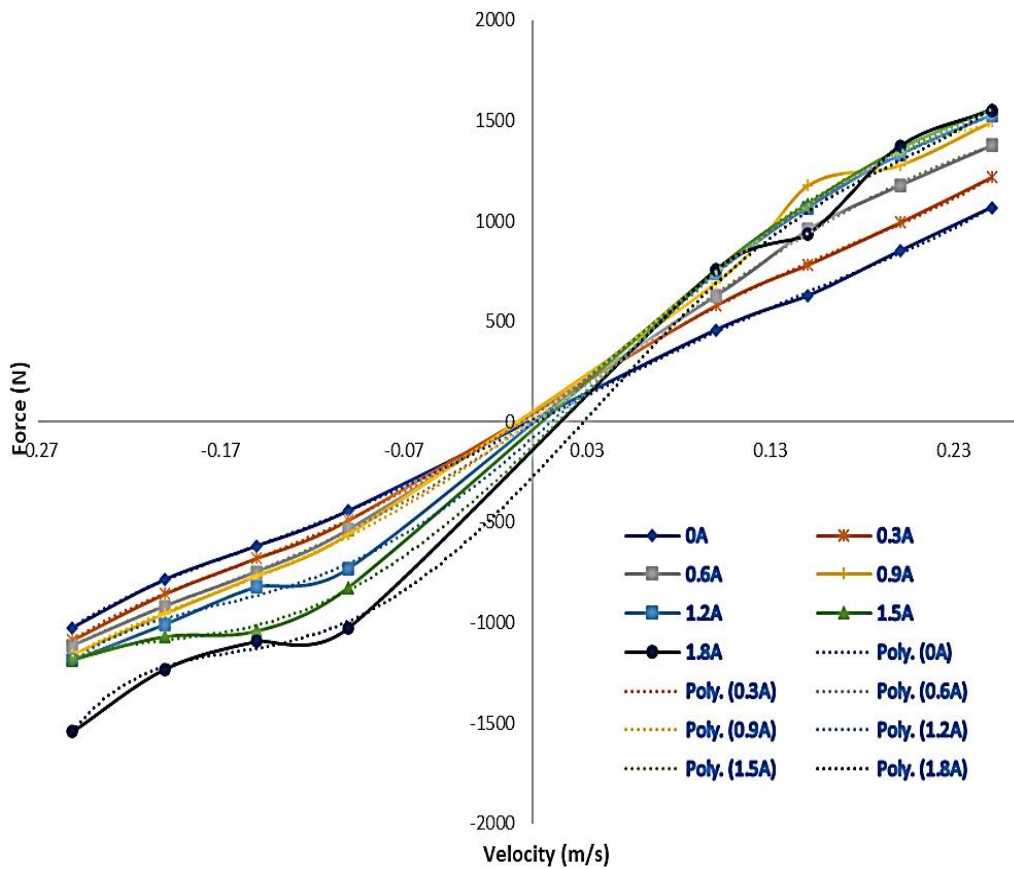


Figure 6.16 Force – velocity curves at different currents of HRFP based MR damper

### 6.7 RESPONSE OF MMQ USING HRFP BASED MR DAMPER

The quarter car model considering the parameters specified in table 6.6 in association with the polynomial model have been implemented with the sliding mode control strategy. The analysis of quarter car suspension model with off-state, sliding mode control and 1.2 A constant current semi-active suspension system has been carried out under a continuous sinusoidal input with an amplitude of 0.01m, 3hz frequency is considered for the road input profile.

Table 6.6 Parameters of the Quarter Car Model with HRFP based MR damper

Quarter car Parameters	Value of the parameter
Sprung mass $M_s$	150 Kg
Unsprung Mass $M_{us}$	15.82 Kg
Sprung stiffness $K_s$	24000 N/m
Unsprung stiffness $K_{us}$	180000 N/m

The sprung mass acceleration responses of suspension are illustrated in figure 6.17. It is observed that the peak sprung mass acceleration has been reduced to 12.87% in case of sliding mode-controlled suspension system when compared with the off state.

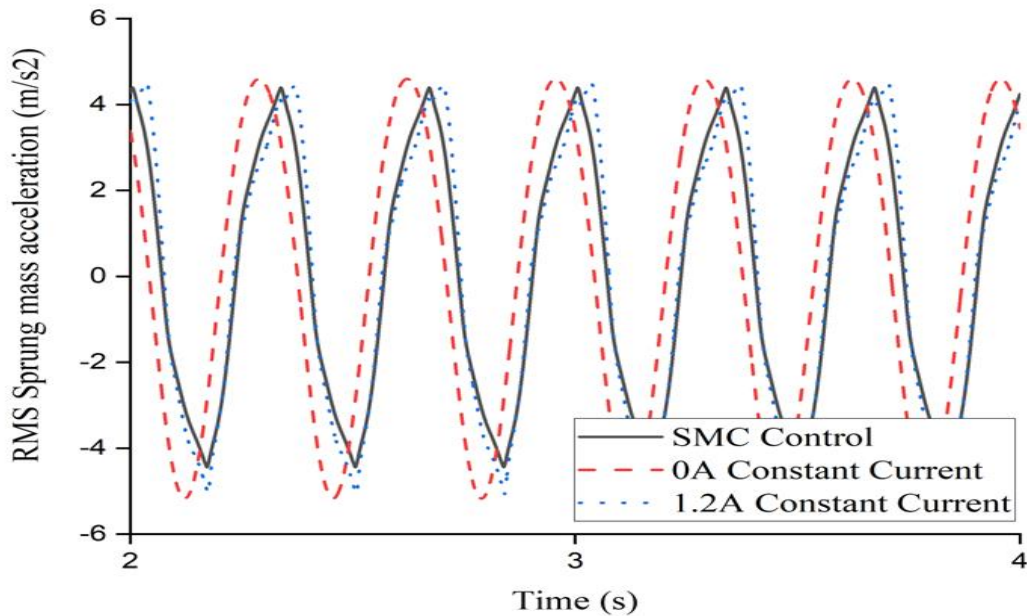


Figure 6.17 Sprung mass acceleration of MMQ with HRFP based MR damper

The RMS acceleration response of the quarter car system specifies  $3.512\text{m/s}^2$  and  $2.985\text{m/s}^2$  with MR damper off-state and the implementation of sliding mode control respectively. The road holding characteristics of the suspension system provides  $0.008771\text{m}$  with off-state and  $0.005501\text{m}$  stability to the vehicle with sliding mode control by making significant contact with the ground. Thus, the control provides an improvement of 15.01% on RMS acceleration and 37.28% of RMS road holding with respect to the off-state response of the MR damper.

## 6.8 RESPONSE OF MMT USING HRFP BASED MR DAMPER

The parameters of the two-wheeler vehicle were considered with reference to Karanam (2016) to develop the two-wheeler model. The parameters are listed in table 6.7. The two-wheeler mathematical model was subjected to random road excitation as specified in the equation 3.15.

Table 6.7 Parameters for two-wheeler mathematical model with HRFP MR damper

Parameters	Value
Wheelbase ( $a_1 + a_2$ )	1.26 m
Sprung mass ( $M_s$ )	155.6 kg
Front unsprung mass ( $M_{uf}$ )	12.28 kg
Front tire damping ( $C_{tf}$ )	700 Ns/m
Distance of front unsprung from center of gravity ( $a_1$ )	0.6237 m
Front tire stiffness ( $K_{tf}$ )	180000 N/m
Front spring stiffness ( $K_{sf}$ )	24000 N/m
Distance of rear unsprung from centre of gravity ( $a_2$ )	0.6363 m
Rear unsprung mass ( $M_{ur}$ )	15.82 kg
Rear tire damping ( $C_{tr}$ )	700 Ns/m
Rear tire stiffness ( $K_{tr}$ )	180000 N/m
Rear spring stiffness ( $K_{sr}$ )	24000 N/m
Inertia ( $I_y$ )	1105 kgm <sup>2</sup>

In this study sliding mode control is designed to control the two-wheeler suspension model. The suspension deflection is measured and sent to the SMC controller to produce the required control signal. This control signal is fed to the current amplifier to produce the required current for the MR damper. In order to ensure that the current fed to the damper is under the physical limitation of the damper, a current limiter is provided to limit the current between 0 to 1.2 A.



The bounded current (limited current) including the suspension deflection are fed to the MR damper. The detailed design of the control strategy is illustrated in the figure 6.18.

The sliding mode control parameters i.e.,  $\lambda$  and  $G$  which are sliding mode constant and the current gain are selected based on the obtained expected force and the damping force. The obtained values for the MR damper fit MMT are  $\lambda=1$  and  $G=0.8$ .

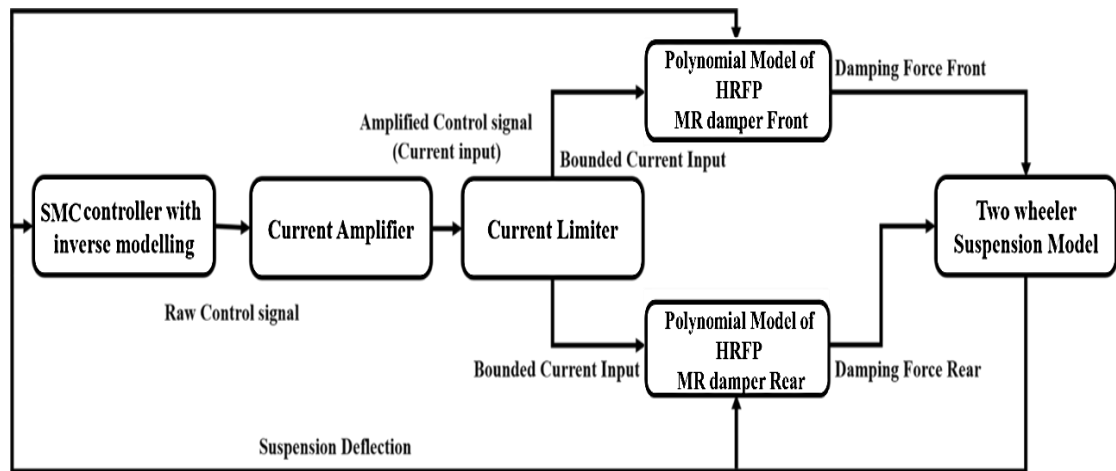
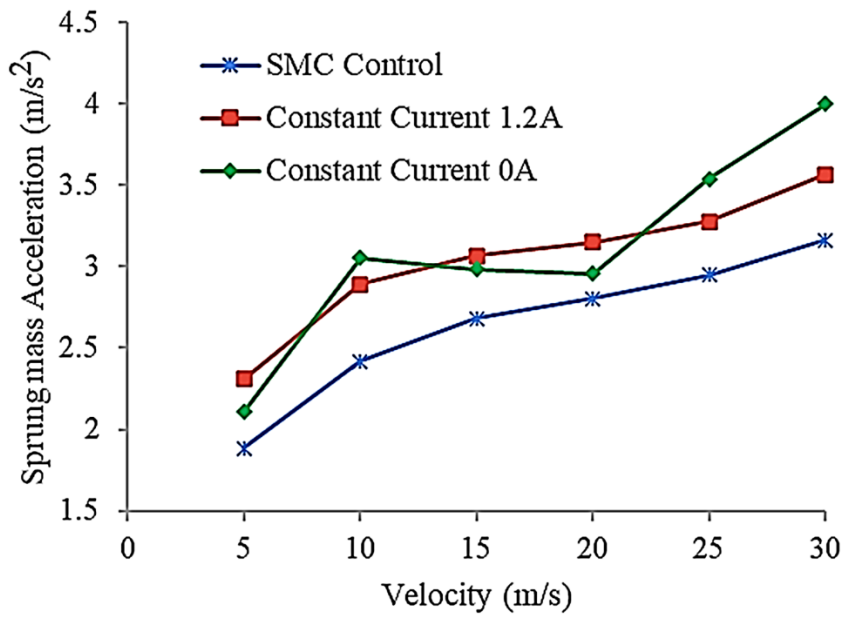


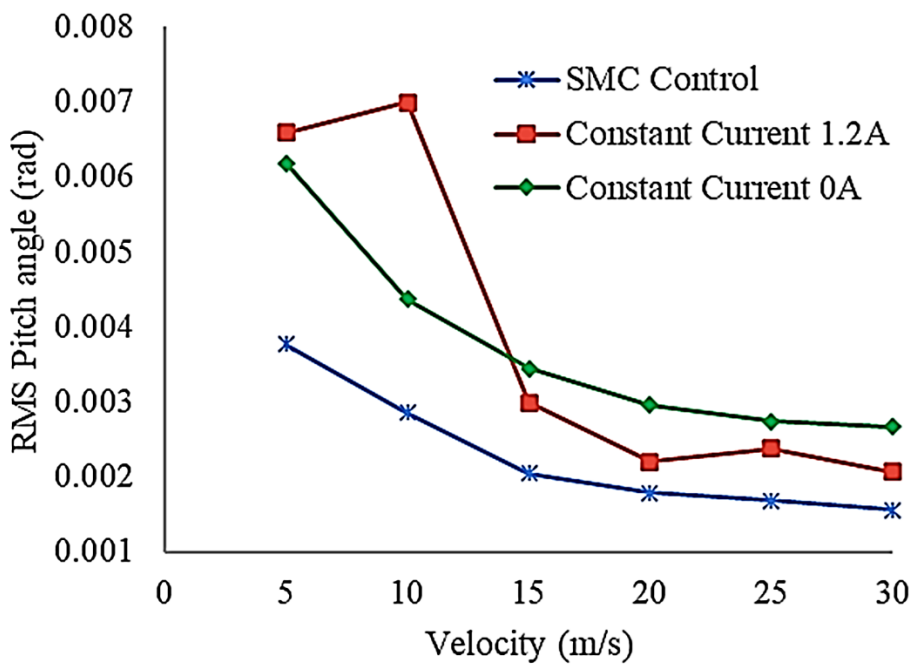
Figure 6.18 Block diagram representation of the SMC on two-wheeler suspension

The analysis of two-wheeler semi active suspension model with off state, sliding mode control and 1.2 A constant current semi-active suspension system has been carried out under random irregularities for different vehicle velocities.

The vertical acceleration responses of semi-active two-wheeler suspension at various speeds are illustrated in figure 6.19(a). It is observed that sprung mass acceleration has been reduced to 10.58% in case of sliding mode-controlled suspension system when compared with the off state at 5 m/s vehicular velocity.



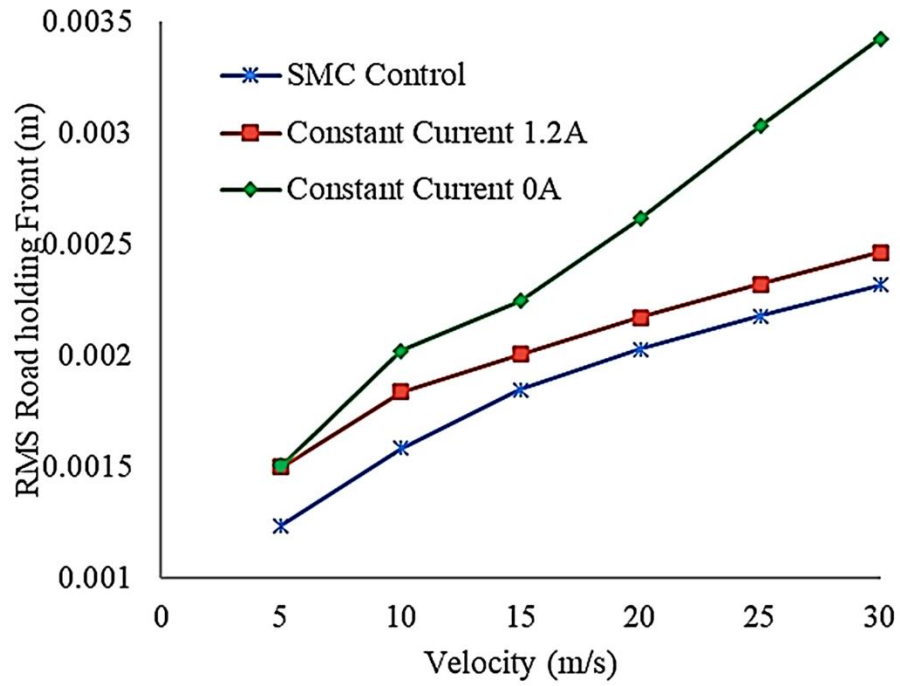
(a)



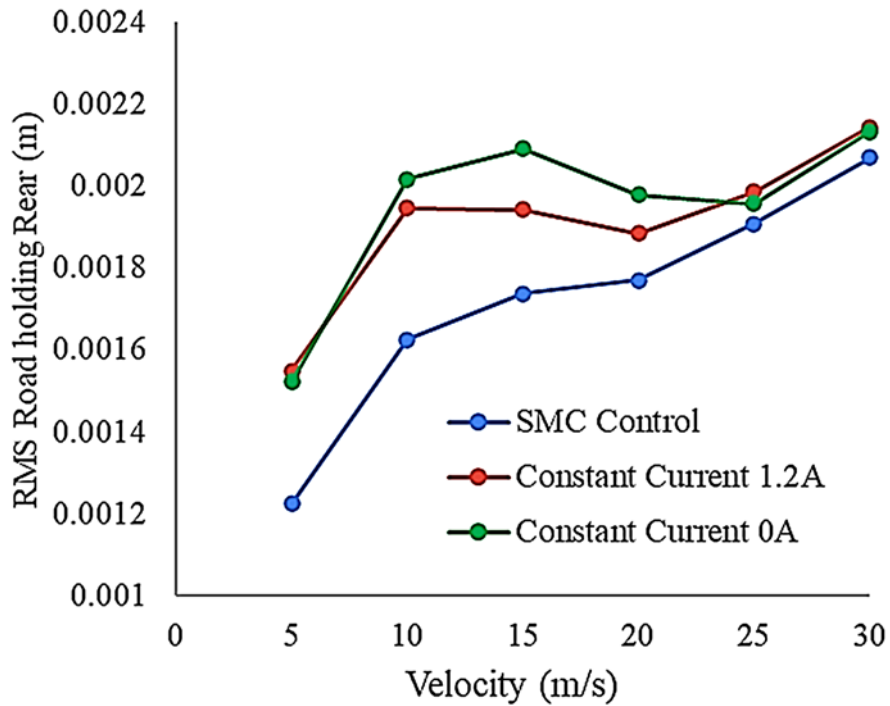
(b)

Figure 6.19 (a) Sprung mass RMS acceleration and (b) pitch angle with current inputs

Figures 6.20 (a) and (b) demonstrate the road holding nature of the two-wheeler suspension at front and rear wheel respectively with different vehicle velocity.



(a)



(b)

Figure 6.20 Road holding of (a) front and (b) rear for different velocity inputs

It is observed that two-wheeler model with developed polynomial modelled MR based suspension system provides about 32.28% improved road holding (at front

wheel) with sliding mode controlled current input than with off-state condition. But it was also observed that the performance of the system was not up to the mark at rear position in terms of road holding. Hence, still there is a scope for improving the damper performance at rear position. The analysis of pitch angle motion of the sprung mass showed good improvement using MR damper with SMC controller when compared to off-state condition (figure 6.19(b)).

The developed MR damper in two-wheeler semiactive suspension model showed a good improvement in performance with SMC controller in terms of RMS acceleration of sprung mass and road holding at front unsprung position of the vehicle. Although rear road holding is not similar to that of the front road holding, the SMC control was showing better results compared to that of the off-state and reduced improvement with increase in the velocity is noted.

## **6.9 SUMMARY**

A novel design of HRF based MR damper was designed and fabricated which can house both the axial and radial fluxes within the piston core. The fabricated damper was able to provide effective change in the damping force with respect to the off-state and also with the individual steps of current change until saturation. The analysis of the prototype damper in the quarter car and two-wheeler models also signify that the damper would be effective for implementation in real-time, provided, the damper must be re-designed based on the space constraints of the respective vehicle.

## CHAPTER 7

### SUMMARY AND CONCLUSIONS

#### 7.1 SUMMARY

The entire study has put forth the design of various types of mono tube MR dampers with the implementation of different piston designs. The designed dampers can be categorised into three categories based on the flux flow path and its distribution. They are:

- ❖ Axial flux design
- ❖ Radial flux design
- ❖ Hybrid Radial flux design

Two different axial flux and radial flux dampers were designed considering the application i.e., for two-wheeler motor vehicle and for the E-bicycle. A new damper with a novel piston design has also been fabricated. The novel design makes an effective flow of magnetic flux combining both axial and radial flux flows in the piston created with in it. This design results in the reduction of the material used in the design of the MR damper piston.

##### 7.1.1 Axial flux design-based Two-wheeler motor vehicle MR damper

Two-wheeler axial flux design-based MR damper, as specified, was fabricated considering the dimensions of the two-wheeler vehicle's (Splendor plus Make: Hero moto corp.) rear suspension. The damper internal dimensions i.e., the piston design, cylinder size, fluid flow gap etc are considered using the Matlab optimization tool box and the obtained parameters are put in the FEMM software tool resulting in a 0.307T magnetic flux density in the fluid flow gap.

In order to avoid the turbulent effect in the specified design the entire piston is fitted with a sheet of brass fitted over the entire piston causing the piston to be leakproof and not allowing the fluid to flow into the piston area. This design has the disadvantage of reducing the flux generated at the poles of the piston making the entire damper to

produce weak additional damping force aiding to the existing hydraulic damping force (off-state damping).

The Kwok modeling of the produced axial flux damper provides an effective mathematical model considering the force-velocity curves of the damper. This model, as specified, would not give better results if used to the dampers force-velocity curves doesn't match with the ideal characteristic curves of the damper. Thus, polynomial modelling is considered for further studies as this modelling depending on the maximum and minimum damping force with respect to the velocity. This modelling on the other hand is also suitable for implementation of real-time control as the modelling does not involve in complex mathematical equations and analysis of multiple modelling parameters.

The sprung mass acceleration graphs obtained in the quarter car suspension models show 10.56% reduction in the RMS acceleration when compared with the off-state value. Similarly, 19.3% RMS acceleration reduction in the sprung mass is observed in the two-wheeler suspension model at 5m/s vehicular velocity using PID control to that of the off-state response. The real time implementation of the damper also shows the effectiveness of the MR damper under off-state and constant current condition providing about 40% reduction of rms sprung mass acceleration. Even though the RMS acceleration is showing considerable reduction it was considered on the single bump with no control scheme applied. Similar design was implemented in radial flux-based design and e-bicycle application with control schemes to obtain its effectiveness.

### **7.1.2 Radial flux design-based Two-wheeler MR damper**

The radial flux damper has been designed and fabricated considering the dimensions of the two-wheeler vehicles (pulsar 200 make: Bajaj Auto corp.) rear suspension so as to be implemented in real-time testing. The dampers dimensional characteristics are obtained using the optimization tool box available in the MATLAB. The designed damper parameters are fit in FEMM software tool to obtain the estimated flux density. The magnetic flux density obtained in the analysis is 0.38T around the fluid flow gap which is 20% higher than the axial flux design.

As the brass fitting over the piston was providing a very low magnetic flux density in the fluid flow gap the piston gaps create turbulent flows which are avoided by filling them with glue or wax. the winding provides a concentrated magnetic field which actually is contrary to the axial flux design providing the distributed magnetic flux. The only disadvantage with this design is that the complexity in designing the piston core and the difficulty in winding the coil over the magnetic poles. The magnetic flux obtained from this design is quite effective and provide good dynamic range implementing in the vehicular suspension.

The modelling of the damper was performed using the polynomial model considering the maximum force with respect to the velocity. The mathematical modeling is effective in the implementation of real-time control of the MR damper in the vehicle.

The real-time implementation of MR damper on the vehicle to be moving at a speed of 25km/h provides sprung mass acceleration reduction of 29.17 % peak value under crest condition and 29.3% under trough condition with sliding mode control with respect to the off-state condition of the MR damper.

### **7.1.3 E-bicycle Axial flux design-based MR damper**

A prototype MR damper with axial flux design was designed and fabricated considering the dimensions of the custom modified E-bike vehicle (Crest Make: Atlas Bicycles.) seat suspension which can also be considered as the rear suspension as there are other heavy equipment on the sprung mass. The designed MR damper was providing a value of 0.48T flux density in the fluid flow gap considering the open source FEMM software tool. In order to reduce the turbulent effect electrical insulation resin is used in filling the piston gaps which was good yet problem with the air trapped inside the damper (being smaller in size and absence of the accumulator) causes wavy pattern instead of smoother response for the force-displacement and the force-velocity curves. The fabricated damper fits effectively on the E-bicycle.

The modelling of the damper was performed using the polynomial model considering the maximum force with respect to the velocity. The mathematical

modeling is effective in the implementation of real-time control of the MR damper in the vehicle. the mathematical model implementation in the quarter car model and two-wheeler model provides around an average of 14.94% and 24.26% reduction of sprung mass acceleration respectively using sliding mode control design with respect to the off-state of the MR damper.

The real-time implementation of MR damper on the vehicle to be moving at a speed of 20km/h provides sprung mass acceleration reduction of 24.11% peak value with sliding mode control with respect to the off-state condition of the MR damper

#### **7.1.4 E-bicycle Radial flux design-based MR damper**

A radial flux piston-based design was designed and fabricated considering the dimensions of the custom modified E-bicycle vehicle seat suspension. The designed damper was providing a value of 0.51T magnetic flux density yet could not provide proper characterization results due to following issues

- The irregular shaping of the poles and the bottlenecks created in the flux flow path of the piston.
- The finishing of the damper was not proper as the cost and complexity of the design are quite high considering the vehicle it needs to be deployed in.
- The flux passage might have a severe issue with the internal passage drilled for coil through the piston.
- The size of the hole reduces the maximum material in the piston between the poles creating a bottleneck for the magnetic flux to pass through.

Modelling of the specified damper was considered using radial basis function approach to provide the effective predicted force. The modelling was also unable to predict the force and its respect.

#### **7.1.5 Hybrid Radial Flux Piston based MR Damper**

1. The designed and fabricated hybrid radial flux piston (HRFP) is able to provide considerable magnetic flux density in the MR fluid flow path creating a considerable damping force with respect to the change in the current.



2. The HRFP MR damper is able to provide both axial and radial fluxes in the MR fluid flow gap.
3. For 2Hz operating frequency the damping force recorded was 1kN at off state condition and 1.6kN at 1.8A excitation which shows the capability of the damper in reaching higher damping forces.
4. The damper coil measures  $3\Omega$  and 144.25 mH satisfying the mean value for reducing the surges and time delay in damper operation.
5. The peak force change for pulsed excitation was recorded as 0.35 kN for the 3Hz operating frequency.
6. The reduction in rms sprung mass acceleration was observed to be 15% in quartercar suspension and 10.58% for the two-wheeler suspension system respectively for the SMC control implementation using HRFP based MR damper.

## **7.2 CONCLUSION**

### **7.2.1 Comparison of Axial and Radial flux piston-based MR dampers**

From the above analysis and experimentation certain conclusions can be drawn out. They are:

1. Both the axial and radial flux designs provide effective damping force in its own way but in this case axial design was providing effective variation in the damping force with respect to current.
2. In order to provide an effective radial flux design precise fabrication of the piston is an important factor considering high complexity in fabrication process axial flux design would be a most common low-cost alternative for radial flux designs.
3. One of the major disadvantages of radial flux design is the remanent flux which would be present in the piston poles creating further more complexity in continuous control and real time applications.
4. Axial flux design is much effective in the applications where size of the damper plays a crucial part.

5. Radial flux designs offer better performance where size of the piston is not a constraint.

### **7.2.2 Real time control of two-wheeler and e-bicycle with MR damper**

1. The real time implementation of axial flux-based two-wheeler MR damper was performed on two-wheeler (Splendor plus) with manual change in current. The results show 40% reduction in the dampening of body vibrations when compared with the off- state condition on a random bump road profile.
2. The real-time implementation of radial flux-based two-wheeler MR damper was performed on the vehicle (Pulsar 200) to be moving at a speed of 25km/h provided a reduced body vibrations of 29.17 % peak value under crest condition and 29.3% under trough condition with sliding mode control with respect to the off-state condition of the MR damper.
3. The real-time implementation of axial flux MR damper on the e-bicycle to be moving at a speed of 20km/h provided a reduced vibration of 24.11% peak value with sliding mode control with respect to the off-state condition of the MR damper.

### **7.2.3 Hybrid Radial flux piston-based MR damper**

1. The hybrid radial flux piston (HRFP) is capable of providing considerable magnetic flux density in the MR fluid flow path creating a uniform damping force with respect to the change in the current supply until the magnetic saturation occurs.
2. The instantaneous surges in the control signal will have a larger impact on the MR damper if the Resistance and Inductance values of the damper coil are low and vice versa
3. The parabolic curve in the force surges is due the inductance of the damper coil, which means the higher the inductance, more the time delay to achieve the maximum force at that point.

4. The voltage or the current surges in the power source of the MRD may result in the destruction of the damper coil. This can be reduced by increasing the inductance of the damper coil and also by employing a surge protection circuit between the damper and the power source.

### **7.3 SCOPE FOR THE FUTURE WORK**

Although extensive work has been carried out in terms of design and implementation of different MR dampers for the vehicular applications there is always scope for improvement in various aspects. Some of them are specified below:

- The radial flux design can be easily implemented in four-wheeler vehicles due to larger space availability for the piston design.
- The remanent magnetic field formed in the radial flux piston design can be reduced by changing the piston core with the silicon steel. Example: M-19.
- The designed HRFP based MR damper can be implemented in two-wheeler and four-wheeler vehicular suspension in real-time.
- The coil wound in various designs discussed earlier can be modified to create rotating magnetic field in the fluid flow gap which can reduce or nullify the sedimentation issue of the iron carbonyl particles in the MR fluid.



## REFERENCES

- Acharya, S., Saini, T. R. S., and Kumar, H. (2019). "Determination of optimal magnetorheological fluid particle loading and size for shear mode monotube damper". *J. Braz. Soc. Mech. Sci. Eng.*, 41(10), 1-15.
- Ahmadian, M. (2017). "Magneto-rheological suspensions for improving ground vehicle's ride comfort, stability, and handling". *Veh. Syst. Dyn.*, 55(10), 1618-1642.
- Ahmadian, M., and Sandu, C. (2008). "An experimental evaluation of magneto-rheological front fork suspensions for motorcycle applications". *Int. J. Veh. Syst. Model. Test.*, 3(4), 296-311.
- Ahmadian, M., and Sandu, C. (2008). An experimental evaluation of magneto-rheological front fork suspensions for motorcycle applications. *Int. J. Veh. Syst. Model. Test.*, 3(4), 296-311. <https://doi.org/10.1504/ijvsmt.2008.025405>.
- Ambhore, N., Hivarale, S., and Pangavhane, D. (2013). "A study of Bouc-Wen model of magnetorheological fluid damper for vibration control". *Int. J. Eng. Res.*, 2(2), 1-6.
- Aruna, M. N., Rahman, M. R., Joladarashi, S., and Kumar, H. (2019). "Influence of additives on the synthesis of carbonyl iron suspension on rheological and sedimentation properties of magnetorheological (MR) fluids". *Mater. Res. Express*, 6(8), 086105.
- Ata, W. G., and Salem, A. M. (2017). "Semi-active control of tracked vehicle suspension incorporating magnetorheological dampers". *Veh. Syst. Dyn.*, 55(5), 626-647.
- Aydar, G., Wang, X., and Gordaninejad, F. (2010). "A novel two-way-controllable magneto-rheological fluid damper". *Smart. Mat. Struct.*, 19(6), 065024.
- Baig, W. M., Hou, Z., and Ijaz, S. (2017). "Fractional order controller design for a semi-active suspension system using nelder-mead optimization". *Proc. 29th Chinese Control and Decision Conf. CCDC 2017.*, Chongqing, China, 2808-2813.

- Boese, H., and Ehrlich, J. (2010). "Performance of magnetorheological fluids in a novel damper with excellent fail-safe behavior". *J. Intell. Mater. Syst. Struct.*, 21(15), 1537-1542.
- Bossis, G., Lacin, S. and Meunier, A. (2002). "Magnetorheological fluids". *J. Magn. Mater.* 224-228.
- Breese, D. G., and Gordaninejad, F. (2000). "Semiactive field-controllable magnetorheological fluid dampers for mountain bicycles". *Proc. Smart. Struct. and Mat. 2000: Industrial and Commercial Applications of Smart. Struct. Tech. SPIE.*, 3991(1), 283-293.
- Chen, B. C., Shiu, Y. H., & Hsieh, F. C. (2011). "Sliding-mode control for semi-active suspension with actuator dynamics". *Veh. Syst. Dyn.*, 49(1-2), 277-290.
- Chang, C. C., and Zhou, L. (2002). "Neural network emulation of inverse dynamics for a magnetorheological damper". *J. Struct. Eng.*, 128(2), 231-239.
- Charalampakis, A. E. (2010). "Parameters of Bouc-Wen hysteretic model revisited". In *Proc. of the 9th HSTAM International Congress on Mechanics*.
- Chen, C., Chan, Y. S., Zou, L., and Liao, W. H. (2018). Self-powered magnetorheological dampers for motorcycle suspensions. *Proc. Int. J. Mech. Eng. Part D: J. Auto Eng.*, 232(7), 921-935. <https://doi.org/10.1177/0954407017723761>.
- Chen, Y. (2009). "Skyhook surface sliding mode control on semi-active vehicle suspension system for ride comfort enhancement". *Sci. eng. res.*, 1 (1). pp. 23-32. ISSN 1947-3931
- Cheng, M., Chen, Z. B., and Xing, J. W. (2018). "Design, analysis, and experimental evaluation of a magnetorheological damper with meandering magnetic circuit". *IEEE Trans. Magn.*, 54(5), 1-10.
- Chi, Z., He, Y., and Naterer, G. F. (2008). "Design optimization of vehicle suspensions with a quarter-vehicle model". *Trans. Can. Soc. Mech. Eng.*, 32(2), 297-312.

- Cortes R, J. A., Villarreal-Gonzalez, L. S., and Martinez M, M. (2005). "Characterization, modeling and simulation of magnetorheological damper behavior under triangular excitation". *Adv. Technol. Mater. Mater. Process. J.*, 7(2), 135.
- Desai, R. M., Jamadar, M. E. H., Kumar, H., Joladarashi, S., and Raja Sekaran, S. C. (2019). "Design and experimental characterization of a twin-tube MR damper for a passenger van". *J. Braz. Soc. Mech. Sci. Eng.*, 41(8), 1-21.
- Desai, R. M., Jamadar, M. E. H., Kumar, H., Joladarashi, S., and Sekaran, S. R. (2019). Design and experimental characterization of a twin-tube MR damper for a passenger van. *J. Braz. Soc. Mech. Sci.*, 41(8), 1-21.
- Desai, R. M., Jamadar, M. E. H., Kumar, H., Joladarashi, S., Rajasekaran, S. C., and Amarnath, G. (2019). "Evaluation of a commercial MR damper for application in semi-active suspension". *SN Appl. Sci.*, 1(9), 1-10.
- Devikiran, P., Puneet, N. P., Hegale, A., and Kumar, H. (2021). "Design and development of MR damper for two wheeler application and Kwok model parameters tuning for designed damper". *Proc. Int. J. Mech. Eng. Part D: J. Auto Eng.*, 236(7), 1595-1606.
- Dong-Rak, L. E. E., & Jin, M. H. (2010). "Piston valve assembly and damper including the same." *U.S. Patent Application 12/499,173*, filed January 14, 2010.
- Du, H., Lam, J., and Zhang, N. (2006). "Modelling of a magneto-rheological damper by evolving radial basis function networks". *Eng. Appl. Artif. Intell.*, 19(8), 869-881.
- Duchanoy, C. A., Moreno-Armendáriz, M. A., Moreno-Torres, J. C., and Cruz-Villar, C. A. (2019). "A deep neural network based model for a kind of magnetorheological dampers". *Sensors*, 19(6), 1-18.
- El-Kafafy, M., El-Demerdash, S. M., and Rabeih, A. A. M. (2012). "Automotive ride comfort control using MR fluid damper". *Sci. eng. res.*, 4(1), 179-187

Eriksen, E. O., and Gordaninejad, F. (2000). "Magneto-rheological fluid shock absorber for suspension of an off-road motorcycle: a theoretical study". *Proc. Smart. Struct. and mat. 2000: industrial and commercial applications of smart. Struct. Tech. SPIE.*, 3991(1), 273-282.

Eshkabilov, S. (2016). "Modeling and simulation of non-linear and hysteresis behavior of magneto-rheological dampers in the example of quarter-car model". *J. Eng. Math.*, 1(1), 19-38.

Florian, P., Vrátník, P., and Čermák, R. (2015). "Modelling and Experimental Analysis Of Motorcycle Dynamics Using Matlab". In *Tech. Computing Prague 2015. Praha: University of Chemistry and Technology*.

Gadekar, P., Kanthale, V. S., and Khaire, N. D. (2017). "Magnetorheological fluid and its applications". *Int. J. curr. eng. technol.*, 7(1), 32-37.

Georgiou, G., Verros, G., and Natsiavas, S. (2007). "Multi-objective optimization of quarter-car models with a passive or semi-active suspension system". *Veh. Syst. Dyn.*, 45(1), 77-92.

Gołdasz, J. (2013). "Electro-mechanical analysis of a magnetorheological damper with electrical steel laminations". *Przegląd Elektrotechniczny*, 89(2a), 8-12.

Goldasz, J. (2013). "Study of a magnetorheological fluid damper with multiple annular flow gaps". *Int. J. Veh. Des.*, 62(1), 21-41.

Gołdasz, J. (2019, May). "Magnetostatic study of a dual-gap MR valve". In *2019 20th Int. Conf. Ind. Mechatron. Autom. (REM)* (pp. 1-5). IEEE.

Goldasz, J. P., Szklarz, Z. W., Alexandridis, A. A., Nehl, T. W., Deng, F., and Valee, O. (2005). *U.S. Patent No. 6,948,312*. Washington, DC: U.S. Patent and Trademark Office.

Gołdasz, J., and Bogdan, S., (2014). *Insight into Magnetorheological Shock Absorbers. Switzerland: Springer International Publishing*.



- Goldasz, J., Sapiński B. (2015) Introduction. In: “Insight into Magnetorheological Shock Absorbers”. *Springer, Cham*.
- Gong, X. L., Zhang, X. Z. and Zhang, P. Q. (2005). “Fabrication and characterization of isotropic magnetorheological elastomers”. *Polymer Testing*, 24(5), 669-676.
- Guan, X. C., Guo, P. F., and Ou, J. P. (2011). “Modeling and Analyzing of Hysteresis Behavior of Magneto Rheological Dampers”. *Procedia Eng.*, 14, 2756-2764.
- Guo, P., Xie, J., and Guan, X. (2018). “Dynamic model of MR dampers based on a hysteretic magnetic circuit”. *Shock. Vib.*, 4(3). 2018.
- Gurubasavaraju, T. M., Hemantha, K., and Arun, M. (2018). “A study of influence of material properties on magnetic flux density induced in magneto rheological damper through finite element analysis”. *MATEC Web Conf.*, 144, 02004.
- Gurubasavaraju, T. M., Kumar, H., and Arun, M. (2017). Optimisation of monotube magnetorheological damper under shear mode. *J. Braz. Soc. Mech. Sci. Eng.*, 39(6), 2225-2240. <https://doi.org/10.1007/s40430-017-0709-9>
- Gurubasavaraju, T. M., Kumar, H., and Mahalingam, A. (2018). “An approach for characterizing twin-tube shear-mode magnetorheological damper through coupled FE and CFD analysis”. *J. Braz. Soc. Mech. Sci. Eng.*, 40(3), 139.
- Hato, M. J., Choi, H. J., Sim, H. H., Park, B. O., and Ray, S. S. (2011). “Magnetic carbonyl iron suspension with organoclay additive and its magnetorheological properties”. *Colloids and Surfaces A: Physicochemical and Engineering Aspects*, 377(1), 103-109.
- Havelka, F., and Musil, M. (2012). “Optimal semi-active preview control of a quarter car model with magnetorheological damper with respect to tire lift off”. *Eng. Mech.*, 175.

Hegale, A., Puneet, N. P., Kumar, H., and Gangadharan, K. V. (2020, July). The effect of inclination angle of shock absorber on ride comfort and road holding of two-wheeled vehicle. *In AIP Conf. Proc.* (2247(1)). <https://doi.org/10.1063/5.0003891>.

Hemanth K. “Dynamic analysis of magnetorheological (MR) fluid based semiactive suspension system for vehicular application using nonparametric approach”. *Doctoral Dissertation*, National Institute of Technology Karnataka, Surathkal, 2016.

Hemanth, K., Ganesha, A., Kumar, H., and Gangadharan, K. V. (2014). “Analysis of MR damper based on finite element approach”. *Appl. Mech. Mater.*, 592, 2006-2010.

Hemanth, K., Kumar, H., and Gangadharan, K. V. (2018). “Dynamic analysis of half car model with MR damper as semi-active suspension element”. *Int. J. Acoust. Vib.*, 23, 13846.

Hu, G., Liu, F., Xie, Z., and Xu, M. (2016). “Design, analysis, and experimental evaluation of a double coil magnetorheological fluid damper”. *Shock. Vib.*, 2016(1), 1-13.

Hu, G., Liu, Q., Ding, R., and Li, G. (2017). “Vibration control of semi-active suspension system with magnetorheological damper based on hyperbolic tangent model”. *Adv. Mech. Eng.*, 9(5), 1687814017694581.

Hu, G., Liu, Q., Ding, R., and Li, G. (2017). “Vibration control of semi-active suspension system with magnetorheological damper based on hyperbolic tangent model”. *Adv. Mech. Eng.*, 9(5), 1687814017694581.

Hu, G., Yi, F., Liu, H., and Zeng, L. (2020). Performance Analysis of a Novel Magnetorheological Damper with Displacement Self-Sensing and Energy Harvesting Capability. *J. Vib. Eng. Technol.*, 1-19. <https://doi.org/10.1007/s42417-020-00212-7>.

Hudha, K., Jamaluddin, H., Samin, P. M., and Rahman, R. A. (2005). “Effects of control techniques and damper constraint on the performance of a semi-active magnetorheological damper”. *Int. J. Veh. Auton. Syst.*, 3(2-4), 230-252.

- Imaduddin, F., Mazlan, S. A., and Zamzuri, H. (2013). "A design and modelling review of rotary magnetorheological damper". *Mater. Des.*, 51, 575-591.
- Jaehwan, K. and Kyoung-Mi, P. (2004). "Material characterization of MR fluid at high frequencies". *J. Sound Vibr.*, 121-133
- Jamadar, M. E. H., Desai, R. M., Saini, R. S. T., Kumar, H., and Joladarashi, S. (2021). "Dynamic analysis of a quarter car model with semi-active seat suspension using a novel model for magneto-rheological (MR) damper". *J. Vib. Eng. Technol.*, 9(1), 161-176.
- Jamali, M. S., Ismail, K. A., Taha, Z., and Aiman, M. F. (2017). "Development of Matlab Simulink model for dynamics analysis of passive suspension system for lightweight vehicle". *J. Phys. Conf. Ser.*, 908, 012066.
- Jastrzębski, Ł., & Sapiński, B. (2016). "Electrical interface for a self-powered MR damper-based vibration reduction system". *Acta Mech. et Autom.*, 10(3).
- Jayabalan, A., and Kumar, N. K. S. (2018). "Vibration suppression of quarter car using sliding-mode and internal model-based skyhook controller". *J. Vib. Eng. Technol.* 6(2), 117-126. <https://doi.org/10.1007/s42417-018-0022-7>.
- Jiang, W., Zhang, Y., Xuan, S., Guo, C., and Gong, X. (2011). "Dimorphic magnetorheological fluid with improved rheological properties". *J. Magn. Magn. Mater.*, 323(24), 3246-3250
- Jun, J. B., Uhm, S. Y., Ryu, J. H. and Suh, K. D. (2005). "Synthesis and characterization of monodisperse magnetic composite particles for magnetorheological fluid materials". *Colloids and Surfaces A: Physicochemical and Engineering aspects*, 260(1), 157-164.
- Kamble, V. G., and Kolekar, S. (2014). "Analysis of rheological properties of MR fluid based on variation in concentration of iron particles". *American J. Nanotechnology*, 5(2), 12.

Karanam, V. M. (2016). “Studies In the Dynamics of Two and Three Wheeled Vehicles” *Doctoral Dissertation*, Indian Institute Science, Bangalore, 2016.

Karnopp, D. (1995). “Active and semi-active vibration isolation”. *ASME J. Vib. Acoust.*, 117(B), 170 – 174.

Kashem, S. B. A., Roy, S., and Mukharjee, R. (2014). “A modified skyhook control system (SKDT) to improve suspension control strategy of vehicles”. *2014 Intl. Conf. on Informatics, Electronics & Vision*. 14(1), 1-8.

Kciuk., S. K. and Turczyn, R. (2009). “Magnetorheological characterization of carbonyl iron-based suspension”. *J. Achiev. Mater. Manuf. Eng.*, V33.

Keshav, M., Bhagyarajan, A., and Chandramohan, S. (2019). “Regression models for magnetic flux density using DoE techniques and geometric optimization of MR valve”. *Smart Mater. Struct.*, 28(7), 075008.

Khot, S. M., Patil, S., and Bhaye, N. A. (2017, January). “Simulation study of MR damper for bump road profile”. *Int. Conf. on Nascent Technol. Eng. (ICNTE)*, 2017 (pp. 1-6). IEEE.

Kim, W. H., Park, J. H., Kaluvan, S., Lee, Y. S., and Choi, S. B. (2017). “A novel type of tunable magnetorheological dampers operated by permanent magnets”. *Sens. Actuators A: Phys.*, 255, 104-117.

Kolekar, S., Venkatesh, K., Oh, J. S., and Choi, S. B. (2019). Vibration controllability of sandwich structures with smart materials of electrorheological fluids and magnetorheological materials: a review. *J. Vib. Eng. Technol.*, 1-19. <https://doi.org/10.1007/s42417-019-00120-5>

Krishna, H., Kumar, H., and Gangadharan, K. (2017). “Optimization of magnetorheological damper for maximizing magnetic flux density in the fluid flow gap through FEA and GA approaches”. *J. Inst. Eng. (India) Ser. C*, 98(4), 533-539.

- Krishnan Unni, R., and Tamilarasan, N. (2018). "Design and analysis of a magnetorheological damper for an all-terrain vehicle". *MS and E*, 310(1), 012128.
- Kubík, M., Macháček, O., Strecker, Z., Roupec, J., Mazůrek, I., (2017). "Design and testing of magnetorheological valve with fast force response time and great dynamic force range". *Smart. Mater. Struct.* (7(26)). <https://doi.org/10.1088/1361-665X/aa6066>.
- Kumar, H., and Gangadharan, K. V. (2016). "Dynamic Analysis of Magnetorheological (MR) Fluid Based Semiactive Suspension System for Vehicular Application Using Nonparametric Approach" Doctoral dissertation, National Institute of Technology Karnataka, Surathkal.
- Kumar, M. S. (2008). "Development of active suspension system for automobiles using PID controller". *Proc. Int. Conf. Eng. Sci. Appl.*, 2(1), 1-6.
- Kumbhar, B. K., and Patil, S. R. (2014). "A study on properties and selection criteria for magneto-rheological (MR) fluid components". *Int. J. ChemTech Research*, 6, 3303-3306.
- Kwok, N. M., Ha, Q. P., Nguyen, T. H., Li, J., and Samali, B. (2006). "A novel hysteretic model for magnetorheological fluid dampers and parameter identification using particle swarm optimization". *Sens. Actuator A Phys.*, 132(2), 441-451.
- Li, W. H., Du, H., and Guo, N. Q. (2003). "Design and testing of an MR steering damper for motorcycles". *Int. J. Adv. Manuf. Technol.*, 22(3), 288-294.
- Lisenker, I., Hopkins, P. N., and Kruckemeyer, W. C. (2002). "Magnetorheological dampers with improved wear resistance". *U.S. Patent No. 6,464,051*. Washington, DC: U.S. Patent and Trademark Office.
- Liu, C., Chen, L., Yang, X., Zhang, X., and Yang, Y. (2019). "General theory of skyhook control and its application to semi-active suspension control strategy design". *IEEE Access*, 7(1), 101552-101560.

Lopez Jr, J. L., and Skarbek, J. S. (2013). "Magnetorheological (MR) piston ring and MR damper having same." *U.S. Patent No. 8,490,762*. Washington, DC: U.S. Patent and Trademark Office.

Lv, H., Zhang, S., Sun, Q., Chen, R., and Zhang, W. J. (2020). "The Dynamic Models, Control Strategies and Applications for Magnetorheological Damping Systems: A Systematic Review". *J. Vib. Eng. Technol.*, 1-17. <https://doi.org/10.1007/s42417-020-00215-4>

Lv, H., Zhang, S., Sun, Q., Chen, R., and Zhang, W. J. (2021). "The dynamic models, control strategies and applications for magnetorheological damping systems: a systematic review". *J. Vib. Eng. Technol.*, 9(1), 131-147.

Madhavrao Desai, R., Acharya, S., Jamadar, M. E. H., Kumar, H., Joladarashi, S., and Sekaran, S. R. (2020). Synthesis of magnetorheological fluid and its application in a twin-tube valve mode automotive damper. *Proc. Inst. Mech. Eng. Pt. L J. Mater. Des. Appl.*, 234(7), 1001-1016.

Manjeet, K., and Sujatha, C. M. (2018). "Modeling and optimization of non-linear Herschel-Bulkley fluid model based magnetorheological valve geometry". *IEEE/ASME Inter. Conf. Adv. Intell. Mechatron.*, 413-420.

Meng, F., and Zhou, J. (2019). "Modeling and control of a shear-valve mode MR damper for semiactive vehicle suspension". *Math. Probl. Eng.*, 2019.

Morales, A. L., Nieto, A. J., Chicharro, J. M., and Pintado, P. (2018). "A semi-active vehicle suspension based on pneumatic springs and magnetorheological dampers". *J. Vib. Control*, 24(4), 808-821.

Nam, Y. J., and Park, M. K. (2009). "Electromagnetic design of a magnetorheological damper". *J. Intell. Mater. Syst. Struct.*, 20(2), 181-191.

Namuduri, C. S., Alexandridis, A. A., Madak, J., and Rule, D. S. (2001). *U.S. Patent No. 6,279,701*. Washington, DC: U.S. Patent and Trademark Office 01.

Naserimojarad, M. M., Tadayoninejad, A., and Eghtesad, M. (2011, December). "An innovative design of fast current controller circuit for MR dampers". *2nd Int. J. instrum. control autom. (ICCIA)*, 2011 (pp. 1086-1090). IEEE.

Nehl, T. W., Alexandridis, A. A., Foister, R. T., Kruckemeyer, W. C., and Deng, F. (2012). *U.S. Patent No. 8,286,763*. Washington, DC: U.S. Patent and Trademark Office.

Nguyen, Q. H., and Choi, S. B. (2009). "Optimal design of MR shock absorber and application to vehicle suspension". *Smart Mat. Struct.*, 18(3), 035012.

Nielens, H., and Lejeune, T. (2004). "Bicycle shock absorption systems and energy expended by the cyclist". *Sports Med.*, 34(2), 71-80.

Oliver, M. L., and Kruckemeyer, W. C. (2002). *U.S. Patent No. 6,481,546*. Washington, DC: U.S. Patent and Trademark Office.

Oliver, M., Kruckmeyer, W., and Bishop, T. (2003). "Magnetorheological damper piston with bypass valving." *U.S. Patent Application 09/894,443*, filed January 2, 2003.

Omar, M., El-Kassaby, M. M., and Abdelghaffar, W. (2017). "A universal suspension test rig for electrohydraulic active and passive automotive suspension system". *Alexandria Eng. J.*, 56(4), 359-370.

Park, B. J., Fang, F. F., and Choi, H. J. (2010). "Magnetorheology: materials and application". *Soft Matter*, 6(21), 5246-5253

Park, J. H., Kim, W. H., Shin, C. S., and Choi, S. B. (2016). "A comparative work on vibration control of a quarter car suspension system with two different magnetorheological dampers". *Smart Mater. Struct.*, 26(1), 015009.

Pavel Kuzhir., George Bossis., Victor Bashtovi and Olga Volkova (2003). "Flow of magnetorheological fluid through porous media". *Eur. J. Mech. B/Fluids*, 22, 331-343

Peng, G. (2011). "Development of MR fluid damper for motorcycle steering", Master of Engineering – *Research thesis*, Faculty of Engineering, University of Wollongong.

Peng, G. R., Li, W. H., Du, H., Deng, H. X., and Alici, G. (2014). “Modelling and identifying the parameters of a magneto-rheological damper with a force-lag phenomenon”. *Appl. Math. Model.*, 38(15-16), 3763-3773.

Peng, G. R., Li, W. H., Du, H., Deng, H. X., and Alici, G. (2014). Modelling and identifying the parameters of a magneto-rheological damper with a force-lag phenomenon. *Appl. Math. Model.*, 38(15-16), 3763-3773. <https://doi.org/10.1016/j.apm.2013.12.006>.

Peng, Y., Yu, M., Du, X., Xu, X., and Fu, J. (2017). “An experimental study of vehicle suspension semi-active control with skyhook controller and magneto-rheological dampers”. *Proc. 29th Chinese Control and Decision Conf. CCDC 2017*, 7427-7429.

Phule, P. P. (2001). “Magnetorheological (MR) fluids: principles and applications”. *Smart Mater. Bull.*, 2001(2), 7-10.

Prabakar, R. S., Sujatha, C., and Narayanan, S. (2009). “Optimal semi-active preview control response of a half car vehicle model with magnetorheological damper”. *J. Sound Vib.*, 326(3-5), 400-420.

Prabakar, R. S., Sujatha, C., and Narayanan, S. (2013). “Response of a quarter car model with optimal magnetorheological damper parameters”. *J. Sound Vib.*, 332(9), 2191-2206.

Priyandoko, G., Nizam, M., and Yahya, I. (2014). “Modeling of magnetorheological damper using back propagation neural network”. *In Adv. Mater. Res.* (896), pp. 396-400). <https://doi.org/10.4028/www.scientific.net/amr.896.396>.

Rabinow, J. (1948). “The magnetic fluid clutch”. *Elect. Eng.*, 67(12), 1167-1167. <https://doi.org/10.1109/ee.1948.6444497>

Rahman, M., Ong, Z. C., Julai, S., Ferdous, M. M., and Ahamed, R. (2017). “A review of advances in magnetorheological dampers: their design optimization and applications”. *J. Zhejiang Univ. Sci. A*, 18(12), 991-1010.



- Rajendiran, S., Lakshmi, P., and Rajkumar, B. (2017). "Fractional order fuzzy sliding mode controller for the quarter car with driver model and dual actuators". *IET Intell. Transp. Syst.* 7(2), 145-153.
- Rao, L. G., and Narayanan, S. (2008). "Preview control of random response of a half-car vehicle model traversing rough road". *J. Sound Vib.*, 310(1-2), 352-365.
- Rao, L. G., and Narayanan, S. (2008). "Preview control of random response of a half-car vehicle model traversing rough road". *J. Sound Vib.*, 310(1-2), 352-365.
- Şahin, İ., Engin, T., and Çeşmeci, Ş. (2010). "Comparison of some existing parametric models for magnetorheological fluid dampers". *Smart. Mater. Struct.*, 19(3), 035012.
- Şahin, İ., Engin, T., and Çeşmeci, Ş. (2010). Comparison of some existing parametric models for magnetorheological fluid dampers. *Smart. Mat. Struct.*, 19(3), 035012. <https://doi.org/10.1088/0964-1726/19/3/035012>.
- Saini, R.S., Chandramohan, S., Sujatha, S., and Kumar, H., (2021). "Design of bypass rotary vane magnetorheological damper for prosthetic knee application". *J. Intell. Mater. Syst. Struct.* 32:931–42. <https://doi.org/10.1177/1045389X20942577>.
- Salem, M. M. M., and Aly, A. A. (2009). "Fuzzy control of a quarter-car suspension system". *World Acad. Sci. Eng. Technol.*, 53(5), 258-263.
- Sapiński, B. (2003). "Non-parametric representations of MR linear damper behaviour". *In IUTAM Symposium on Dynamics of Advanced Mat. Smart. Struct.*, 347-356, Springer, Yonezawa, Japan.
- Savaresi, S. M., Poussot-Vassal, C., Spelta, C., Sename, O., and Dugard, L. (2010). "Semi-active suspension control design for vehicles". *Elsevier*.
- Seid, S., Chandramohan, S., and Sujatha, S. (2019). "Design Evaluation of a Mono-tube Magnetorheological (MR) Damper Valve". *In Innovative Design, Analysis and Development Practices in Aerospace and Auto. Eng. (I-DAD 2018)* 145-151 Springer, Singapore.

Seung-Bok Choi, Young-Min Han (2012), “Magnetorheological Fluid Technology: Applications in Vehicle Systems” *CRC press*.

Sharma, S. K., Saini, U., and Kumar, A. (2019). Semi-active control to reduce lateral vibration of passenger rail vehicle using disturbance rejection and continuous state damper controllers. *J. Vib. Eng. Technol.*, 7(2), 117-129. <https://doi.org/10.1007/s42417-019-00088-2>

Shiao, Y. J., and Nguyen, T. S. (2015). “Using magnetorheological fluids in an innovative hybrid bicycle damper”. *IOP Conf. Ser.: Mater. Sci. Eng.*, 103(1), 1-8.

Shiao, Y. J., Nguyen, Q. A., and Lai, C. C. (2013). “Application of Magneto Rheological Damper on Semi-Active Suspension System”. *Appl. Mech. Mater.* (Vol. 284, pp. 1754-1758). Trans Tech Publications.

Shivaram, A. C., and Gangadharan, K. V. (2007). “Statistical modelling of a magnetorheological fluid damper using the design of experiments approach”. *Smart Mater. Struct.*, 16(4), 1310.

Simon, T. M., Reitich, F., Jolly, M. R., Ito, K., and Banks, H. T. (2001). “The effective magnetic properties of magnetorheological fluids”. *Math. Comput. Model. Dyn. Syst.*, 33(1), 273284.

Spaggiari, A., Castagnetti, D., Golinelli, N., Dragoni, E., and Scirè Mammano, G. (2019). “Smart materials: Properties, design and mechatronic applications”. *Proc. Inst. Mech. Eng. Pt. L J. Mater. Des. Appl.*, 233(4), 734-762.

Strecker, Z., Jeniš, F., Kubík, M., Macháček, O., and Choi, S. B. (2021). “Novel approaches to the design of an ultra-fast magnetorheological valve for semi-active control”. *Materials*, 14(10), 2500.

Sultoni, A. I., Sutantra, I. N., and Pramono, A. S. (2014). “Modeling, prototyping and testing of regenerative electromagnetic shock absorber”. *Appl. Mech. Mater.*, 493, 395400.

- Sunil Jha and Jain, V. K. (2009). "Rheological characterization of magnetorheological polishing fluid for MRAFF". *Int. J. Adv. Manufac. Tech.*, 42: 656-668
- Tharehalli Mata, G., Kumar, H., and Mahalingam, A. (2019). Performance analysis of a semi-active suspension system using coupled CFD-FEA based non-parametric modeling of low-capacity shear mode monotube MR damper. *Proc. Int. J. Mech. Eng. Part D: J. Auto Eng.*, 233(5), 1214-1231.
- Trikande, M. W., and Rajamohan, V. (2016). "MR damper characterization for implementation of semi-active suspension control". *Indian J Sci Technol.*, 9(30), 1-11.
- Trikande, M. W., and Rajamohan, V. (2016). MR damper characterization for implementation of semi-active suspension control. *Indian J. Sci. Technol.*, 9(30), 1-11. <https://doi.org/10.17485/ijst/2016/v9i30/95756>.
- Upadhyay, R. V., Laherisheth, Z., and Shah, K. (2013). "Rheological properties of soft magnetic flake shaped iron particle based magnetorheological fluid in dynamic mode". *Smart Mater. Struct.*, 23(1), 015002.
- Verros, G., Natsiavas, S., and Papadimitriou, C. (2005). "Design optimization of quartercar models with passive and semi-active suspensions under random road excitation". *J. Vib. Control*, 11(5), 581-606.
- Wang, D. H., Ai, H. X., and Liao, W. H. (2009). "A magnetorheological valve with both annular and radial fluid flow resistance gaps". *Smart. Mater. Struct.*, 18(11), 115001.
- Wang, D. H., and Liao, W. H. (2011). Magnetorheological fluid dampers: a review of parametric modelling. *Smart. Mat. Struct.*, 20(2), 023001. <https://doi.org/10.1088/0964-1726/20/2/023001>.
- Wen, S., Chen, M. Z., Zeng, Z., Yu, X., & Huang, T. (2016). "Fuzzy control for uncertain vehicle active suspension systems via dynamic sliding-mode approach". *IEEE Trans. Syst., Man, and Cybernetics: Systems*, 47(1), 24-32.

Wong, P. L., Bullough, W. A., Feng, C., and Lingard, S. (2001). "Tribological performance of a magneto-rheological suspension". *Wear*, 247(1), 33-40.

Yang, G., Spencer, B. F., Carlson, J. D., and Sain, M. K. (2002). "Large-scale MR fluid dampers: modelling and dynamic performance considerations". *Eng. Struct.*, 24(3), 309-323

Yao, G. Z., Yap, F. F., Chen, G., Li, W., and Yeo, S. H. (2002). "MR damper and its application for semi-active control of vehicle suspension system". *Mechatronics*, 12(7), 963-973.

Yerrawar, R. N., and Arakerimath, R. R. (2017). "Development of methodology for semi active suspension system using MR damper". *Mater. Today: Proc.*, 4(8), 9294-9303.

Zhang, H. H., Liao, C. R., Chen, W. M., and Huang, S. L. (2006). "A magnetic design method of MR fluid dampers and FEM analysis on magnetic saturation". *J. Intell. Mater. Syst. Struct.*, 17(8-9), 813-818.

Zhang, S., Shi, W., and Chen, Z. (2021). "Modeling and parameter identification of MR damper considering excitation characteristics and current". *Shock. Vib.*, 2021(1), 1-17.

## LIST OF PUBLICATIONS

The following are the list of Journals and conferences communicated till date

### International Journals

1. Devikiran, P., Puneet, N. P., Hegale, A., and Kumar, H. (2021). "Design and development of MR damper for two-wheeler application and Kwok model parameters tuning for designed damper". *Proc. Inst. Mech. Eng., Part D: J. Automob. Eng.*, 236(7), 1595-1606. Doi: 10.1177/09544070211036317. (Q2) SCI indexed, Impact factor 1.828.
2. Devikiran, P., Puneet, N. P., Saini T.R.S., and Kumar, H. "Hybrid Radial Flux Piston: Novel design of Electro Magnetic piston for Magneto Rheological Damper in Vehicular applications." *J. Vib. Eng. Technol.* (Q2) SCI indexed, Impact factor 2.333 (Under Review).
3. Devikiran, P., Puneet, N. P., Shravya, P., and Kumar, H. "Real Time Control of Radial Flux MR Damper for Two-Wheeler Light Motor Vehicle with Sliding Mode Controller" *Veh. Syst. Dyn.* (Q2) SCI indexed, Impact factor 3.749. (Under review).
4. Devikiran, P., Puneet, N. P., Shravya, P., and Kumar, H. "Reduction of Seat Vibrations in E-Bicycle using Axial Flux Piston Based MR Damper" *World J. Eng.* (Q3) ESCI & Scopus indexed, 3.3 Cite score. (Under review)

### International Conferences

1. Devikiran, P., Puneet, N. P., Hegale, A., and Kumar, H. (2021) "Sliding Mode Control Design for MR Damper in Vehicular Applications" *Prime 2021 conference organised by NIT Patna. 5-7 August 2021.*
2. Devikiran, P., Shravya, P., Puneet, N. P., and Kumar, H. (2022). "Design, characterization and control of MR damper for two-wheeler applications." *Mater. Today: Proc.* Doi: <https://doi.org/10.1016/j.matpr.2022.02.512>.

3. Devikiran, P., Shravya, P., Puneet, N. P., and Kumar, H. (2022). “Comparison of Axial and Radial Flux Piston Designs for Vehicular Applications with MR Damper”. *3rd International Conference on Mechanical Materials and Renewable Energy conference organised by Sikkim Manipal Institute of Technology, Sikkim.* 11-12 February 2022.
4. Devikiran, P., Shravya, P., and Kumar, H. (2022). “Design and Analysis of Radial Flux MR Damper for E-bike applications using Radial Basis Function with different control strategies”. *17th International Conference on Vibration Engineering and Technology of Machinery (VETOMAC 2022), Katmandu, Nepal.* 15-17 December 2022.

#### **Patents**

1. Hybrid Radial Flux Based Multi-Pole Piston for Magneto Rheological Damper, Patent application No.: 202141012329, Filed Date: 23/03/2021. (FER received).

## APPENDIX

### Specification of instruments used

#### Lord Wonder box



Lord Wonder box

Parameter	Specification
Overall Dimensions (LxWxH), mm (in)	63.5 x 27.9 x 88.9 (2.5 x 1.1 x 3.5)
Input Receptacle	1 mm, Female
Pulse Width Modulation (PWM) Frequency, kHz	30
Output Current, Amp	2 maximum

### Lord MRF 132 DG

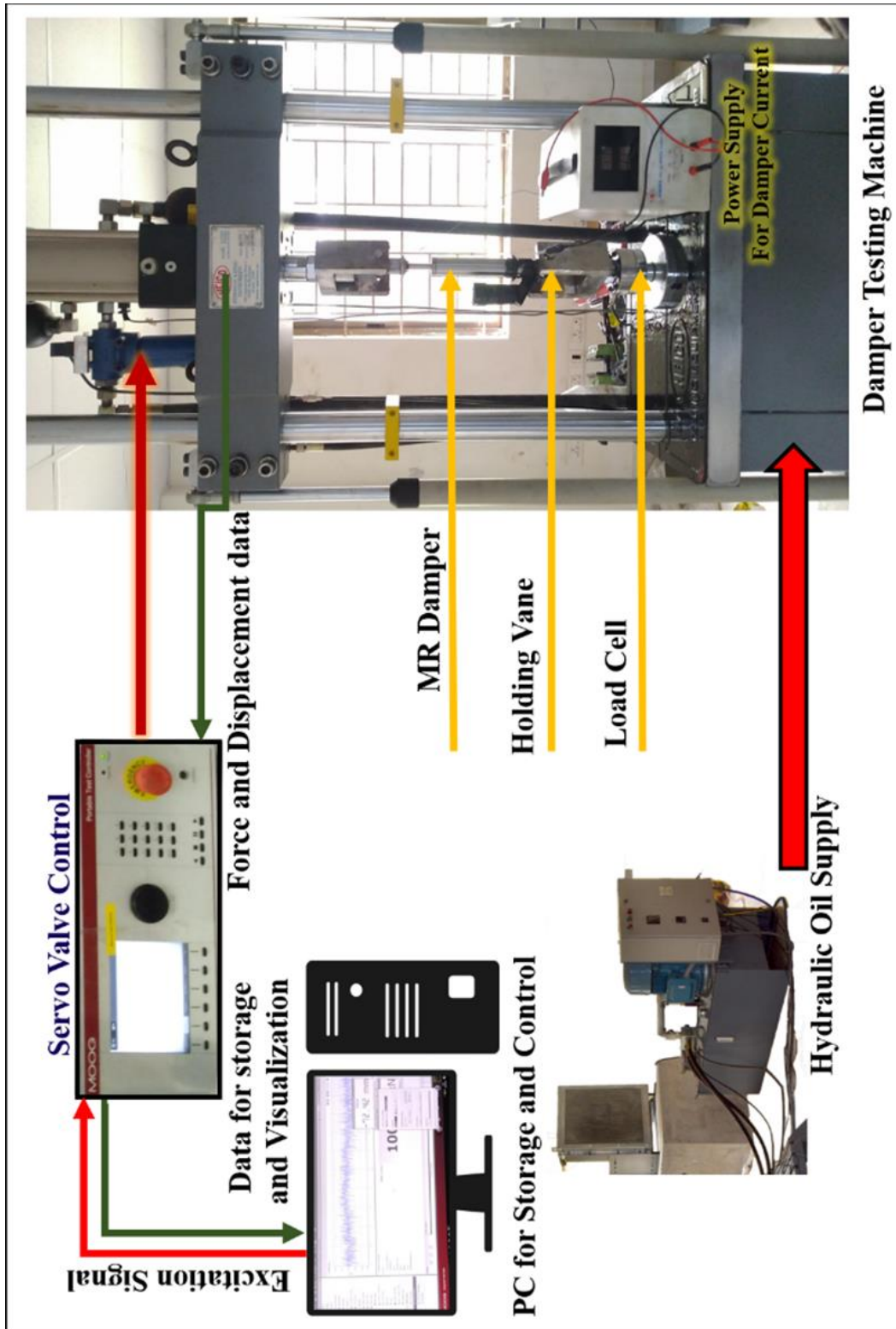


Lord MR fluid MRF 132 DG

<b>Parameter</b>	<b>Specification</b>
Appearance	Dark Gray Liquid
Viscosity, Calculated as slope 800-1200 sec <sup>-1</sup> , Pa-s @ 40°C (104°F)	0.112 ± 0.02
Density, g/cm <sup>3</sup> (lb/gal)	2.95-3.15 (24.6-26.3)
Solids Content by Weight, %	80.98
Flash Point, °C (°F)	>150 (>302)
Operating Temperature, °C (°F)	-40 to +130 (-40 to +266)



# HEICO Damper testing machine at NITK



Schematic test setup of damper testing machine

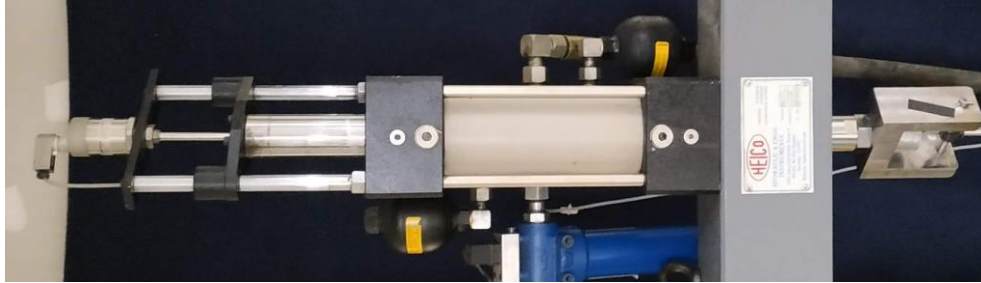
## 1. Hydraulic power pack



Hydraulic power pack

<b>Parameter</b>	<b>Specification</b>
Flow of the pump	64 LPM
Max. Operating Pressure	210 bars
Oil tank capacity	200 litres
Power rating of motor	40 HP
Length of hoses	5 m. (each)
Electric power supply	440V, 3 phase (AC supply)

## 2. Hydraulic actuator



Hydraulic actuator

Parameter	Specification
Type	Double acting double ended
Capacity	+/- 20 kN
Stroke	150 mm (+/- 75 mm)
Max. working pressure	210 bars
Max. sustained velocity	0.8 m/s
Peak velocity	1.2 m/s
Servo valve	63 LPM
Pressure line filter	180 LPM with 3 microns filtration
Accumulator (2 No.)	0.36 litre capacity

A servo valve with pressure line filter and accumulators (1.5 litres) in pressure and return valve is fitted on the manifold block. It controls the movement of the ram as per given command signal from control electronics. The servo valve is a throttle valve for 4-way applications and rated for a pressure drop of 1,000 PSI (70 kg/cm<sup>2</sup>). The output stage is a closed centre four way sliding spool. The servo valve is of MOOG make with a flow rate of 63 LPM.

### 3. Force transducer



Force transducer

Parameter	Specification
Capacity	+/- 30 kN
Resolution	0.001 kN
Full scale output	2 mV/V
Excitation Voltage	10 Volts DC
Non-linearity	< +/- 0.15 % FSO
Safe overload	150 %
Operating temperature	0 to +60 deg. C
Accuracy	0.5% of indicated value as per ISO7500-1

#### 4. Position sensor/ Displacement transducer



Position sensor/ Displacement transducer

<b>Parameter</b>	<b>Specification</b>
Range	200 mm
Make	Gefran/Balluff
Full scale output	10 volts
Repeatability	<0.01 mm
Maximum Pressure	Up to 600 bars
Excitation voltage	24 volts DC
Sampling rate	2 kHz
Operating temperature	-30 to +75 deg. C

## 5. Signal conditioning and controlling unit



Computer with signal conditioning and controlling unit

- Signal conditioning unit consists of conditioning modules for different transducers (position transducer, load cell etc.) that receives output signal from these sensors and processes the signal as per the requirement and transfers it to the computer where it is accepted by the data acquisition system.
- The controlling unit controls the movement of the ram with respect to the signal input on feedback basis either from force transducer or displacement transducer.
- It consists of a dedicated Servo-controller card that gives the desired processed signal through an automatic PID controller to the servo valve to operate in load mode or displacement mode.
- It also sends the signal to the computer and accepts the command from the software to operate in the desired manner.

### Specifications of servo controller

- Auto PID operation with auto zeroing, auto tuning and auto-adjustment feature servo operation.
- Digital signal processing (DSP) based closed loop servo controller with closed loop update rate of 10 kHz.
- Number of control channels - 4 (Load/Displacement/External channel strain 1 and strain2).
- Demand wave generation - Sine, Triangular, Square and ramp signal.

- High-speed 32-bit data acquisition with 6 kHz sampling rate on all primary channels.
- Auto calibration and digital auto zero capability.

**6. Computer with control software for controlling and data acquisition**

The system consists of a computer (Laptop) of latest available configuration with NI LabVIEW and latest OS installed. Computer configuration consists of AMD Ryzen5 processor with 8GB RAM and 512 GB SSD, 3 USB ports.

Control software in the system is the Windows based user-friendly software. The loading can be given in the form of sine, triangular, square and ramp signal. Multi-velocity performance and plotting with desired parameters make this software user friendly.

**1. Uniaxial accelerometer (PCB make)**



Uniaxial accelerometers (2 Nos.)

Parameter	Specification
Sensitivity	$\pm 100$ mV/g
Range	$\pm 50$ g
Frequency	0.5 to 10kHz
Resonance frequency	Greater than or equal to 50 kHz

**DAQ and semi-active controller (NI CDAQ 9174, NI 9234, NI 9403)**



NI CDAQ 9174

Parameter	Specification
Input FIFO size	127 samples per slot
Timing accuracy	50 ppm of sample rate
Timing resolution	12.5 ns
Resolution (Timers and counters)	32 bits
No. of slots for modules	4 slots





NI 9234 C series

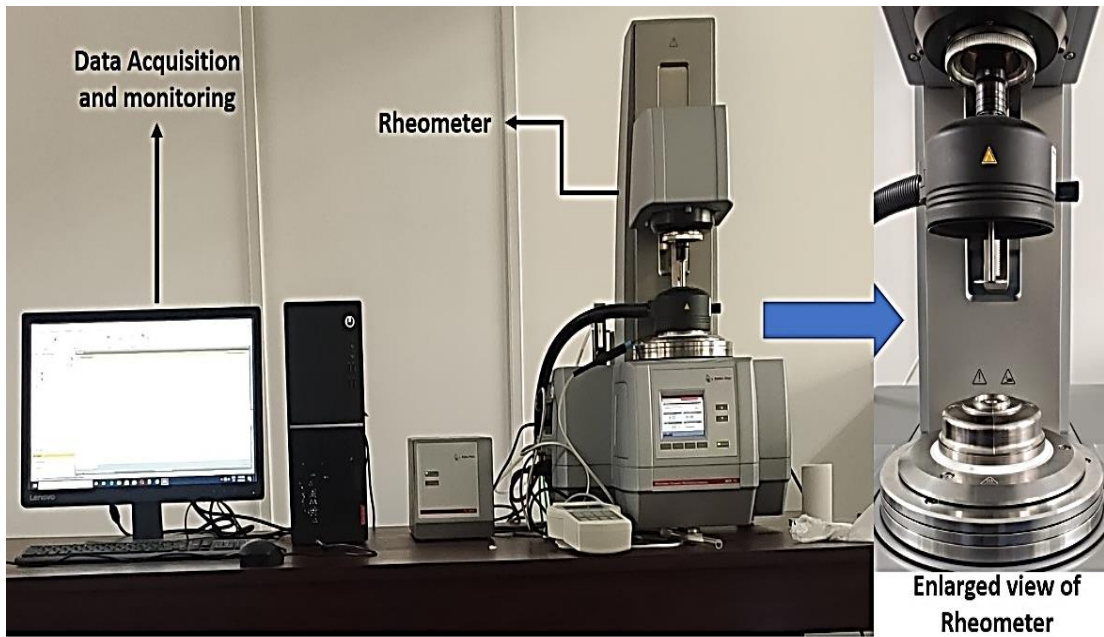
Parameter	Specification
IEPE channels	4 channel sound and vibration input
Resolution	24-bit resolution
Operational Range	±5 V, 0 to 20mA Input range
Connectivity type	BNC connectivity only
Sampling rate	51.2 kS/s



NI 9403 with DSUB 32 Ch, TTL Digital Input/Output Module

Parameter	Specification
Module type	5V, TTL digital I/O
No. of input output channels	32 - Channel
Speed of operation	7 μS
Isolation	60 VDC, CAT I
Operational Temperature	-40 °C to 70 °C
Operating Acceleration	5 g vibration, 50 g shock

## Anton Paar Rheometer MCR 702



Anton Paar Rheometer

Parameter	Specification
Minimum torque, rotation	1 nNm
Maximum torque, rotation	230 mNm
Minimum torque, oscillation	0.5 nNm
Maximum angular frequency	628 rad/s
Normal force range	0.005 to 50 N
Maximum temperature range	-160 to +1000 °C
Pressure range	up to 1000 bar
Rheometer Software RheoCompass™ Professional	Running under Microsoft Windows 7/8/8.1/10 (64bit versions only) - Recommended hardware: Intel i5,

	2.67 GHz or higher, 8 GB RAM or more, SSD with 240 GB or more
Magnetorheological Device Cell	Magnetic Flux density up to 1 Tesla Temperature range -10 to 170°C
Hood with Peltier Heating/Cooling	Temperature range: -40 to 200 °C
Compressor	230/50 V/Hz, 55 l/min, OILFREE Motor Power: 0.55 kW Output (5 bar): 55 l/min max. Pressure: 8 bar Tank Volume: 10 l Weight: 59 kg
Peltier Temperature Control Device	Temperature range: -5 to 200 °C
Power Supply Magneto Cell	230V HCP 14-12500,12.5,1 mA
Tesla meter	1 Tesla

### DC Power supply (Scientific make)



DC Power supply (Scientific PSD 3005)

<b>Parameter</b>	<b>Specification</b>
Make	Scientific
Model	PSD 3005
DC output	0 to 30V / 5A
Settling resolution	V: 10 mV, I: 5 mA
Load Regulation	$\leq \pm(0.05\% + 10 \text{ mV})$
Input Supply	230 AC $\pm 10\%$ / 50-60 Hz
Internal resistance	$\leq 10 \text{ m}\Omega$

- Built in over-heat and over-voltage protection.
- Constant current and constant voltage operation.
- Digital display for voltage and current.
- Adjustable current limiter.
- Protection against over-load and short circuit.
- Compact and light weight.

## Real-time controller (NI cRIO 9045)



NI cRIO 9045

- 1.30 GHz Dual-Core CPU,
- 2 GB DRAM ,
- 4 GB Storage, -20 °C to 55 °C,
- Kintex-7 70T FPGA,
- 8-Slot CompactRIO Controller

## MATLAB software details

Parameter	Specification
Name of the software	MATLAB/SIMULINK
Version	R2018b to R2022a
Licensed to	NITK
Company	MathWorks

### FEMM software details

<b>Parameter</b>	<b>Specification</b>
Name of the software	Finite Element Method Magnetics
Version	4.2 (Current version)
Licensed to	Open-Source software

<b>Parameter</b>	<b>Specification</b>
Name of the software	ANSYS
Licensed to	NITK, Surathkal

### LabVIEW software

<b>Parameter</b>	<b>Specification</b>
Name of the software	LabVIEW
Version	2017
Licensed to	NITK
Company	National Instruments
Tool boxes	Real time tool box, FPGA

## BIO DATA

**Name** : PINJALA DEVI KIRAN  
**Date of Birth** : 21-08-1989  
**Mobile No.** : 9032390251/9441114765  
**Email Id** : devikiranpro@gmail.com  
pinjaladevikiran@gmail.com



**Address** : H.No.1-23-314, Bhudevinagar, Thirumalgiri Post, Secunderabad.  
Pin:500015

### Qualification

Degree	University	Percentage/CGPA	Year
Ph.D (Course Work)	NITK, Surathkal	8.0 CGPA	2018
M.Tech (Power Electronics and Drives)	K.L. University	8.8 CGPA	2011-13
B. Tech (Electrical and Electronics Engineering)	JNTU-Hyderabad	74.22%	2007-11

### Experience

S. No.	Name of the Institute/organization	Designation	From	To
1.	Shri Vishnu Engineering College for Women	Assistant Professor	Nov, 2013	Nov, 2017
2.	National Institute of Technology Karnataka	Junior Research Fellow (JRF)	Dec, 2017	Aug, 2019

**Journal Publications: 7**

**Conferences: 9**